Curso 2006/07
CIENCIAS Y TECNOLOGÍAS/14
I.S.B.N.: 978-84-7756-759-2

NANCY DEL CARMEN ELÍAS DE LA ROSA

Thermonuclear Supernovae in environments with significant extinction

Directores
JOHN E. BECKMAN
MASSIMO TURATTO
STEFANO BENETTI
ENRICO CAPPELLARO

SERVICIO DE PUBLICACIONES
UNIVERSIDAD DE LA LAGUNA

SOPORTES AUDIOVISUALES E INFORMÁTICOS
Serie Tesis Doctorales

a mi familia

¡va por ustedes!

Resumen

¿Las supernovas (SN/SNs) son herramientas útiles para el estudio del polvo en otras galaxias? ¿Tienden a explotar en regiones donde las propiedades de los granos de polvo son diferentes de las estándares? Contestar a estas preguntas fue el principal objetivo de esta tesis.

Durante la primera parte de este trabajo, se recopilaron, reducieron y analizaron datos de SNs Ia fuertemente extinguidas: SN 2003cg, SN 2002cv y SN 2006X, aprovechando los telescopios disponibles de la *European Supernova Collaboration*, en las bandas ópticas e infrarrojas. Estos objetos permitieron la realización de un análisis del enrojecimiento que sufren las SNs en las galaxias huésped encontrando, en todos los casos, valores bajos de R_V (razón entre la extinción total y selectiva) para la ley de extinción. Estas determinaciones de R_V fueron obtenidas con varios métodos independientes derivados de la fotometría y la espectroscopía, basados en la comparación de las distribuciones espectrales de la energía de nuestras SNs enrojecidas con las de otras SNs Ia no enrojecidas.

En la segunda parte de esta tesis se estudiaron los resultados obtenidos para estas tres SNs en base a nuestro conocimiento actual de las propiedades del polvo. Usando las curvas de extinción derivadas de estas SNs Ia, se pudo estimar el tamaño medio de los granos del polvo a lo largo de las líneas de vista en dirección de las SNs. También en este trabajo se realizó un nuevo estudio sobre la relación entre la anchura equivalente (EW) de la línea interestelar del Na ID y el E(B-V) con un nuevo y más completo grupo de SNs. Durante su análisis se comprobó que muchos efectos contribuyen a la dispersión de los puntos del diagrama EW(Na ID) - E(B-V) y que por lo tanto, sólo pueden ser establecidos límites inferiores de la extinción de la SN.

En este contexto, la tesis está organizada como sigue:

El **Capítulo 1** introduce al fenómeno "supernova" e ilustra los problemas relacionados con el estudio de las supernovas termonucleares (SNs Ia).

El **Capítulo 2** describe la instrumentación empleada para obtener los datos presentados en esta tesis y una breve explicación de las técnicas de reducción usadas.

El **Capítulo 3** presenta los resultados obtenidos del estudio de SN 2003cg, cuarta supernova observada por la *European Supernova Collaboration*. Tanto sus curvas de luz como sus espectros son similares a los de SNs de tipo Ia "normales", pero con un enrojecimiento muy alto. Después de usar diversos métodos para estimar la extinción, adoptando siempre una ley de extinción de Cardelli, Clayton & Mathis (1989) y dejando R_V como parámetro libre, se estimó $A_V = 2.39 \pm 0.13$, y $R_V = 1.80 \pm 0.19$.

El **Capítulo 4** está dedicado al análisis de las observaciones de SN 2002cv. Dos características principales hacen de esta SN un extraño caso: la primera es la coincidencia de explotar en la misma galaxia huésped y casi simultáneamente con otra SN Ia, SN 2002bo; la segunda es su extinción extremadamente alta: $A_V = 8.54 \pm 0.89$ y $R_V = 1.75 \pm 0.55$. Estos valores hacen de SN 2002cv una de las SNs más enrojecidas jamás observada.

El **Capítulo 5** se centra en el estudio preliminar de la reciente SN 2006X, cuya campaña de observación está todavía en marcha. De este análisis se puede decir que la SN 2006X parece ser un tipo típico de SN de tipo Ia, pero fuertemente extinguida por el polvo. La SN 2006X fue observada en el óptico usando 12 configuraciones instrumentales diferentes y su seguimiento abarca un período de 6 meses. La conclusión principal de este análisis es la clara evolución en el tiempo de las líneas interestelares del Na ID causada probablemente por la presencia de material circumestelar alrededor del lugar de la explosión. También en este caso R_V era menor que el valor estándar ($A_V = 1.98 \pm 0.69$ y $R_V = 1.56 \pm 0.30$).

El **Capítulo 6** presenta las principales características del polvo y del gas tanto en el medio interestelar como en el circumestelar y sus efectos en las supernovas. En particular, del análisis de los pequeños valores de R_V se ha podido dar una estimación del tamaño medio del polvo que produce la extinción. También se presenta en este capítulo el estudio de la relación entre la anchura equivalente de las líneas interestelares de Na ID y el enrojecimiento, para una nueva y más numerosa muestra de SNs.

El **Capítulo 7** resume los resultados principales y conclusiones obtenidas en esta tesis. Por otra parte, presenta alguna aplicaciones futuras de este trabajo.

El **Apéndice A** describe el marco en el cual fue concebida esta tesis, es decir, la *European Supernova Collaboration*, financiada por la Comunidad Europea durante 4 años (2002-2006) y formada por 10 institutos europeos. Esta colaboración fue creada para investigar la naturaleza de las explosiones termonucleares de las supernovas y para entender mejor su física.

El **Apéndice B** presenta el análisis y la clasificación de nuevas supernovas cercanas observadas por el grupo de Padova. Este trabajo ha sido importante para esta tesis porque de la información proporcionada por los primeros espectros ha sido posible determinar si las SNs estaban fuertemente enrojecidas y, por consiguiente, comenzar mi estudio.

Riassunto

Le supernove (SN/SNe) sono strumenti utili per lo studio della polvere in altre galassie? Tendono ad esplodere nelle regioni dove le proprietá dei grani di polvere sono diverse di quelle standard? Rispondere a queste domande è stato lo scopo principale di questa tesi.

Durante la prima parte del lavoro, i dati di SNe di tipo Ia altamente estinte (SN 2003cg, SN 2002cv e SN 2006X) sono stati raccolti nelle bande ottiche ed IR, ridotti e analizzati sfruttando i telescopi disponibili alla *European Supernova Collaboration*. Lo studio di questi oggetti ha permesso di effettuare un'analisi del loro arrossamento nelle galassie ospite trovando, per tutti i casi, valori bassi di R_V (rapporto fra estinzione totale e estinzione selettiva) per la legge di estinzione. Queste determinazioni di R_V sono state ottenute con parecchi metodi indipendenti, basati fra confronto delle distribuzioni spettrali di energia delle SNe studiate (derivati dalla fotometria e la spettroscopia) con quelle di altre SNe Ia non arrossate.

Nella seconda parte di questa tesi sono stati analizzate i risultati ottenuti per tutte e tre SNe nel contesto della nostra conoscenza attuale della polvere. È stato possibile derivare la dimensione media dei grani di polvere seguendo le linee di vista verso le SNe. Inoltre si è tentato un nuovo studio sul rapporto della larghezza equivalente della linea interstellare del Na ID in funzione di E(B-V) con un nuovo campione ingrandito. Si é visto che molti effetti contribuiscono a disperdere i punti nel diagramma EW(Na ID) - E(B-V) e che, quindi, possono essere stabiliti solo i limiti all'estinzione delle SN.

Sotto questo contesto, la tesi è organizzata come segue:

Il **Capitolo 1** introduce al fenomeno "supernova" ed illustra il problemi relazionati con lo studio delle supernovae termonucleari (SNe Ia).

Il **Capitolo 2** descrive la strumentazione usata per ottenere i dati presentati in questa tesi e da una breve discussione sulle tecniche di riduzione dei dati.

Il **Capitolo 3** presenta i risultati ottenuti per SN 2003cg, la quarta supernova osservata dalla *European Supernova Collaboration*. Tanto le sue curve di luce come gli spettri sono simili a quelli di altre SNe di tipo Ia "normali" ma con un arrossamento molto alto. Dopo aver usato differenti metodi per valutare l'estinzione, adottando sempre una legge di estinzione di Cardelli, Clayton & Mathis (1989) con R_V come parametro libero, si sono stimati i seguenti valori: $A_V = 2.39 \pm 0.13$ e $R_V = 1.80 \pm 0.19$.

Il **Capitolo 4** è dedicato all'analisi delle osservazioni di SN 2002cv. Due fatti principali rendono SN 2002cv un evento raro: il primo è la coincidenza di esplodere nella stessa galassia ospite e praticamente nello stesso periodo con un altra SN Ia, SN 2002bo; il secondo è la sua estremamente alta estinzione: $A_V = 8.54 \pm 0.89$ e $R_V = 1.75 \pm 0.55$. Ciò fa di SN 2002cv una delle SNe piú arrossate mai osservata prima.

Il **Capitolo 5** è centrato sullo studio preliminare della recente SN 2006X, il cui monitoraggio è ancora in progresso. Da questa analisi, SN 2006X sembra effettivamente essere una tipica SN di tipo Ia, ma fortemente estinta dalla polvere. SN 2006X è stata osservata nell'ottico usando 12 differenti configurazioni strumentali coprendo un arco di tempo di 6 mesi. La principale conclusione di questa analisi è la chiara evoluzione nel tempo delle linee di assorbimento di Na ID, che potrebbe essere causata dalla presenza di materiale circumstellare nelle vicinanze della posizione della esplosione. Inoltre anche in questo caso R_V è più basso del valore standard ($A_V = 1.98 \pm 0.69$ e $R_V = 1.56 \pm 0.30$).

Il **Capitolo 6** introduce le caratteristiche principali della polvere nel mezzo interstellare e circumstellare ed i relativi effetti sulle supernove. In particolare, un'analisi del R_V basso ha fornito una stima media della dimensione della polvere che produce l'estinzione. Anche in questo capitolo si presenta lo studio sul rapporto fra la larghezza equivalente delle linee interstellari di Na ID e l'arrossamento utilizzando un campione di SNe piú grande.

Il **Capitolo 7** riassume i risultati principali di questa tesi le conclusioni raggiunte. Inoltre presenta alcune possibili estenzioni e applicazioni future di questo lavoro.

L'**Appendice A** descrive la struttura della collaborazione internazionale entro cui questo lavoro è stato sviluppato, cioè, la *European Supernova Collaboration*, finanziata dalla Comunità Europea per 4 anni (2002-2006) e costituito da 10 istituzioni europee. Questa collaborazione è stata supportata per studiare la natura delle esplosioni termonucleari delle supernove e per capire meglio la loro fisica.

L'**Appendice B** presenta l'analisi e la classificazione di una frazione di nuove supernove vicine osservate dal gruppo di Padova. Dalle informazioni fornite dai primi spettri è stato possibile capire se le SNe fossero fortemente arrossate e, conseguentemente, includerle nel mio studio.

Abstract

Are the supernovae (SN/SNe) useful tools in studying of the dust in other galaxies? Do they tend to explode in regions where dust grain properties are far from standard? Answering to these questions was the main purpose of this thesis.

During the first part of this work, data of the highly extinguished Type Ia SNe SN 2003cg, SN 2002cv and SN 2006X were collected, reduced, and analyzed by exploiting the available telescopes to the *European Supernova Collaboration* in the optical and in infrared wavelength bands. These objects allowed me to carry out an analysis of the reddening suffered by them in the host galaxies finding, in all cases, low values of the total-to-selective extinction ratio (R_V) for the extinction law. These determinations of R_V were obtained with several independent methods based on the comparison of the Spectral Energy Distributions derived both from photometry and spectroscopy with those of other unreddened SNe Ia.

In the second part of this thesis I studied the results obtained for the three SNe in the context of our present knowledge of dust. It has been possible to derive the average size of the dust grains along the lines of sight toward the SNe. I have also attempted a new study on the relation of equivalent width (EW) of the Na ID vs. E(B-V) with a new enlarged sample. I have seen that many effects contribute to disperse the points in the diagram and that, therefore, only lower limits to the SN extinction can be set.

Under this context, the thesis is organized as follow:

Chapter 1 introduces to the supernova phenomenon and illustrates the problematic related to the study of the thermonuclear supernovae (SNe Ia).

Chapter 2 describes the instrumentation used to obtain the data presented in this thesis and a short discussion about the data reduction techniques.

Chapter 3 presents the results relative to SN 2003cg, the fourth supernova monitored by the *European Supernova Collaboration*. Its light curves and spectra are similar to those of a *normal* Type Ia SNe but for the very high reddening suffered. After using different methods to estimate extinction, adopting a Cardelli, Clayton & Mathis (1989) extinction law with R_V as free parameter, I estimated $A_V = 2.39 \pm 0.13$, and $R_V = 1.80 \pm 0.19$.

Chapter 4 is devoted to the analysis of the observations of SN 2002cv. Two main facts make SN 2002cv a rare event: the first is a coincidence in the time of explosion with another Type Ia SN, SN 2002bo, in the same host galaxy; the second one is its extremely high extinction: $A_V = 8.54 \pm 0.89$ and $R_V = 1.75 \pm 0.55$ inside the host galaxy. This makes SN 2002cv one of the most reddened SNe ever observed.

Chapter 5 focuses on the preliminary study of the recent SN 2006X, whose monitoring is still in progress. From this analysis, SN 2006X seems indeed to be a typical Type Ia SN, but heavily extinguished by dust. SN 2006X was observed in the optical using 12 different instrumental configurations and the follow-up spans a period of 6 months. The main conclusion of this analysis is the clear time evolution of the Na ID absorption features which could be caused by the presence of circumstellar material in the vicinity of the explosion location. Also in this case R_V was lower than the canonical value ($A_V = 1.98 \pm 0.69$ and $R_V = 1.56 \pm 0.30$).

Chapter 6 introduces the main features of the dust and gas in the interstellar and circumstellar medium and its effects on the supernovae. In particular, an analysis of the low R_V has provided the average size of the dust producing the extinction. The study of the relation between the equivalent width of Na ID interstellar lines and reddening for a new large sample of SNe is presented.

Chapter 7 summarizes the main results of this thesis and the conclusions obtained. Moreover, it presents some future application of this work.

Appendix A describes the framework in which this thesis was prepared, i.e. the *European Supernova Collaboration* funded by the European Community for 4 years (2002-2006) and formed by 10 European Institutions. This collaboration was born to investigate the nature of thermonuclear supernova explosions and to better understand their physics.

Appendix B presents the analysis and classification performed by me on a large fraction of the new, nearby supernovae observed by the Padova SNe Group. From the information provided by the first spectra has been possible to understand whether the SNe were heavily reddened and, consequently, to start my intensive study.

Contents

Resumen **v**

Riassunto **ix**

Abstract **xiii**

1 Why Are Supernovae Important? **9**
1.1 How were the supernovae discovered? 9
1.2 How many types of supernovae are there? 12
1.3 What are the general properties of SNe? 15
1.4 Thermonuclear Supernovae 17
1.4.1 What are the observational characteristics of the Thermonuclear Supernovae? 17
1.4.2 Why SNe Ia do explode? 32
1.4.3 Are all SNe Ia similar? 36
1.4.4 Why are SNe Ia useful in cosmology? 39
1.5 Why do I devote this thesis to the SN study? 43

2 Data acquisition and processing **45**
2.1 Data acquisition 45
2.2 Telescopes and instrumentation 46
2.3 Data reduction 54
2.3.1 Preliminary reduction 54
2.3.2 Photometry 55
2.3.3 Spectroscopy 65

3 Supernova 2003cg **67**
3.1 Data acquisition and reduction 68

3.1.1 Photometric observations 69
3.1.2 Spectroscopic observations 70
3.1.3 Correction to standard photometric bands 70
3.2 The reddening 82
3.2.1 Reddening estimate - Standard procedure 83
3.2.2 Reddening estimate - an anomalous extinction law 84
3.2.3 Effects of a light echo? 89
3.3 Photometry 91
3.3.1 Light curves 91
3.3.2 Colour curves 96
3.3.3 Absolute magnitudes and the *uvoir* light curve 97
3.4 Spectroscopy 99
3.4.1 Optical spectra 100
3.4.2 Near-infrared spectra 101
3.4.3 Velocity gradient 106
3.4.4 Spectral modelling 111
3.5 Summary 115

4 Supernova 2002cv 117
4.1 Photometry 118
4.1.1 Data acquisition and reduction 118
4.1.2 Light curves 121
4.1.3 Colour and pseudo bolometric Curves 125
4.2 Spectroscopy 130
4.2.1 Data reduction 130
4.2.2 Optical and NIR spectra 130
4.3 The reddening estimate 133
4.4 Photometric parameters 138
4.4.1 VRI decline rates vs. Δm_{15}(B) 138
4.4.2 I magnitudes and Δm_{15}(B) 143
4.4.3 Parameters of SN 2002cv 147
4.5 Summary 149

5 Supernova 2006X 151
5.1 Data acquisition and reduction 152
5.2 Photometry 153
5.2.1 Light curves 153
5.2.2 Colour curves 155
5.3 Spectroscopy 157
5.3.1 Spectral evolution 157

5.3.2 Velocity gradient . . . 161
5.4 Extinction . . . 162
5.4.1 Reddening estimate . . . 162
5.4.2 Sodium lines . . . 165
5.5 Summary . . . 167

6 Dust 169
6.1 Interstellar medium . . . 170
6.1.1 Dust grain properties . . . 171
6.2 Circumstellar medium . . . 180
6.3 Dust and Supernovae . . . 183
6.4 Diffuse interstellar bands in supernovae . . . 187
6.5 Estimation of the relative grain sizes . . . 189
6.6 EW of Na ID line and reddening in SNe . . . 192
6.7 Low total-to-selective extinction ratios in SNe . . . 206

7 Conclusions 211
7.1 Future work . . . 214

A European Supernova Collaboration 217
A.1 Research objectives . . . 217
A.2 Major successes . . . 218
A.3 Research results . . . 219

B Spectroscopic Classification of Supernovae 223
B.1 Supernova 2003hg in NGC 7771 . . . 224
B.2 Supernova 2003ie in NGC 4051 . . . 225
B.3 Supernova 2004G in NGC 5668 . . . 226
B.4 Supernova 2004aq in NGC 4012 . . . 227
B.5 Supernova 2004aw in NGC 3997 . . . 227
B.6 Supernova 2004dg in NGC 5806 . . . 229
B.7 Supernova 2004go in IC 270 . . . 230
B.8 Supernova 2005G in UGC 8690 . . . 230
B.9 Supernova 2005H in NGC 838 . . . 231
B.10 Supernova 2005I in IC 983 . . . 232
B.11 Supernova 2005W in NGC 691 . . . 233
B.12 Supernova 2005ab in NGC 4617 . . . 234
B.13 Alleged Supernova in NGC 4656 . . . 234
B.14 Supernova 2006G in NGC 521 . . . 235
B.15 Supernova 2006W in UGC 9265 . . . 236

B.16 Supernova 2006dk in NGC 4161 237
B.17 Supernova 2006en in MCG +05-54-41 238
B.18 Supernova 2006et in NGC 232 239
B.19 Supernova 2006gy in NGC 1260 240
B.20 Supernova 2006jc in UGC 4904 241

Bibliography **243**

List of Tables

1.1 Historical supernovae 10
1.2 General characteristics of the three well-separated clusters of SNe Ia 39
1.3 Properties within which a SN Ia can be considered normal . . . 39

3.1 Original optical photometry of SN 2003cg 71
3.2 Magnitudes for the local sequence stars identified in the field of SN 2003cg 74
3.3 Original near-IR photometry of SN 2003cg 75
3.4 Optical spectroscopy of SN 2003cg 76
3.5 Infrared spectroscopy of SN 2003cg 77
3.6 Optical S-correction to be added to the data in Table 3.1 78
3.7 NIR S-corrections to be added to the data in Table 3.3 81
3.8 Values of the colour excess and the ratio of total-to-selective extinction derived from different methods 88
3.9 Main data of SN 2003cg and its host galaxy 92
3.10 Decline rates of SN 2003cg at late phases 95
3.11 Absolute B magnitude of SN 2003cg derived from different methods 100

4.1 Magnitudes for the local sequence stars identified in the field of SN 2002cv 120
4.2 S-corrected optical photometry of SN 2002cv 122
4.3 Original near-IR photometry of SN 2002cv 123
4.4 Main data of SN 2002cv and its host galaxy 129
4.5 Optical and IR spectroscopic observation of SN 2002cv 130
4.6 Basic input data to find the values of A_V, R_V and μ by multi-dimensional maximum likelihood estimation 136

4.7 Values of the total host extinction in the V band and the ratio of total-to-selective extinction 137
4.8 Main parameters for the SNe Ia sample 142
4.9 Absolute I magnitude of SN 2002cv 148

5.1 Optical photometry of SN 2006X 154
5.2 Optical spectroscopy of SN 2006X 155
5.3 Main data of SN 2006X and its host galaxy 156

6.1 Classification of Interstellar Cloud Types. 172
6.2 Diffuse Interstellar Bands of SN 2003cg 189
6.3 R_λ values and relative (mean) grain sizes 192
6.4 Sample of SNe treated in this section 195
6.5 Ratio of EWs of the components of the NaI D doublet 206
6.6 Size Domains of Interstellar Grains 208

B.1 Summary of the SNe classified 242

List of Figures

1.1 Number of SN discoveries per year 12
1.2 Supernova taxonomy 13
1.3 Spectra of the various supernova types and subtypes at maximum light, 3 months and one year after maximum 14
1.4 Light curves of the various supernova types and subtypes 15
1.5 Typical P-Cygni line profile 16
1.6 V light curve of SN 1987A 18
1.7 Spectral evolution of a typical SN Ia 20
1.8 Light curves of a normal SN Ia (SN 1992A) 21
1.9 Colour evolution of several SNe Ia 22
1.10 B-V colour evolution for SNe Ia 23
1.11 Absolute magnitude vs. Δm_{15}(B) relation 24
1.12 Light curve timescale stretch factor corrected 25
1.13 J, H and K band light curve of several bright SN Ia 26
1.14 NIR absolute magnitudes of Type Ia SNe at maximum as a function of Δm_{15}(B) 27
1.15 V minus IR colours of SN Ia with decline rates $0.81 \leq \Delta m_{15}$(B) ≤ 1.00 28
1.16 Early NIR spectra of several SNe Ia 29
1.17 Ultraviolet and optical light curves of SN 2005ke 30
1.18 UVOT Grism Spectra of SN2005am 31
1.19 Double Degenerate schematic evolution 34
1.20 Single Degenerate schematic evolution 35
1.21 Schematics of the explosion of a white dwarf near the Chandrasekhar mass 36
1.22 Observed magnitude versus redshift for well-measured distant and nearby Type Ia SNe 40
1.23 Hubble Diagram for Supernova Cosmology Project 41

1.24 Confidence regions for Ω_M vs Ω_Λ 42

2.1 Example of PSF-fitting technique 56
2.2 Example of Template Subtraction Technique 58
2.3 Differences between the magnitudes obtained with the PSF-fitting and Template Subtraction Techniques 59
2.4 BVRI global passbands transmission function 61
2.5 Late epochs evolution of δB, δV and δR introduced by different instruments 64
2.6 BVRI Bessell and WFI passbands overplotted on spectrum of SN 1992A 65

3.1 V band image of SN 2003cg and local sequence stars 68
3.2 First monodimensional spectrum of SN 2003cg taken with the WHT+ISIS on 2003 March 22 69
3.3 Summary of the S-corrections adopted for the BVRI bands at early and late time 80
3.4 Summary of the S-corrections adopted for the NIR bands at early time 81
3.5 Detail of the interstellar Na ID region 82
3.6 (B-V) colour curve of SN 2003cg 83
3.7 Intrinsic optical and NIR colour curves of SN 2003cg 86
3.8 Differences between the observed colour excesses and those computed for $R_V = 3.1$ and $R_V = 2.0$ 87
3.9 Best fit of theoretical CCM laws to empirical extinction curves of SN 2003cg 90
3.10 S-corrected optical and IR light curves of SN 2003cg at early phases 94
3.11 S-corrected BVRIJHK light curves for SN 2003cg covering early and late phases 96
3.12 Intrinsic (B-V) colour curve of SN 2003cg 98
3.13 *uvoir* light curve for SN 2003cg 99
3.14 Optical spectral evolution of SN 2003cg 102
3.15 Ca II IR triplet profiles in the earliest spectra of SN 2003cg and other Type Ia SN 103
3.16 Comparison between optical spectra of SN 2003cg with those of other SNe 104
3.17 NIR spectral evolution of SN 2003cg 105
3.18 Comparison between the NIR spectra of SN 2003cg and those of other SNe 107

3.19 Combined optical and IR spectra of SN 2003cg 108
3.20 Evolution of the expansion velocity derived from the minima of Si II 6355 Å for SN 2003cg 109
3.21 Evolution of the expansion velocity derived from the minima of S II 5640 Å for SN 2003cg 109
3.22 Pre-maximum evolution of $\mathcal{R}$(Si II) for SN 2003cg 110
3.23 $\mathcal{R}(\mathrm{Si\,II})_{max}$ vs. Δm_{15}(B) and $\dot{v}$ vs. Δm_{15}(B) for Si IIλ 6355 . . . 110
3.24 Spectral models of SN 2003cg at day $-7.6/-6.5$ 112
3.25 Spectral model of SN 2003cg at day -0.6 114

4.1 R band image of SN 2002cv and local sequence stars 118
4.2 Summary of the S-corrections derived for the VRI bands of the different instruments at early times 121
4.3 Comparison between the VRI band light curves of SN 2002cv . . 124
4.4 S-corrected VRIJHK light curves of SN 2002cv 125
4.5 Comparison between the I band light curve of SN 2002cv and other Type Ia SNe with different Δm_{15}(B) 126
4.6 Colour evolution of SN 2002cv compared with those of other SNe Ia 127
4.7 Colour evolution of SN 2002cv compared with those of other SNe of different types 127
4.8 Pseudo-bolometric (RIJHK) light curve for SN 20002cv 128
4.9 Optical spectral evolution of SN 2002cv 131
4.10 NIR spectral evolution of SN 2002cv 132
4.11 Comparison between the combined optical and IR spectra of SN 2002cv 133
4.12 One of the best fit of theoretical CCM laws to empirical extinction curves of SN 2002cv 135
4.13 Multi-dimensional maximum likelihood estimation to derived A_V and R_V 137
4.14 Colour evolution of SN 2002bo compared with those of other SNe Ia 140
4.15 Graphical representation of the parameters defined in Sections 4.4.1 and 4.4.2 141
4.16 V light curve decline rates 144
4.17 R light curve decline rates 144
4.18 I light curve decline rates 145
4.19 Difference of magnitude between the primary and secondary maxima of I light curve, ΔI_{max}, vs. $\Delta m_{15}(B)_{obs}$ 145

4.20 Difference in phase between primary and secondary maxima of I light curve ($\Delta t_{max}(I)$) vs. $\Delta m_{15}(B)_{obs}$ . . . 146
4.21 M_I^{max} vs. $\Delta t_{max}(I)$ . . . 146
4.22 M_I^{max} vs. Δm_{40}(I) . . . 147

5.1 V band image of SN 2006X and local sequence stars . . . 152
5.2 Optical light curves of SN 2006X at early phases . . . 157
5.3 Comparison between the B band light curve of SN 2006X and other Type Ia SNe with different Δm_{15}(B) . . . 158
5.4 Best B template giving the stretch factor for SN 2006X . . . 158
5.5 (B-V) and (V-R) colour curves of SN 2006X . . . 159
5.6 Optical spectral evolution of SN 2006X . . . 160
5.7 Comparison between optical spectra of SN 2006X and those of SN 2002bo . . . 161
5.8 Evolution of the expansion velocity derived from the minima of Si II 6355 Å for SN 2006X . . . 163
5.9 Best fit of theoretical Cardelli, Clayton & Mathis (1989) laws to empirical extinction curves of SN 2006X . . . 164
5.10 Detail of the interstellar Na ID region of SN 2006X . . . 166

6.1 Interstellar Reddening . . . 172
6.2 Schematic illustration of the Pair Method . . . 175
6.3 Average interstellar extinction curve . . . 176
6.4 Extinction curves by Cardelli, Clayton & Mathis (1989) . . . 177
6.5 Schematic representation of the evolution of cosmic dust . . . 178
6.6 Extinction curve model for the average Galactic extinction . . . 181
6.7 Histogram of the host galaxy extinction . . . 184
6.8 Variation of λ_{eff} with time for various levels of extinction in the B bands . . . 186
6.9 Variation with time of the selective to total extinction ratio in UBVRI bands for Type Ia SNe . . . 186
6.10 Diffuse Interstellar Bands of SN 2003cg . . . 190
6.11 Extinction curves for the parent galaxies in the direction to the three highly extinguished SNe Ia of this thesis compared with the canonical curve for the Milky Way for comparison . . . 191
6.12 Relation between equivalent width of Na ID and reddening for the 90 SNe of our sample . . . 194
6.13 Relation between Na I D equivalent width and extinction for the SNe of our sample in the range EW(Na I D) < 2 Å and E(B−V) < 0.5 . . . 198

6.14 Curve of growth 200
6.15 EW(Na ID) vs. A_V 202
6.16 Superimposition of curves of growth on plane EW(Na ID) vs. E(B−V) 204
6.17 Same as Figure 6.12 where we have highlighted the region of linear growth and those of saturation 205
6.18 Limits on the plane EW(Na ID) vs. E(B−V) 207
6.19 Variation in the time of extinction properties in UBVRI bands for Type Ia SNe considering dust scattering 209

B.1 Spectral comparison of SN 2003hg 225
B.2 Spectral comparison of SN 2004G 226
B.3 Spectral comparison of SN 2004aq 227
B.4 Spectral comparison of SN 2004aw 228
B.5 Spectral comparison of SN 2004dg 229
B.6 Spectral comparison of SN 2004go 230
B.7 Spectral comparison of SN 2005G 231
B.8 Spectral comparison of SN 2005H 232
B.9 Spectral comparison of SN 2005I 233
B.10 Spectral comparison of SN 2005W 234
B.11 Spectral comparison of SN 2005ab 235
B.12 Spectral comparison of an alleged supernova in NGC 4656 . . . 236
B.13 Spectral comparison of SN 2006W 237
B.14 Spectral comparison of SN 2006dk 238
B.15 Spectral comparison of SN 2006en 239
B.16 Spectral comparison of SN 2006et 240
B.17 Spectral comparison of SN 2006gy 241

1

Why Are Supernovae Important?

Se pone al fuego agua muy abundante con sal,
y cuando rompe a hervir se echan los espaguetis ...
Simone Ortega

Time by time, in a galaxy far far away, a star explodes. This star explodes so violently that for a few weeks it outshine its parent galaxy. This kind of extremely powerful explosions are called Supernovae (hereafter SNe). More precisely, *a supernova is an explosive event disrupting a star at the end of its (single or binary) evolution, returning to the interstellar medium all (or most) the gas synthetized during its evolution and explosion.* SNe are responsible for producing some of the most energetic cosmic rays in the universe, and they generate prodigious quantities of neutrinos; they lead to the formation of neutron stars and, occasionally, black holes; their shock waves may also trigger vigorous bursts of star formation by compressing dense molecular clouds, and some types of supernovae are exceedingly useful tools, as we will see, for measuring distance of galaxies billions of light-years away. In other words, SNe are playing a crucial role in determining the age, global structure, and evolution of our universe.

1.1 How were the supernovae discovered?

The exceptional and unexpected apparition in the sky of source extremely luminous and of their mysterious disappearance after some months fascinated the men from antiquity.

Temporary stars, comets and novae, as well as occasional supernovae, were

TABLE 1.1— Historical supernovae.

year date	constel.	RA - DEC	mag	comments
185 AD	Cen	14:43.1 -62:28	-2	SNR: G135.4-2.3/RCW 86
393/396 AD	Sco	17:14 -39.8	-3	3 radio sources candidates for SNR
1006 Apr 30	Lup	15:02.8 -41:57	-9	SNR: PKS 1459-41
1054 Jul 4	Tau	05:34.5 +22:01	-6	M1 Crab Nebula
1181 Aug 6	Cas	02:05.6 +64:49	-1	3C 58
1572 Nov 6	Cas	00:25.3 +64:09	-4	Tycho
1604 Oct 9	Oph	17:30.6 -21:29	-3	Kepler
1680? 1667?	Cas	23:23.4 +58:50	6?	Cas A SN

fairly frequently recorded in East Asian history. Stephenson & Green (2005) considered historical Galactic SNe, from the ancient (East and West) chronicles, those temporary stars with long duration of visibility (preferably more than three months), with a fixed location and low Galactic latitude (usually less than 10^o), also with no evidence of significant angular extent and unusual brilliance (e.g. daylight visibility) and, finally, objects whose information comes from several independent records. In Table 1.1 there are listed these historical SNe from Stephenson & Green (2005).

In the 1920's scientists begun to realise that there was a particular class of very bright novae (Lundmark 1920, Curtis 1921). It was Lundmark who said: *It is quite possible that we have to deal with two distinct classes of Novae: one "upper class" having comparatively few members and reaching an absolute magnitude more or less equal to the absolute magnitude of the system in which they appear: one "lower class" in the mean 10 magnitudes fainter ....* A decade later, Baade (1938) and Zwicky (1938), at the California Institute of Technology, defined them as "supernovae". The distinction between novae and supernovae was at first based on twelve objects discovered between 1895 and 1930, plus the galactic SN observed by Tycho in 1572.

Between 1936 and 1941, the first systematic supernova search was started by Baade and Zwicky using the Palomar 18-inch Schmidt telescope and led to the discovery of 19 SNe.

During this same period, the convention was introduced of cataloguing the SNe by identifying them with the discovery year followed by a letter of the alphabet which indicates the chronological order of discovery.

Two SNe discovered in 1937, 1937C and 1937D, provided the first well sampled light curves and spectra. In the following years, a few SNe of a different kind were discovered, and Minkowski (1941) "provisionally" divided SNe into Type I and II, distinguished by the lack or presence of Hydrogen lines in their

early spectra, respectively.

In the following years, the improvement of the instrumentation, the construction of new telescopes and also the numerous progresses in the understanding of the stellar evolution, stimulated the research and cataloguing of the SNe. With this aim, in 1957, several Schmidt telescopes were devoted to SN searches in Zimmerwald (Switzerland) by P. Wild, Asiago (Italy) by L. Rosino, Tonantzintla (Mexico) by G. Haro and E. Chavira and in 1958, the Palomar 48-inch Schmidt telescope began another deeper SN search. By the Sixties, thanks to international SN searches coordinated by Zwicky, $\sim$ 100 SNe were discovered and three other SN types were added (III, IV and V). All these SNe had peculiar light curves and evidence of hydrogen in the spectra. The prototype of the Type V objects was the famous SN 1961V and this Type survived several years more. Now we believe that the Type V objects are likely not genuine SNe, but superficial outbursts resembling η Carinae. Also in 1968 the first SN discovered by an amateur was reported (SN 1968L discovered by J. Bennet).

By the Eighties, with the introduction of the CCD and the construction of telescopes of increasing diameter which allow the observations of relatively large areas of the sky, not only did the number of SNe observed grow but it was possible also to obtain spectra with better resolution and to study the evolution of the luminosity of the SNe for long times. The SNe classification became consequently more complex due mainly to more careful comparison among the SNe. These technological advances also allowed a high redshift SN search at z = 0.2 - 0.4.

The optical band has played a fundamental role in the knowledge and classification of the SNe, but with the technological progress, it has been possible to observe the SNe in the IR bands, and in the radio, ultraviolet (UV) and X-ray. In particular, with the explosion of the SN 1987A in the LMC, the closest extragalactic SN observed (50 kpc), it has been possible also to observe for the first time the SN progenitor and the neutrino flux produced during the explosion.

With modern technology we can estimate the discovery of $\sim$ 300 extragalactic SNe per year using the visual and automated methods of research (mainly by amateurs). Figure 1.1 shows the increase of the number of known SNe with time.

Among the most important recent search projects, we note the *LOSS* (Lick Observatory supernova Search), which using the robotic telescope KAIT (Katzman Automatic Imaging Telescope) has been one of the most successful projects for the discovery of SNe in the local Universe. Also important were the *SCP* (Supernova Cosmology Project) and the High z SuperNovae Search, which searched for SNe at high redshift and determined the fundamental cosmological parame-

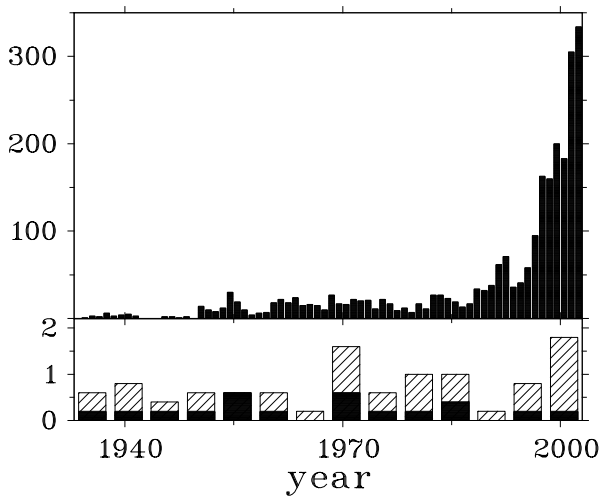

FIGURE 1.1— *Top panel*: number of SN discoveries per year. *Bottom panel*: number of SNe within a distance smaller than 10 Mpc (shaded area) or 5 Mpc (filled area), averaged over 5 years (from Cappellaro 2005).

ters Ω_M and Ω_Λ[1].

In the future, *SNAP* (Supernova Acceleration Probe) will study the evolution of the Universe by searching for SNe with even higher redshift (~ 1.7) by mean of a satellite telescope. Also the *JWST* (James Webb Space Telescope, expected by 2013) and *ELTs* (Extremely Large Telescopes, expected after 2015) with diameters of 30 and 60 meters will help in the search for SNe for cosmological purposes.

1.2 How many types of supernovae are there?

As we see before, the first fundamental classification was given by Minkowski (1941) who distinguished the SNe in two different classes based on the lack (SNe I) or presence (SNe II) of hydrogen lines in their early spectra. Since SNe can be very different one from another as to spectral features (i.e. chemical composition, physical conditions), photometry, overall SED (Spectral Energy Distribution), time evolution, radio and X-ray properties, ..., in the 1980s subclasses were introduced such as Ib, Ic, IIn, II-L, II-P, IIb which are related to characteristics of their spectra (small letter) or light curves (capital letter).

[1] Ω_M is the matter (dark and baryonic) density, and Ω_Λ is the density parameter corresponding to a cosmological constant.

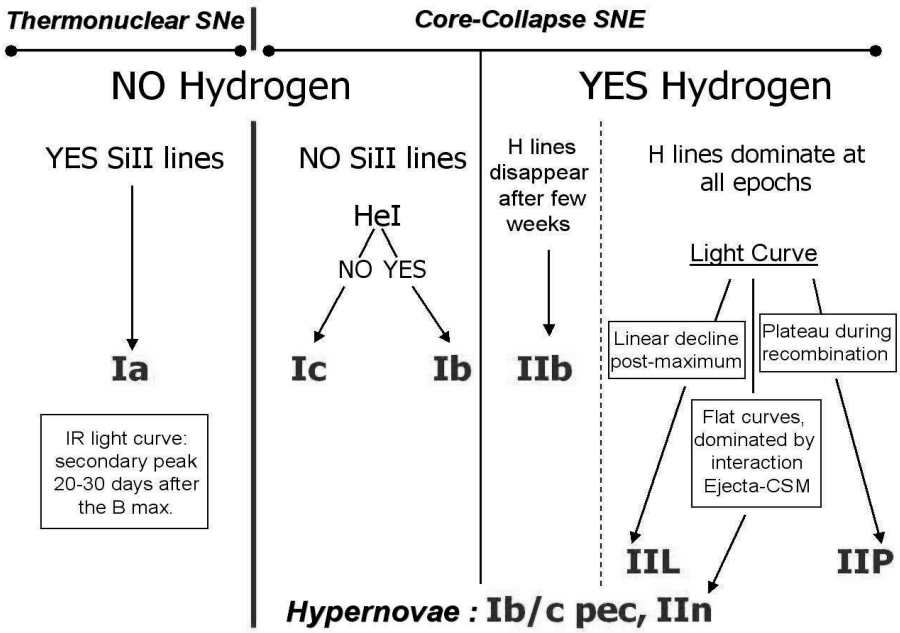

FIGURE 1.2— Supernova taxonomy (courtesy of A. Pastorello).

In Figure 1.2 a sketch of the classification system is shown, which highlights the main characteristics used to differentiate between the various types and subtypes and their relation to each other.

The SNe of type I are subdivided in three subclasses, depending on the presence or lack of Si II and He I in the spectra. Type Ia SNe present the line of Si II at 6150 Å in their spectra (recognized to be due to the doublet of Si II at 6355 Å), while the spectra of the SNe Ib do not have this feature but are characterized by pronounced lines of He I, as that at 5876 Å. Finally, the SNe Ic do not present Si II nor He I lines (or He I is very weak)(see Figure 1.3).

The class of the SNe II is formed by four main subclasses and their spectra are dominated by H lines at all epochs. The SNe IIP and SNe IIL constitute the most numerous subclasses and are characterized by the shape of the light curve[2] (see Figure 1.4), but they do not show deep spectral differences. The light curve of SNe IIP shows, afterwards the luminosity declines for a few days, a relatively constant luminosity, or plateau, with a duration of approximately 2-3 months. The light curve of SNe IIL shows instead, a linear decline starting shortly past maximum. The SNe IIn (narrow emission lines) present spectra in

[2]A light curve, as we will see, is the variation of the object luminosity with time.

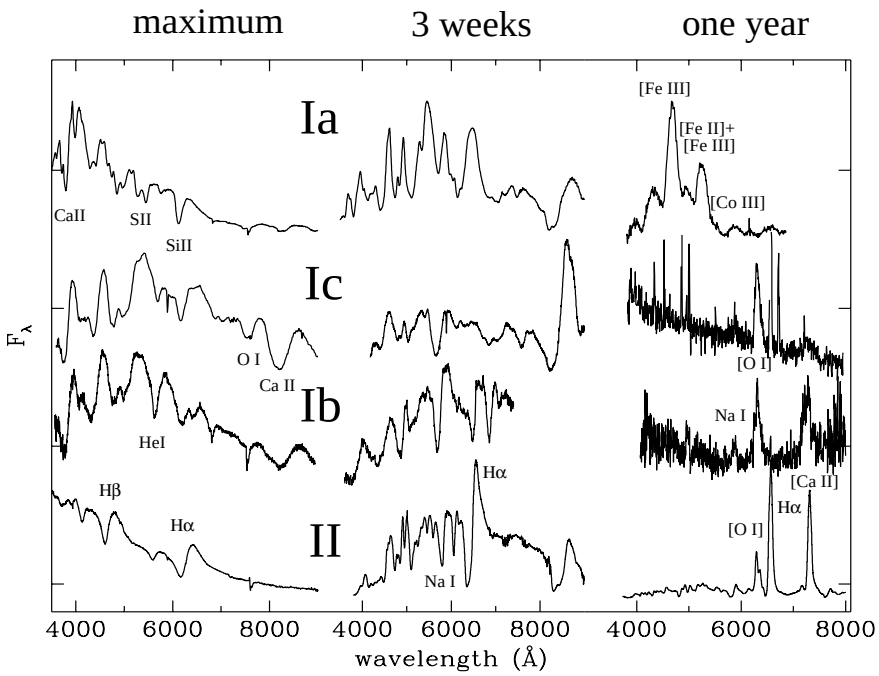

FIGURE 1.3— Spectra of the various supernova types and subtypes at maximum light, 3 months and one year after maximum (from Turatto 2003a).

which the Balmer emission lines are formed by several components that evolve in the time in various ways. The spectrum of the SNe IIb, finally, is similar, during maximum light, to that of the SNe IIP and IIL, i.e. it has strong lines of H, but in the following week it metamorphoses to that of SNe Ib, thus pointing out a physical link between these two classes.

This classification, based on early phase spectra, is normally used in the IAU Circulars when a new SN candidate is confirmed, but it is not always accurate, as it is not related to the physical characteristics of the objects but only to their spectral and photometric appearance soon after the explosion.

It has been seen in many cases that the appearance of a SN can change in time due to the characteristics of the progenitor or to those of the circumstellar material. Therefore, it is preferable to divide SNe according to the physical character of the explosion rather than the morphology of the spectra or light curves. Nowadays we divide supernovae in two categories: Core-Collapse and Thermonuclear explosions (see Figure 1.2). The former class shows great observational diversity, which is supposedly due to the large variety in size of the progenitor and to environmental conditions. Some of the most powerful among

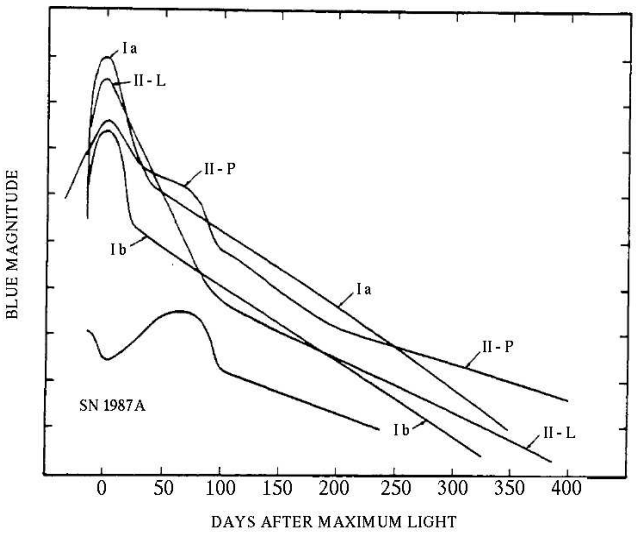

FIGURE 1.4— Light curves of the various supernova types and subtypes (from Wheeler & Harkness 1990).

these events seem to be related to Gamma-ray Bursts, and are called Hypernovae (Nomoto et al. 2005). The latter include only SNe Ia, which will be the subject of our discussion in next sections and of this thesis, in general.

1.3 What are the general properties of SNe?

As a consequence of the explosion, a large quantity of material (ejecta) (M = 1 to 10 $M_{\odot}$), is expelled with large velocity, in to the surrounding medium of the progenitor.

Quickly after the explosion, the ejecta expand with velocity proportional to the distance from the center of the explosion (homologous expansion). They are compact, dense and opaque. The density profile of the ejected matter and its composition depends strongly on the type of SN.

As the expansion progresses, the ejecta density and their temperature decrease. This reduction guides the spectral and luminosity evolution of the SN. Analyzing the spectra and the light curve for a given phase of the expansion, and comparing them to theoretical models, it is possible to reconstruct the composition, the velocity and the density of the ejecta in that phase and, finally, find the SN progenitor and the mechanism of explosion.

The spectroscopic evolution of the ejecta is usually divided in two phases: the photospheric and nebular phases, with a smooth transition between them.

In the first phase, the high density of the ejecta determines the formation of a photosphere with a black body emission with temperature of 10000 - 20000 K. The optical spectrum is characterized by lines with P-Cygni profiles over a blue continuum. The P-Cygni profile, shown in Figure 1.5, is characterized by a blueshifted absorption and an emission features at the rest wavelength of the transition. From the measure of the position of the absorption minimum, it is possible to estimate the expansion velocity of the photosphere.

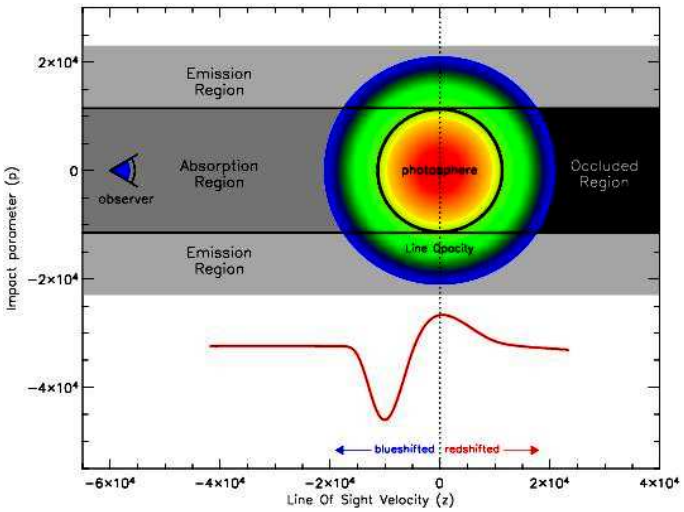

FIGURE 1.5— Typical P-Cygni line profile (http://supernova.lbl.gov/∼dnkasen/tutorial/).

As the expansion proceeds, the photosphere and the region of the line formation recede more deeply in the ejecta and the P-Cygni width decreases. The spectral energy distribution is shifted redwards as consequence of the temperature decrease and the ratio between the emission lines and the continuum grows in favor of first former.

In a few months the optical depth of the expelled matter decreases and even the innermost regions are exposed. The photosphere disappears and the SN enters the so-called nebular phase. The profiles of these lines change and only the emissions are left. The density is now so low that even forbidden lines can appear. In this phase, the energy is supplied by the radioactive decays together with progressive γ ray transparency of the ejecta during the long-time exponential light decay. The synthesized ^{56}Ni during the explosion decays to ^{56}Co, which in turn decays to ^{56}Fe. While the first reaction has an average life of 6.1 days and, therefore, influences the first phases of the evolution of the

light curve, the second one has an average life of 77.7 days and determines the course of the curve of light on longer temporal scales. At very late epochs (after about 1000 days) can also become important the contributions of the decays of ^{57}Co and of ^{44}Ti.

In general, the SNe light curves present steep rise to the maximum light followed by slower decrease. However, there are a great variety of shapes among the light curves, depending on the dimension and mass of the progenitor on the explosion intensity and on the possible presence of circumstellar medium (hereafter CSM) interaction.

With the passing of time, the differences generated from the various initial conditions are overwhelmed by the fast expansion of the ejecta. The light curves of the various types of SNe, some months after the explosion, in the nebular phase, show a slow and gradual decline, with an exponential tail typical of radioactive decays (Figure 1.6). In fact, as mentioned above, the source of energy in this period is the radioactive decay of the elements synthesized during the explosion.

Moreover, depending on the mass of the ejecta, i.e. on their ability in trapping the γ rays produced in the radioactive decays, the slope can be steep (low mass ejecta, SNe Ia/b/c) or flatter (large ejecta mass, SNe II).

In the last phases, the formation of dust within the ejecta and the interaction with CSM become important in shaping the light curve. Often at later phases (but sometimes also quite early), the expelled matter can interact with the CSM, if it is present. The interaction of the ejecta with the CSM, which moves much more slow than the ejecta, produces two shock waves: the *reverse shock*, which spread towards the inside, and the *forward shock*, moves outward in the CSM. The physical processes generated from the propagation of these shock waves influence the emission spectrum of the SN, mainly in the radio and X-ray bands. The analysis of the interaction of the ejecta with the CSM give us information about the density, the structure and the chemical composition of both of them.

1.4 Thermonuclear Supernovae

1.4.1 What are the observational characteristics of the Thermonuclear Supernovae?

The main characteristic of thermonuclear supernovae (or SNe Ia) is their homogeneity which, together with their appearance in early type galaxies, provides indication that they descend from old progenitors which are in the same configuration at the explosion, in particular from C-O white dwarf (hereafter

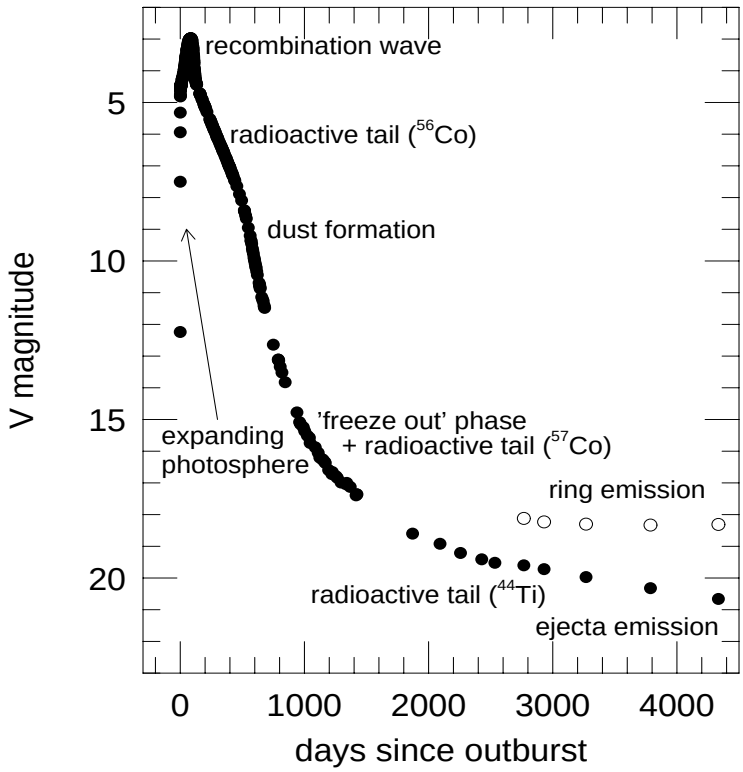

FIGURE 1.6— V light curve of SN 1987A. The various phases of the ejecta luminosity evolution are labelled (from Leibundgut & Suntzeff 2003).

WD) reaching the Chandrasekhar limit by accretion from a companion (Section 1.4.2). In recent years however, an increasing number of pieces of observational evidence show that differences do exist also among SNe Ia (Section 1.4.3).

- What is the spectroscopic evolution of normal SNe Ia?

  We have seen before that the SN Ia spectrum is characterized, at every phase, by the absence of the emission lines of H.

  The very early phase spectra of SNe Ia (about 2 weeks before maximum light) show broad lines with the characteristic P-Cygni profiles, produced in an expanding atmosphere. The wide features at a velocity of about 25 - 30000 km s^{-1} are due to intermediate mass elements such as Ca, Si, S or Mg. At a phase earlier than -14 days from maximum light, lines are difficult to identify due to heavy blanketing effect, although the H and K lines of Ca II and, at a smaller velocity, C II are visible. Later on lines become easier to identify, and they are mostly due to Ca II, Si II

and Si III, S II and Mg II. A few days before maximum light the Si II line at 6355 Å becomes evident and characterizes the spectra of SNe Ia for over one month. Si II expands at around 15000 $\mathrm{km\,s^{-1}}$ at maximum light, and its velocity decreases at a slower rate than the rest of the photosphere in the following days indicating that the layer is detached. The continuum at this stage is similar to that of a B star. A week or so after maximum light, Ni-Co-Fe lines from the core start to appear, as the photosphere is retreating towards the inner regions of the expanding envelope. Eventually, at around three weeks after maximum light, Fe lines dominate the entire spectrum with some leftover Si and, a couple of months after maximum light, with Co, Cr II and Na I. In Figure 1.7 are shown optical spectra of SNe Ia at various phases.

- What do we know about SNe Ia spectro-polarimetry[3]?

  Most of the SNe Ia are only slightly polarized in continuum light, about 0.3 %, but polarization as high as 2 % is found across some spectral lines. This low level of continuum polarization implies that the SNe Ia photospheres are, in general, approximately spherical. Since the polarization in SNe Ia decreases with time and vanishes around 2 weeks past optical maximum, this suggests that the outermost layers of the ejecta are more aspherical than the inner most regions. More detailed information on spectropolarimetry of SNe Ia can be found in Wang, Baade & Patat (2006b) and the references therein.

- What are the photometric characteristics of SNe Ia?

  The B light curves of SNe Ia show a rather steep rise to maximum light, which is reached 17 to 20 days after the explosion. After a few days spent around maximum, the SN luminosity suffers a fast linear decline with a dimming rate of about 0.1 mag per day until the so-called *inflection point*, reached usually at a month past maximum. Afterward the decline become less steep and the SN settles on the so-called exponential tail with average slope 0.015 mag/day. This phase lasts until the SN becomes invisible with the available instrumentation, approximately 2 - 3 years, depending on the distance and the extinction suffered. The V light curves show similar behaviour, with the maximum light generally occurring between 0.5 and 2 days after B maximum. At times, the V light curves show a shoulder, corresponding in phase to a plateau always visible in the R light curve,

[3]The polarized emission from a supernova is caused by electron scattering in its ejecta and is sensitive to its geometric structure (Höflich 1991).

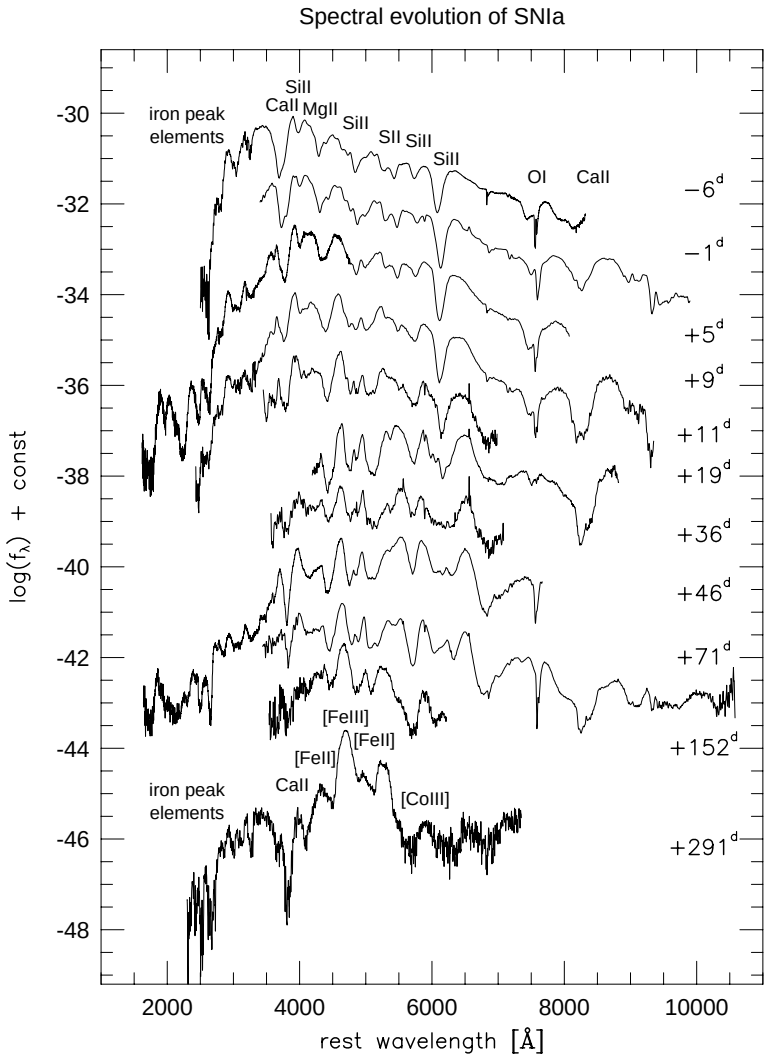

FIGURE 1.7— Spectral evolution of a typical SN Ia from 6 days before maximum to about 300 days after (from Wheeler & Benetti 2000).

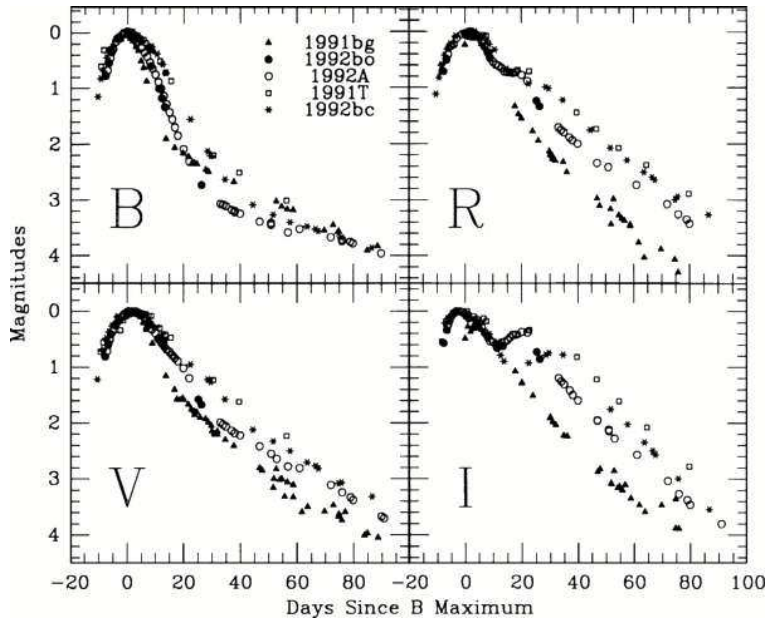

FIGURE 1.8— Light curves of a normal SN Ia (SN 1992A) and of a few peculiar ones (from Suntzeff 1996).

which in turn becomes a pronounced secondary maximum in the I light curve around 20 - 25 days after the primary maximum. The origin of the secondary maximum have remained in many ways, and to many people, obscure. According of Kasen (2006), this probably is due to the change of opacity and concentration of iron-peak elements in the central regions during these first days. Examples of SN Ia light curves in various bands are visible in Figure 1.8.

As a consequence of the homogeneity of the light curves, also the colour evolutions of SNe Ia are similar with an average value B-V $\sim$ 0 at maximum followed by a rapid reddening due to the expansion up to about 30 days. Afterward, the SN starts to enter to the nebular phase, the reddening halts and, because of the emergence of emission lines, the colour becomes bluer (see Figure 1.9). The slope of the B-V color curve of a SN Ia is constant between 30 and 90 days from maximum light (Figure 1.10). Lira (1995) showed that the evolution at these phases is remarkably uniform for SNe Ia in general. This can be used to calibrate the intrinsic colours of these objects at maximum light and to estimate the reddening inside the host galaxy, as we will see later in this work.

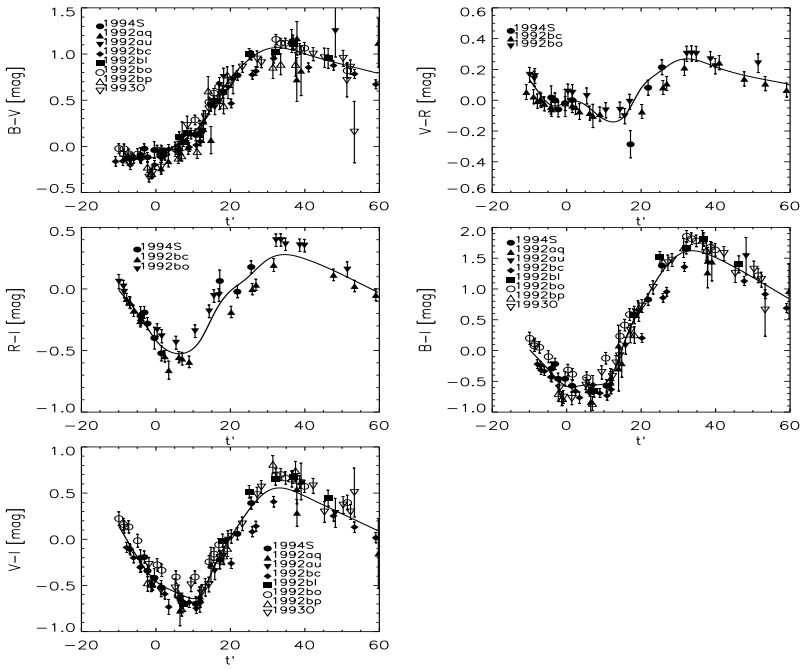

FIGURE 1.9— Colour evolution of several SNe Ia from the Calán/Tololo sample Hamuy et al. (1996c) and the CfA sample Riess et al. (1999a) (from Nobili et al. 2003).

Comparing the shape of light curve with absolute magnitude of SN Ia, Phillips (1993) and Hamuy et al. (1995) pointed out the magnitude-decline rate relation (M_B^{max} vs. Δm_{15}(B)) where Δm_{15}(B) is the difference in magnitude between maximum light and 15 days later. The coefficients of this relation have changed significantly over the last few years (see Figure 1.11) as the distance and extinction correction have been refined (Phillips 1993, Hamuy et al. 1996a, Altavilla et al. 2004, Prieto, Rest & Suntzeff 2006). A similar way of comparing the relation between light curve shape and absolute magnitude of SN Ia, the stretch factor, is described in Perlmutter et al. (1997). By broadening or narrowing a SN light curve with respect to the standard shape the luminosity of the object can normalise a light curve to the standard luminosity. See Figure 1.12 for an example of the effectiveness of this technique, which has later been improved with the Multi-Color Light Curve Shape method by Riess et al. (1996a). CMAGIC (Color-Magnitude Intercept Calibration, Wang et al. 2003) is a method to find the luminosity of a SN Ia observed after maximum light. It is based on the fact that the colour index in SNe Ia remains uniform for about a month after maximum.

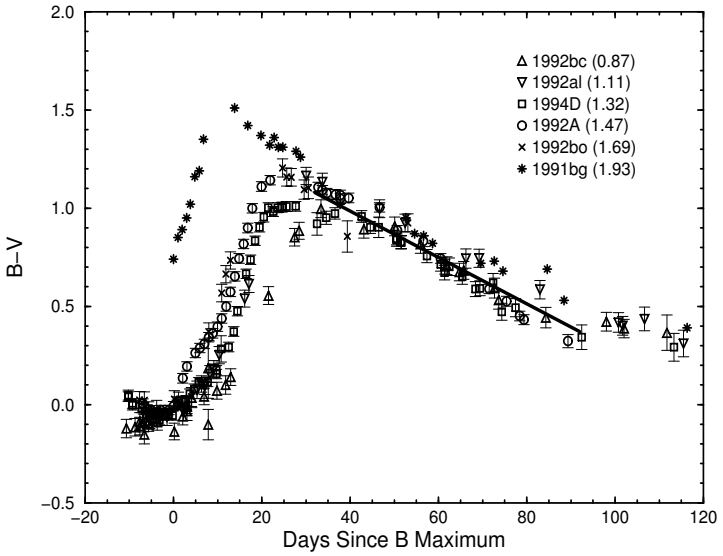

FIGURE 1.10— B-V colour evolution for six SNe that likely suffer little or no reddening from dust in their host galaxies. These six events, whose Δm_{15}(B) parameters are indicated in parenthese, cover a wide range of initial decline rates and peak luminosities. The solid line represents the Lira locus (from Lira 1995, Phillips et al. 1999).

These relations and other more recent analogues have allowed us to standardize the absolute magnitudes of SNe, strengthening confidence in the utilization of SNe Ia as distance indicators.

- How do SNe Ia behave at other wavelengths?

  The observations of Type Ia SNe in JHK bands start in the eighties with the works of Elias et al. (1981, 1985), but became systematic only few years ago (Hernandez et al. 2000, Meikle 2000, Krisciunas et al. 2001, Krisciunas et al. 2004a). In Figure 1.13 the J, H and K light curves from Meikle (2000) show the characteristic second maximum already visible in the I band.

  The major advantage to studying SNe in the near IR (NIR) is that at those wavelengths the absorption due interstellar material is a order of magnitude smaller than in the optical range. Therefore, J, H and K photometry is less subject to systematic error due to dust extinction along the line of sight. Moreover the analysis of the available data provide a hint that in the near infrared bands SNe Ia show a higher degree of

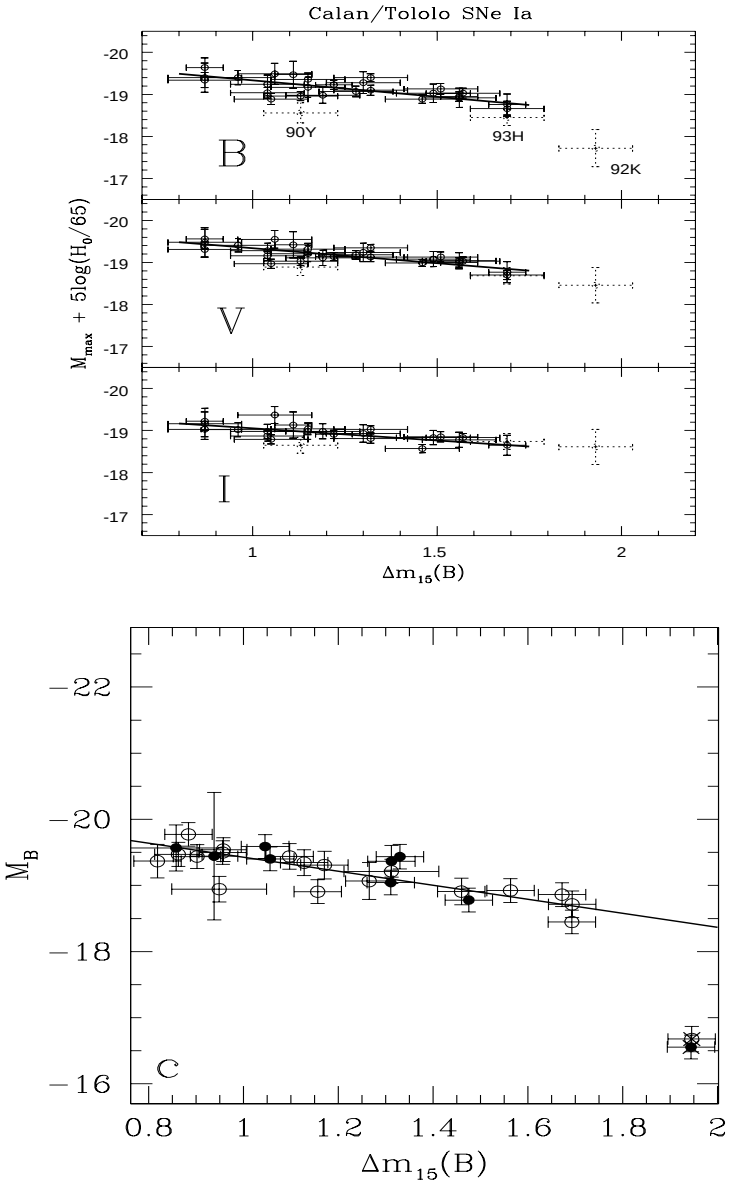

FIGURE 1.11— BVI absolute magnitude vs. Δm_{15}(B) relation from Hamuy et al. (1996a) (top panels). B absolute magnitude vs. Δm_{15}(B) relation from Altavilla et al. (2004) (bottom panel).

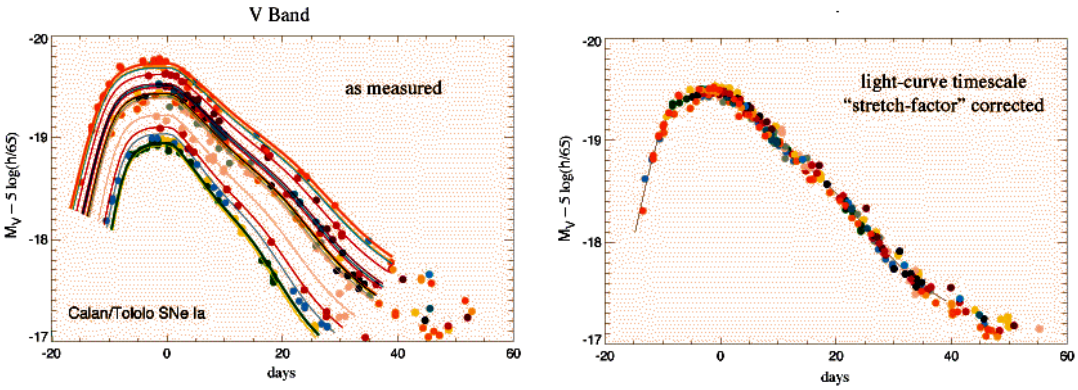

FIGURE 1.12— Left panel: the range of light curves for low-redshift SNe of known relative brightness discovered by the Calán/Tololo Supernova Survey. Right panel: the same light curves after calibrating the SN brightness using the stretch of the timescale of the light curve as an indicator of brightness (from Perlmutter et al. 1997).

homogeneity than in the optical. In particular, the absolute luminosity seems to be nearly constant in the J, H and K bands, making SNe Ia excellent standard candle in the infrared (Krisciunas et al. 2004b, see Figure 1.14). Krisciunas et al. (2004a) proposed also a new method to estimate the reddening suffer by SNe Ia comparing the V - J, V - H and V - K with the templates reported in Figure 1.15. This method gives a partially independent estimation of the reddening, the V band is in fact involved in the colour, providing a value of E(B-V) with a precision comparable with that obtained using only optical data. An advantage of this method is that the V - NIR colours seem to be quite homogeneous for all Type Ia SNe. The templates are in fact only two: one for slow decliner and the other for mid-range decliner SNe (Krisciunas et al. 2004a).

The NIR spectra of the SNe Ia complete the information we obtain in the optical region, probing different depths at the same epoch within the exploded white dwarf (Wheeler et al. 1998) even if relatively few NIR spectra have been published, especially regarding the early SN phase. Moreover, in the NIR the line identification and measurement of their strength and evolution is a easier task than in the optical because NIR lines suffer less from contamination by primordial elements. Nevertheless, ground based NIR observations are limited by the atmospheric bands between 1.31 and 1.38 and 1.78 and 1.88 μm which reduce the transmission down to 10%. This makes difficult or prevents, at least from the ground, full exploitation of the NIR window.

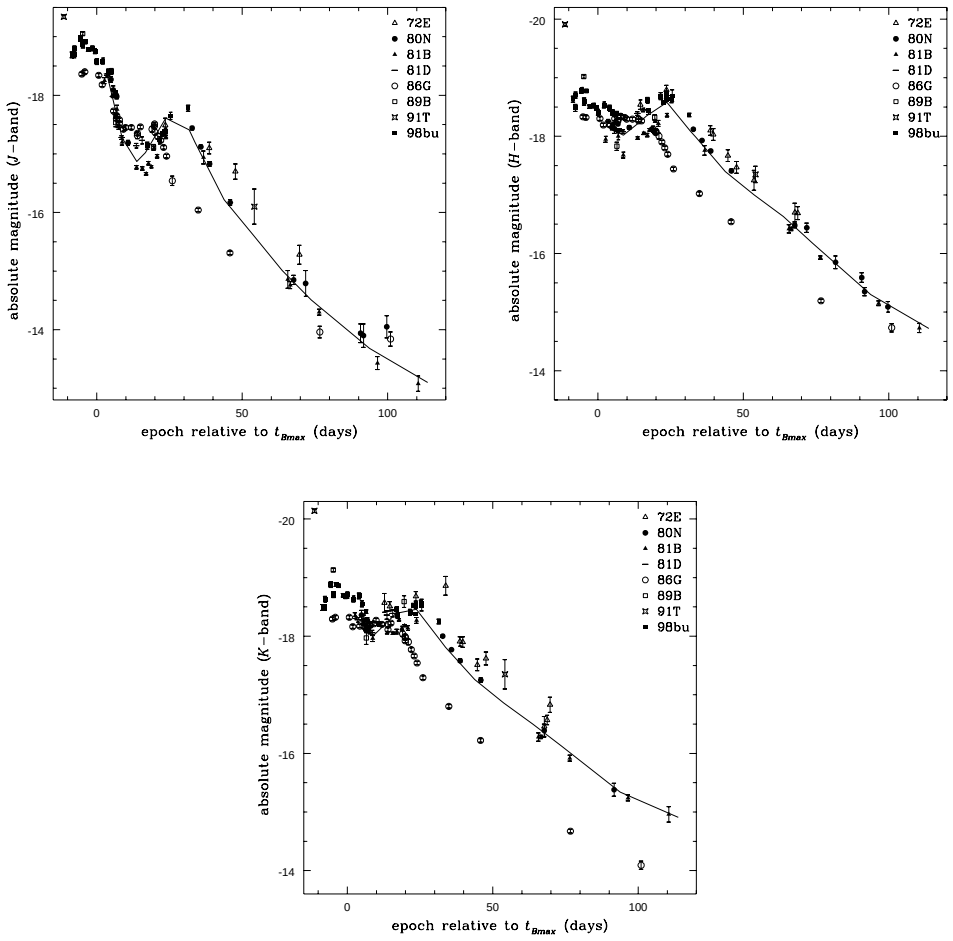

FIGURE 1.13— J (top left panel), H (top right panel) and K (bottom panel) band light curve of several bright SN Ia. (from Meikle 2000).

At early epochs, the NIR SN Ia SED approximates well a black body continuum (Figure 1.16). Especially at very early time the spectrum is almost featureless with few lines due to single ionized intermediate mass elements: Ca II, Mg II, Si II. Around maximum brightness a broad P-Cygni feature due to a blend of strong Ca II lines from 1.23 to 1.29 μm appears. A few days after maximum light, the photosphere has receded well within the Ca-rich layer and the line becomes too weak to be observed. The absorption minimum near 1.60 μm is part of a P-Cygni-like

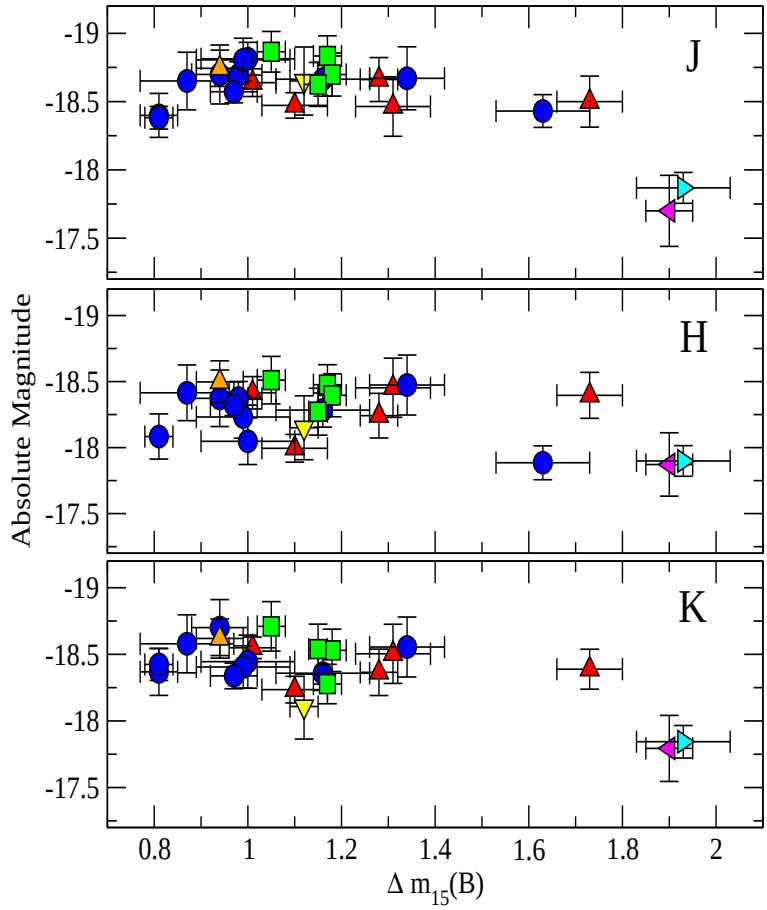

FIGURE 1.14— NIR absolute magnitudes of Type Ia SNe at maximum on the H_0 = 72 km s^{-1} Mpc^{-1} scale as a function of Δm_{15}(B) (with decline rates in the range 0.8 - 1.7). The average values found are M_J^{max} = -18.61 ± 0.13, M_H^{max} = -18.28 ± 0.15 and M_K^{max} = -18.44 ± 0.14 (from Krisciunas et al. 2004b).

feature with an emission peak near 1.68 μm. This feature is likely due to blend of Si II (1.691 μm) and Mg II (1.676 μm and the others) with the Si II dominant. After maximum, lines start to be detected in the NIR spectra due to the iron group element (Fe, Ni and Co) and at later epochs they become the dominant features.

Also UV observations are important for understanding the behaviour of SNe. Observations of SNe in the UV can be used to distinguish between different explosion models, as the UV emission probes the metallicity of

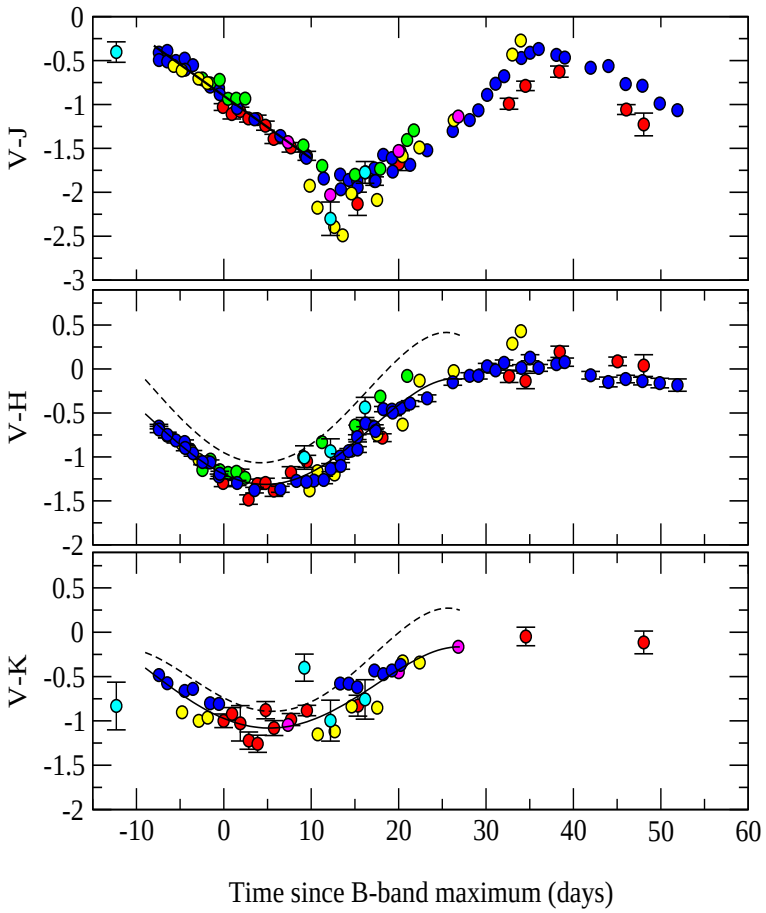

FIGURE 1.15— V minus IR colours of SN Ia with decline rates $0.81 \leq \Delta m_{15}(\mathrm{B}) \leq 1.00$. The solid line in the top plot shows the range of uniformity of V-J. The dashed lines in the bottom two plots are the loci for midrange decliners (Krisciunas et al. 2000, Krisciunas et al. 2003). The solid lines in the bottom two plots are the fourth-order polynomial fits to the data from -8 to 27 days with respect to the B-band maximum light (from Krisciunas et al. 2004a).

the progenitor, as well as the degree of mixing of the synthesized ^{56}Ni (Blinnikov & Sorokina 2000). Unfortunately, observations of SNe in the UV are limited because they require space-based observatories.

Only a small number of SNe Ia have been observed in the UV, e.g. SN 1992A (Kirshner et al. 1993), SN 2004dt, SN 2004ef, and SN 2005M (Wang et al., in prep.), SN 2005am (Brown et al. 2005), SN 2005ke (Immler et al 2006) or SN 2006X (Elias-Rosa et al., in prep.).

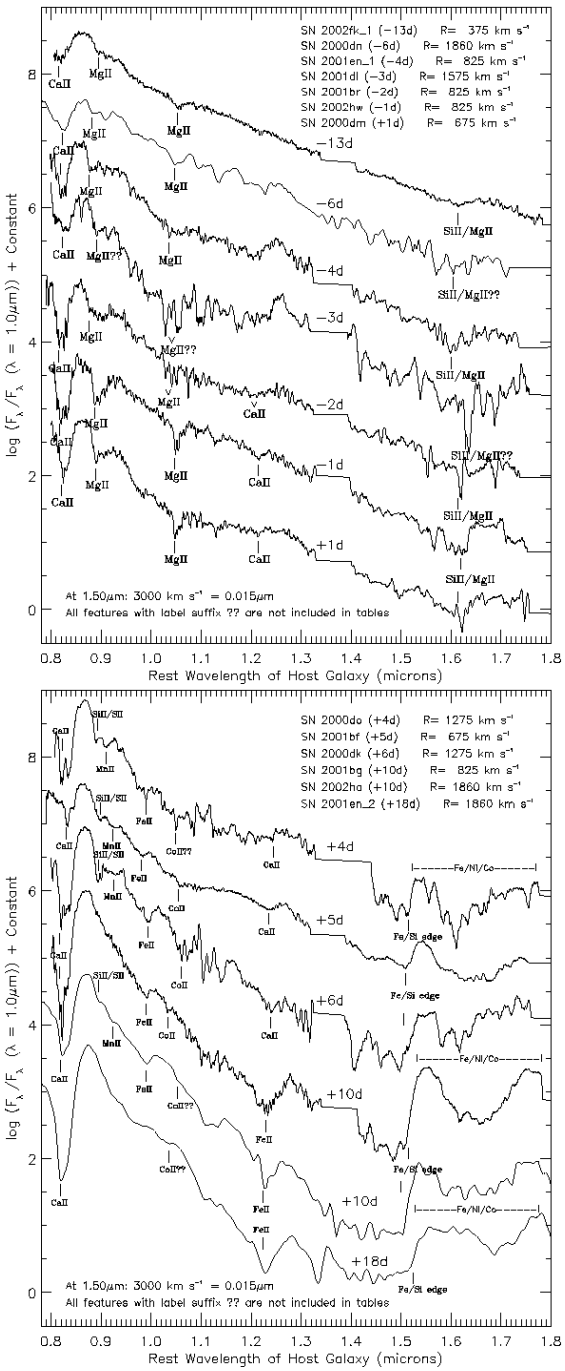

FIGURE 1.16— NIR spectra of several SNe Ia from -13 days to +1 days (top panel) and from 4 days to 18 days past maximum light (bottom panel). Tentative identification of some lines is also labeled. The straight line between 1.3 and 1.4 μm replaces the region of the spectrum absorbed by strong atmospheric bands (from Marion et al. 2003).

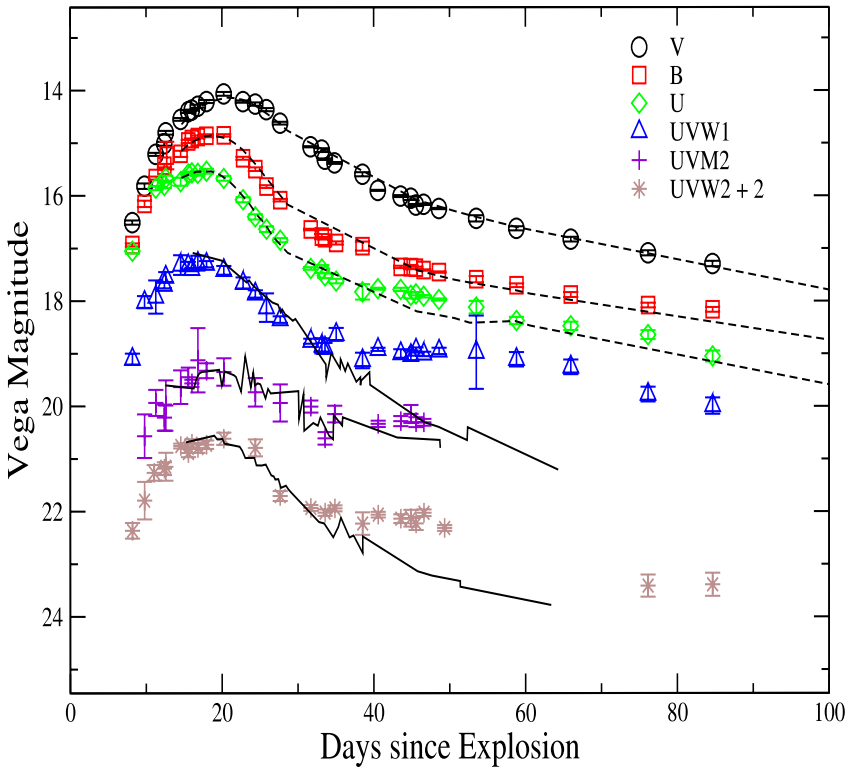

FIGURE 1.17— Ultraviolet and optical light curves of SN 2005ke in all six UVOT filters, ranging from days to weeks after the outburst. Multiple exposures were obtained in the V, B, U, UVW1 (181321 nm), UVM2 (166268 nm), and UVW2 (112264 nm) UVOT filters. Overlaid are the V, B and U light curves of the Type Ia SN 1999by (Garnavich et al. 2004) and the UV (UVW1, UVM2, UVW2) light curves of SN 2005am (Brown et al. 2005) for comparison (from Immler et al 2006).

The UV photometry is important in helping to determine, by means of UV light curves, the photometric evolution and bolometric luminosity of Type Ia SNe (Figure 1.17). In the pre-maximum and near maximum light epochs, the UV contributes significantly to the bolometric luminosity, although it is less important than the optical (e.g. Leibundgut et al.

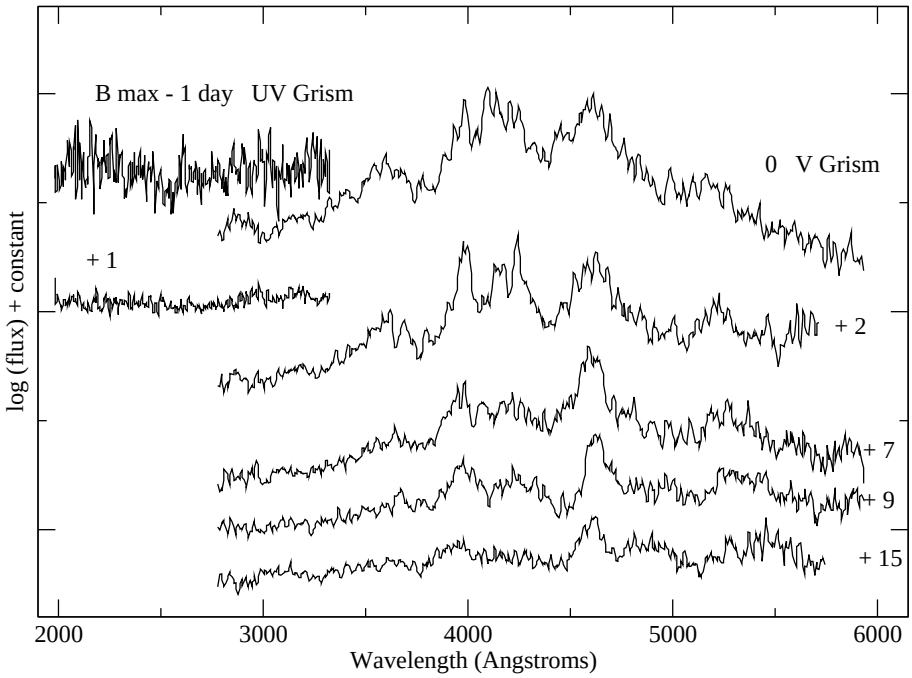

FIGURE 1.18— UVOT Grism Spectra of SN2005am. Each spectrum is labelled with its epoch in days from B_{max}. The vertical scale is given in logarithmic units of ergs s^{-1} cm^{-2} $Å^{-1}$. The spectra were trimmed from their full size to avoid contamination by other spectral orders (from Brown et al. 2005).

1991). One feature is that the decay rate in the UV is actually shallower than in the U and B bands. UV observations of SNe such as these could be useful for interpreting high redshift SNe observed in the optical bands, e.g. a rest frame SN observed with UVOTs UVW2 filter (UVOT is a instrument onboard the Swift Observatory, Gehrels et al. 2004) should match a B band observation of a SN at a redshift of z $\approx$ 1.5.

The UV spectra are also important for the study of Type Ia SNe because these spectra are formed mainly by a blanketing of iron peak element lines. The UV continuum is suppressed by deep absorption from blends of iron peak elements. Broad peaks on either side of 3000 Å resemble those seen in other SNe observed in the UV (Benvenuti et al. 1982) and identified by Branch & Venkatakrishna (1986) as blended lines of Fe II and Co II (Figure 1.18).

At early epochs, hard X-rays are created in SNe Ia by gamma-rays, pro-

duced in the decays of ^{56}Ni synthesized in the SN explosion. These gamma-rays scatter off of electrons in the ejecta via Compton scattering. The down-scattered photons can either escape the ejecta, be further down-scattered, or be absorbed via bound-free absorption. Further, energetic electrons created by the interaction of these gamma-ray photons are slowed down in the ejecta, generating bremsstrahlung emission which produces photons in the 0.1 - 100 keV energy range. X-rays in SNe are also caused by shocks of the expanding SN shell interacting with the nearby medium. Type Ia SNe are not expected to be bright in shock-induced X-ray emission because older, degenerate systems are expected to contain very little circumstellar material. Notwithstanding, excesses of X-ray counts are detected from the position of SNe Ia like SN2005am (Brown et al. 2005) and SN 2005ke (Immler et al 2006), corresponded to an upper limit of the X-ray luminosity.

Unlike Type II and Type Ib/c SNe, no SN Ia has yet been detected as a radio emitter, even when observed quite promptly after explosion or quite nearby. This implies that SNe Ia have a very low density for any possible circumstellar material established by the progenitor, or progenitor system, before explosion. Using model predictions of radio emission from SNe (e.g. Weiler et al. 2002) and assuming that the radio properties of SNe Ia would be relatively similar to those of SNe Ib/c (at least for some progenitor system models), but with a wind-established CSM from a less massive pre-SN system, we can place constraints on the mass-loss rate from such systems (Panagia et al. 2006).

- Formation environment

  SNe Ia explode in galaxies of all morphological types, from ellipticals to irregulars. In general, in spiral galaxies the SNe Ia are observed in the disc, and, rarely in the arms or near regions of star formation. Since the spiral arms of a galaxy are sites of stellar formation and, therefore, are populated by young stars, SNe Ia belong to a intermediate or old stellar population. This is consisted with the fact that the SNe Ia are observed also in the elliptical galaxies, characterized by old stellar population.

1.4.2 Why SNe Ia do explode?

SNe Ia have been widely believed to be the thermonuclear explosion of a WD that has reached the Chandrasekhar limit by accretion of mass from a companion star. The short duration of the peak of the light curve and the small

mass of the ejecta suggest that the exploding object is a compact star. The fact that the declining light is powered by the radioactive decay of ^{56}Ni supports the theory of little ejected mass compared with the ejecta of a SN II (Starrfield 2003). The nature of the companion star in these systems, however, has not been fully understood to date. We can only infer that it must be an evolved star, as we do not see any H or He in the ejecta of SNe Ia, so this kind of mass cannot be the material that the WD accretes.

It is currently believed (Nomoto et al. 2003) that the WD accreting mass from the companion star explodes when it reaches the critical mass M $\sim$ 1.37 - 1.38 $M_{\odot}$, near the Chandrasekhar mass (1.4 M$\odot$). At this point the star begins to contract, causing carbon ignition in the central region and a thermonuclear runway occurs. The star is eventually completely destroyed by the explosion. The synthetic spectra produced with this explosion model are in excellent agreement with the observed ones, although there might be peculiar events whose behaviour is better described by sub-Chandrasekhar mass models (in this case, the SN originates from a WD of C-O in a phase of accretion of He, after the He-flash, and have a M < M_{Ch}).

There are two favoured scenarios where a WD accretes mass up to the Chandrasekhar limit: the double-degenerate (DD, Figure 1.19) in which two C+O WDs merge, and the single-degenerate (SD, Figure 1.20) in which H-rich matter accretes from a binary companion. The DD scenario is likely to produce a SN with little or no H and He, which is consistent with a SN Ia event, but it seems more likely to produce a core collapse SN rather than a thermonuclear explosion. The SD scenario is therefore the more promising of the two as far as SNe Ia are concerned. Several types of binary systems have been proposed at different times as progenitors for SNe Ia. However, many of them (Classical Novae, Dwarf Novae, Symbiotic Variables and Symbiotic Novae) would produce too much H and He, that we do not see in the spectra (it has been estimated that SN Ia can eject only 0.1 $M_{\odot}$ or less of H (Baron et al. 2001, private communication to Starrfield). Two probable systems that might generate a SN Ia according to the SD scenario are: a WD+RG (red giant) system (symbiotic system), which should be observable as symbiotic star, luminous supersoft X-ray source or recurrent nova, and a WD+MS (main-sequence) system, in which the C+O WD is formed from a red giant that transfers part of its outer envelope on the companion main-sequence star. Such systems should be observable as supersoft X-ray sources and some recurrent novae, like U Sco.

The short duration of the peak of the light curve and the relatively steep light curve at late time, are both consistent with a low mass, compact exploding star. This is also consistent with the absence of (significant) H lines in the spectra and with the appearance of SNe Ia in early type galaxies, formed by

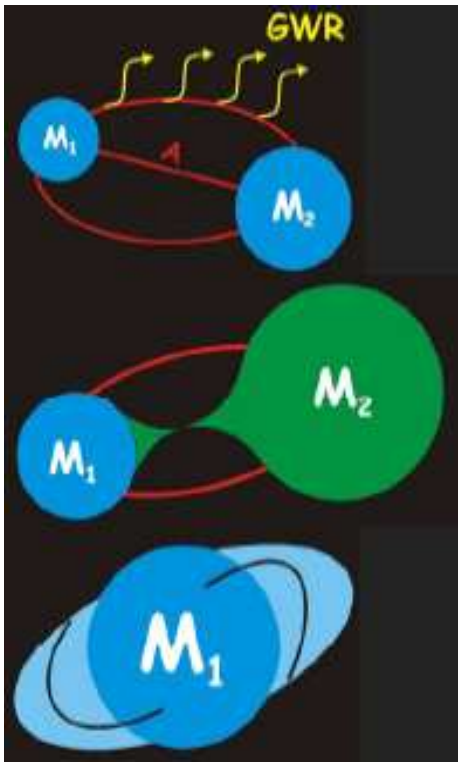

FIGURE 1.19— Double Degenerate schematic evolution. Top panel: shrinkage of the orbits due to GWR emission; middle panel: dynamical mass transfer from M_2 to M_1; bottom panel: disruption of M_2 and formation of an accretion disk. $M_1 + M_2 > M_{Ch}$, A (orbital separation) $\sim$ 1 -10 $R_\odot$ (courtesy of Tornambè A. & Piersanti L.).

relatively low mass, evolved stars.

For the last thirty years, theorists have used one-dimensional, spherically symmetric models to describe the observed behavior of SN Ia. High accretion rates cause a higher central temperature and pressure, favoring lower ignition densities. A flame front then propagates as a deflagration (subsonic velocity) wave due to heat transport across the front. These models can reproduce the observed characteristics of SN Ia events by parameterizing the thermonuclear flame speed and if necessary the density at which a spontaneous transition to supersonic burning (detonation) occurs. Multidimensional calculations of deflagrations, on the other hand, allow to determine the energy generation rate independently from the local value of the flame speed. In the past couple of years three-dimensional modelling of SN Ia has become possible (Niemeyer et al. 2003). 3-D hydrocodes account well for the deformation of the flame

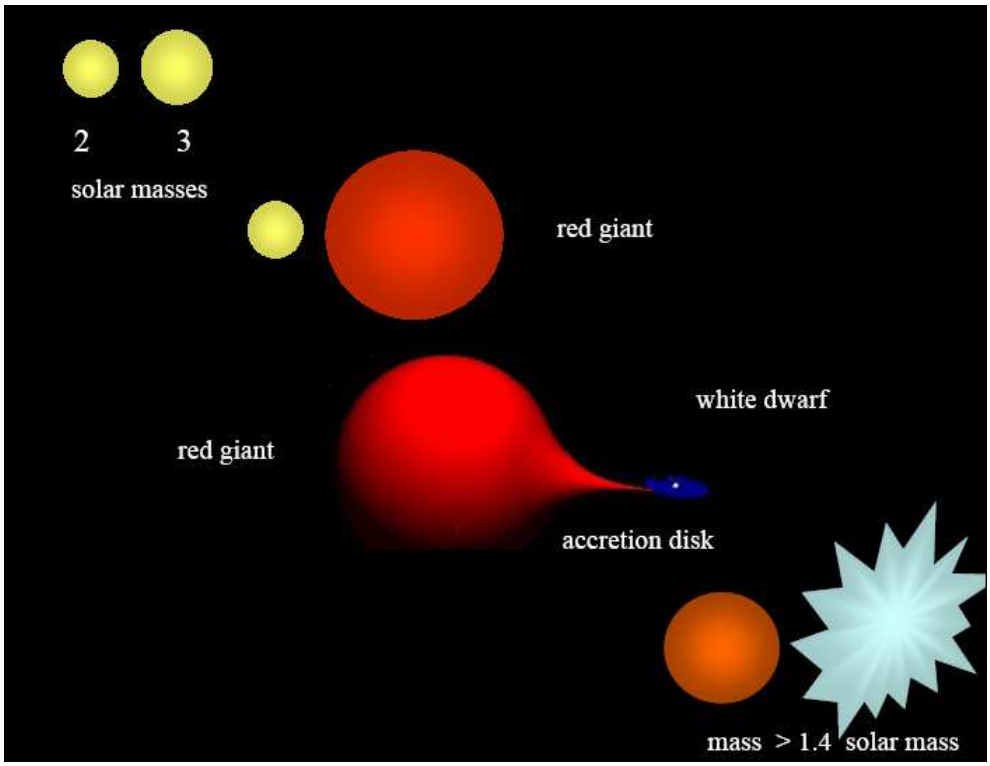

FIGURE 1.20— Single Degenerate schematic evolution.

surface, which determines the acceleration of the fuel consumption rate, using the initial configuration of the flame as the main free parameter. The ability of these models to reproduce observations strongly depends on the resolution of the simulation.

The current preliminary results show that the Chandrasekhar mass scenario with pure turbulent deflagration is a viable candidate for SN Ia explosions, but a self consistent multidimensional initial model is not yet available. García-Senz & Bravo (2003) find in their 3-D calculations that ^{56}Ni and the intermediate mass elements show a large dispersion in velocity space. The irregular distribution of fuel and ashes they find may provide a natural way to explain SN Ia diversity. Very high resolution 3D-calculations seem not to be able to obtain the correct amount of radioactive ^{56}Ni to reproduce SN Ia light curves, while different 3D-approaches of turbulent flame fronts seem to achieve this goal with a pure deflagration model (Thielemann et al. 2003). Such a model could explain SN Ia diversity using a number of possible parameters: for example the

progenitor C/O ratio, its metallically, and the central density at ignition (Röpke & Hillebrandt 2005). Multi-spot ignition scenarios might be able to eliminate some of the issues of current deflagration models (Röpke et al. 2006a). Diversity might also be caused by off-center detonations of the transition from deflagration to detonation (delayed detonation, Livne 1999). Multi-dimensional codes are crucial to investigate all these possible sources of diversity. A simplified model of SN Ia (from Höflich et al. 2003) is shown and described in Figure 1.21.

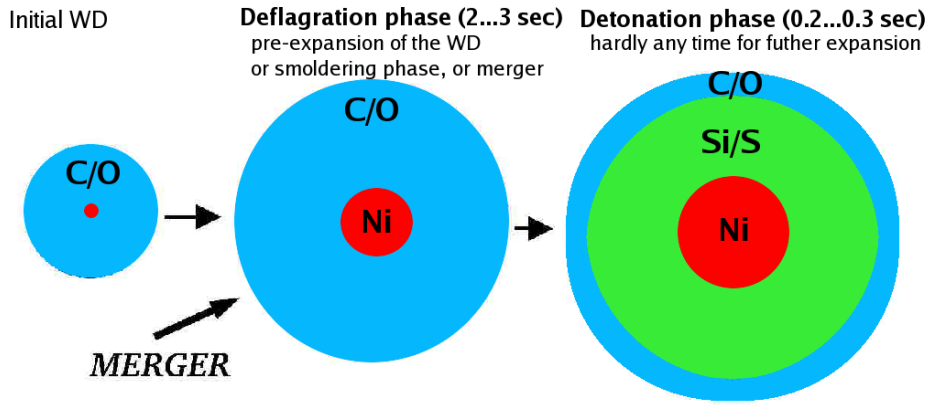

FIGURE 1.21— Schematics of the explosion of a white dwarf near the Chandrasekhar mass. A thermonuclear runaway occurs near the centre and a burning front propagates outwards. Initially, the burning front must start as a deflagration to allow a pre-expansion because, otherwise, the entire WD would be burned to Ni. Alternatively, the pre-expansion may be achieved during the non-explosive burning phase just prior to the thermonuclear runaway. Subsequent burning is either a fast deflagration or a detonation. In pure deflagration models, a significant amount of matter remains unburned in the outer layers, and the inner layers show a mixture of burned and unburned material. In contrast, the models making a transition to a detonation produce the observed layered chemical structure with little unburned matter, wiping out the history of deflagration. Note that all scenarios have a similar, pre-expanded WD as an intermediate state (from Höflich et al. 2003).

1.4.3 Are all SNe Ia similar?

We already discussed the photometric diversity of SNe Ia in Section 1.4.1. The homogeneity of SN Ia spectra at the various phases is such that one can determine the phase of a SN Ia by simply comparing its spectrum with a sequence of reference spectra. Nonetheless, the study of good quality data demonstrates that spectroscopic differences do exist between SNe Ia in general.

The ejecta of SNe Ia do not always have the same velocity at a given phase (see e.g. Branch 1987). The smallest ejection velocities are generally found among SNe Ia in elliptical galaxies (Filippenko 1989, Branch & van den Bergh 1993b). A spectroscopic distinction between SNe Ia in spiral and elliptical galaxies indicates that there are real physical differences among SNe Ia; the dissimilar ejection velocities cannot be a consequence of viewing an asymmetric explosion from different angles. The most luminous SNe Ia seem to occur in young stellar populations (Hamuy et al. 1995, Branch, Romanishin & Baron 1996). The extinction law, considered until now similar among the SNe, is another important factor of diversity which will be extensively discussed in the course of this thesis.

Moreover, a specific variable observed is that the continuum is bluer in SNe with lower values of Δm_{15}(B), which seems to be related to variations in temperature. The relation between the B absolute magnitude and the ratio of the Si II absorption lines at 5800 Å and 6150 Å described by Nugent et al. (1995) might also be temperature-related. Benetti et al. (2004a) suggest that this relation breaks down at low values of Δm_{15}(B). Nugent et al. (1995) find a relation between the ratio of the H and K Ca II absorptions and the B absolute magnitude, while Mazzali et al. (1998) find a relation between the FWHM of the 4700 Å Fe line in very late spectra and the Δm_{15}(B). All these relations between photometric and spectroscopic characteristics of SNe Ia and their absolute magnitude have supported the hypothesis that one parameter is sufficient to describe the differences between the various objects. This was, therefore, the general belief among the supernova community at the end of the last decade. The new decade, and the new century, have brought with them a number of objects which defy this paradigm, and the tools to investigate the issue further.

Some peculiar SNe Ia have light curves that are significantly different from the average. In general, they require a different theoretical model as a basis for their observed characteristics to be reproduced. A good example is the already known SN 1991T. It was the first peculiar SN Ia to be discovered, although SN 1986G (Phillips et al. 1987) had already cast some doubts on the uniformity of the class. The early-phase spectra of SN 1991T are nearly featureless and only after maximum light this object starts showing SN Ia characteristics. Its light curves are not peculiar, although its decline rate is slower than average and its luminosity seems to be higher than average. Together with the normal SN 1998bu (Cappellaro 2001), this is the only SN Ia to have produced a light echo. SN 1991bg, the second peculiar SN Ia discovered, has opposite characteristics: its light curves show a much faster decline than average and its spectra show Ti at bluer wavelengths, which is not visible in normal events. Its spectra remain

peculiar also at late phases and its I-band light curve does not show the usual secondary maximum. These characteristics, and a much fainter magnitude than average, are the signature of a very low-energy event. Like SN 1991T, SN 1991bg is now the representative of a well-populated class of objects. SN 2002ic (Hamuy et al. 2003) might also be considered the representative of a subclass formed by a few objects, although even its attribution to the class of SNe Ia is still controversial (Benetti et al. 2006c). Indeed, its spectra show a strong H line, which is the defining characteristics of Type II SNe, but this feature comes from a circumstellar shell, surrounding what has been claimed to be a normal SN Ia event. Other objects, such as SNe 1998Z, 1997cy, 1999E and 2005gj show somehow similar characteristics. Some peculiar objects are the only representatives of their class: this is the case for SNe 2000cx and 2002cx. The former was the brightest SN discovered in the year 2000 and it was extensively observed by Li et al. (2001a). Its light curves show a different rate between rise and decline - a speedy rise to maximum light and then a slow decline - the colour curves show an unusual evolution and the spectra, initially similar to those of SN 1991T, are different from the average until after maximum light. SN 2002cx (Li et al. 2001c) shows an opposite discrepancy in its light curve: a slow rise and a fast decline, together with a much fainter magnitude than any known SN Ia. Its spectra, apart from the early ones which are featureless like SN 1991T, remain different from the average at all phases.

Finally, one of the most recent studies on the observed diversity of SNe Ia (Benetti et al. 2005a) has analysed a set of observational parameters, namely the expansion velocity from Si II measured 10 days past maximum (v_{10}(Si II)), the average daily rate of decrease of the expansion velocity of this line ($\dot{v}$ = -Δv/Δt), the $\mathcal{R}(\mathrm{Si\,II})_{max}$ (the ratio of the depths of the Si II 5972 Å and 6355 Å absorptions measured at maximum light, Nugent et al. 1995), the B absolute magnitude and the Δm_{15}(B). They found that SNe Ia can be grouped in three main families called FAINT (faint SNe Ia with low expansion velocities and rapid evolution of the Si II velocity), HVG ('normal' SNe Ia with high velocity gradients, brighter absolute magnitudes and higher expansion velocities than the FAINT SNe) and LVG ('normal' and SN 1991T-like SNe Ia with small velocity gradients) whose characteristics are mainly governed by the nature of the explosion mechanism (same explosion mechanism, possibly distinguishing LVG and HVG or a totally different kind of explosion, which may be the case especially for the FAINT group). A brief summary of the main characteristics of these groups are listed on Table 1.2.

The discovery of these peculiar objects divides the SNe Ia in three groups: *normal* (the majority), *underluminous* (1991bg-like) and *overluminous* (1991T-like). Currently, with the improvement of the observations, it is possible to

TABLE 1.2— General characteristics of the three well-separated clusters of SNe Ia (from Benetti et al. 2005a).

	$\langle\Delta m_{15}(\mathrm{B})\rangle$	$\langle M_B\rangle$	$\langle\dot{v}\rangle$ ($\mathrm{km\,s^{-1}}\,d^{-1}$)	$\langle v_{10}(\mathrm{Si\,II})\rangle$ (1000 $\mathrm{km\,s^{-1}}$)	$\langle\mathcal{R}(\mathrm{Si\,II})_{max}\rangle$	note
FAINT	1.83	-17.2	87	9.2	0.58	91bg-like
HVG	1.20	-19.3	97	12.2	0.20	NIa
LVG	1.10	-19.2	37	10.3	0.25	NIa + 91T-like

NIa = normal Ia

TABLE 1.3— A set of properties within which a SN Ia can be considered normal (from Salvo 2006).

- Hydrogen lines absent from spectra
- *w*-shaped S II feature at 5200-5700 Å in spectra near max has EW > 50 Å
- Si II 6355 Å line near maximum light has EW > 50 Å
- B light curve fitted by stretched template curve with RMS < 0.1 mag
- $\Delta m_{15}(\mathrm{B}) < 1.8$
- $(\mathrm{B\text{-}V})_{0,max} < 0.2$
- Presence of secondary maximum in I band

detect subtle differences even between the more typical objects. When these discrepancies are not large enough to cause these objects to be defined as *peculiar*, they are often termed *unusual*.

Conversely we can consider 'normal' a Type Ia SNe having the observed parameters within the ranges given Table 1.3 (Salvo 2006).

1.4.4 Why are SNe Ia useful in cosmology?

Despite the differences discussed in the previous section, SNe Ia are extensively used as distance indicators (Trimble 1982).

A perfect standard candle for Cosmology should satisfy a number of conditions: it should be extremely bright, have always exactly the same absolute magnitude, its absolute magnitude should not depend on the environment, should not evolve with z (redshift), should need no or very small corrections and should be easy to calibrate. Type Ia SNe are therefore not according to this definition but, as discussed in Section 1.4.1 and subsequent, they are standardizable with the relations between the light curve shape and the luminosity. Moreover, thank to their very high luminosity, they are visible across billions of light years.

In the local universe, SNe Ia can be used to determine accurate values of H_0 (e.g. Hamuy et al. 1996b) and to test peculiar motions and the Great Attractor theory (Germany 2000).

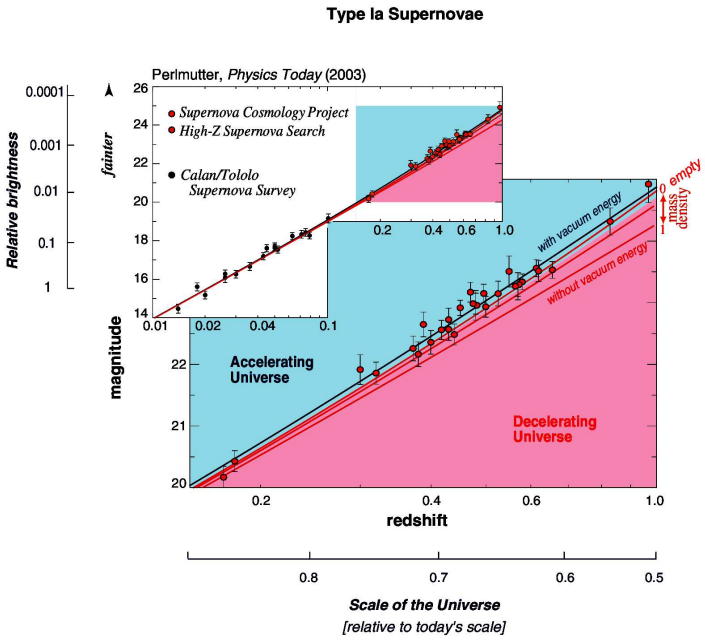

FIGURE 1.22— Observed magnitude versus redshift for well-measured distant and nearby Type Ia SNe (from http://panisse.lbl.gov/).

By 1999 more than 100 SN Ia had been discovered and studied at redshifts higher than 0.3 by two independent groups: The Supernova Cosmology Project (SCP, Perlmutter et al. 1998, Perlmutter et al. 1999) and The High z Super-Novae search (Riess et al. 1998). The two teams consistently found that SNe Ia at redshifts z $\sim$ 0.5 appear dimmer than expected by $\sim$ 0.3 magnitudes. This suggests that the expansion of the Universe is accelerating, propelled by dark energy[4] with $\Omega_\Lambda \sim 0.75$ (see Figures 1.22 and 1.23). Of course, this re-

[4]The dark energy is a hypothetical form of energy that permeates all space and has strong negative pressure (Peebles & Ratra 2003). According to the Theory of Relativity, the effect of such a negative pressure is qualitatively similar to a force acting in opposition to gravity at large scales. It is "dark" because it is not known what form the energy takes: it is not directly visible and has not been detected in particle physics experiments. The dark energy

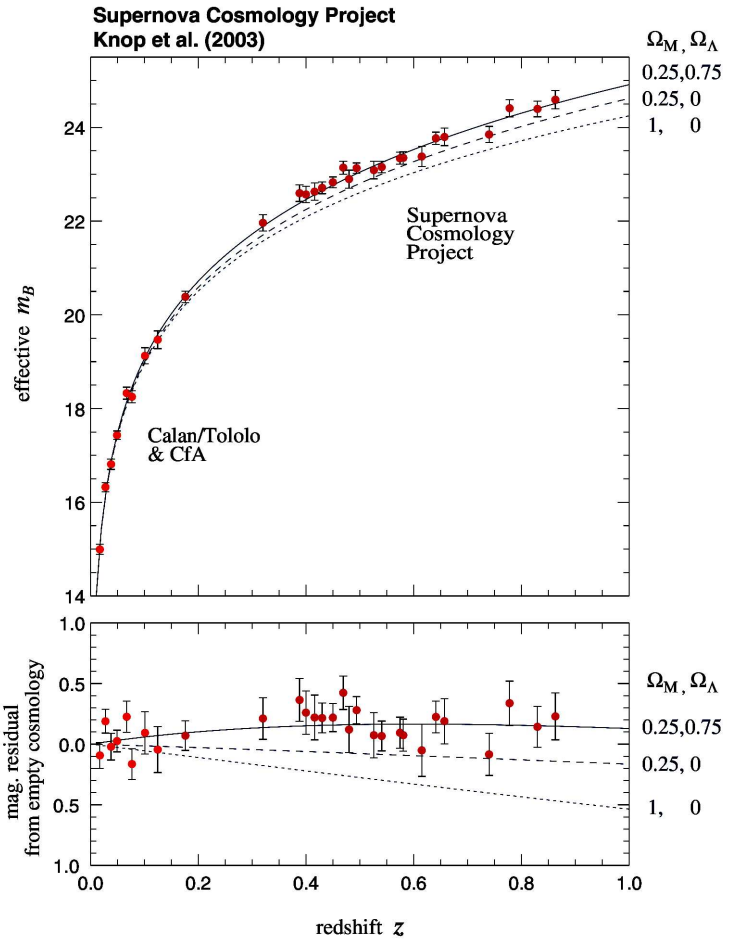

FIGURE 1.23— *Top panel*: Hubble Diagram for Supernova Cosmology Project with a low-extinction subsample. *Bottom panel*: residuals relative to an empty universe (from Knop et al. 2003).

sult might be affected by several selection effects which need to be taken into account, and rely on the assumption that distant SNe Ia are the same as the nearby ones. Nevertheless these results have been corroborated by several independent sources: the Cosmic Microwave Background (CMB) and gravitational

is thought to be responsible for the acceleration of the Universe.

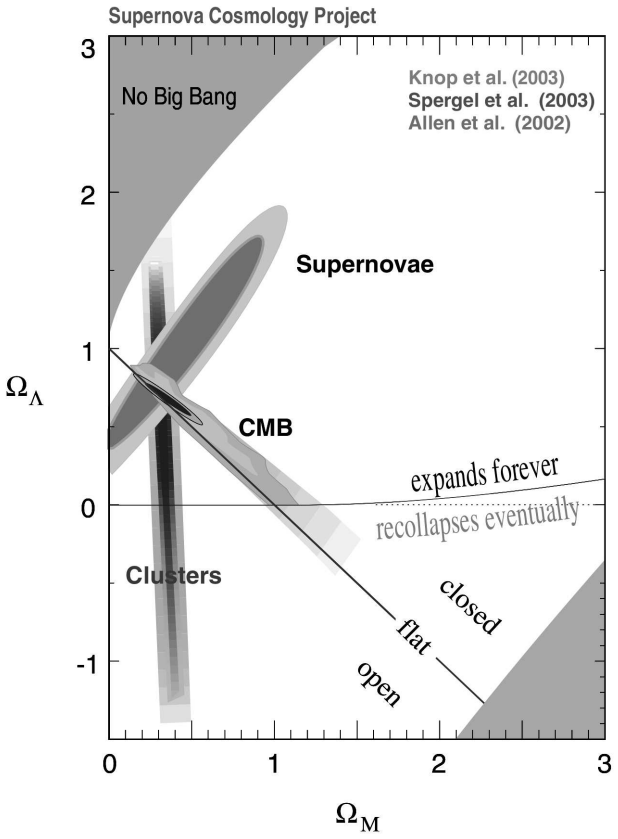

FIGURE 1.24— Confidence regions for Ω_M vs Ω_Λ with results from Cosmic Microwave Background (CMB) and galaxy cluster data added (from Knop et al. 2003).

lensing, as well as improved measurements of the supernovae (see Figure 1.24). Recent estimation of the cosmological parameters given $\Omega_M \approx 0.3$ and $\Omega_\Lambda \approx 0.7$ (Riess et al. 2004, Astier et al. 2006, Wood-Vasey et al. 2007).

1.5 Why do I devote this thesis to the SN study?

We have seen in the previous sections that SNe are a very hot topics in astrophysics. However a large number of open questions remain on the nature of the exploding stars, on the explosion mechanisms and on the amount of extinction suffered by the SN light in its travels up to us. The extinction reduces the precision of our measured of the energy of the explosion, required to fully understand the physics, and also, limits our ability to use SNe as distance indicators. Indeed we have shown that thermonuclear SNe (SNe Ia) are a reasonably homogeneous (though not perfect) class of objects now widely used as distance indicators. Thus this property, the homogeneity can be exploited to derive the properties of the dust along the line of sight toward the SNe and the associated extinction laws.

Questa tesi è incentrata a questo tema.

We will show that the detailed study of three highly extinguished SNe Ia (SN 2003cg, SN 2002cv and SN 2006X) reveals unexpected results: the extinction laws in all the three cases do not follow the classical Cardelli, Clayton & Mathis (1989) law with the canonical total-to-selective extinction ratio $R_V = 3.1$, but show peculiar behaviour with R_V from 1.56 to 1.80.

This tells us that in external galaxies there are lines of sight where the dust can have properties deviating from the average ones that we observe in the Galaxy. This has a two-fold effect: it warns us of peculiar reddening toward some cosmological Type Ia SNe forcing us to be cautious in their utilization as distance indicators, and it provides us another element in the discussion about their progenitors, often simply considered to be old stars exploding in regions depleted of dust and gas.

2

Data acquisition and processing

Minaccia sereno.
Tecnico d'Asiago

As we have seen in the previous chapter, questions about supernovae (SN/SNe) remain still open and a new observational effort is required. We need a complete coverage of the SN evolution from few days after explosion all the way to the nebular phase and from the U to the near-infrared (NIR) bands, and a detailed redaction and calibration of the data. In this chapter we describe the requirement of the data acquisition (Section 2.1) and the instrumentation used to observe the SNe discussed in this thesis (Section 2.2), and the techniques of photometric (Section 2.3.2) and spectroscopic (Section 2.3.3) data reduction.

2.1 Data acquisition

Our observational campaigns begin after the discovery of the SN (see also Appendix B) which turns out to be before or close to maximum light. According to the statistic of the last few years, 2 - 3 objects/semester are accessible from the telescopes available to our team. Because of the restrictions on the scheduling of specific instruments, a complete dataset can only be achieved through the effort of several observatories and telescopes.

We attempt to observe a target in both imaging and spectroscopy. UBVRI-JHK photometry of nearby SNe are needed for the construction of bolometric light curves and colour curves (important for the estimation of the extinction). In addition, we obtain the detailed monitoring of the high signal-to-noise spectroscopic observations (in general, SNe do not require high-resolution spec-

troscopy because SNe spectral features are broad) both at optical and infrared wavelengths in order to follow the evolution of the physical conditions of the ejecta such as temperature, density, chemical compositions and kinematics.

The scheduling of the observations depends on the visibility period of the SN and on its type, and is planned at the beginning of a follow-up (taking into account the availability of each telescope). For a typical SN Ia, considering the light curve and spectra characteristics of these targets, the strategy is to get as many observations are possible during the first 2 weeks after maximum ($\sim$ B_{max} + 1 mag), then every fourth night until one month after maximum, every week up two months, every two weeks from 2 - 4 months after maximum, and finally, two observations during the nebular phase.

With this basic strategy, I have prepared several proposals for observations at the 1.82m Copernico Telescope in Asiago, at telescopes of the Roque de los Muchachos Observatoy (La Palma, Spain, see Section 2.2) and the ESO Telescopes in La Silla and Paranal (Chile). Since SNe are highly variable objects and their discovery is unpredictable we usually require for *Target of Opportunity* mode (ToO) in these telescopes. I have administrated most of the ToO from Padova and I have also observed in visitor mode in several occasions.

Along with material from literature, in this thesis we present data for three SNe Ia extensively studied by the *European Supernova Collaboration* (hereafter ESC - see Appendix A). This material is the result of the combined efforts of several researchers from different institutions of the collaboration between years 2002 and 2006, using many different telescopes and instrumental configurations. Each of the people involved gave a specific contribution and all of them contributed to the success of the global work.

This thesis was born as part of this collaborative effort. The large set of data here analyzed includes more than 50 spectra and 465 photometric points of SNe not published before. For this work, I have organized the observations, the calibration and the systematic analysis of the whole set of data.

2.2 Telescopes and instrumentation

One of the difficulties of SN follow-up is to get a good spectral coverage during all its evolution from optical to near IR. Because we do not have access to a dedicated telescope, we had to distribute the extensive observational campaign on several telescopes available to the ESC.

In the following, we will briefly describe the main technical characteristics of the different instrumental configurations used for the observations of the SNe presented in this thesis.

ESO 2.2m + WFI imager WFI (operated by the European Southern Observatory (ESO) at La Silla, Chile) is a wide field camera with a mosaic of 8 2k×4k chips, Read-Out-Noise (RON) between 4.9 and 5.5 $e^-$and Conversion Factor (CF) between 1.99 and 2.26 e^-/ADU. The pixel scale is 0.238 arcsec/pixel, and the total field of view $34' \times 33'$. The observations have been obtained with filters U/50 (ESO#77), B/99 (ESO#842), V/89 (ESO#843), Rc/162 (ESO#844), I/203 (ESO#879).
http://www.ls.eso.org/lasilla/sciops/2p2/E2p2M/WFI/

ESO 3.6m + EFOSC2 The Multi-Mode instrument EFOSC2 (ESO Faint Object Spectrograph and Camera), operated by ESO at La Silla (Chile), has a pixel size of 15 μm, pixel scale of 0.157 arcsec/pixel and the field of view is $5\farcm4 \times 5\farcm4$. In Slow mode are estimated CF = 1.33 e^-/ADU, RON = 8.0 $e^-$and dark current $\sim$ 7 e^-/px/hr. The observations have been obtained with Bessel filters V, R and Gunn i.
http://www.ls.eso.org/lasilla/sciops/3p6/efosc/

ESO NTT + EMMI EMMI (ESO Multi-Mode Instrument at La Silla, Chile) has two "arms" optimized for different wavelengths. Each arm is available both for imaging and spectroscopy.

- Blue arm: the detector (ESO CCD 31) is a Tektronix TK1034 chip, 1024×1024 pixels, with pixel size of 24 μm, pixel scale of 0.37 arcsec/pixel, field of view of $6\farcm2 \times 6\farcm2$, CF = 2.88 e^-/ADU, RON = 6.5 e^-, dark current 6.9 e^-/pixel/hour in normal mode. The wavelength range 3000-5000 Å.
- Red arm: the pixel scale of 0.1665 arcsec/pixel, pixel size of 15 μm, field of view of $9\farcm1 \times 9\farcm9$, CF $\sim$ 1.35 e^-/ADU, RON $\sim$ 5.84 e^-, dark current 0.3 e^-/pixel/hour. The wavelength range 4000-10000 Å.

We used Bessel V, R and Gunn i filters. For low-dispersion spectroscopy, grism 2 (range 3800-9200 Å, dispersion 1.74 Å/px).
http://www.ls.eso.org/lasilla/sciops/ntt/emmi/index.html

ESO NTT + SofI SofI (Son of Isaac), which is operated by ESO at La Silla (Chile), provides both infrared spectroscopy and imaging. For imaging, it has been used with the large Field Objective, with pixel scale 0.288 arcsec/pixel and field of view $4\farcm94 \times 4\farcm94$. The detector is a HgCdTe 1024×1024 Hawaii array with 18.5 μm pixels. The RON is about 12

e$^-$and the CF is about 5.4 e$^-$/ADU. We used the SofI filters J, H, Ks and, for low-resolution spectroscopy, the grism GBF (range 9500-16400 Å, dispersion 6.96 Å/px) and GRF (range 15300-25200 Å, dispersion 10.22 Å/px). The resolution of the spectra obtained with the GBF was about 30 Å, and $\sim$ 40 Å for GRF.
http://www.ls.eso.org/lasilla/sciops/ntt/sofi/index.html

ESO VLT UT1 + ISAAC The ESO Very Large Telescope (VLT) is located at Paranal (Chile). UT1 (Unit Telescope 1) was used with ISAAC (Infrared Spectrometer And Array Camera), an IR (1-5 μm) imager and spectrograph. It has two arms, one equipped with a 1024×1024 Hawaii Rockwell array (it is used at short wavelengths - SW, from 1 to 2.5 μm), and the other with a 1024×1024 InSb Aladdin array (it is used predominantly at long wavelengths - LW, from 3 to 5 μm) from Santa Barbara Research Center. Our observations were obtained from SW - Rockwell, with a pixel size of 18.5 μm, a CF = 4.5 e$^-$/ADU and a RON = 11 e$^-$. The pixel scale is 0.1484 arcsec/pixel and the field 2′.5×2′.5, using the filters J, H and Ks.
http://www.eso.org/instruments/isaac/

ESO VLT UT2 + FORS1 FORS1 (FOcal Reducer/low dispersion Spectrograph 1) detector (at Paranal, Chile) is a Tektronix 2048 × 2048 pixel CCD of 24 μm pixel size, with an average CF = 1.61 e$^-$/ADU, and a RON $\approx$ 5.15 e$^-$and dark current at -120^oC about 8 e$^-$/pixel/hour in high gain mode. The pixel scale in the configuration used was 0.2 arcsec/pixel and the field of view 6′.8×6′.8. The filters Bessel B, V, R, I and the grism 300V+GC435 (wavelengths range 4450-8650 Å, dispersion 112 Å/mm, resolution 30 Å) have been used.
http://www.eso.org/instruments/fors1/

Danish 1.54m + DFOSC The telescope is a Danish national facility, operated by ESO at La Silla, Chile. DFOSC (Danish Faint Object Spectrograph and Camera) is a focal reducer type of instrument. It allows wide field imaging $\sim$ 13′.7×13′.7 field of view with a pixel scale of 0.39 arcsec/pixel, a pixel size of 15 μm, a CF = 0.76 e$^-$/ADU and a RON = 3.21 e$^-$. . The observations have been obtained with filters Bessel B, V, R and Gunn i.
http://www.ls.eso.org/lasilla/sciops/2p2/D1p5M/

INT + IDS The Isaac Newton 2.5m Telescope (INT) is located at La Palma (Spain). The CCD of IDS (Intermediate Dispersion Spectrograph) is

a EEV10 (2148×4200 pixels, size 13.5 μm, scale 0.19 arcsec/pixel, CF = 0.96 e^-/ADU, RON = 3.27 e^-). The spectra were obtained with a low resolution grating (R632V, useful range 3500-9250 Å, dispersion 0.85 Å/pixel).
http://www.ing.iac.es/Astronomy/instruments/ids/

INT + WFC The WFC (Wide Field Camera) is an optical mosaic camera at the prime focus of the 2.5m Isaac Newton Telescope. It consists of 4 thinned EEV 2kx4k CCDs, with pixel size of 13.5 μm corresponding to 0.33 arcsec/pixel and a field of view of $34' \times 34'$. SN 2002cv was observed with the filters Harris V, R and Sloan Gunn r', i' in the CCD#4 or A5382-1-7 which CF = 2.9 e^-/ADU and RON = 5.8 e^-.
http://www.ing.iac.es/Astronomy/instruments/wfc/

WHT + ISIS A single spectrum of SN 2003cg was obtained with the William Herschel 4.2m Telescope (WHT) at La Palma (Spain) equipped with ISIS, on which was mounted the CCD EEV12 (2148×4200 pixels, pixel size 13.5 μm, scale 0.19 arcsec/pixel). The blue arm used the R600B grating (4227-6000 Å with a dispersion of 0.45 Å/pixel) and the red arm used the R1200 grating (5900 to 6891 Å with a resolution of 0.23 Å/pixel). ISIS has a CF = 2.3 e^-/ADU and RON = 6 e^-.
http://www.ing.iac.es/Astronomy/telescopes/wht/index.html

JKT + JAG The Jacob Kaptein 1.0m Telescope (JKT) is located at La Palma (Spain). It was used with the Acquisition and Guiding unit (JAG) and the SITe2 2048×2048 (24 μm) pixels detector. For SITe2 the image scale is 0.33 arcsec/pixel, giving an unvignetted field of view of about $10' \times 10'$. Main characteristics of the detector are: CF = 1.95 e^-/ADU and RON = 6 e^-in slow mode. We used Harris V, R and I.
http://www.ing.iac.es/Astronomy/telescopes/jkt/index.html

LT + RATCAM We obtained photometric data with the optical RATCAM CCD Camera of the 2m robotic Liverpool Telescope (LT) at La Palma (Spain). The CCD is a 2048×2048 pixel EEV CCD42-40, with pixel size 13.5 μm, pixel scale $\sim$ 0.135 arcsec/pixel and field of view $4\farcm6 \times 4\farcm6$. The CF is 2.72 e^-/ADU and the RON is < 5 e^-. Part of the photometry of SN 2006X was obtained from this telescope using the Sloan u', r', i', z' and the Bessell B, V filters.
http://telescope.livjm.ac.uk/

NOT + ALFOSC Two different detectors were used for the ALFOSC (Andalucia Faint Object Spectrograph and Camera) instrument mounted at

the 2.5m Nordic Optical Telescope (NOT) in La Palma (Spain) during the period of our observations:

- before September 2003, our observations were performed using a 2048×2048 Provenance Loral/Lesser detector (CCD7), with pixel size 15 μm and scale 0.188 arcsec/pixel. The estimated CF was ~ 1 e^-/ADU and RON ~ 6 e^-.
- After September 2003, a new detector was installed: a EEV42-40 2Kx2K Manufacturer (CCD42-40) back illuminated, a 2048×2048 chip of pixel size 13.5 μm and 0.19 arcsec/pixel. The CF has been estimated to be 0.726 e^-/ADU and the RON = 5.3 e^-.

For the photometry we used U, B, V, R and I Bessell filters and for the spectroscopy we used the grism#4 (low resolution visual grism, range 3200-9100 and dispersion 3.0 Å/pixel) and grism#5 (low resolution red grism, range 5000-10250 and dispersion 3.1 Å/pixel).
http://www.not.iac.es/instruments/alfosc/

NOT + StanCam StanCam (Stand-by CCD camera) is less sensitive and has smaller field of view than ALFOSC. The pixel size is 24 μm, the scale is 0.176 arcsec/pixel, and the field of view of about $3' \times 3'$. The RON is 6.5 e^- and the CF is 1.68 e^-/ADU. The instrument allows optical imaging with UBVRI Bessell filters.
http://www.not.iac.es/instruments/stancam/

TNG + Dolores Dolores (Device Optimized for the LOw RESolution) is installed at the Nasmyth B focus of the TNG (Telescopio Nazionale Galileo in La Palma - Spain). The detector is a Loral thinned and back illuminated 2048×2048 CCD. The scale is 0.275 arcsec/pixel (μm 15), which yields a field of view of about $9'.4 \times 9'.4$. The CF is 0.97 e^-/ADU and the RON ~ 2 e^-. The instrument allows imaging as well as spectroscopic observations. We used the Johnson filters U, B, V, and Cousins R, I; for the spectroscopy we used LR-B (wavelength range between 3000 and 8800 Å, dispersion 2.8 Å/pixel and resolution 11 Å with a $1''$ slit) and LR-R (wavelength range between 4470 and 10360 Å, dispersion 2.9 Å/pixel and resolution 11 Å with a $1''$ slit).
http://www.tng.iac.es/instruments/lrs/

TNG + OIG OIG (Optical Imager Galileo) is a CCD camera for direct imaging, mounted on the Nasmyth A Adapter interface of TNG. OIG is equipped with a mosaic of two thinned and back illuminated EEV 42-80

CCDs, with 2048×4096 pixels each (pixel size of 13.5 μm). The resulting pixel scale is 0.072 arcsec/pixel for a total field of view of about $4'.9 \times 4'.9$. The gap between the two chips is 2.8 arcsec. For a 2×2 binning. CF $\sim$ 1.6 e^-/ADU and RON $\sim$ 10 e^-. The set of filters used was U, B, V, R Johnson stantdard plus Gunn i.
http://www.tng.iac.es/instruments/oig/

2.2m Telescope of Calar Alto + CAFOS We also used the 2.2m telescope of Calar Alto (located in Sierra de Los Filabres, Andalucía, Spain) equipped with CAFOS (Calar Alto Faint Object Spectrograph), a 2048×2048 SITe#1d CCD (pixel size 24 μm, image scale 0.53 arcsec/pixel, total field $18' \times 18'$, CF = 2.3 e^-/ADU and RON = 5.060 e^-). The Johnson U, B, V, R, I filters were used as well as grism B-200 (range 3200-7000 Å and spectral resolution 13 Å) and R-200 (range 6300-11000 Å).
http://w3.caha.es/alises/cafos/cafos.html

Asiago-Ekar 1.82m Copernico Telescope + AFOSC The Asiago Observatory is located in Italy. AFOSC (Asiago Faint Object Spectrograph and Camera) is equipped with a Tektronix TK1024 Thinned Back Illuminated CCD, 1024×1024, with pixel size 24 μm, pixel scale 0.473 arcsec/pixel, and a field of view is $8'.14 \times 8'.14$. The estimated CF and RON were 2 e^-/ADU and 7.8 e^-respectively until June 2003. After this, a new similar CCD was mounted and the new values were 1.86 e^-/ADU and 9.6 e^-. For photometry were used Johnson U, B, V, R and Gunn i filters, and for spectroscopy, were used the grism#2 (wavelength region 3720-10200 Å, dispersion 15.67 Å/pixel and resolution 38 Å with the 2.1″ slit) and grism#4 (wavelength region 3500-8450 Å, dispersion 4.99 Å/pixel and resolution 22 Å with the 2.1″ slit).
http://www.oapd.inaf.it/asiago/2000.html

Asiago-Pennar 1.22m Galilei Telescope + B&C The Boller and Chivens (B&C) spectrograph has been equipped with the "Dioptric Blue Galileo Camera". There are five gratings available for the B&C spectrograph. Dispersion range from 1.01 Å/pixel to 8.14 Å/pixel. The scale of the CCD along the slit is 1.11 arcsec/pixel. The 300 mm^{-1} grooves grating was usually used to get spectra with a dispersion of 4.06 Å/pixel.
http://www.oapd.inaf.it/asiago/4000.html

UKIRT + CGS4 Near IR spectra of SN 2003cg and SN 2002cv were obtained with the 3.8 meters United Kingdom InfraRed Telescope (UKIRT), equipped with the CGS4 (Cooled Grating Spectrometer Mk 4), a 1-5

μm multi-purpose 2D grating containing a 256×256 InSb array, sited in Hawaii near the summit of Mauna Kea. We used CGS4 with the 40 l/mm grating (pixel scale 1.22 arcsec/pixel). This gives a resolving power of R=800 in the IJ band (roughly 15 Å) and R=400 in the HK band (roughly 50 Å).
http://www.jach.hawaii.edu/UKIRT/instruments/cgs4/cgs4.html

2.3m SSO Telescope + DBS The 2.3m telescope of Siding Spring Observatory (Australia) works with:

- the optical imager (available until October 2004) equipped with a SITe 1024×1024 thinned CCD with 24 μm pixels (CCD#11), with 0.59 arcsec/pixel, field of view 6′.62×6′.62, CF = 1 e^-/ADU and RON = 6 e^-;
- a Double Beam Spectrograph (DBS) equipped with two SITe 1752×532 CCDs, ST-D06AB, thin, back illuminated, AR coated, 15 μm pixel devices, labeled CCD 7 and CCD 9 (and associated with DBS-B and DBS-R arms, respectively). The RON is about 6 $e^-$and the CF $\sim$ 1 e^-/ADU.

We used both instruments to obtain spectra and imaging (in U, B, V, R and I bands).
http://www.mso.anu.edu.au/observing/telescopes/2.3m.php

KAIT of Lick Observatory + CCD camera Some imaging of SN 2002cv was obtained with the Katzman Automatic Imaging Telescope (KAIT) at Lick Observatory atop Mount Hamilton (California). It is an entirely robotic telescope dedicated to the search for supernovae and the monitoring of celestial objects. It is a 76 cm diameter reflecting telescope equipped with a 500×500 Peltier cooled CCD camera back illuminated and coated to enhance the blue response. The pixel size is 24 μm and the pixel scale is 0.8 arcsec/pixel. CF = 3.8 e^-/ADU and RON = 9 e^-.
http://astron.berkeley.edu/∼bait/kait.html

Nickel 1m Telescope of Lick Observatory in Direct imaging This telescope was used to get photometry (V, R and I Bessel) of SN 2002cv. The Nickel CCD camera, a direct imaging, is a SITe 1024×1024 thinned CCD, with a pixel scale of 0.28 arcsec/pixel, CF = 4.4 e^-/ADU, RON = 1.7 $e^-$and dark = 0.76 e^-/1000 s.
http://mthamilton.ucolick.org/techdocs/telescopes/Nickel/nickel.html

Shane 3m Reflector at Lick Observatory + KAST Some of the spectra of SN 2002cv were obtained with the Shane 3m Reflector and KAST, a double spectrograph with simultaneous red/blue spectra (wavelength range 3300-10000 Å, RON $\sim$ 8.7 $e^-$and CF $\sim$ 1.4 e^-/ADU).
http://mthamilton.ucolick.org/techdocs/telescopes/Shane/

AZT-24 Telescope + SWIRCAM The AZT-24 is a 108 cm-aperture telescope located in Campo Imperatore (Italy). The telescope is equipped with the near-infrared camera SWIRCAM (1.1 - 2.5 μm). The detector was a 256×256 HgCdTe PICNIC array with a pixel size 40 μm, pixel scale of 1.04 arcsec/pixel and field of view of more than $4'.4\times4'.4$. The CF is 5.95 e^-/ADU and the RON is about 11 e^-.
http://www.te.astro.it/attivitascientifica/telescopi/azt24/azt24_eng.html

TNT + TK512CB1-1 CCD Teramo-Normale Telescope (TNT), located at Terano, Italy, is a Ritchey-Chretien of 72 cm equipped with a 512×512 pixel Tektronics TK512CB1-1 CCD with pixel size 27 μm, 0.46 arcsec/pixel, field of view $3'.92\times3'.92$, CF = 4 e^-/ADU, RON = 7.9 $e^-$and dark current 0.09 e-/pixel/s. V, R and I filters were used.
http://www.te.astro.it/attivitascientifica/telescopi/tnt/tnt_home.htm

Loiano + BFOSC It is a 1.52m telescope with a Ritchey-Chretien optical configuration located in Bologna (Italy). BFOSC (Bologna Faint Object Spectrograph and Camera) is equipped with an EEV 1340×1300 CCD camera with a scale of 0.58 arcsec/pixel, a pixel size of 20 μm, a field of view of $13'.0\times12'.6$, a CF = 2.13 e^-/ADU and a RON = 1.73 e^-. It were used B, V, R and I Johnson filters.
http://www.bo.astro.it/loiano/152cm.html

0.60m Reflector of BAO + CCD The 0.60m Reflector at Xinglong Station of the Beijing Astronomical Observatory (BAO) in China was used to observe SN 2003cg. The CCD camera was a Texas Instruments T1-215, with 1024×1024 pixels and a field of view of $16'.8\times16'.8$ (pixel scale 0.45 arcsec/pixel, RON = $e^-$and CF = 2.5 e^-/ADU). We obtained with this configuration photometric points in Johnson's B, V and Cousins's R and I.
http://www.bao.ac.cn/english/Telescope.asp

2.16m Telescope of BAO + CCD One spectrum of SN 2003cg was obtained with the 2.16m Optic Telescope at Xinglong Station of the Beijing Astronomical Observatory (BAO) and the OMR spectrograph (Tektronix 1024×1024 CCD). We used the grating 300g mm^{-1}, with a RON = 3.75

$e^-$and a CF = 0.86 e^-/ADU with an useful spectral range between 4000 and 8500 Å.
http://www.bao.ac.cn/english/Telescope.asp

2.3 Data reduction

The SNe observations were processed using IRAF[1] and FIGARO[2] routines. For photometry we used a collection of tasks developed in the IRAF environment by the Padova-Asiago SN Group.

2.3.1 Preliminary reduction

To use our images we need first to remove any peculiar instrumental signature due to the detector and the telescope. A brief description of the necessary pre-reduction steps are the following:

Bias subtraction. The bias level is an electronic offset added to the signal from the CCD to make sure that the Analogue-to-Digital Converter (ADC) always receives a positive value. The ADC samples the charge accumulated in a CCD pixel and returns a digital value. This value is proportional to the actual number of electrons detected in the pixel and is measured in Analogue-to-Digital Units (ADUs). The relation between ADU and the number of photons (charge) is a scale factor known as the gain. It is common practice to create a "master bias" image from the average of several ($\sim$ 10) bias images (frames obtained with exposure time of 0 seconds and closed shutter closed) in order to gain a better statistics, to reduce the read-out noise (RON) and to get rid of cosmic rays.

Overscan correction. In principle the bias level is constant, but it can slightly change during the night because of external factors (like temperature variations). To monitor this effect, the bias level of each image is measured in the "overscan" region (a stripe of a few columns/row at the edge of the CCDs, which is not exposed to the light) and removed from the whole frame.

Trimming. After use, the overscan region can be cut off trimming the images. With this action, it is also possible to cut off the edge of the images, often

[1]IRAF is distributed by the National Optical Astronomy Observatories, which are operated by the Association of Universities for Research in Astronomy, Inc, under contract with the National Science Foundation.

[2]http://www.aao.gov.au/figaro/

affected by irregular response and degraded, and to delimit the useful area for the scientific analysis.

Flat-fielding. Due to construction faults and to variation of transmissivity of the CCD coating, and to dust contamination, the CCD response to the incident light is not uniform and can shows variation on different scales from that of the whole frame to pixel-to-pixel. So, it is necessary to divide the data by a "sensitivity map" (flat-field) created from calibration exposures. Usually, a flat-field is obtained by imaging a uniformly illuminated screen inside the telescope dome (dome-flats) or, better, the sky at twilight/dawn (sky-flat). Since the detector efficiency changes with the wavelength, flat exposures are required in all the bands used for the scientific frames. In order to have a better statistic, to reduce the read-out-noise and to get rid of cosmics, a number of flats are averaged to obtain a "master-flat". To the spectroscopic master-flats we add another process, their normalization along the dispersion axis.

2.3.2 Photometry

The photometric observations of our objects were obtained with a number of instruments equipped with broadband UBVRIzJHK filters. The observations consist of short exposures at early times and dithered multiple exposures at late epochs. In the latter case, the images in each filter were first geometrically aligned (registered) and then combined to produce a single deep image.

Reduction Techniques and magnitudes estimate

A major complication in supernovae photometry is separating the light from the SN itself from the underlying galaxy contribution at the SN position. Poor subtraction of the background light can produce large errors in the supernova light curve shapes and colours. The importance of the galaxy contribution change from event to event, it depends on the SN position (close or far from the nucleus of the host galaxy) but also on the phase of the SN and distance of the galaxy. Thus we have used different techniques: for the early-time optical photometry, the instrumental optical magnitudes [3] of the SN were measured using the IRAF Point Spread Function[4] (PSF) fitting routine while at late phases, when the SN magnitude is comparable to that of the background features, determination of the SN magnitudes made use of template subtraction:

[3] it is *-2.5* times the *log* of the sum of all counts coming from the object.

[4] The Point Spread Function or PSF is the analytic 2D function which describes the light distribution of a point source on the detector after passing through the turbulent atmosphere and the optics.

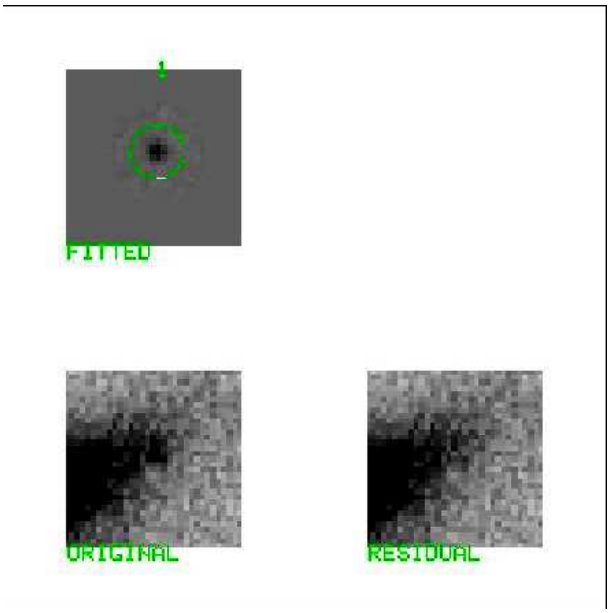

FIGURE 2.1— PSF-fitting technique in the case of SN 2002cv: original image of the SN region (bottom-left panel); SN contribution (fitted star), obtained after that the background at the SN position has been estimated fitting the region with a bidimensional polynomial of fixed degree (top-left panel); and residual background (bottom-right panel).

PSF-Fitting Technique. This technique consists in performing the fit of stellar profile and subtract the background galaxy contamination at the SN position. For this purpose the Padova team developed SNOoPY (SuperNOvaPhotometrY), a package originally designed by F. Patat and later implemented in IRAF by E. Cappellaro. It is based on DAOPHOT which allows to fit the SN profile with a PSF obtained from a set of local, unsaturated stars. This procedure is used when the host galaxy template is missing, the SN exploded onto a relatively flat background region or when its luminosity largely dominates that of the surrounding background.

In Figure 2.1 is shown a example of the application of this method in the case of SN 2002cv (Chapter 4) when the SN was around the maximum light.

Template Subtraction Technique. This technique is mandatory when the SN explode in a complex background area e.g. close to the galactic nucleus, H II region, spiral arms, and in general when the SN is faint. It consists of the cancellation of the host galaxy contribution removing an image

acquired when the supernova was not present. The procedure makes use of the ISIS template subtraction program (Alard 2000) and runs in the IRAF environment. For the application of this technique it is necessary to have a reference image of the host galaxy taken in each passband and obtained before or long after the SN explosion, when the SN luminosity has faded away, and this is often a limitation for the application of the method. Ideally, the templates should be obtained with the same telescope and with similar seeing as the scientific image containing the SN. Since this is not typically the case, a number of preliminary operation are required. The first step is the geometrical and photometrical registration of both images in order to correct for different instrumental pixel scales (image stretching), spatial orientation and position (frame rotation and shifting). After that, the image with better-seeing is degraded to that with poorer one and both images are scaled to the same intensity. Finally the reference (template) image is subtracted from the SN image.

The resulting frame is flat in the ideal case, except for variable objects in the field (SN, variable galactic nuclei, variable star), accidental bodies (asteroids, meteors, artificial satellites, and so on). But in real case, a number of blemishes show up (saturated stars, cosmic rays, hot pixels and bad columns).

At this point, the instrumental magnitude of the SN can be measured using the aperture photometry (e.g. IRAF task imexamine) or the PSF-fitting photometry (SNOoPY package) on the image obtained from the subtraction (without the host galaxy).

An example of the results of this method is shown for the same SN in Figure 2.2. The SN is clearly visible in the difference image along with residuals of stars and the galaxy nucleus.

We have used both techniques to get instrumental magnitudes of SN 2002cv, SN 2003cg and SN 2006X. It was found that the PSF-fitting and template-subtraction methods produced results in excellent agreement for a variety of instrumental configurations when the SN was bright. In Figure 2.3 is presented an example of comparison of B, V and R band photometry of SN 1999bw (Bufano 2003) obtained with the PSF-fitting and template subtraction techniques. In this case, the two methods provided similar results, with range -0.08 and 0.04 magnitudes and mayor differences only when the SN is faint (magnitudes ≥ 19). At this level the SN magnitude was comparable to that of the background and the most reliable results are provided by the template subtraction. Therefore we conclude that the template subtraction is the ideal method, but the PSF

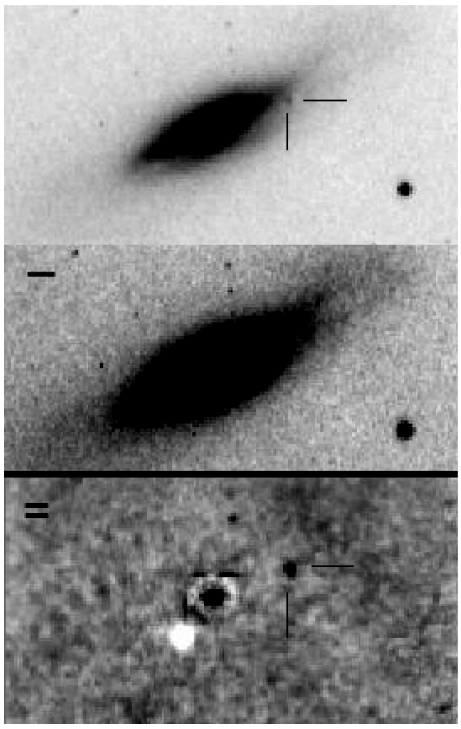

FIGURE 2.2— Template Subtraction Technique in the case of SN 2002cv at magnitude $\sim$ 17.2 in I band: original image containing the SN (top), reference frame (template) of the host galaxy without SN (center), subtracted image (bottom).

method provides the same results when the SN is bright (indicatively down to magnitude $\sim$ 19) and the seeing and the image sampling are adequate.

Calibration

The instrumental magnitudes obtained with either method must be scaled to a reference exposure time (e.g. 1 sec.) and corrected for the atmospheric extinction via

$$m_\lambda = m'_\lambda + 2.5log(t_{exp}) - K_\lambda \times airmass \tag{2.1}$$

where m' is the instrumental magnitude, t_{exp} the exposure time and K_λ the atmospheric extinction coefficient which depend from the observing site and season.

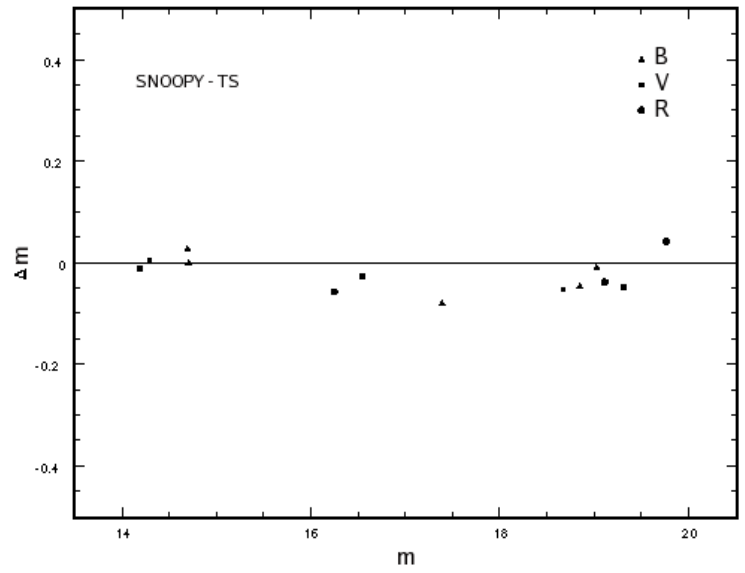

FIGURE 2.3— Differences between the B (triangles), V (squares) and R (circles) band magnitudes obtained with the PSF-fitting and template subtraction techniques applied to the same set of images of SN 1999bw (Bufano 2003), as a function of the measures estimate with the PSF-fitting.

Since SNe are variable objects each observation is unique and non reproducible. For this reason an effort is done to use all available data, even those obtained under non ideal conditions. In order to calibrate the photometry obtained in non-photometric nights we make use of a set of local standards in each SN field. These stars are chosen among the isolated stars in the field in order to avoid the contamination by nearby objects. Also they should be non-variable star and neither too bright to saturate during the long exposures at late phases nor too faint to be dominated by the photon noise. In turn, the local stars are a posteriori calibrated by mean of observations of standard stars during a subset of photometric nights. The observation of standard stars allows us also to determinate the colour terms for the various instrumental setups. To this aim we observe standard Landolt fields (Landolt 1992) on the photometric nights. In detail, for each night and instrumental configuration, the observation of the Landolt stars provide a system of colour equations of the form:

$$\Delta m_\lambda = M_\lambda - m_\lambda = a_\lambda + b_\lambda \times (colour)_\lambda \tag{2.2}$$

where M_λ is the standard magnitude of each star, m_λ is its instrumen-

tal measurement normalized at 1 second exposure time and corrected for atmospheric extinction, using average values for the extinction coefficients. a_λ and b_λ characterize the instrumental configuration. a_λ usually called the zero point and b_λ is the colour term. Solving the system of equations, we obtain a_λ and b_λ for all filters and we can determinate the standard magnitude M_λ for the SN and the local standard stars for all bands.

Finally a check of the photometric quality of the night was performed on the local sequence. If Δm_λ represents the mean difference between the magnitude of the sequence stars in a non-photometric night and those of the photometric ones, a correction was applied to the a_λ terms of the colour equations. The new values of the constant terms allow to estimate the final calibrated magnitude M_λ of the object.

For the IR magnitudes, additional reduction steps were required. Particular care was devoted to sky subtraction from all science frames due to the rapid variation in the IR and to image coaddition due to very short integration time of each exposure to improve the signal-to-noise.

As for the optical photometry, the IR magnitudes were obtained using PSF-fitting. For night-to-night calibration we also used a local sequence. However, as the number of IR standard fields observed each night was small, we adopted average colour terms provided by the telescope teams.

It is necessary to notice that the Ks band filter used in observation with SofI had a transmission curve slightly different from that of a standard K filter. Following Lidman (2002) we have transformed the Ks magnitudes to K by mean of the relation

$$K - Ks = -0.005 \times (J - K) \tag{2.3}$$

Errors of measurements

Uncertainties in the instrumental photometry (via PSF-fitting or template subtraction) were estimated by placing artificial stars with the same magnitude and profile as the SN, at positions close (within a few arcsec) to that of the SN, and then computing the deviations of the artificial star magnitudes. For the calibration error we adopted the r.m.s. of the observed magnitudes of the local sequence stars obtained during photometric nights only. The final errors of the SN magnitudes reported in respectively tables (see Chapter 3, 4 and 5) are computed as the square root of the quadratic sum of instrumental, calibration and S-correction (next section) errors.

Correction to standard photometric bands

In principle, the SN magnitudes can be calibrated to the standard photometric system using the colour corrections obtained with the equations 2.2. However, it is well-known that these colour corrections do not work well for SNe because of their peculiar spectra. Indeed, significant systematic differences between photometry obtained with different instruments are often observed (see Figure 2.4).

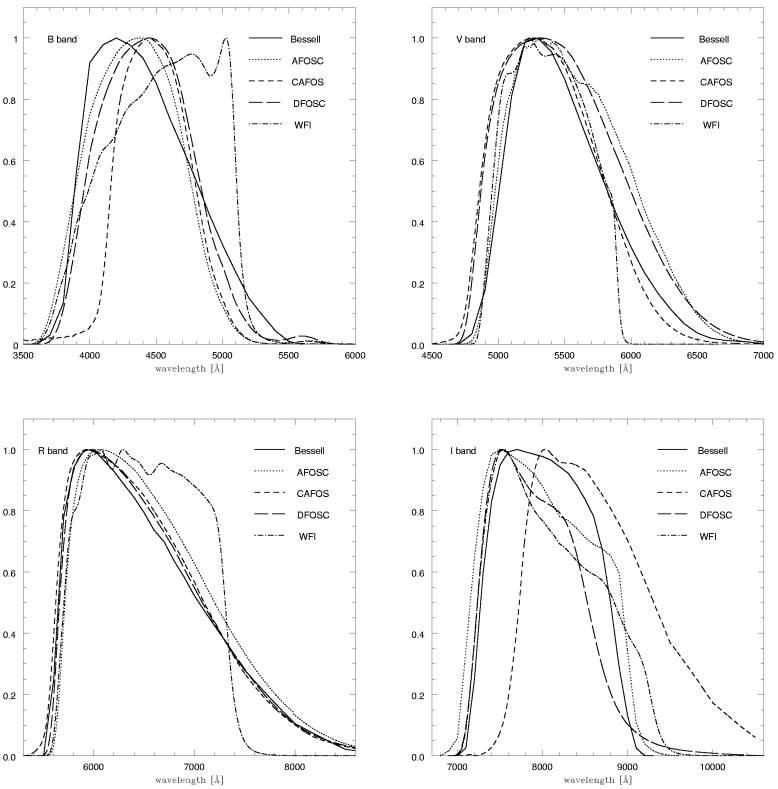

FIGURE 2.4— BVRI global passbands transmission function of AFOSC (dotted line), CAFOS (dashed line), DFOSC (long-dashed line) and WFI (dashed-dotted line). All the response function are normalized at maximum (Pignata 2004b).

Several authors Suntzeff (2000), Stritzinger et al. (2002), Krisciunas et al. (2003), Pignata et al. (2004a) and Pignata (2004b) have shown that with a

careful treatment it is possible to overcome such problems and obtain very homogeneous photometry. The procedure is sometimes called the S-correction (Stritzinger et al. 2002). The essence of the methods is that, if the SED (Spectral Energy Distribution) of the object and the response of the instruments used for the observations are both accurately known, one can put the photometry in any well-defined photometric system by means of synthetic photometry. We applied the S-correction to the photometry of the SNe of our sample following the method of Pignata et al. (2004a) who, in order to reduced the correction uncertainty introduced, do not use the colour equation (usual approach for the S-correction) and compute the calibrated SN magnitude using the following relation referred here to the B band:

$$B_{SN_{ph}} = b_{SN_{ph}} + zp_B - k_B Z + zp_B(S) \tag{2.4}$$

where $B_{SN_{ph}}$ and $b_{SN_{ph}}$ are the corrected and the instrumental SN magnitude, zp_B is the instrumental zero point at the time of the observation, k_B and Z are the absorption coefficient and airmass, and $zp_B(S)$ is a variable zero point correction that depends on the passband and the SN SED or, in other words, the difference between the SN synthetic magnitude measured using the standard passband (B_{sy}) and that computed using the instrumental passband (b_{sy}):

$$\begin{aligned} zp_B(S) = B_{sy} - b_{sy} = -2.5log \int_{-\infty}^{+\infty} F(\lambda)\, S_{st}(\lambda)\, d\lambda + zp_{B_{sy}} \\ +2.5log \frac{hc}{\lambda_{eff}} \int_{-\infty}^{+\infty} N(\lambda)\, S_{in}(\lambda)\, d\lambda + zp_{b_{sy}} \end{aligned} \tag{2.5}$$

where $F(\lambda)$ is the SED of a set of spectrophotometric standard stars (Hamuy et al. 1992; Hamuy et al. 1994) for the optical, or that of Vega, Sirius and the Sun for the IR, $N(\lambda)$ is the photon number distribution ($N(\lambda) = \frac{F(\lambda)\lambda}{hc}$, where h is the Plank constant and c the light speed), $S_{st}(\lambda)$ and $S_{in}(\lambda)$ are the standard and instrumental B passband, respectively, and $zp_{B_{sy}}$ and $zp_{b_{sy}}$ are the zero points. $N(\lambda)$ is used instead of $F(\lambda)$ for the instrumental passband because CCD are photon counting devices, therefore in CCD photometry, photons are integrated across the band.

In order to determine the instrumental passband $S_{in}(\lambda)$, we need take into account the following terms:

$$S_{in}(\lambda) = F(\lambda) QE(\lambda) A(\lambda) M(\lambda) L(\lambda) \tag{2.6}$$

where $F(\lambda)$ is the filter transmission function, $QE(\lambda)$ is the detector quantum efficiency, $A(\lambda)$ is the continuum atmospheric transmission profile, $M(\lambda)$ is the mirror reflectivity function and $L(\lambda)$ is the lens throughput. The main challenge was to obtain $S_{in}(\lambda)$ for all the facilities for which we could obtain the previously mentioned information. Once the instrumental response functions were constructed, we calculated an instrumental zero-point for each passband. With this information we then calculated the S-corrections for the BVRIJHK bands[5] by using the best flux-calibrated spectra of each SNe. Sometimes, as the epochs of our spectra did not always match the photometric coverage, we enhanced the S-correction spectral database by adding a set of spectra of other normal SNe Ia with similar features, artificially reddened to match those of the SNe of our study and properly redshifted (see Chapters 3 and 4 for more details).

Once the synthetic magnitudes for each instrumental setup were obtained, we fitted a low order polynomial to the correction terms (δM, difference between the standard magnitude measured directly using the standard passband and that computed for the instrumental setup). Some dispersion in the S-corrections for a given instrument, resulted from flux calibration errors in the observed spectra. Assuming that for each instrument the S-correction changed smoothly with time, we calculated the r.m.s. deviation with respect to the polynomial fit and used this as an estimate of the S-correction errors.

It is important to emphasize that the S-correction should be computed individually for each SN because it is a strong function of redshift, reddening and, to a lower extent, possible spectral peculiarities.

The S-correction for SNe Ia at early times is generally small. It is ≤ 0.1 in the optical and NIR bands. We note that in the R band these corrections are smallest probably because here the differences between the instrumental and standard bands are smaller. The largest corrections are those in the I band.

The differences of δM between one instrument and the other are more pronounced that those of different SNe. It is also important to note that for all instruments δB, δV and δR seem to remain constant during all the phase range. A typical example of δM evolution with time is reported in Figure 2.5. At late phases SNe Ia emit most of their flux in the B and V bands (see Figure 2.6). In this figure we see that the strong emission line at 4700 Å (Fe III) falls where the B band of WFI is almost at the peak of the sensitivity, while the Bessell filter is only around 60%, we therefore expect a significant S-correction for SNe Ia at

[5]We did not compute an S-correction for the U band since very few spectra covered this wavelength range.

this epoch measured with WFI. In general, the δM in the BVR bands at late time are larger that around maximum brightness and even if at these epochs other sources of errors become important (e.g. low signal-to-noise ratio and galaxy background contamination), they could be the dominant systematics especially in the B band.

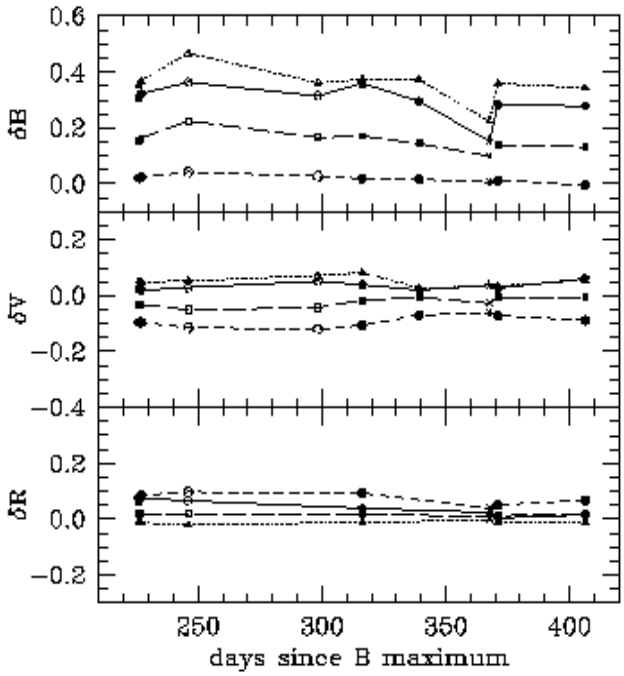

FIGURE 2.5— Late epochs evolution of δB, δV and δR introduced by different instruments for SN 1992A (filled symbols), SN 1996X (open symbols) ans SN 2002bo (skeletal symbols). The symbols connected with solid, dotted, dashed and long-dashed line refer to WFI, CAFOS, AFOSC and DFOSC, respectively.

K correction

In order to compare the intrinsic properties of objects at different redshift, one has to apply the so called K-correction, which accounts for the fact that the photometric bands sample different parts of the emitted spectrum because of the Doppler shift[6]. We have not applied the K-correction to the magnitudes of our SNe because our objects have z between 0.0041 and 0.0052 hence the K

[6]Because of Doppler effect, redshift occurs when the visible light from an object is shifted towards the red end of the spectrum. For visible light, red is the color with the longest

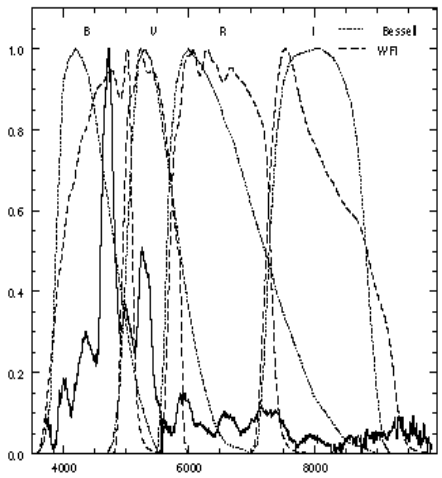

FIGURE 2.6— The BVRI Bessell (dotted line) and WFI (dashed line) passbands overplotted on spectrum of SN 1992A at 226 days after B maximum brightness.

correction is of the order of a few hundreds of a magnitude, therefore comparable to the measurement errors.

2.3.3 Spectroscopy

The spectra were reduced using standard IRAF tasks from the *ctioslit* package (used for optical and IR reduction) or FIGARO routines (used for IR reduction only) after the preliminary removal of detector signatures which includes bias, overscan (only for the optical spectra) and flat field correction as mentioned in Section 2.3.1.

Then, the one-dimensional spectrum of the SN is extracted and the galaxy contribution along with the night sky lines are subtracted via a polynomial fit. The observation of lamp spectra (usually He-Ne, He-Ar, Hg-Cd lamps), obtained with the same instrumental configuration, allows the wavelength calibration of the SN spectrum. The identification of the lines allow us to match pixel to wavelength coordinates through a WCS (World Coordinate System) transformation. As we have said, the spectrum of a calibration lamp is usually taken at the position of the supernova, in order to compensate for the bending of the instrument. The accuracy of the wavelength calibration is verified against the position of the background sky lines in the spectra and is in general

wavelength. The corresponding shift to shorter wavelengths produced by a motion toward the observer, is called blueshift.

1- 2 Å.

The next step is very important: the flux calibration. The response curve of the instrumental configuration is obtained observing spectroscopic standard stars from the lists of Oke (1990), Hamuy et al. (1992), Hamuy et al. (1994). This response curve is obtained by comparing the observed standard star spectrum to the flux tabulated for that star. The flux calibration is typically accurate within 20%. Errors can be produced because the supernova and/or the flux standard star have been observed under poor photometric conditions or when the object has not been perfectly centered in the slit.

Broad telluric absorptions contaminate the SN spectra which can be removed if a spectrum of a standard star obtained with the same resolution is available. Telluric absorptions are identified and removed from the observed spectrum which is then divided by the original one. The resulting spectrum (equal to 1 everywhere, except in coincidence with the telluric bands) is multiplied by the object spectrum.

For the atmospheric extinction correction, we used the average extinction curves available for each site.

To obtain full wavelength coverage in the optical region, we combined the spectra obtained using different grating/grisms. The absolute flux calibration of the spectra is checked against photometry and when necessary, the flux scale is adjusted to match the photometry. To this, we use the Pogson formula

$$\delta I_i = 10^{-0.4(M_{i,phot} - M_{i,spec})} \tag{2.7}$$

where δI_i is the factor needed to scale the original spectrum.

It is important to point out that most spectra were obtained with the slit oriented along the parallactic angle in order to minimize differential losses due to atmospheric refraction (Filippenko 1982).

Additional processing required for the analysis of SN spectra are the correction for redshift of the host galaxy (it is necessary to identify the spectral lines and to estimate the expansion velocities) and the correction for interstellar extinction (it is necessary to compute the continuum temperature and obtain accurate measures).

The near-IR spectra were reduced using standard procedures in IRAF and FIGARO 4 environments. Wavelength calibration was carried out using a Xe arc and the accuracy of the solution was checked using OH sky lines. Flux calibration was carried out with respect to near-IR standard stars observed close in time and airmass to the SN. Flux calibration was checked against the photometry as in the optical and scaled to match the latter.

3

Peculiar extinction towards the Type Ia SN 2003cg

Stanley è un'astronauta
poporo poporo.
Demetrio Magrin

We present in this Chapter the optical and near-infrared photometry and spectroscopy of the unusually reddened Type Ia SN 2003cg and discuss the techniques applied for data reduction in Section 3.1. The large set and the high quality of the data along with the high reddening allow a detailed study of the reddening law toward this, otherwise normal SN Ia. The reddening law results atypical findings a small value of R_V (see Section 3.2). A detailed analysis of the light curves and spectra are described on Sections 3.3 and 3.4, respectively.

SN 2003cg was discovered on 2003 March 21.51 UT by Itagati and Arbour (IAUC 8097) at 14″E and 5″N from the centre of the nearby spiral galaxy NGC 3169 (Figure 3.1). The SN is projected on a dust lane, already suggesting that the SN light might be heavily extinguished. Some days later, Kotak, Meikle & Patat (2003) and Matheson et al. (2003) classified SN 2003cg as a highly-reddened normal Type Ia SN, of epoch a few days before maximum. Indeed the Si II line at λ6355, typical of these type of SNe was visible (see Figure 3.2) with a expansion velocity estimate around 11500 $\mathrm{km\,s^{-1}}$. The spectrum shows very strong, multicomponent Na ID interstellar absorption lines at the velocity of the host galaxy. Several other narrow absorptions are present in the spectrum

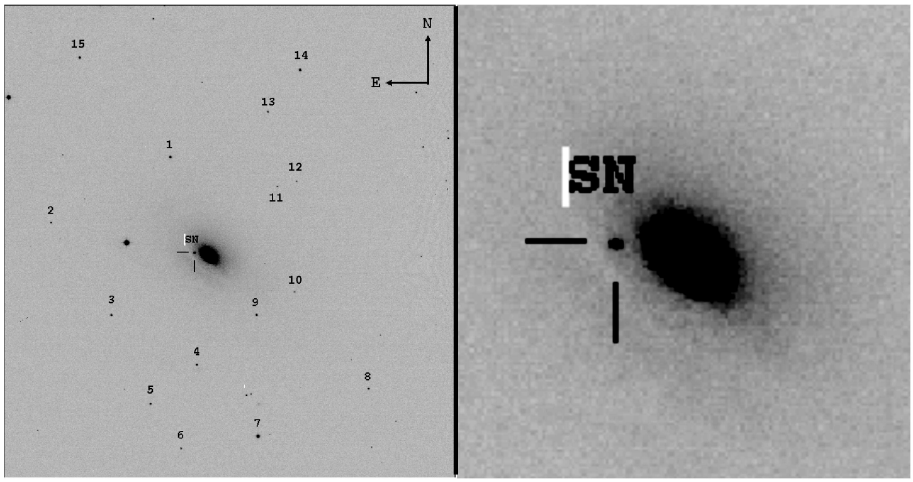

FIGURE 3.1— V band image of SN 2003cg in NGC 3169 taken with the ESO/MPI 2.2m+WFI on 2003 April 03 (FoV $\sim 8'.5 \times 9'.0$). Local sequence stars are indicated (cf. Table 3.2).

that appear coincident with known diffuse interstellar bands (e.g., 5449, 5780, 6283 Å, etc) at the host velocity. The overall shape of the spectrum declines toward the blue, implying that the supernova is heavily extinguished by dust. The object appeared therefore an ideal target for studying to absorption toward Type Ia SNe.

SN 2003cg exploded in NGC 3169, a nearby (v_r=1238 km s^{-1}), elongated Sa galaxy with narrow, distorted arms. It has a total B magnitude of 11.08 with a prominent dust lane. SN 1984E also exploded in NGC 3169. This was a Type IIL SN with a B magnitude at maximum of 15.2. A comparison of the colour curve with the intrinsic ones of other Type II SNe (Metlova 1985) yielded E(B−V) = 0.1 ± 0.05 for this older event. It exhibited evidence of pre-explosion superwinds (Dopita et al. 1984; Gaskell 1984; Gaskell & Keel 1986; Henry & Branch 1987) similar to those of SNe 1994aj, 1996L and 1996al (Benetti 2000).

3.1 Data acquisition and reduction

In view of the early discovery epoch of the SN, its favorable position on the sky ($\alpha = 10^h14^m15\overset{s}{.}97, \delta = +03^o28'02\overset{''}{.}50$, 2000.0) and the proximity of the host galaxy (v_r=1238 km s^{-1}), an extensive observational campaign was immediately triggered with all the telescopes available to the ESC. Using 13 different

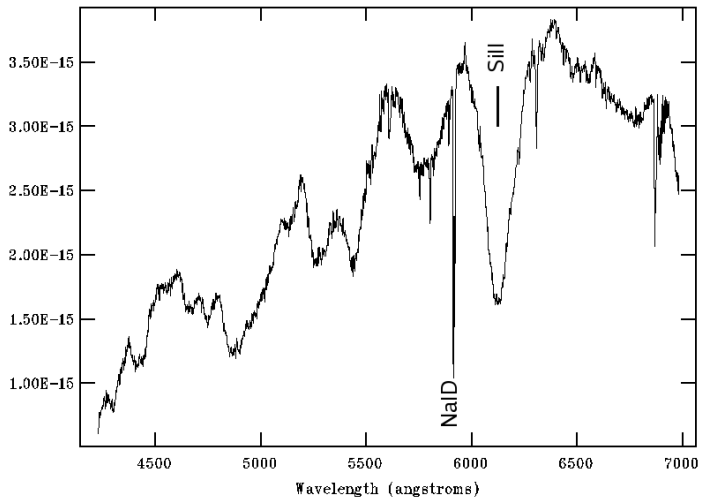

FIGURE 3.2— First monodimensional spectrum of SN 2003cg taken with the WHT+ISIS on 2003 March 22 used by Kotak, Meikle & Patat (2003) for the classification of this SN. Pointed out are also the Si II line (λ6355) and the multicomponent Na ID interstellar absorption lines.

instrumental configurations, we obtained optical and NIR data from day -8.5 to +414 relative to B band maximum light. The observational programme comprised 74 photometric epochs and 35 spectra.

3.1.1 Photometric observations

The SN 2003cg observations were processed as described in Chapter 2. Standard pre-processing (trimming, overscan and bias corrections, flat-fielding) was first carried out. Then, for the early-time optical photometry, the instrumental optical magnitudes of the SN (Table 3.1) and the local standards (Table 3.2) were measured using the IRAF point-spread-function (PSF) fitting routine. These local standards in the SN field (see Figure 3.1) were also used to calibrate the SN brightness on non-photometric nights. To calibrate the local standards, and to find the colour terms for the various instrumental setups, average values for 20 photometric nights were obtained (marked in Table 3.1). These were then calibrated via standard Landolt fields (Landolt 1992).

For the early-time IR magnitudes, additional reduction steps were required viz. sky subtraction, and image coaddition to improve the signal-to-noise (see

Table 3.3). As for the optical photometry, the IR magnitudes were obtained using PSF-fitting. For night-to-night calibration we used a smaller local sequence than in the optical. However, as the number of IR standard fields observed each night was small, we adopted average colour terms provided by the telescope teams. The IR magnitudes of the local sequence stars are given in Table 3.2.

SN 2003cg was also observed at late phases. In this case, determination of the SN magnitudes made use of template subtraction. The template images were taken with VLT-UT2+FORS1 on February 1, 2005, around 673 days post-explosion, when the supernova was no longer visible. The late-time magnitudes of SN 2003cg are included in Table 3.1.

3.1.2 Spectroscopic observations

The spectra were reduced using standard IRAF (used for optical and IR reduction) or FIGARO (used for IR reduction only) routines (see Section 2.3.3 for more details). For most spectra the errors in the wavelength calibration are $< \pm$ 2 Å and the flux calibration is typically accurate within $\pm$ 10 - 20%. The details of the spectroscopic observations are summarised in Tables 3.4 & 3.5. The tables give the observation date, the Modified Julian Day, the phase relative to B_{max}, the wavelength range and the instruments used.

3.1.3 Correction to standard photometric bands

As indicated in Tables 3.1 & 3.3, we used ten different instruments to collect the photometry of SN 2003cg from U to K band. In order to convert the photometry of the target to a standard system we applied S-corrections to our data following the method of Pignata et al. (2004a) (see Section 2.3.2).

We computed the S-corrections for the BVRIJHK by using the best flux-calibrated spectra of SN 2003cg and considering also a set of spectra of SN 1994D (Patat et al. 1996), artificially reddened to match those of SN 2003cg (see Section 3.2 for more details) in order to have a complete set for every date. Indeed the features of the SNe 1994D and 2003cg spectra are very similar. At late times (nebular phase) we have only one optical spectrum of SN 2003cg. We therefore used the spectra of other normal SNe Ia: 1992A (Suntzeff 1996); 1994D (Patat et al. 1996), 1996X (Salvo et al. 2001), 2002bo (Benetti et al. 2004a), 2002dj (Pignata et al. in preparation) and 2004eo (Pastorello et al. in preparation).

TABLE 3.1— Original optical photometry of SN 2003cg.

date	JD (+2400000.00)	Phase* (days)	U	B	V	R	I	Instr.
13/03/03	52711.80	-18.1	-	-	-	19.0	-	UNF
22/03/03	52720.80	-9.1	-	-	-	14.9	-	UNF
23/03/03◁	52722.44	-7.5	17.03 ± 0.19	16.49 ± 0.06	15.27 ± 0.04	14.58 ± 0.02	14.14 ± 0.07	CAF
24/03/03◁	52723.04	-6.9	16.91 ± 0.08	16.35 ± 0.03	15.24 ± 0.03	14.55 ± 0.02	14.07 ± 0.02	SSO
24/03/03	52723.06	-6.9	-	16.34 ± 0.03	15.21 ± 0.04	14.50 ± 0.03	14.00 ± 0.03	BAO
25/03/03◁	52723.94	-6.0	16.77 ± 0.04	16.22 ± 0.01	15.09 ± 0.01	14.44 ± 0.02	13.95 ± 0.01	SSO
26/03/03	52725.03	-4.9	-	16.13 ± 0.20	14.99 ± 0.36	14.29 ± 0.06	-	BAO
26/03/03	52725.32	-4.7	-	16.09 ± 0.02	14.92 ± 0.03	14.29 ± 0.02	13.85 ± 0.03	ASI
27/03/03	52726.35	-3.6	-	16.03 ± 0.02	14.84 ± 0.03	14.27 ± 0.02	13.84 ± 0.04	ASI
28/03/03◁	52726.52	-3.5	16.67 ± 0.02	16.08 ± 0.03	14.85 ± 0.02	14.24 ± 0.03	13.77 ± 0.02	WFI
28/03/03	52727.01	-3.0	-	16.02 ± 0.19	14.82 ± 0.03	14.19 ± 0.04	13.82 ± 0.03	BAO
29/03/03	52727.52	-2.5	-	15.99 ± 0.04	14.78 ± 0.06	14.18 ± 0.03	13.84 ± 0.03	ASI
29/03/03	52728.07	-1.9	-	15.98 ± 0.06	14.82 ± 0.02	14.17 ± 0.05	13.80 ± 0.05	BAO
01/04/03	52731.33	1.4	-	15.97 ± 0.03	14.72 ± 0.05	14.15 ± 0.05	13.86 ± 0.03	ASI
02/04/03◁	52731.66	1.7	16.79 ± 0.03	16.05 ± 0.02	14.74 ± 0.06	14.15 ± 0.02	13.88 ± 0.03	WFI
04/04/03◁	52733.62	3.7	16.87 ± 0.09	16.10 ± 0.02	14.76 ± 0.03	14.18 ± 0.02	13.95 ± 0.04	WFI
04/04/03	52734.12	4.2	-	16.04 ± 0.05	14.79 ± 0.05	14.19 ± 0.04	13.97 ± 0.03	BAO
04/04/03	52734.39	4.4	16.89 ± 0.10	16.05 ± 0.03	14.83 ± 0.03	14.24 ± 0.03	14.00 ± 0.06	TGD
07/04/03	52737.01	7.1	-	16.22 ± 0.08	14.93 ± 0.04	14.35 ± 0.05	14.12 ± 0.03	BAO
07/04/03	52737.30	7.3	-	16.25 ± 0.04	14.92 ± 0.04	14.39 ± 0.07	14.08 ± 0.05	ASI
09/04/03◁	52739.40	9.4	17.26 ± 0.02	16.45 ± 0.01	14.99 ± 0.03	14.56 ± 0.02	14.27 ± 0.04	TGD
11/04/03	52741.37	11.4	17.51 ± 0.01	16.65 ± 0.05	15.13 ± 0.03	14.68 ± 0.04	14.37 ± 0.03	TGD
12/04/03◁	52742.40	12.4	17.69 ± 0.04	16.79 ± 0.01	15.17 ± 0.02	14.73 ± 0.04	14.33 ± 0.06	CAF
14/04/03◁	52743.57	13.6	18.06 ± 0.13	16.93 ± 0.01	15.19 ± 0.02	14.78 ± 0.01	14.36 ± 0.02	WFI
15/04/03	52744.52	14.6	18.10 ± 0.03	17.13 ± 0.01	15.26 ± 0.02	14.81 ± 0.01	14.37 ± 0.02	WFI

date	JD (+2400000.00)	Phase* (days)	U	B	V	R	I	Instr.
16/04/03	52745.58	15.6	18.40 ± 0.03	17.22 ± 0.04	15.30 ± 0.03	14.82 ± 0.02	14.30 ± 0.03	WFI
17/04/03	52746.59	16.6	18.78 ± 0.05	17.34 ± 0.03	15.33 ± 0.02	14.83 ± 0.02	14.24 ± 0.02	WFI
18/04/03	52747.61	17.6	18.93 ± 0.04	17.42 ± 0.02	15.41 ± 0.02	14.84 ± 0.01	14.24 ± 0.02	WFI
19/04/03	52748.54	18.6	19.04 ± 0.02	17.57 ± 0.02	15.42 ± 0.03	14.85 ± 0.02	14.22 ± 0.02	WFI
20/04/03◁	52749.57	19.6	19.26 ± 0.05	17.68 ± 0.03	15.47 ± 0.01	14.85 ± 0.01	14.20 ± 0.02	WFI
21/04/03◁	52750.64	20.7	19.29 ± 0.02	17.77 ± 0.02	15.53 ± 0.02	14.87 ± 0.02	14.17 ± 0.01	WFI
21/04/03	52751.48	21.5	19.30 ± 0.03	17.92 ± 0.02	15.54 ± 0.02	14.90 ± 0.02	14.17 ± 0.01	WFI
23/04/03◁	52752.51	22.5	19.48 ± 0.02	17.98 ± 0.01	15.60 ± 0.01	14.90 ± 0.01	14.15 ± 0.01	WFI
23/04/03	52753.45	23.5	-	18.09 ± 0.08	-	14.93 ± 0.02	14.16 ± 0.03	ASI
24/04/03◁	52753.69	23.7	19.57 ± 0.09	18.17 ± 0.02	15.65 ± 0.03	14.92 ± 0.01	14.11 ± 0.02	WFI
25/04/03◁	52754.51	24.5	19.73 ± 0.03	18.26 ± 0.01	15.69 ± 0.08	14.93 ± 0.01	14.15 ± 0.01	WFI
25/04/03◁	52755.50	25.5	19.84 ± 0.02	18.34 ± 0.01	15.78 ± 0.01	14.99 ± 0.02	14.13 ± 0.01	WFI
26/04/03	52756.35	26.4	-	-	15.90 ± 0.02	15.02 ± 0.02	-	CAF
27/04/03◁	52756.61	26.6	19.91 ± 0.02	18.46 ± 0.01	15.82 ± 0.01	15.06 ± 0.01	14.12 ± 0.01	WFI
28/04/03◁	52757.50	27.5	19.90 ± 0.02	18.57 ± 0.01	15.94 ± 0.01	15.09 ± 0.01	14.16 ± 0.01	WFI
29/04/03	52759.01	29.1	-	-	-	15.18 ± 0.03	14.23 ± 0.04	BAO
30/04/03	52759.63	29.7	20.24 ± 0.04	18.80 ± 0.01	16.08 ± 0.01	15.23 ± 0.01	14.25 ± 0.02	WFI
30/04/03	52760.00	30.0	-	-	16.12 ± 0.11	15.23 ± 0.04	14.30 ± 0.09	BAO
02/05/03	52761.65	31.7	20.28 ± 0.02	18.94 ± 0.03	16.14 ± 0.05	15.38 ± 0.02	14.44 ± 0.02	WFI
02/05/03	52762.49	32.5	20.31 ± 0.03	18.98 ± 0.05	16.19 ± 0.02	15.44 ± 0.02	14.52 ± 0.02	WFI
04/05/03	52763.51	33.5	20.48 ± 0.05	19.06 ± 0.03	16.25 ± 0.02	15.52 ± 0.02	14.58 ± 0.01	WFI
05/05/03	52765.49	35.5	20.43 ± 0.03	19.05 ± 0.02	16.41 ± 0.01	15.63 ± 0.03	14.70 ± 0.01	WFI
07/05/03◁	52766.51	36.5	20.43 ± 0.03	19.04 ± 0.01	16.44 ± 0.01	15.69 ± 0.02	14.80 ± 0.01	WFI
07/05/03	52767.35	37.4	-	-	16.47 ± 0.07	-	-	ASI
07/05/03	52767.49	37.5	20.55 ± 0.05	19.10 ± 0.02	16.50 ± 0.01	15.73 ± 0.02	14.87 ± 0.02	WFI

date	JD (+2400000.00)	Phase* (days)	U	B	V	R	I	Instr.
08/05/03◁	52768.35	38.4	-	19.10 ± 0.09	-	15.79 ± 0.03	14.91 ± 0.05	ASI
09/05/03	52768.87	38.9	-	19.05 ± 0.07	16.66 ± 0.03	15.80 ± 0.05	14.96 ± 0.01	SSO
17/05/03	52777.02	47.1	-	-	16.99 ± 0.04	16.15 ± 0.03	15.29 ± 0.05	BAO
22/05/03	52782.44	52.5	20.64 ± 0.07	19.26 ± 0.03	17.03 ± 0.04	16.37 ± 0.04	15.66 ± 0.04	TGD
23/05/03	52783.34	53.4	-	-	17.03 ± 0.10	16.39 ± 0.05	15.69 ± 0.03	ASI
31/05/03	52791.42	61.5	20.78 ± 0.09	19.33 ± 0.02	17.39 ± 0.04	16.60 ± 0.02	16.14 ± 0.08	TGO
07/06/03	52797.86	67.9	-	-	-	-	16.22 ± 0.12	SSO
19/06/03◁	52809.52	79.6	-	19.58 ± 0.03	17.75 ± 0.01	17.21 ± 0.01	16.76 ± 0.02	WFI
25/06/03	52815.51	85.5	-	19.60 ± 0.02	17.95 ± 0.02	17.38 ± 0.03	16.91 ± 0.07	WFI
20/11/03	52963.70	233.7	-	-	21.09 ± 0.09	20.75 ± 0.06	-	ASI
31/01/04	53035.73	305.8	-	23.02 ± 0.18	21.68 ± 0.04	21.23 ± 0.28	20.01 ± 0.17	TGD
19/04/04	53114.58	384.6	-	24.12 ± 0.07	22.95 ± 0.12	22.59 ± 0.08	21.58 ± 0.02	FOR
07/05/04	53133.47	413.5	-	24.74 ± 0.17	22.92 ± 0.14	22.22 ± 0.05	21.89 ± 0.04	FOR
14/12/04	53353.79	623.8	-	> 23.60	> 22.63	> 23.18	> 21.53	WFI

* Relative to B_{max} (JD=2452729.90)

◁ Photometric night

UNF = Unfiltered CCD frames taken with a 0.60-m, Japan (Itagati & Arbour 2003); CAF = Calar Alto 2.2m + CAFOS + CCD SITe 0.53″/px; SSO = Siding Spring Observatory 2.3m + CCD 0.59″/px; BAO = Beijing Astronomical Observatory 0.85m + CCD 0.45″/px; ASI = Asiago 1.82m Copernico telescope + AFOSC 0.47″/px; TGD = Telescopio Nazionale Galileo + DOLORES 0.28″/px; TGO = Telescopio Nazionale Galileo + OIG 0.07″/px; WFI = ESO/MPI 2.2m + WFI 0.24″/px; FOR = ESO VLT-UT2 + FORS1 0.20″/px

TABLE 3.2— Magnitudes for the local sequence stars identified in the field of SN 2003cg coded as in Figure 3.1.

star	U	B	V	R	I	J	H	K
1	17.15 ± 0.01	16.04 ± 0.01	14.97 ± 0.01	14.27 ± 0.01	13.73 ± 0.01	13.18 ± 0.03	12.63 ± 0.02	12.45 ± 0.01
2	17.39 ± 0.01	17.46 ± 0.01	16.85 ± 0.01	16.49 ± 0.01	16.08 ± 0.01	-	-	-
3	18.43 ± 0.02	17.32 ± 0.01	16.14 ± 0.01	15.37 ± 0.01	14.69 ± 0.01	14.00 ± 0.04	13.26 ± 0.04	13.11 ± 0.03
4	16.96 ± 0.01	16.67 ± 0.01	15.91 ± 0.01	15.47 ± 0.01	15.03 ± 0.01	14.63 ± 0.03	14.10 ± 0.03	13.98 ± 0.04
5	19.70 ± 0.03	18.55 ± 0.01	17.09 ± 0.01	16.18 ± 0.00	15.27 ± 0.02	-	-	-
6	20.54 ± 0.07	19.52 ± 0.01	18.07 ± 0.01	17.18 ± 0.02	16.41 ± 0.02	-	-	-
7	13.70 ± 0.01	13.75 ± 0.01	13.25 ± 0.01	12.88 ± 0.01	12.55 ± 0.02	-	-	-
8	17.56 ± 0.01	17.29 ± 0.01	16.52 ± 0.01	16.13 ± 0.01	15.69 ± 0.01	-	-	-
9	16.41 ± 0.01	16.34 ± 0.01	15.61 ± 0.01	15.19 ± 0.01	14.75 ± 0.01	14.26 ± 0.02	13.77 ± 0.01	13.67 ± 0.02
10	18.22 ± 0.01	18.32 ± 0.01	17.79 ± 0.01	17.48 ± 0.01	17.10 ± 0.01	16.74 ± 0.04	16.48 ± 0.02	16.37 ± 0.01
11	-	21.18 ± 0.01	19.57 ± 0.02	18.24 ± 0.01	16.41 ± 0.01	15.08 ± 0.03	14.48 ± 0.03	14.21 ± 0.04
12	18.08 ± 0.01	17.95 ± 0.01	17.28 ± 0.01	16.90 ± 0.01	16.54 ± 0.01	16.21 ± 0.03	15.85 ± 0.01	15.85 ± 0.04
13	19.73 ± 0.01	18.41 ± 0.01	17.16 ± 0.01	16.37 ± 0.01	15.75 ± 0.01	-	-	-
14	14.67 ± 0.02	14.46 ± 0.01	14.27 ± 0.01	14.12 ± 0.01	13.98 ± 0.01	-	-	-
15	18.70 ± 0.01	17.42 ± 0.01	16.05 ± 0.01	15.19 ± 0.01	14.32 ± 0.01	-	-	-

TABLE 3.3— Original near-IR photometry of SN 2003cg.

Date	JD (+2400000.00)	Phase* (days)	J	H	K	Instr.
25/03/03◁	52723.56	-6.4	13.71 ± 0.04	13.68 ± 0.05	13.50 ± 0.01	SofI
28/03/03◁	52726.55	-3.4	13.56 ± 0.08	13.61 ± 0.10	13.42 ± 0.01	SofI
10/04/03◁	52740.46	10.5	15.18 ± 0.01	14.03 ± 0.01	13.90 ± 0.02	SofI
12/04/03◁	52742.48	12.5	15.24 ± 0.12	13.92 ± 0.10	13.75 ± 0.01	SofI
20/04/03◁	52749.67	19.7	14.89 ± 0.17	13.66 ± 0.01	13.59 ± 0.01	SofI
24/04/03◁	52753.68	23.7	14.76 ± 0.13	13.61 ± 0.03	13.51 ± 0.02	SofI
01/05/03◁	52760.53	30.6	14.49 ± 0.01	13.83 ± 0.02	13.82 ± 0.02	SofI
09/05/03◁	52769.48	39.5	15.15 ± 0.09	14.26 ± 0.10	14.34 ± 0.09	SofI
28/05/03◁	52788.45	58.5	16.55 ± 0.08	15.08 ± 0.01	15.11 ± 0.02	SofI
16/04/04◁	53111.17	381.2	19.80 ± 0.81	19.00 ± 0.51	20.48 ± 0.69	Isaac
18/05/04◁	53143.51	413.5	20.09 ± 0.21	19.29 ± 0.13	20.55 ± 0.32	Isaac

* Relative to B_{max} (JD=2452729.40)
◁ Photometric night
SofI = ESO NTT + SofI 0.29″/px; Isaac = ESO VLT-UT1 + Isaac 0.15″/px

For the early-time NIR corrections we used the extensive spectral sequences of SN 2002bo (Benetti et al. 2004a) together with the spectra of SN 2003cg. NIR S-corrections at nebular epochs were not computed owing to the lack of contemporary IR spectra.

The S-corrections for SN 2003cg in the BVRI bands at early times are generally small (≤ 0.09), as seen in Table 3.6 and in Figure 3.3 (top). The 0.85m Beijing telescope data were not S-corrected since it was not possible to find the basic information needed to calculate the global response. Since they are in good agreement with the S-corrected data from other instruments as can be seen in Section 3.3.1, they have been used without S-correction. As explained in Section 2.3.2, the S-correction adopted is a low order interpolation of the data of each instrument. Our S-correction values are comparable to those obtained by Pignata et al. (2004a) for other SNe Ia observed with the same instruments the largest corrections being those in the I band. As in Pignata et al. (2004a), the WFI filter passbands differ from the standard ones by more than those of any other instrument.

The bottom panel of Figure 3.3 shows the S-correction estimated for the SN 2003cg BVRI magnitudes from 200 to 450 days after B maximum. This

TABLE 3.4— Optical spectroscopy of SN 2003cg.

Date	JD (+2400000.00)	Phase* (days)	Range (Å)	Instr.
22/03/03	52721.49	-8.5	4227-6981	WHT
23/03/03	52722.39	-7.6	3700-9350	CAF
24/03/03	52723.06	-6.9	3650-9132	SSO
25/03/03	52723.95	-6.0	3720-9153	SSO
26/03/03	52725.39	-4.6	3650-9350	ASI
29/03/03	52727.56	-2.4	4000-7773	ASI
29/03/03	52728.10	-1.9	4000-8500	BAO
30/03/03	52729.40	-0.6	3750-9196	CAF
01/04/03	52731.40	1.4	3900-9350	ASI
04/04/03	52734.40	4.4	3500-7968	TGD
07/04/03	52737.37	7.4	3700-7752	ASI
10/04/03	52739.58	9.6	3380-7970	TGD
11/04/03	52741.39	11.4	3400-8050	TGD
12/04/03	52742.36	12.4	3400-9250	CAF
16/04/03	52746.40	16.4	3500-9250	INT
19/04/03	52749.38	19.4	3800-8050	INT
23/04/03	52753.41	23.4	3800-7750	INT
23/04/03	52753.42	23.5	3800-7750	ASI
26/04/03	52756.39	26.4	3800-9350	CAF
28/04/03	52758.50	28.5	4250-7750	INT
08/05/03	52768.39	38.4	4000-7770	ASI
09/05/03	52768.87	38.9	6100-8920	SSO
13/05/03	52773.43	43.5	3810-9250	INT
22/05/03	52782.47	52.5	3500-8050	TGD
19/04/04	53114.58	384.6	4000-8050	FOR

* Relative to B_{max} (JD=2452729.40)
WHT = William Herschel Telescope + ISIS; CAF = Calar Alto 2.2m + CAFOS; SSO = Siding Spring Observatory 2.3m + Double Beam Spectrograph; ASI = Asiago 1.82m Copernico Telescope + AFOSC; BAO = Beijing Astronomical Observatory 0.85m + CCD; TGD = Telescopio Nazionale Galileo + DOLORES; INT = Isaac Newton Telescope + IDS; FOR = ESO VLT-UT2 + FORS1

TABLE 3.5— Infrared spectroscopy of SN 2003cg.

Date	JD (+2400000.00)	Phase* (days)	Range (Å)	Instr.
25/03/03	52723.64	-6.5	7970-24984	SofI+UKI
27/03/03	52725.85	-4.1	14002-25035	UKI
28/03/03	52726.52	-3.5	9367-24980	SofI
04/04/03	52733.92	3.9	14242-25030	UKI
14/04/03	52743.90	13.9	10378-25037	UKI
20/04/03	52749.60	19.6	9405-24990	SofI
21/04/03	52750.73	20.8	9400-25000	SofI
24/04/03	52753.78	23.8	10381-25033	UKI
30/04/03	52760.60	30.5	9398-24990	SofI
10/05/03	52770.10	40.1	9397-24990	SofI

* Relative to B_{max} (JD=2452729.40)
SofI = ESO NTT + SofI; UKI = United Kingdom Infrared Telescope + CGS4

work represents one of only a few examples where the S-correction has been computed at late phases. As Pignata (2004b) has already discussed, these corrections are generally larger than those around maximum light, especially in the B band. In fact, at late epochs the SNe Ia emit most of their flux in a few strong emission lines and so even small shifts in the filter passbands can produce significant variations in the instrumental magnitudes. We find evidence of dispersion in the late-time S-correction due to the low signal-to-noise ratio of the spectra and to residual galaxy background contamination, but there are no trends in the corrections for each instrument and therefore we have adopted an average constant value.

Table 3.7 and Figure 3.4 contain the NIR S-corrections for SofI. We used the same method as described above to place the magnitudes on the standard system of Persson et al. (1998). As we have mentioned before, to determine the colour terms we used the synthetic photometry of Vega, Sirius and the Sun. The corrections were, in general, quite small for SN 2003cg in JK but increased to about 0.13 magnitudes for the H band.

The final magnitudes used for the analysis of SN 2003cg are therefore the algebraic sum of the values of Tables 3.1 & 3.6 for the optical bands, and 3.3 & 3.7 for the NIR bands.

TABLE 3.6— Optical S-correction to be added to the data in Table 3.1, in order to convert the SN magnitudes to the Bessell (1990) system.

date	JD (+2400000.00)	Phase* (days)	B	V	R	I	*Instr.*[1]
23/03/03	52722.44	-7.5	−0.002(±0.010)	−0.041(±0.006)	0.006(±0.001)	−0.065(±0.003)	CAF
24/03/03	52723.04	-6.9	−0.015(±0.008)	0.005(±0.003)	−0.006(±0.005)	−0.006(±0.002)	SSO
25/03/03	52723.94	-6.0	−0.015(±0.008)	0.006(±0.003)	−0.006(±0.005)	−0.007(±0.002)	SSO
26/03/03	52725.32	-4.7	−0.015(±0.004)	0.006(±0.009)	−0.016(±0.005)	0.000(±0.009)	ASI
27/03/03	52726.35	-3.6	−0.016(±0.004)	0.003(±0.009)	−0.016(±0.005)	0.002(±0.009)	ASI
28/03/03	52726.52	-3.5	−0.064(±0.010)	−0.042(±0.009)	0.012(±0.008)	−0.014(±0.007)	WFI
29/03/03	52727.52	-2.5	−0.016(±0.004)	−0.001(±0.009)	−0.016(±0.005)	0.003(±0.009)	ASI
01/04/03	52731.33	1.4	−0.016(±0.004)	−0.011(±0.009)	−0.014(±0.005)	0.010(±0.009)	ASI
02/04/03	52731.66	1.7	−0.064(±0.010)	−0.026(±0.009)	0.011(±0.008)	0.012(±0.007)	WFI
04/04/03	52733.62	3.7	−0.064(±0.010)	−0.020(±0.009)	0.009(±0.008)	0.021(±0.007)	WFI
04/04/03	52734.39	4.4	−0.004(±0.006)	−0.050(±0.008)	−0.020(±0.002)	−0.042(±0.005)	TGD
07/04/03	52737.30	7.3	−0.018(±0.004)	−0.024(±0.009)	−0.013(±0.005)	0.021(±0.009)	ASI
09/04/03	52739.40	9.4	0.001(±0.006)	−0.039(±0.008)	−0.021(±0.002)	−0.027(±0.005)	TGD
11/04/03	52741.37	11.4	0.002(±0.006)	−0.036(±0.008)	−0.021(±0.002)	−0.022(±0.005)	TGD
12/04/03	52742.40	12.4	−0.031(±0.010)	−0.020(±0.006)	0.009(±0.001)	0.012(±0.003)	CAF
14/04/03	52743.57	13.6	−0.067(±0.010)	0.006(±0.009)	−0.005(±0.008)	0.052(±0.007)	WFI
15/04/03	52744.52	14.6	−0.068(±0.010)	0.008(±0.009)	−0.007(±0.008)	0.054(±0.007)	WFI
16/04/03	52745.58	15.6	−0.068(±0.010)	0.010(±0.009)	−0.009(±0.008)	0.057(±0.007)	WFI
17/04/03	52746.59	16.6	−0.069(±0.010)	0.013(±0.009)	−0.011(±0.008)	0.059(±0.007)	WFI
18/04/03	52747.61	17.6	−0.069(±0.010)	0.014(±0.009)	−0.013(±0.008)	0.060(±0.007)	WFI
19/04/03	52748.54	18.6	−0.070(±0.010)	0.016(±0.009)	−0.015(±0.008)	0.062(±0.007)	WFI
20/04/03	52749.57	19.6	−0.070(±0.010)	0.018(±0.009)	−0.017(±0.008)	0.064(±0.007)	WFI
21/04/03	52750.64	20.7	−0.071(±0.010)	0.020(±0.009)	−0.019(±0.008)	0.066(±0.007)	WFI
21/04/03	52751.48	21.5	−0.071(±0.010)	0.021(±0.009)	−0.021(±0.008)	0.067(±0.007)	WFI
23/04/03	52752.51	22.5	−0.072(±0.010)	0.023(±0.009)	−0.023(±0.008)	0.068(±0.007)	WFI

date	JD (+2400000.00)	Phase* (days)	B	V	R	I	*Instr.*[1]
23/04/03	52753.45	23.5	−0.049(±0.004)	−0.041(±0.009)	−0.011(±0.005)	0.046(±0.009)	ASI
24/04/03	52753.69	23.7	−0.072(±0.010)	0.024(±0.009)	−0.025(±0.008)	0.069(±0.007)	WFI
25/04/03	52754.51	24.5	−0.073(±0.010)	0.025(±0.009)	−0.027(±0.008)	0.070(±0.007)	WFI
25/04/03	52755.50	25.5	−0.073(±0.010)	0.026(±0.009)	−0.029(±0.008)	0.071(±0.007)	WFI
26/04/04	52756.35	26.4	−0.069(±0.010)	−0.006(±0.006)	0.012(±0.001)	−0.108(±0.003)	CAF
27/04/03	52756.61	26.6	−0.074(±0.010)	0.027(±0.009)	−0.031(±0.008)	0.072(±0.007)	WFI
28/04/03	52757.50	27.5	−0.074(±0.010)	0.028(±0.009)	−0.032(±0.008)	0.073(±0.007)	WFI
30/04/03	52759.63	29.7	−0.075(±0.010)	0.030(±0.009)	−0.036(±0.008)	0.075(±0.007)	WFI
02/05/03	52761.65	31.7	−0.076(±0.010)	0.030(±0.009)	−0.039(±0.008)	0.076(±0.007)	WFI
02/05/03	52762.49	32.5	−0.077(±0.010)	0.031(±0.009)	−0.040(±0.008)	0.076(±0.007)	WFI
04/05/03	52763.51	33.5	−0.077(±0.010)	0.031(±0.009)	−0.042(±0.008)	0.077(±0.007)	WFI
05/05/03	52765.49	35.5	−0.078(±0.010)	0.031(±0.009)	−0.044(±0.008)	0.078(±0.007)	WFI
07/05/03	52766.51	36.5	−0.078(±0.010)	0.031(±0.009)	−0.046(±0.008)	0.078(±0.007)	WFI
07/05/03	52767.35	37.4	−0.049(±0.004)	−0.040(±0.009)	−0.011(±0.005)	0.054(±0.009)	ASI
07/05/03	52767.49	37.5	−0.078(±0.010)	0.030(±0.009)	−0.047(±0.008)	0.078(±0.007)	WFI
08/05/03	52768.35	38.4	−0.049(±0.004)	−0.040(±0.009)	−0.011(±0.005)	0.055(±0.009)	ASI
09/05/03	52768.87	38.9	−0.016(±0.008)	0.003(±0.003)	−0.003(±0.005)	0.016(±0.002)	SSO
22/05/03	52782.44	52.5	0.011(±0.006)	−0.026(±0.008)	−0.022(±0.002)	0.001(±0.005)	TGD
23/05/03	52783.34	53.4	−0.048(±0.004)	−0.033(±0.009)	−0.011(±0.005)	0.054(±0.009)	ASI
31/05/03	52791.42	61.5	0.009(±0.006)	−0.026(±0.008)	−0.022(±0.002)	−0.002(±0.005)	TGO
07/06/03	52797.86	67.9	−0.016(±0.008)	−0.007(±0.003)	−0.002(±0.005)	0.017(±0.002)	SSO
19/06/03	52809.52	79.6	−0.070(±0.010)	0.013(±0.009)	−0.051(±0.008)	0.086(±0.007)	WFI
25/06/03	52815.51	85.5	−0.070(±0.010)	0.013(±0.009)	−0.051(±0.008)	0.086(±0.007)	WFI
20/11/03	52963.70	233.7	0.029(±0.008)	−0.096(±0.021)	0.070(±0.028)	0.097(±0.097)	ASI
31/01/04	53035.73	305.8	0.162(±0.027)	0.158(±0.051)	0.052(±0.021)	0.102(±0.023)	TGD
19/04/04	53114.58	384.6	−0.017(±0.009)	−0.092(±0.022)	0.073(±0.024)	0.053(±0.019)	FOR
07/05/04	53133.47	413.5	−0.017(±0.009)	−0.092(±0.022)	0.073(±0.024)	0.053(±0.019)	FOR

* Relative to B_{max} (JD=2452729.40)

[1] See note to Table 3.1 for the telescope coding.

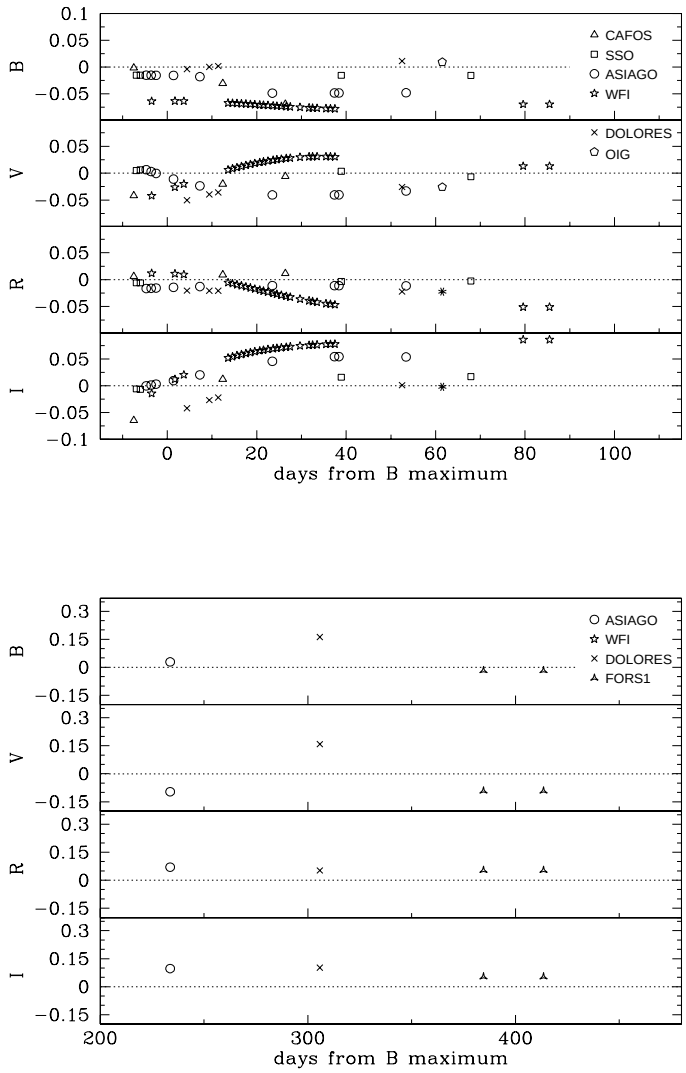

FIGURE 3.3— Summary of the S-corrections adopted for the BVRI bands of the different instruments (see legend) at early (top panel) and late (bottom panel) times. These corrections should be added to the first-order corrected SN 2003cg magnitudes (Table 3.1) in order to convert to the standard system values. The dotted line shows the zero correction.

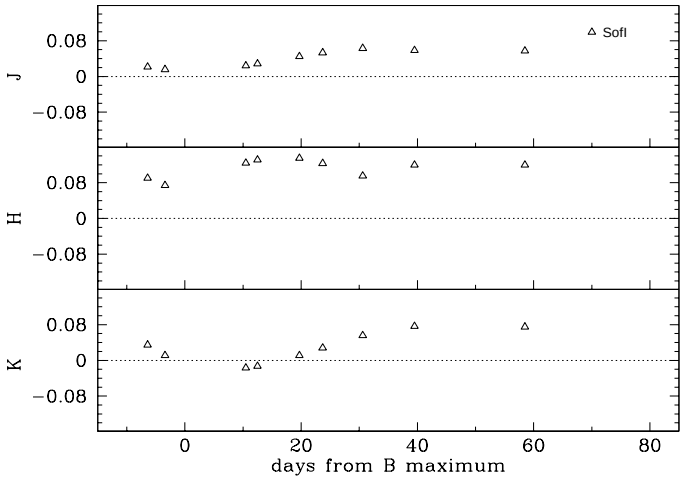

FIGURE 3.4— Summary of the S-corrections adopted for the NIR bands of the different instruments (see legend) at early time. These corrections should be added to the first-order corrected SN 2003cg magnitudes (Table 3.3) in order to convert to the standard system values. The dotted line shows the zero correction.

TABLE 3.7— NIR S-corrections to be added to the data in Table 3.3 in order to convert the SN magnitudes to the Persson et al. (1998) system.

date	JD (+2400000.00)	Phase* (days)	J	H	K	*Instr.*[1]
25/03/03	52724.06	-6.4	0.021(±0.017)	0.090(±0.023)	0.035(±0.019)	SofI
28/03/03	52727.05	-3.4	0.016(±0.017)	0.074(±0.023)	0.011(±0.019)	SofI
10/04/03	52740.96	10.5	0.024(±0.017)	0.124(±0.023)	−0.017(±0.019)	SofI
12/04/03	52742.98	12.5	0.028(±0.017)	0.131(±0.023)	−0.013(±0.019)	SofI
20/04/03	52750.17	19.7	0.045(±0.017)	0.135(±0.023)	0.011(±0.019)	SofI
24/04/03	52754.18	23.7	0.053(±0.017)	0.123(±0.023)	0.028(±0.019)	SofI
01/05/03	52761.03	30.6	0.063(±0.017)	0.095(±0.023)	0.056(±0.019)	SofI
09/05/03	52769.98	39.5	0.058(±0.017)	0.120(±0.023)	0.077(±0.019)	SofI
28/05/03	52788.95	58.5	0.057(±0.017)	0.120(±0.023)	0.075(±0.019)	SofI

* Relative to B_{max} (JD=2452729.40)

[1] See note to Table 3.3 for the telescope coding.

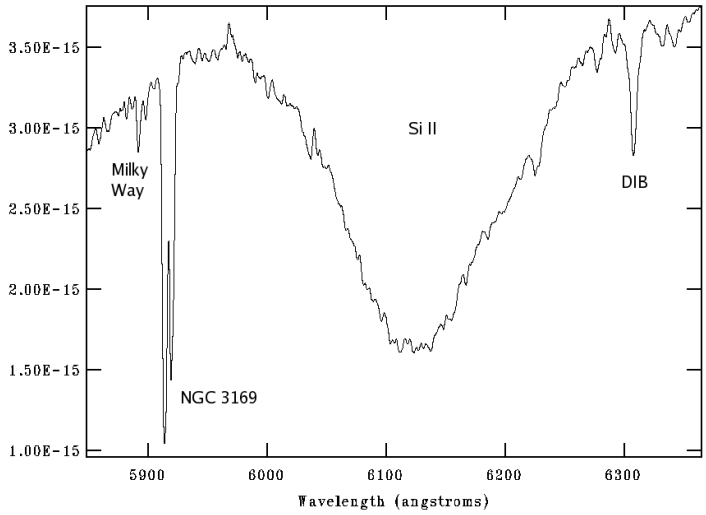

FIGURE 3.5— Detail of the interstellar Na ID region in the classification spectrum of SN 2003cg obtained on 2003 March 23 with the William Herschel Telescope (+ISIS). The components due to the Galaxy and NGC 3169 are clearly distinguishable. Also visible is a narrow absorption of a DIB at $\sim$ 6282 Å (in the rest frame).

3.2 The reddening

SN 2003cg appears projected onto a dust lane of NGC 3169 (Figure 3.1) and there are a number of indications that reddening is an important issue for this supernova. The SN 2003cg spectra exhibit strong interstellar Na ID lines at the rest wavelength of the host, plus weaker absorption at the Milky Way rest wavelength (Figure 3.5). In addition, there is a narrow absorption at $\sim$ 6282 Å not seen in normal SN Ia spectra (see Figure 3.5) which coincides with a *diffuse interstellar band* (DIB) measured in e.g. HD 183143 at 6283.86 Å by (Herbig 1995). This feature tends to be seen in the spectra of stars heavily obscured and reddened by interstellar dust, and is probably due to a variety of interstellar polyatomic molecules based on carbon (see Chapter 6). Moreover, the SED is very red at all phases.

Adopting a Virgo distance of 15.3 Mpc (Freedman et al. 2001) and a relative distance from Virgo of 1.18 for NGC 3169 (Kraan-Korteweg 1986), we estimate a distance modulus for SN 2003cg of $\mu = 31.28$. Given the observed magnitude at maximum (see Section 3.3.1), we obtain an absolute V magnitude $M_V^{max} \sim$

-16.56 before any reddening correction. This compares with $M_V^{max} = -19.46 \pm 0.05$ for a sample of nearby dereddened SNe Ia sample (Gibson et al. 2000). In addition, as we will see in Section 3.3.2, the $(B-V)_{max}$ colour is ~ 1.08 redder than typical SNe Ia, which have $(B-V)_{Bmax} \simeq 0.00 \pm 0.04$ (Schaefer 1995), again pointing to heavy reddening (see Section 3.3.2 and Figure 3.6).

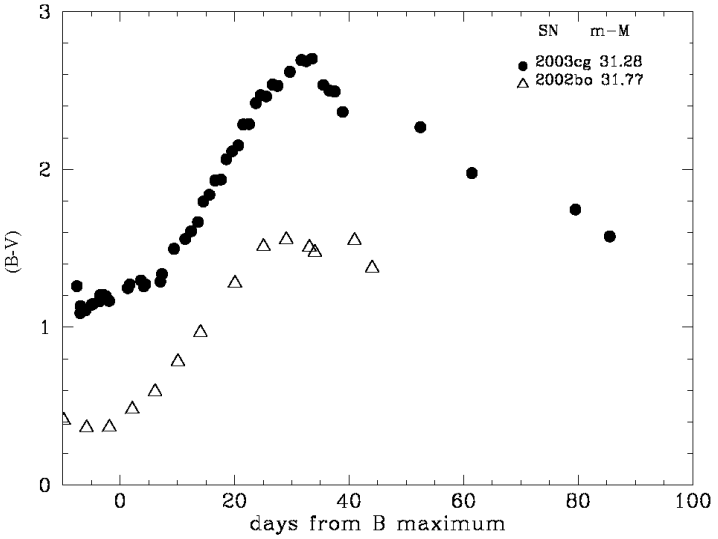

FIGURE 3.6— (B-V) colour curve of SN 2003cg (filled circles) compared with that of SN 2002bo (Benetti et al. 2004a) (empty triangles) no corrected for extinction.

From these various indicators we conclude that the light emitted by SN 2003cg is heavily reddened. We have mentioned in Chapter 1, the main property of thermonuclear SNe is their homogeneity. In this respect, SN 2003cg seems intrinsically similar to other normal SNe Ia (cf. next sections). The comparison of SN 2003cg with other SNe Ia offers therefore the rare opportunity to study the properties of the dust surrounding the SNe by the comparison of its spectroscopic and photometric properties.

3.2.1 Reddening estimate - Standard procedure

In general, extinction is a function of wavelength. For the V band it is related to the colour excess E(B−V) through the relation,

$$A_V = R_V \times E(B-V) = R_V \times (A_B - A_V), \tag{3.1}$$

where the dimensionless R_V, the ratio of total-to-selective absorption, is the slope of the extinction curve. Therefore, the problem of estimating the extinction becomes that of measuring the colour excess. Lira (1995) found that the B−V colour curve of SN Ia in the +30–+90 day interval is identical for all SNe, independent of their light curve and in particular of their Δm_{15}(B) (the B magnitude decline between the maximum and 15 days later, Phillips 1993). This indicates an E(B−V) of 1.35 for SN 2003cg (Figure 3.6). Using the standard value of $R_V = 3.1$, we obtain an intrinsic absolute magnitude of $M_V^{max} \sim$ -20.91 to be compared to the mean $M_V^{max} =$ -19.34 ± 0.05 obtained by (Gibson et al. 2000) (for $H_0 = 72$ km s^{-1} Mpc^{-1}). This implies that either this SN was exceptionally luminous, or that the adopted R_V is too large[1].

R_V has been well determined in our Galaxy by comparing the colour of reddened and unreddened stars of identical spectral type. Apart from a small dispersion at the shorter wavelengths (Seaton 1979; Savage & Mathis 1979; Cardelli, Clayton & Mathis 1989 (hereafter CCM); O'Donnell 1994; Calzetti 2001), there seems to be a remarkable homogeneity in the optical portion of the interstellar extinction curve in various Galactic directions, with a mean value of $R_V = 3.1$. However, for a few directions values ranging from $R_V =$ ∼2 to ∼5.5 have been found (Fitzpatrick 2004; Geminale & Popowski 2005). Moreover, we have relatively poor information about the extinction parameters in other galaxies (Chini & Wargau 1990; Jansen et al. 1994; Clayton 2004). In fact, several SNe Ia studies have yielded statistical evidence for lower values of R_V: 0.70 ± 0.33 (Capaccioli et al. 1990), 0.5 (Branch & Tammann 1992), 2.3 ± 0.2 (Della Valle & Panagia 1992), 2.5 ± 0.4 (Phillips et al. 1999), 1.8 (Krisciunas et al. 2000), 2.5 (Knop et al. 2003; Altavilla et al. 2004), 1.55 (Krisciunas et al. 2006), 1.1 and 3.1 (2 components) (Pozzo et al. 2006). Since R_V is related to the characteristics of dust clouds along the line-of-sight, SNe Ia may prove to be a useful probe of the grain properties.

3.2.2 Reddening estimate - an anomalous extinction law

In order to obtain a precise extinction estimate, we examine more closely the relation between A_λ and E(B−V). CCM provided analytic expressions for the average extinction law A_λ/A_V for the wavelength range $0.125\mu m \leq \lambda \leq 3.5\mu m$ parameterized with $R_V = A_V$ / E(B−V). Their analytic formulae reproduce

[1]The high luminosity of SN 2003cg could be due to a *super*-Chandrasekhar mass progenitor as it is the case of SNLS-03D3bb (SN 2003fg, Howell et al. 2006). But, after a comparison of their spectra, we can see that they are different, e.g. SN 2003cg does not present features with unusually low velocity as in SNLS-03D3bb.

the Galactic mean extinction curve (Seaton 1979; Savage & Mathis 1979) with R_V close to 3.1.

Photometric determination of the extinction

One might compute the extinction from the colour excess, E(B-V), assuming a given value of R_V. As mentioned above in the case of SN 2003cg, this yields an extinction incompatible with the absolute magnitude of SNe Ia. For SN 2003cg, we have several colour curves available which compared to the average ones of SNe Ia can provide us the extinction law. Assuming the CCM absorption law:

$$\frac{A_\lambda}{A_V} = a_\lambda + \frac{b_\lambda}{R_V}, \tag{3.2}$$

where a_λ and b_λ are wavelength-dependent coefficients, we can write the following expression:

$$E(\lambda_i - \lambda_j) \quad = \quad A_V \left[(a_{\lambda_i} - a_{\lambda_j}) + \frac{b_{\lambda_i} - b_{\lambda_j}}{R_V} \right]. \tag{3.3}$$

For the fit we have adopted the values of a_λ and b_λ given by CCM. Other values of these coefficient better suited to SNe Ia are also given by Krisciunas et al. (2006) but they are valid only around maximum light. The parameters of this equation were adjusted simultaneously to provide the values of A_V and R_V which gave the best (minimum residual) simultaneous matches to the normal SN Ia colour curves. (cf. Figure 3.7). This was achieved with $A_V = 2.62 \pm 0.29$ and $R_V = 1.97 \pm 0.29$, definitely a smaller value than the canonical $R_V = 3.1$.

Figure 3.8 shows the average differences between the observed colours and those expected for $R_V = 3.1$ and $R_V = 2.0$ (~ 1.97). This plot confirms our result that R_V is small: indeed for $R_V = 2.0$ the residuals are practically zero. In turn this provides us an estimate of the colour excess E(B-V) = 1.33 ± 0.28 (Table 3.8).

Spectroscopic determination of the extinction

An independent method for determining the extinction is via the equivalent width (EW) of the narrow interstellar Na ID doublet (see Chapter 6). This is believed to be related to the amount of dust between us and the source (Barbon et al. 1990; Munari & Zwitter 1997). Turatto, Benetti & Cappellaro (2003b) (hereafter TBC) studying a sample of SNe Ia, found that the points appear to cluster around two separate relations between EW (Na ID) and E(B−V):

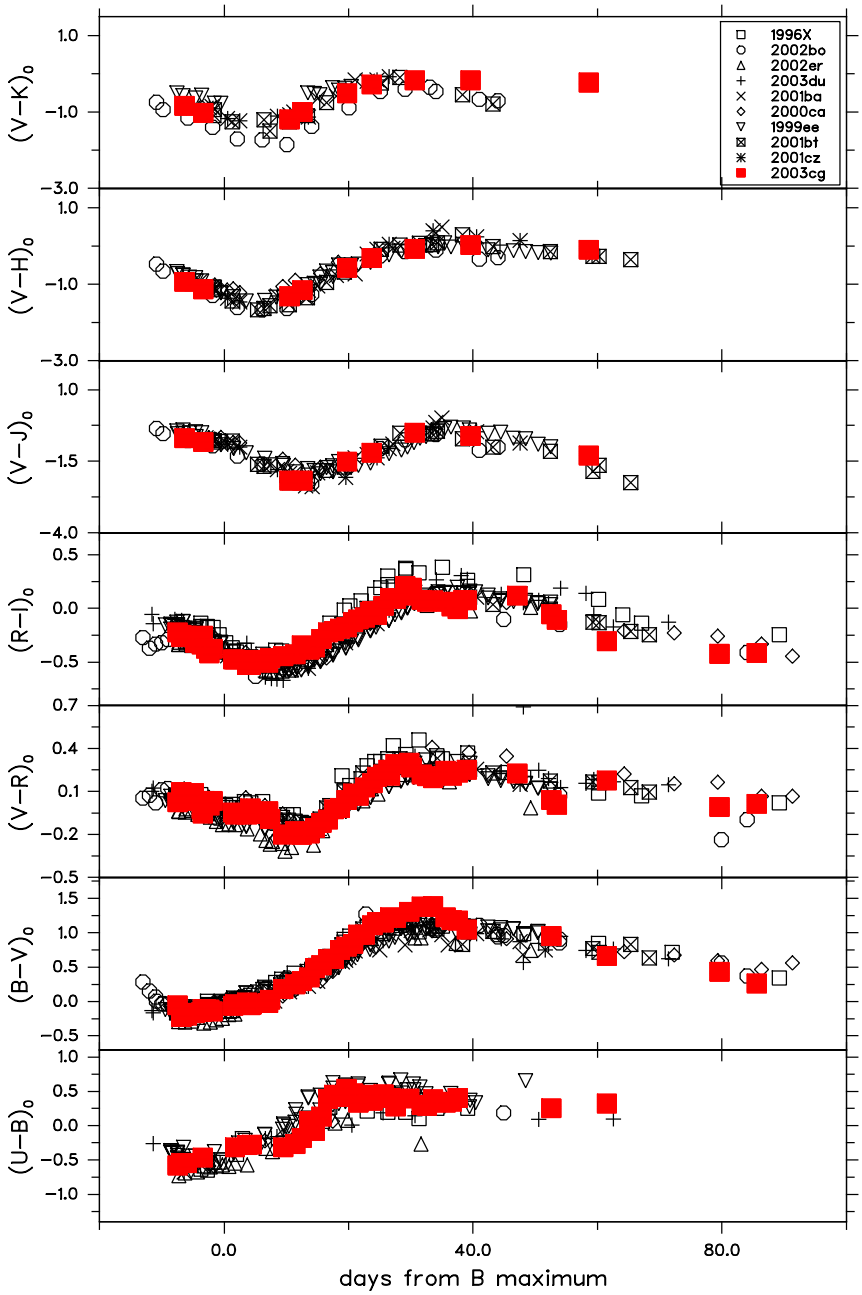

FIGURE 3.7— Intrinsic optical and NIR colour curves of SN 2003cg compared with those of SNe 2003du (Stanishev et al. in preparation), 2002er (Pignata et al. 2004a), 2002bo (Benetti et al. 2004a; Krisciunas et al. 2004b), 1996X (Salvo et al. 2001), 2001bt, 2001cz (Krisciunas et al. 2004b), 1999ee, 2000ca and 2001ba (Krisciunas et al. 2004a). For a discussion on the reddening adopted, see Section 3.2.2 ($A_V = 2.62 \pm 0.29$ and $R_V = 1.97 \pm 0.29$).

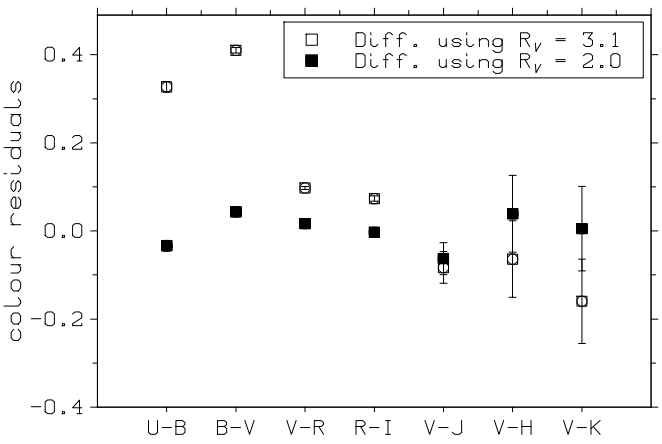

FIGURE 3.8— Differences between the observed colour excesses and those computed for R_V = 3.1 (empty symbols) and R_V = 2.0 (full symbols).

$$E(B-V) = 0.16 \times EW(NaID) \tag{3.4}$$

$$E(B-V) = 0.51 \times EW(NaID) \tag{3.5}$$

Averaged over the 25 spectra obtained for SN 2003cg, the Na ID doublet has an EW = 0.63 ± 0.07 Å for the Milky Way and EW = 5.27 ± 0.50 Å for NGC 3169. Using the relations (3.4) and (3.5) we find E(B−V) ∼ 0.10 and E(B−V) ∼ 0.32 for the Milky Way, and E(B−V) ∼ 0.84 and E(B−V) ∼ 2.69 for NGC 3169. The sum of the lower values (from relation 3.4) for the host galaxy and the Milky Way is 0.94 which is about 0.4 lower than those found with the colour curve. However, since the ratio between the Na ID component lines is close to saturation (1.24), we regard this value of E(B−V) as being a lower limit only. We also considered using the EW of the K I (7699 Å) absorption line to estimate the reddening (Munari & Zwitter 1997). Unfortunately, the spectra covering this spectral region were of insufficient resolution to detect this much weaker line.

Another way of determining the extinction law is to use the optical SED (3400-9350 Å) of SN 2003cg. We have developed a script which derives the free

TABLE 3.8— Values of the colour excess E(B−V) and the ratio of total-to-selective extinction derived from different methods.

Method	E(B−V)	R_V	Reference
$E(B\text{-}V)_{tail}$	1.35±0.13	–	Phillips et al. 1999
Colour Evolution	1.33±0.28	1.97±0.29	Section 3.2.2
Comp-CCM (94D)	1.31±0.44	1.61±0.41	Section 3.2.2
Comp-CCM (96X)	1.25±0.33	1.69±0.33	Section 3.2.2
EW of Na ID	0.94	–	TBC

parameters of a CCM extinction law by comparison of the SED of SN 2003cg with those of unreddened SNe Ia, at various coeval epochs. The reference SNe were selected to have similar light curve shapes (Δm_{15}(B)) and spectral features to SN 2003cg. Their spectra were corrected for redshift and Galactic reddening. The reference spectra were then scaled to the distance of SN 2003cg via:

$$f_{ref}^{03cg} = (\frac{d_{ref}}{d_{03cg}})^2 f_{ref}, \tag{3.6}$$

where f_{ref} is the observed flux of the reference SN at its true distance, d_{ref}, d_{03cg} are the distances of the comparison SN and SN 2003cg respectively and f_{ref}^{03cg} is the flux of the reference SN at the distance of SN 2003cg. The script divides the SN 2003cg spectra by the scaled reference spectra and calculates:

$$A_\lambda = -2.5log\frac{f_{03cg}}{f_{ref}^{03cg}}, \tag{3.7}$$

where A_λ is the total extinction at any wavelength and f_{03cg} is the observed flux of SN 2003cg. Finally, in order to compare with the CCM law (relation 3.2), we normalise the derived extinction curve to match the value of A_λ at the V band effective wavelength.

As reference we have used the spectra of SN 1994D (Δm_{15}(B) = 1.32 - Patat et al. 1996; Phillips et al. 1999) and SN 1996X (Δm_{15}(B) = 1.31 - Salvo et al. 2001). We have compared seven pairs of 94D-03cg spectra at different epochs and five pairs of 96X-03cg spectra, obtaining the parameters A_V and R_V in each case. The average values of R_V and the corresponding E(B−V) for each sets of pairs are given in Table 3.8. Two examples of this comparison are shown in Figure 3.9.

From the E(B−V) and R_V values listed in Table 3.8 (but excluding the Na ID measurement) we obtained weighted average values of E(B−V) = 1.33 ± 0.11 and $R_V = 1.80 \pm 0.20$. Using these results we can estimate the NIR colour

excesses using the basic relations between A_V, E(B−V) and R_V: $E(V-J) = 1.92$, $E(V-H) = 2.08$ and $E(V-K) = 2.20$. These values are approximately 10% smaller than those we obtained from the comparison of the colour curves reported in Table 3.9 (see also Section 3.2.2).

Up to this point we have investigated the extinction using methods which either did not involve the value of Δm_{15}(B) or where the reference SNe Ia were of similar light curve shape. If a wider diversity of SNe Ia were employed we would have to correct this parameter for the effects of reddening (see Section 3.3.1). Assuming $\Delta m_{15}(B)_{intrinsic} = 1.25$, we checked the E(B−V) using the prescription given by Reindl et al. (2005) at maximum for a sample of 111 "Branch normal" SNe Ia and tentatively for five 1991T-like, and +35 days for 59 normal SNe Ia. We obtained for the two epochs E(B−V) = 1.21 ± 0.20 and 1.25 ± 0.11 respectively, which are in excellent agreement with the estimates reported before.

This analysis confirms that the light emitted by SN 2003cg was heavily reddened. However, in order to match its intrinsic luminosity and colour evolution to those of other SNe Ia with similar light curve shapes and spectral features, it was necessary to deredden the SN 2003cg data using a value of $R_V = 1.80 \pm 0.20$. This is significantly less than the standard ISM value of 3.1.

3.2.3 Effects of a light echo?

Wang (2005) has suggested that the anomalous reddening seen towards a number of SNe Ia may be due to the effects of a dusty circumstellar cloud. In this "light-echo" (LE) scenario, not only is light scattered out of the beam, but also we see light that has been scattered into our line-of-sight. Thus, in addition to the scattering cross-section we also need to consider the (wavelength-dependent) albedo of the grains. Wang finds that a dust cloud of inner radius 10^{16}cm would produce a significant reduction in R_V. However, we suggest that there are a number of difficulties with this scenario. Firstly, the survival of grains at such a small distance from the supernova is rather unlikely. Adopting the bolometric luminosity of SN 2003cg derived below, and scaling from Dwek's (1983) analysis of SN 1979C we find that the inner radius of a dust cloud around SN 2003cg would exceed $\sim 2 \times 10^{17}$cm. Dust at this large distance would have only a modest effect on R_V (see Wang (2005) Figure 4). In addition, a nearby, dusty CSM would be expected to produce other observable effects at later times. By 50–100 days, the fastest-moving ejecta would collide with the CSM producing characteristic spectral features as seen in interacting SNe. However, no signs

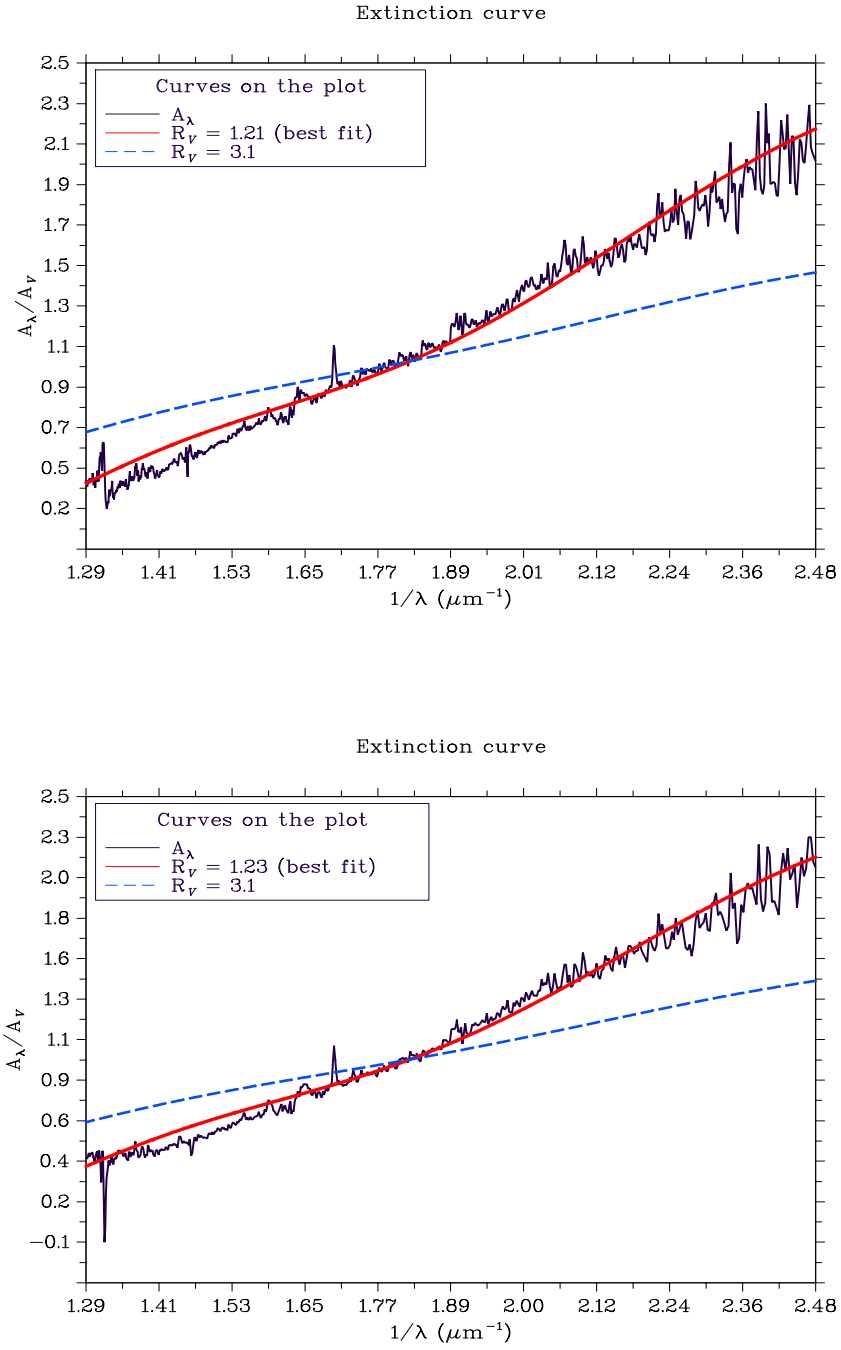

FIGURE 3.9— Best fit of theoretical CCM laws (solid line) to empirical extinction curves of SN 2003cg obtained with the pair 1994D-2003cg (top) and 1996X-2003cg (bottom) on day -2. The CCM extinction curve for $R_V = 3.1$ (dashed line) is plotted for comparison.

of such an interaction are apparent. Moreover, even if some (larger) grains survived the peak luminosity, their high temperature would produce a strong near-IR excess, as seen in types IIn SN 2002ic (Kotak et al. 2004). However, no SN Ia, including SN 2003cg, has shown such an effect. Other LE effects expected but not seen in SN 2003cg, include (a) a reduced $(B - V)$ colour range (so, that after matching the colours at maximum, at later phases one would expect the observed colour to be bluer than that of a LE-free object), (b) temporal variation in the reddening, (c) an anomalously small Δm_{15}, (d) a significantly brighter late phase tail and (e) broader spectral lines (Patat 2005). We conclude that any circumstellar dust, if present, has only a small effect on the extinction behaviour of SN 2003cg.

We conclude that the small value of R_V for SN 2003cg is most likely due to a grain size distribution where the grains are generally smaller than in the local ISM (Geminale 2006).

In the photometric and spectroscopic analysis of SN 2003cg that follows, we adopt E(B−V) = 1.33 ± 0.11 and R_V = 1.80 ± 0.20.

We consider these results one of the major successes of this thesis because (i) we have used several methods to estimate the extinction suffered by a SN, obtaining similar results, (ii) the extinction found implies that the grain size of the dust around the SN is small compared with the average value for the local ISM, and so, we can establish some characteristics of the host galaxy.

3.3 Photometry

3.3.1 Light curves

The light curve shape provides one of the main ways by which we acquire information about individual SNe. It is linked directly to the energy input and to the structure of the exploding star. However, it can also be influenced by intervening dust. In the following sections we discuss the early and late light curve phases of SN 2003cg.

Early phase

The optical (Table 3.1, 3.6) and near-IR photometry (Table 3.3) of SN 2003cg are plotted as light curves in Figure 3.10. Note in particular the excellent sampling of the optical data from –7 to +85 days. Also shown as "*R*-band" data are the unfiltered pre-discovery and discovery points of Itagati & Arbour (2003) (see below). In view of the small redshift of SN 2003cg (z=0.004), we have not applied K-corrections to any of the magnitudes. The shapes of the light curves are typical of a normal Type Ia SN e.g. (a) the occurrence of secondary maxima

TABLE 3.9— Main data of SN 2003cg and its host galaxy.

Host Galaxy Data	NGC 3169	Ref.
α (2000)	$10^h14^m15\overset{s}{.}00$	1
δ (2000)	$03°27'58''$	1
Galaxy type	SA(s)a pec	1
B magnitude	11.08	1
E(B−V)$_{Gal}$	0.031	2
$v_{r,helio}$ (km s^{-1})	1238	1
μ	31.28	3
SN Data	**SN 2003cg**	**Ref.**
α (2000)	$10^h14^m15\overset{s}{.}97$	4
δ (2000)	$03°28'02\overset{''}{.}50$	4
Offset SN-Gal. nucleus	$14''E, 5''N$	4
Discovery date (UT)	2003 March 21.51	4
Discovery date (JD)	2452719.51	4
E(B−V)$_{host}$	1.33 ± 0.11	5
$R_{V\,host}$	1.80 ± 0.20	5
A$_{V\,tot}$	2.49 ± 0.13	5
Date of B max (JD)	2452729.40 ± 0.07	5
Magnitude and epoch	U = 16.64 ± 0.03; -1.6 (days)	5
at max wrt B max	B = 15.94 ± 0.04; 0.0 (days)	5
	V = 14.72 ± 0.04; +0.8 (days)	5
	R = 14.13 ± 0.05; +0.5 (days)	5
	I = 13.82 ± 0.04; -1.7 (days)	5
	J = 13.55 ± 0.05; -2.6 (days)	5
	H = 13.69 ± 0.05; -0.2 (days)	5
	K = 13.40 ± 0.02; -0.7 (days)	5
Magnitude and epoch	I = 14.19 ± 0.02; +26.4 (days)	5
of second IJHK max	J = 14.50 ± 0.06; +31.4 (days)	5
wrt B max	H = 13.74 ± 0.02; +23.1 (days)	5
	K = 13.52 ± 0.02; +22.3 (days)	5
Estimated $\Delta m_{15}(B)_{obs}$	1.12 ± 0.04	5
Estimated $\Delta m_{15}(B)_{intrinsic}$	1.25 ± 0.05	5
t_r(B)	19.9 ± 0.5	5
stretch factor in B	0.97 ± 0.02	5
ΔC_{12}	0.39 ± 0.11	5
Absolute magnitude	M_U^{max} = -19.50 ± 0.94	5
	M_B^{max} = -19.17 ± 0.75	5
	M_V^{max} = -19.00 ± 0.49	5
	M_R^{max} = -18.78 ± 0.35	5
	M_I^{max} = -18.29 ± 0.19	5
	M_J^{max} = -18.22 ± 0.14	5
	M_H^{max} = -17.92 ± 0.11	5
	M_K^{max} = -18.08 ± 0.06	5
$\log_{10}L$	43.01 ± 0.05 (erg s^{-1})	5
E(U-B)	1.08 ± 0.13	5
E(V-R)	0.64 ± 0.06	5
E(R-I)	0.74 ± 0.11	5
E(V-J)	2.03 ± 0.20	5
E(V-H)	2.34 ± 0.09	5
E(V-K)	2.45 ± 0.23	5

(1) NED; (2) Schlegel, Finkbeiner & Davis (1998); (3) Assuming a Virgo distance of 15.3 Mpc (Freedman et al. 2001) and a relative distance from Virgo of 1.18 for NGC 3169 (Kraan-Korteweg 1986); (4) Itagati & Arbour (2003); (5) This work.

longward of the V-band (b) the increased prominence of the secondary maxima in the NIR. Also typical is that maximum light occurred before t_{Bmax} in the U, I and NIR bands, and slightly after in the V and R bands (e.g. Contardo, Leibundgut & Vacca 2000). In order to estimate the maximum light epochs and magnitudes for the different bands, we fitted low order polynomials to the light curves around their respective maxima. The results are given in Table 3.9 together with other parameters for SN 2003cg and its host galaxy.

An important light curve width/shape parameter is Δm_{15}(B). For SN 2003cg we obtain a direct measurement of $\Delta m_{15}(\mathrm{B}) = 1.12 \pm 0.04$. However, the intrinsic light curve shape may be altered by the combined effects of SED evolution and dust extinction. We corrected for this effect using the formula of Phillips et al. (1999) viz. correction = 0.1×E(B−V). For the E(B−V) derived in the previous section this gives a correction of 0.133 and hence an intrinsic value of $\Delta m_{15}(\mathrm{B}) = 1.25 \pm 0.05$. However, in view of the high reddening of SN 2003cg, we decided to check the Δm_{15}(B) correction using synthetic magnitudes obtained from its spectra. We computed Δm_{15}(B) for (a) the observed spectra and (b) the spectra corrected for Galactic and host galaxy reddening (see Sections 3.2 and 3.4). The difference between the two synthetic values is 0.128, very similar to that obtained from the formula given by Phillips et al. (1999), thus indicating that their formula is valid even at high reddening.

Another useful means of characterising the light curve shape is the stretch factor s (Perlmutter et al. 1997; Goldhaber et al. 2001; Altavilla et al. 2004). This is the factor by which an observed B-band light curve must be expanded or contracted to match a standard light curve shape. We find s = 0.97 ± 0.02 for SN 2003cg, in good agreement with that obtained via the relation $\Delta m_{15}(\mathrm{B}) = 1.98 \times (s^{-1} - 1) + 1.13$ (Altavilla et al. 2004).

In Figure 3.10, for comparison we also plot the light curves of two other nearby Type Ia SNe having similar Δm_{15}(B): SN 1994D ($\Delta m_{15}(\mathrm{B}) = 1.32$, Phillips et al. 1999) and SN 2002bo ($\Delta m_{15}(\mathrm{B}) = 1.13$, Benetti et al. 2004a). Both SNe have been: (a) shifted to the SN 2003cg distance (Section 3.3.3), (b) dereddened according to their colour excesses (0.04 - Phillips et al. 1999 and 0.38 - Stehle et al. 2005 respectively) with $R_V = 3.1$, and (c) artificially reddened with the E(B−V) and R_V values of SN 2003cg (Section 3.2). We adopt distance modules of 30.68 and 31.67, for SN 1994D and SN 2002bo, respectively (Patat et al. 1996; Benetti et al. 2004a).

With respect to the other two SNe, SN 2003cg has a broader U-band peak. This can be due to the high reddening towards SN 2003cg which shifted the bandpass to redder effective wavelengths where the light curves are broader.

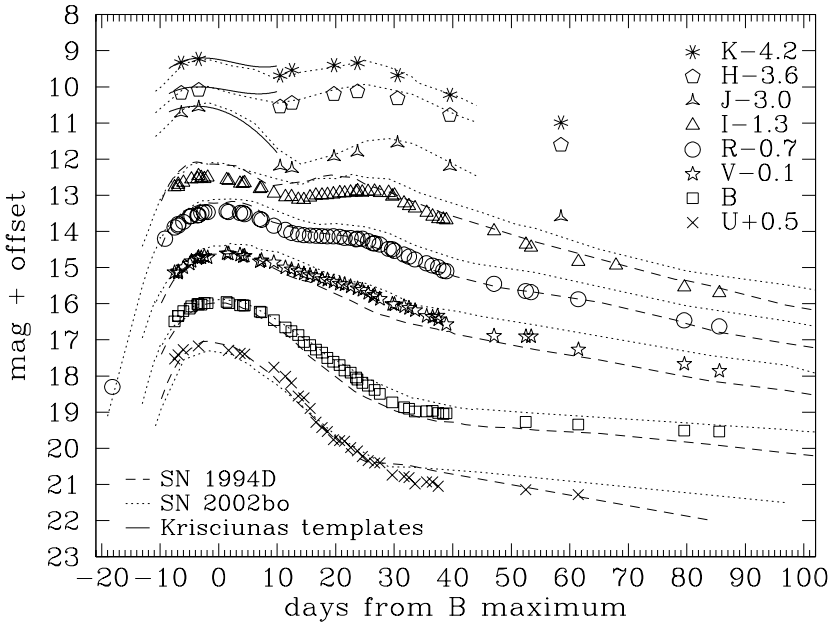

FIGURE 3.10— S-corrected optical and IR light curves of SN 2003cg during the first months post-explosion. The light curves have been shifted by the amount shown in the legend. The dashed, dotted and solid lines represent the light curves of SN 1994D (Patat et al. 1996), SN 2002bo (Benetti et al. 2004a; Krisciunas et al. 2004b) and JHK templates (Krisciunas et al. 2004a), respectively, adjusted to the SN 2003cg distance and reddening (E(B−V) = 1.33 ± 0.11 and $R_V = 1.80 \pm 0.20$).

The same effect is probably responsible for the pronounced shoulder in the V band light curve which correlates with the emergence of the secondary maxima in the light curves in the R, I and longer wavelength light curves.

SN 1994D and SN 2003cg show similar maximum magnitudes in the UBV bands but in R and I SN 1994D is brighter. In addition, the secondary maximum in I occurs approximately 8 days earlier in SN 1994D. SN 2002bo is approximately 0.5 magnitudes brighter than SN 2003cg in the VRI bands, and approximately 0.5 magnitudes fainter in the U band. In contrast with the optical bands, we find similar behaviour between SN 2003cg and SN 2002bo in the NIR bands (no NIR light curves are available for SN 1994D). We note that the H and K light curve minima of both SN 2002bo and 2003cg occur later and are more pronounced than in the Krisciunas et al. NIR template light curves

TABLE 3.10— Decline rates of SN 2003cg at late phases[1].

B	V	R	I
1.40±0.31	1.24±0.14	1.23±0.10	1.99±0.24

J	H	K
0.91±0.51	0.89±0.32	0.22±0.51

[1] Magnitude per 100 days between 233 and 385 days for optical data, and between 381 and 414 for NIR data.

Krisciunas et al. (2004a).

As already mentioned (Section 3.1), SN 2003cg was discovered about 10 days before B maximum. Along with the discovery, Itagati & Arbour (2003) report two unfiltered optical images obtained at –18.1 and –9.1 days (see Table 3.1). We judge that the magnitudes from these images most closely approximate to those which would have been obtained in the R band (Pignata et al. 2004a).

Riess et al. (1999b) suggest that the early ($t_0 \lesssim 10$ days) luminosity is proportional to the square of the time since explosion and derived an estimate of the explosion epoch t_0. Applying this relationship to the SN 2003cg R band light curve (including the two unfiltered points), we obtain $t_0(\mathrm{R}) \lesssim 2452710.0 \pm 0.6$ (JD) i.e. a risetime of 20.4 ± 0.5 days. However, for the B band is $t_r(\mathrm{B}) = 19.9 \pm 0.5$ days, significantly longer then that derived by Riess et al. (1999b) (17.71 days) for a SN Ia with a $\Delta m_{15}(\mathrm{B})$ similar to that of SN 2003cg.

Nebular phase

The optical BVRI and NIR evolution of SN 2003cg was also monitored at late phases (to over one year post-maximum). The complete light curves, covering both early and late phases, are shown in Figure 3.11, together with those of SNe 1992A (Suntzeff 1996; Altavilla et al. 2004), 1994D (Patat et al. 1996; Altavilla et al. 2004) and 1996X (Salvo et al. 2001). The evolution of the SN 2003cg optical fluxes is consistent with exponential declines in each band. The decline rates are given in Table 3.10. The late time optical evolution of the four SNe Ia is broadly similar. The BVRI light curve declines are consistent within the errors with those estimated by Turatto et al. (1990) for SNe Ia. In the NIR, only two points quite close in time are available, and the errors are large. Consequently, little can be said about the NIR decline rate (Table 3.10).

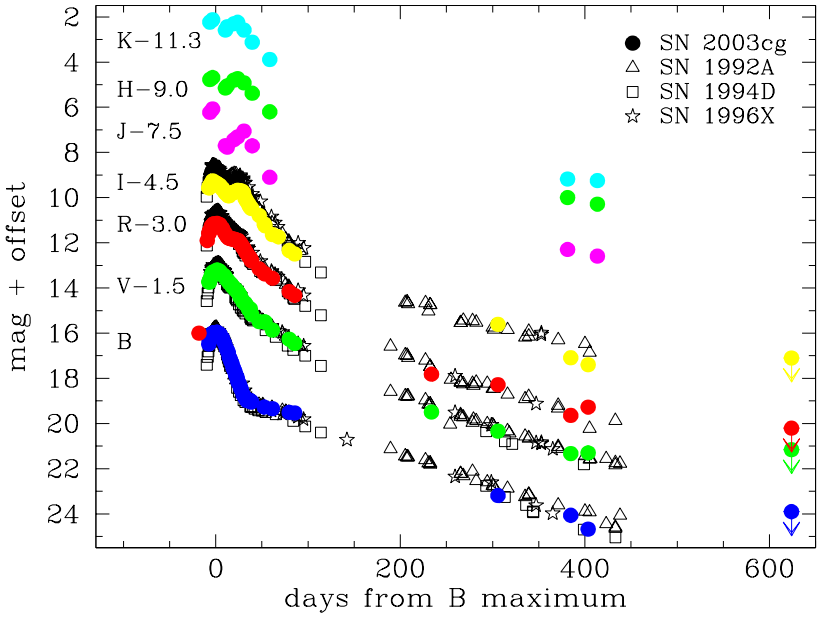

FIGURE 3.11— S-corrected BVRIJHK light curves for SN 2003cg covering early and late phases. For clarity, the light curves have been displaced vertically by the amounts shown on the right. Triangles, squares and stars represent the data of SN 1992A (Suntzeff 1996; Altavilla et al. 2004), SN 1994D (Patat et al. 1996; Altavilla et al. 2004) and SN 1996X (Salvo et al. 2001) respectively. They have been adjusted to the SN 2003cg distance and reddening (E(B−V) = 1.33 ± 0.11 with R_V = 1.80 ± 0.20). The lack of data from 3 to 7 months, and from 13 to 20 months is due to seasonal gaps.

3.3.2 Colour curves

We have already demonstrated that SN 2003cg is a heavily extinguished SN Ia. In Section 3.2 we discussed extensively the reddening of SN 2003cg and the use of the colour as an extinction indicator. In this section we discuss only the intrinsic colour evolution of the supernova.

In Figure 3.7, the intrinsic colour curves of SN 2003cg (corrected for E(B−V) = 1.33 ± 0.11 and R_V = 1.80 ± 0.20) are compared with those of other SNe Ia (cf. Section 3.2). The optical colour curves are generally very similar. The most significant difference is in the $(B-V)_0$ colour around +30 days when SN 2003cg presents a redder bump reaching a $(B-V) \sim 1.4$ (see also Figure 3.12). At maximum, SN 2003cg has $(B-V)_0 \sim -0.28$, and curiously, Phillips

et al. (1999) and Jha (2002) found $(B-V)_{Bmax}$ values of –0.09 and –0.10, respectively, for normal SNe Ia (after correction for Galactic and host galaxy extinctions). Consequently, SN 2003cg would stand out from the majority of points on the colour-colour diagram ($(U-B)_{max}$ vs. $(B-V)_{max}$) of SNe Ia shown in Figure 3.9 of Jha (2002), and so, in our case, his discussion is not applicable.

The $V-J$, $V-H$ and $V-K$ colour curves of SN 2003cg are also shown in Figure 3.7 (top panels). Again, the behaviour of SN 2003cg is very similar to that of the comparison sample. In particular, the IR colour evolution of SN 2003cg matches well that of SN 2001bt (Krisciunas et al. 2004b).

In a recent work Wang et al. (2005) introduced the colour parameter, ΔC_{12}, the (B-V) colour measured 12 days after the B maximum. This parameter depends strongly on the decline rate Δm_{15}(B) and may provide a means of estimating the reddening due to the host galaxy. They also find a correlation between the peak luminosities of SNe Ia and ΔC_{12}. For SN 2003cg, we measure $\Delta C_{12} = 0.39 \pm 0.11$.

In conclusion we emphasise that, given the reddening derived in Section 3.2, the intrinsic colour evolution of SN 2003cg is normal over a wide range of wavelengths.

3.3.3 Absolute magnitudes and the *uvoir* light curve

For a Virgo distance of 15.3 Mpc (Freedman et al. 2001) and a relative distance from Virgo of 1.18 for NGC 3169 (Kraan-Korteweg 1986), the host galaxy of SN 2003cg, we estimate a distance modulus of $\mu = 31.28$. Using the values for A_V and R_V discussed in Section 3.2, we obtain M_B^{max} = -19.17 ± 0.75 and M_V^{max} = -19.00 ± 0.49 which is typical for SNe Ia of its Δm_{15}(B). We have also used distance-independent parameters to estimate M_B^{max}. In Table 3.11 we show the SN 2003cg M_B^{max} values derived using peak luminosity v. Δm_{15}(B) relations (Hamuy et al. 1996a; Phillips et al. 1999; Altavilla et al. 2004; Reindl et al. 2005) scaled to $H_0 = 72$ km s^{-1} Mpc^{-1} (Freedman et al. 2001). We also give M_B^{max} obtained from the parameter ΔC_{12} (Wang et al. 2005). The weighted average M_B^{max} = -19.00 ± 0.06 is consistent with the M_B^{max} value obtained from the observed peak magnitude and adopted distance modulus. (M_B^{max} deduced from the Reindl et al. (2005) relation is somewhat discrepant).

A similar comparison using the stretch factor, s, can be made. SN 2003cg has a stretch factor of 0.97 i.e. almost 1, and so we can directly compare its absolute magnitude of M_B^{max} = -19.17 ± 0.75 with the M_B^{max} = -19.30 value

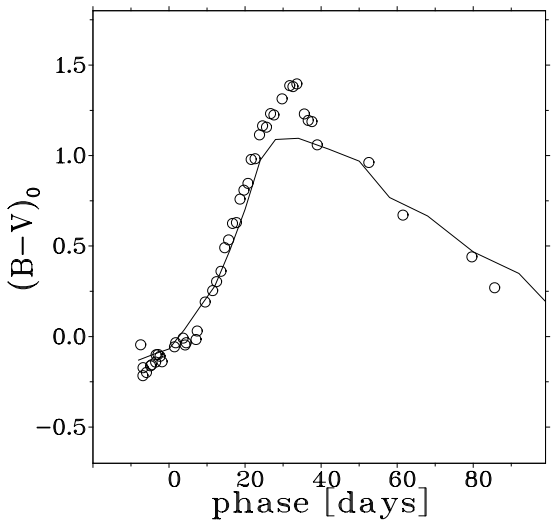

FIGURE 3.12— Intrinsic (B-V) colour curve of SN 2003cg (circles) compared with the average $(B-V)_0$ colour curve (solid line) obtained from SNe 2003du (Stanishev et al. in preparation), 2002er (Pignata et al. 2004a), 2002bo (Benetti et al. 2004a; Krisciunas et al. 2004b), 1996X (Salvo et al. 2001), 2001bt, 2001cz (Krisciunas et al. 2004b), 1999ee, 2000ca and 2001ba (Krisciunas et al. 2004a). For a discussion on the reddening adopted, see Section 3.2.2.

for s = 1 (Nugent, Kim & Perlmutter 2002; Knop et al. 2003). Again the agreement is good.

In contrast with the optical region, the IR magnitudes at maximum (M_J^{max} = -18.22 ± 0.14, M_H^{max} = -17.92 ± 0.12 and M_K^{max} = -18.08 ± 0.05) are between 0.4 and 0.5 mag fainter than the values found by Meikle (2000) and Krisciunas et al. (2004b) for two samples of Type Ia SNe.

The "bolometric" (*uvoir*) luminosity evolution of SN 2003cg is shown in Figure 3.13. It was obtained using the computed distance modulus and reddening, integrating the fluxes in the UBVRIJHK bands (we used a combination of optical and IR spectra having similar epochs) and adding the correction of Suntzeff (1996) for the unknown ultraviolet contribution. The reddening-corrected bolometric luminosity at maximum is $\log_{10}L = 43.01 \pm 0.05$ (erg s^{-1}). Also shown

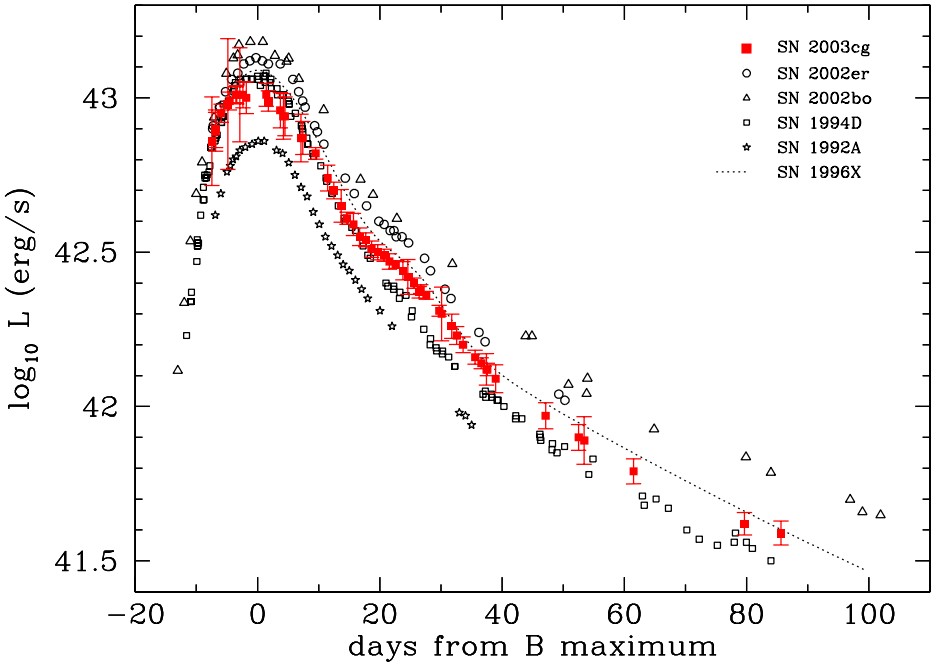

FIGURE 3.13— *uvoir* light curve for SN 2003cg. Filled squares give the *uvoir* light curve of SN 2003cg. Dotted line is the *uvoir* light curve for SN 1996X. Open stars, squares, circles and triangles give the *uvoir* light curves for SNe 1992A, 1994D, 2002er and 2002bo, respectively. Error bars refer only to photometric errors and not to uncertainties in reddening and distance.

in Figure 3.13 are the *uvoir* light curves for five other SNe Ia. The *uvoir* light curve shape of SN 2003cg is clearly similar. In particular, SNe 1996X, 2002er and 2003cg all exhibit prominent bumps around +25 days corresponding to the second NIR maxima. However, SN 2003cg is fainter than SN 1996X around maximum. Differences in the bolometric luminosities at maximum may be due to errors in the distance modulus or reddening estimates for the different SNe.

3.4 Spectroscopy

As can be seen in Figure 3.14, a good set of optical spectra were acquired for SN 2003cg, spanning -8.5 to +52.5 days, plus a nebular spectrum taken 384.6 days after B maximum. We also obtained ten early-time NIR spectra (Figure 3.17) with NTT and UKIRT. This data set constitutes a remarkable sequence of spectra and allows a detailed IR spectroscopic study.

TABLE 3.11— Absolute B magnitude of SN 2003cg derived from different methods.

B	Method	Reference
-19.17±0.75	Distance	This work
-18.91±0.13	M_B^{max} vs. Δm_{15}(B)[a]	Hamuy et al. 1996a[b]
-18.90±0.10	M_B^{max} vs. Δm_{15}(B)	Phillips et al. 1999
-19.21±0.12	M_B^{max} vs. Δm_{15}(B)	Altavilla et al. 2004[c]
-18.22±0.56	M_B^{max} vs. Δm_{15}(B)	Reindl et al. 2005
-19.20±0.22	M_B^{max} vs. ΔC_{12}	Wang et al. 2005

(*a*) $\Delta m_{15}(B)_{intrinsic}$; (*b*) according to the relation given in Table 3 of Hamuy et al. (1996a) (peak luminosity); (*c*) according to the relation given in Table 1 of Altavilla et al. (2004) (ΔY/ΔZ=2.5).

3.4.1 Optical spectra

Figure 3.14 shows the optical spectral evolution of SN 2003cg. It is similar to that of other normal Type Ia SNe apart from the red gradient due to the high reddening. Evidence of high extinction towards SN 2003cg is apparent in all the spectra in the form of strong (EW = 5.27 ± 0.50 Å) Na I D interstellar absorption at $\lambda \sim 5915$ Å. Some of the spectra such as that at -7.6 day also show interstellar Ca II H&K absorption at λ 3934 and 3968 Å. Around maximum light the spectra show the P Cygni profile of Si II at $\sim$ 4130 Å. Also two prominent absorptions are present in SN 2003cg at $\sim$ 4300 Å and at $\sim$ 4481 Å. These are attributed to a combination of Mg II, Fe III and Si III lines. Feature due to Fe III and Si III are again present around 5000 Å. The W-feature at $\sim$ 5300 Å is caused by S II. Between 5960 and 6350 Å the spectra are dominated by Si II lines. The earliest Ca II IR triplet spectra include a weak high velocity component. For the -8.5 day spectrum we find $v \sim 22000$ km s^{-1} for this component (Figure 3.15). The high-velocity feature (HVF) disappears after maximum light (Mazzali et al. 2005). Its strength can be reproduced by synthetical spectra if the abundance of Ca is slightly higher than that at the photosphere [X(Ca) = 0.02 at the photosphere, and 0.03 at the high velocity layers], or by a density jump of a factor 4 and X(H) = 0.30 in the context of the circumstellar medium interaction [X(Ca) = 0.001 (0.0001) without (with) circumstellar medium interaction using a delayed detonation model] (Tanaka et al. 2006).

A single late-phase (nebular) spectrum was secured with the ESO VLT-UT2+FORS1 at +384.5 days. A spectrum at this late phase is particularly

valuable since the ejecta are mostly transparent to optical/NIR light. Thus, via modelling it is possible to estimate directly the total mass of ^{56}Ni synthesised in the explosion. Mazzali et al. (in preparation) estimate $M_{Ni} = 0.53 \pm 0.05$ M$_\odot$ for this SN Ia.

In Figure 3.16 (top) we compare the SN 2003cg optical spectra around maximum light with those of other SNe Ia such as SNe 2003du (Stanishev et al. in preparation), 2002er (Kotak et al. 2005), 2002bo (Benetti et al. 2004a) and 1996X (Salvo et al. 2001). Comparison of the SN 2003cg nebular phase spectrum with those of SNe 2002bo and 1996X is also shown in Figure 3.16 (bottom). The Δm_{15} values of these SNe Ia are in the range 1.07-1.33, close to the average for SNe Ia. In spite of this relative homogeneity there are some clear differences between the spectra. At maximum light both SN 2003cg and SN 2002er show well-developed, structured features due to intermediate mass elements but with clear differences in the P Cygni profiles up to 4500 Å. However, the same features in SN 2003du are less pronounced, possibly due to high expansion velocity or composition effects. The SN Ia-defining Si II λ 6355 line is clearly visible until $\sim$ 28 days after maximum. The line has a fairly symmetrical profile as is also the case for SNe 1996X and 2002er. Somewhat less symmetrical profiles are seen in SNe 2002bo and 2003du. The Si II (λ 6355 Å) trough blueshifts are similar for SN 2003cg and SN 2003du (see Section 3.4.3). However the pre-maximum light Ca II H&K (λ 3934 and 3968 Å) trough blueshifts in SN 2003du are higher by a factor $\sim \times 1.2$ and decline more slowly with time than in SN 2003cg.

In the nebular spectrum of SN 2003cg (Figure 3.16 - bottom) the [Fe II]/[Fe III] emission feature at $\sim$ 4600 Å is comparable to that seen in SN 2002bo but is less pronounced than in SN 1996X. For this feature, the position of SN 2003cg on a plot of FWHM vs. Δm_{15}(B) coincides with the average regression curve for SNe Ia. (Mazzali et al. 1998 - Figure 2). The [Co II] 5900 Å emission (Axelrod 1980) appears barely visible above the noise. The boxy feature between 7000 and 7600 Å may be due to a blend of [Fe II] and [Ca II] (Figure 3.16 - bottom).

3.4.2 Near-infrared spectra

Near-infrared (NIR) spectra are important because there is reduced line blending and lower line opacity. Consequently, line identification is less ambiguous and we may look more deeply into the ejecta. Thus, the line intensities and profiles provide a tool for analysing the ejecta composition and stratification. In Figure 3.17 we show the NIR spectral evolution of SN 2003cg. The spectral evolution is typical of SNe Ia. The earliest spectra are dominated by con-

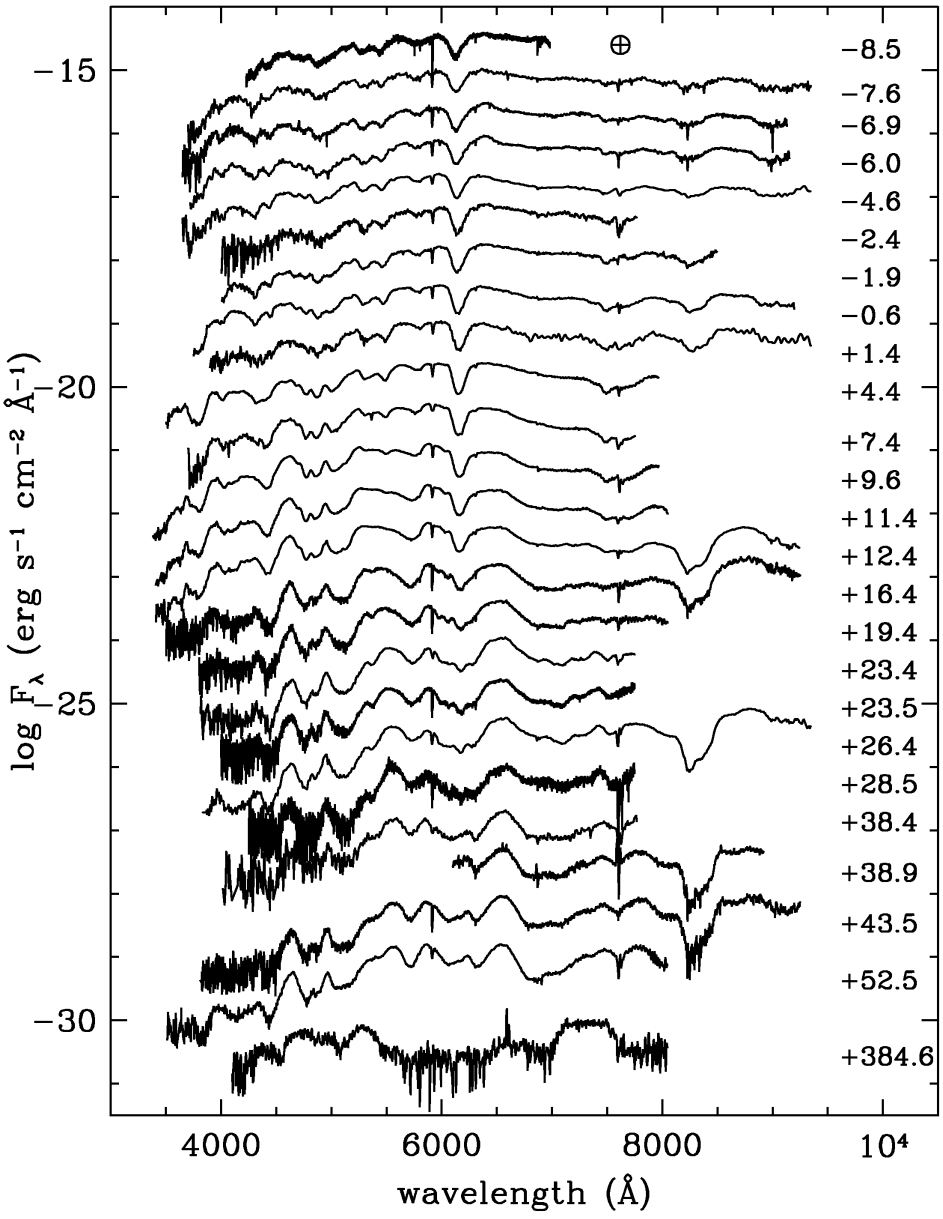

FIGURE 3.14— Optical spectral evolution of SN 2003cg. The ordinate refers to the first spectrum and the others have been shifted downwards by arbitrary amounts. Epochs (in days) are given at the right hand side. The ⊕ indicates the location of the strongest telluric band.

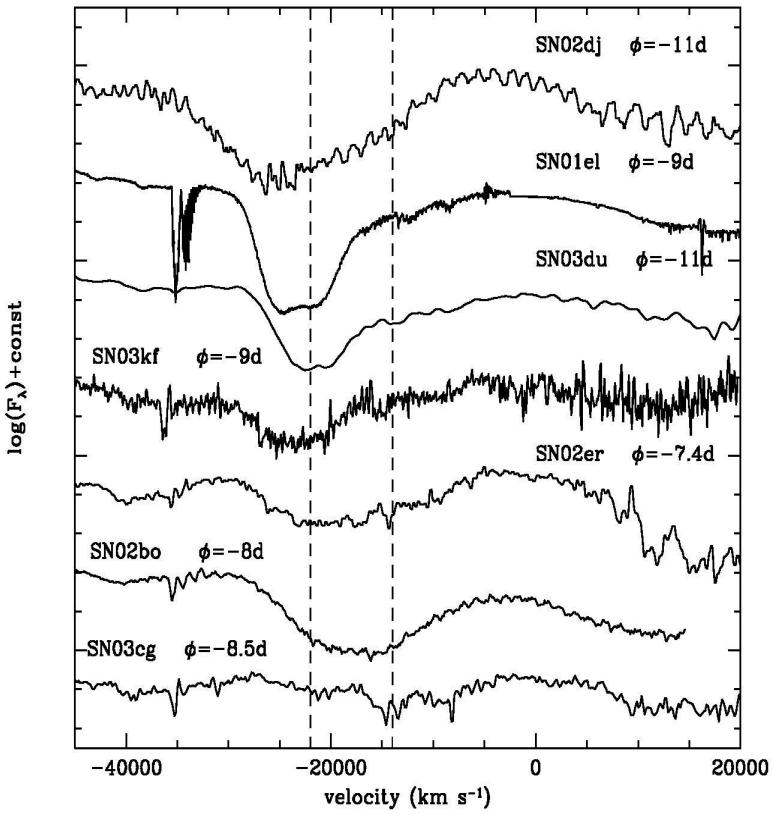

FIGURE 3.15— Ca II IR triplet profiles in the earliest spectra of SN 2003cg and other Type Ia SN. The abscissa shows velocity, taking the average wavelength of the multiplet as the zero point, and the two vertical lines mark the average position of the photospheric components (14000 km s^{-1}) and of the HVFs (22000 km s^{-1}), respectively (see also Mazzali et al. 2005).

tinuum emission but, as the photosphere recedes, the spectra are increasingly dominated by discrete, doppler-broadened features. In Figure 3.18 we compare three early-phase (–6d, +14d, +31d) NIR spectra of SN 2003cg with approximately coeval spectra of SNe 1994D (Meikle et al. 1996), 1999ee (Hamuy et al. 2002), 2002bo (Benetti et al. 2004a) and 2002er (Kotak et al. 2005).

In the pre-maximum spectra of SN 2003cg a weak P Cygni profile is visible at about 10500 Å. This feature was first noted in pre-maximum spectra of SN 1994D by Meikle et al. (1996). This was discussed by Meikle et al. (1996), Maz-

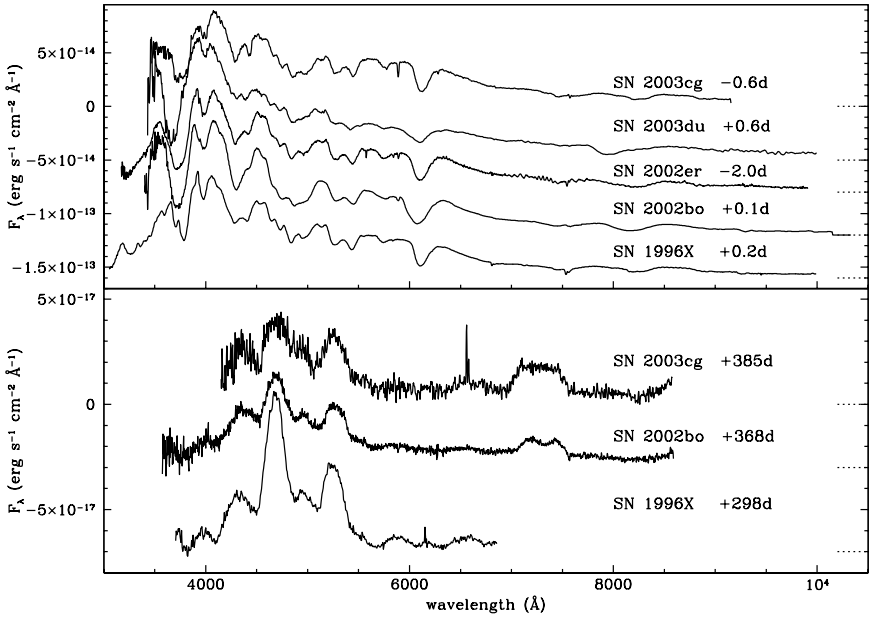

FIGURE 3.16— Comparison between optical spectra of SN 2003cg with those of SNe 2003du (Stanishev et al. in preparation), 2002er (Kotak et al. 2005), 2002bo (Benetti et al. 2004a) and 1996X (Salvo et al. 2001) at maximum light (top) and at late-phase (bottom). The spectra have been displaced vertically for clarity (the zero-flux levels are indicated by the dotted lines). All the spectra have been corrected for redshift and reddening (see text).

zali & Lucy (1998), Hamuy et al. (2002), Benetti et al. (2004a) and attributed to He I 10830 Å or Mg II 10926 Å. On the basis of their modelling, Meikle et al. (1996) and Mazzali & Lucy (1998) concluded that He I, Mg II or a mixture of the two could be responsible for the feature. In contrast, according to the NIR spectral models of Wheeler et al. (1998), the feature must be due almost entirely to Mg II as there is not enough He in the model atmosphere to form a He line. However, simultaneous optical-IR spectral model fits to SN 1994D by Hatano et al. (1999) and examination of the -7 day spectrum of SN 2002cx by Nomoto et al. (2003) has led these authors to challenge the Mg II identification. They find that the Mg II interpretation also predicts non-existent features at other wavelengths. It is possible that the Mg II explanation is only appropriate for faster decliners. Regardless of which identification we adopt, we find that the trough blueshift of SN 2003cg at –6.5 days is similar to that seen in SN 1994D at -8.5 days.

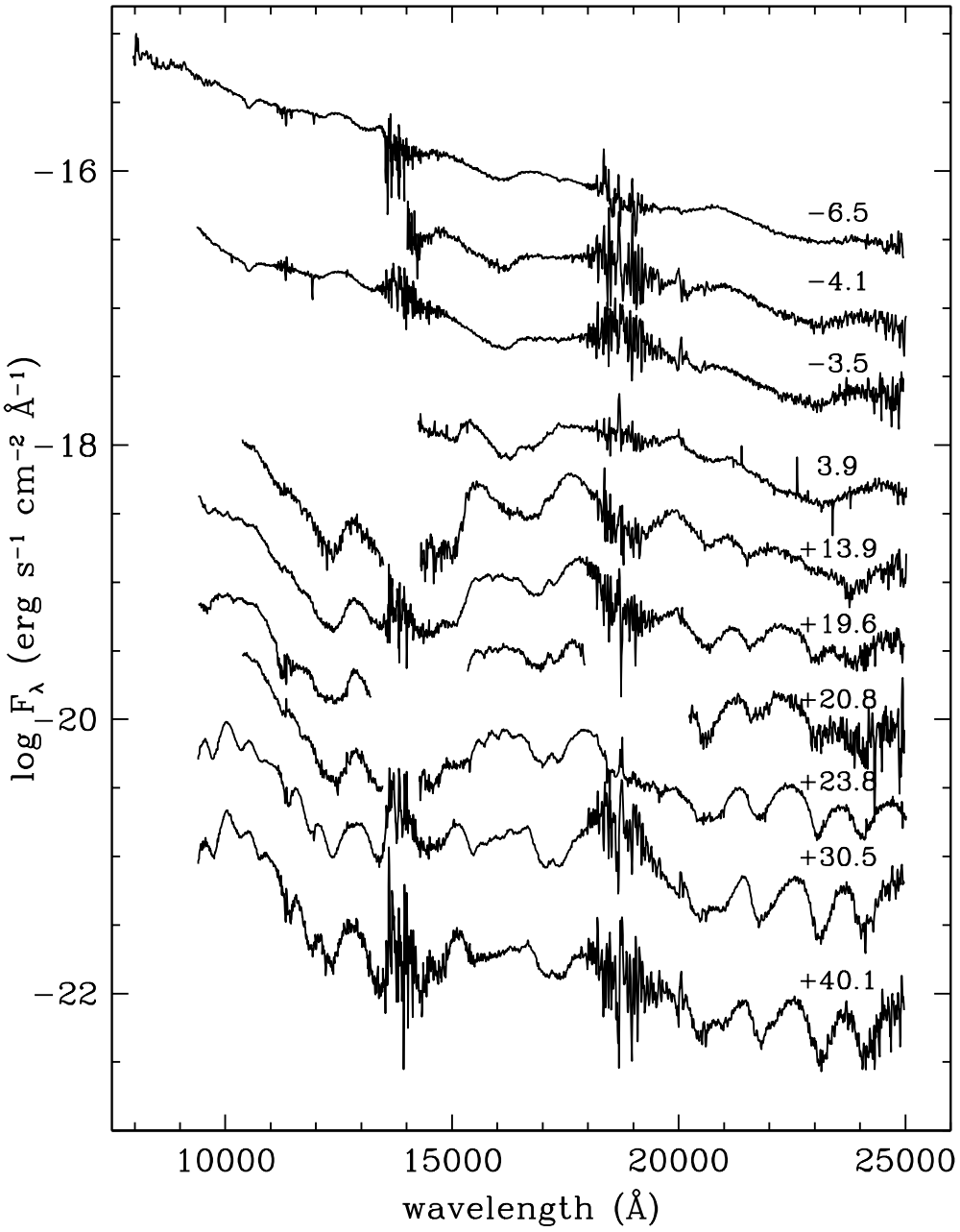

FIGURE 3.17— NIR spectral evolution of SN 2003cg. The ordinate refers to the first spectrum and the others have been shifted downwards by arbitrary amounts. Epochs are shown to the right.

In the SN 2003cg and SN 1999ee spectra Fe III 12550 Å emission is visible (Figure 3.18). In addition, a broad P Cygni-like feature is present at $\sim$ 16700 Å. According to Wheeler et al. (1998), this is due to Si II. In the K-band, emission at 20500 Å is visible in SN 2003cg. This was also seen in SN 2002bo, albeit more weakly, and was identified with Si III (Benetti et al. 2004a).

By +1 to +2 weeks, the weak Mg II/He I $\sim$ 10800 Å absorption has disappeared and strong absorption/emission features have appeared. The prominent emission at 13000 Å is attributed to Si II, while the strong features around 15500-17500 Å are produced by iron group elements such as Co II, Fe II and Ni II (Wheeler et al. 1998). In the K band Si II and Fe-group lines have appeared (Wheeler et al. 1998). This indicates that, by this epoch, the NIR photosphere has already receded through the intermediate mass element zones and has penetrated quite deeply into the Fe-group region. In this respect, SN 2003cg is more similar to SN 2002bo than to SN 2002er whose spectrum was more characterised by lighter elements during this era. Like SN 1999ee, SN 2003cg presents spectral features due to Mg, Ca and the Fe-group elements around 12000 Å but at a lower strength.

By one month post-maximum light the three broad emission peaks in the range 21350-22490 Å, produced by Co, Ni and Si, have become more prominent. This is similar to the behaviour seen in other SNe Ia over this spectral range and phase.

Figure 3.19 shows combined coeval optical and IR spectra of SN 2003cg, allowing a more complete view of the SED evolution. We find that, at -6.5 days the NIR flux (integrated between 10000 and 25000 Å) contribution was about 8% of the total flux, rising to about 14% at +23.8 days. For the same interval, Suntzeff (1996, 2003) estimated the contribution of IR in SNe Ia to be approximately 15% of the total flux.

3.4.3 Velocity gradient

As can be seen in Figure 3.14, SN 2003cg exhibits a deep and symmetric Si II trough at 6355 Å, visible approximately from –8 to +28 days, and shifting rapidly redwards with time. In Figure 3.20, we compare the SN 2003cg Si II velocity evolution with those of a sample of SNe Ia. Clearly, SN 2003cg lies within the low velocity gradient group (hereafter LVG)[2]. The SN 2003cg

[2]Benetti et al. (2005a) have analysed the photometric and spectroscopic diversity of 26 SNe Ia. They identify three groups: FAINT (faint SNe Ia with low expansion velocities and rapid evolution of the Si II velocity), HVG (normal SNe Ia with high velocity gradients,

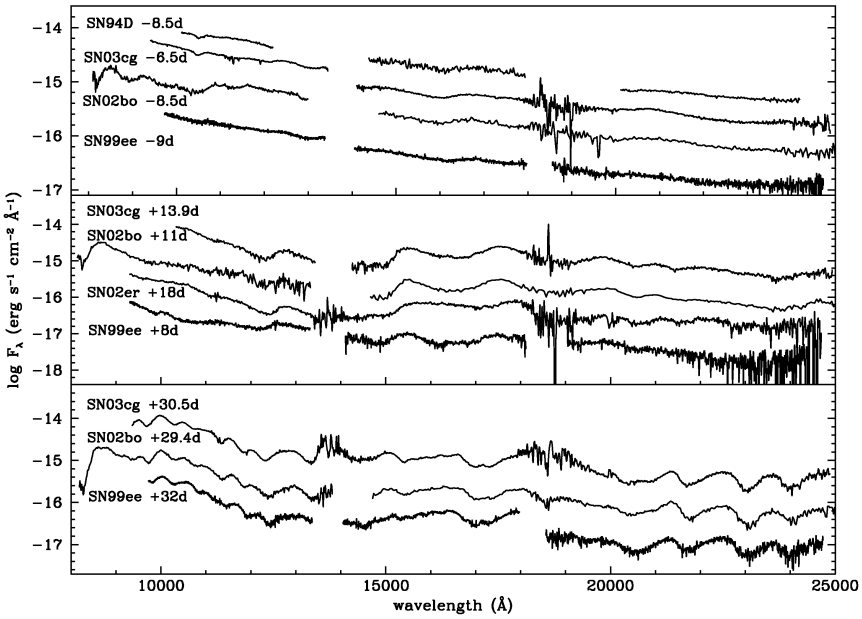

FIGURE 3.18— Comparison between the NIR spectra of SN 2003cg and those of SNe 1994D (Meikle et al. 1996), 1999ee (Hamuy et al. 2002), 2002bo (Benetti et al. 2004a) and 2002er (Kotak et al. 2005) before maximum (top), two weeks after maximum (middle) and one month after maximum (bottom). The spectra have been displaced vertically for clarity. All spectra have been corrected for reddening (see text) and parent galaxy redshift.

velocity gradient $\dot{v}$ (= -Δv/Δt) $\sim 38 \pm 6$ km s^{-1} d^{-1} and its expansion velocity at 10 days past maximum v_{10}(Si II) = 10310 $\pm$ 0.10 km s^{-1}. These are typical LVG values. By way of comparison, we also show in Figure 3.20 the velocity evolutions of the HVG SN 2002bo (HVG) and the FAINT SN 1986G.

In Figure 3.21 we show the velocity evolution of the S II 5640 Å trough blueshift, compared with those of three other normal SNe Ia. This feature tends to disappear more quickly than does Si II, and is generally difficult to discern beyond +10 days. SNe Ia show two types of behaviour here, exhibiting either a steep velocity gradient (e.g. SN 2002bo) or a shallow gradient (e.g. SNe 1994D, 2003du) Benetti (2005b). It may be seen that SN 2003cg falls into

brighter absolute magnitudes and higher expansion velocities than the FAINT SNe) and LVG (normal and SN 1991T-like SNe Ia with small velocity gradients).

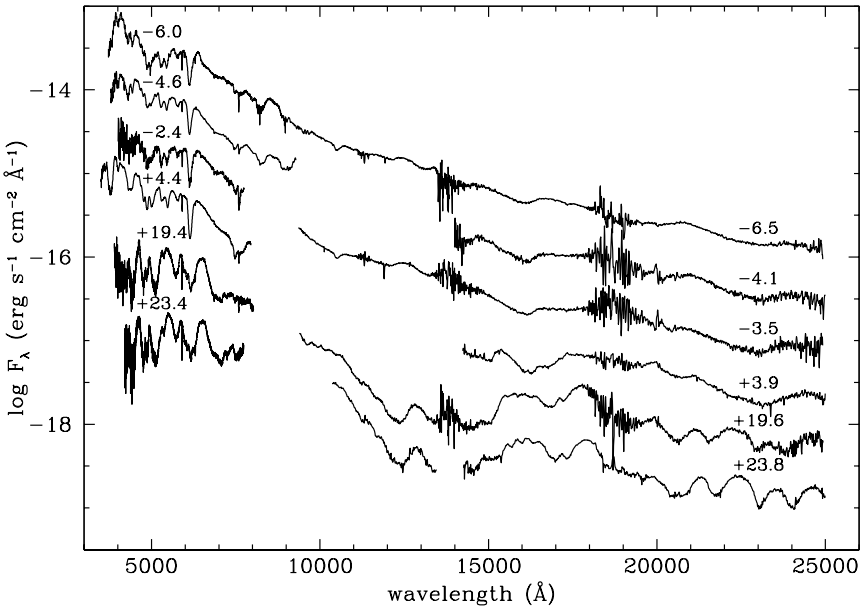

FIGURE 3.19— Combined optical and IR spectra, showing the evolution of SN 2003cg from 1 week before to 3 weeks after maximum light. The spectra have been corrected for reddening due to the Milky Way and the host galaxy.

the latter category.

$\mathcal{R}$(Si II), the ratio of the depths of the Si II 5972 Å and 6355 Å absorptions, was introduced by Nugent et al. (1995) as a potential distance-independent parameter which is related to the luminosity. The parameter was investigated further by Benetti et al. (2005a). For SN 2003cg, $\mathcal{R}(\mathrm{Si\,II})_{max} = 0.30 \pm 0.05$. In Figure 3.22 it may be seen that the pre-maximum evolution of $\mathcal{R}$(Si II) for SN 2003cg is similar to that of other LVG SNe Ia i.e. little or no pre-maximum evolution occurs.

We repeated the Benetti et al. (2005a) cluster analysis including SN 2003cg. We found that this SN does indeed belongs to the LVG cluster (see Figure 3.23). In the five-parameter space [Δm_{15}(B), M_B^{max}, $\dot{v}$, v_{10}(Si II) and $\mathcal{R}(\mathrm{Si\,II})_{max}$], the nearest SNe to SN 2003cg are SN 1994D and SN 1996X. This supports our choice of these SNe for comparison purposes in this work.

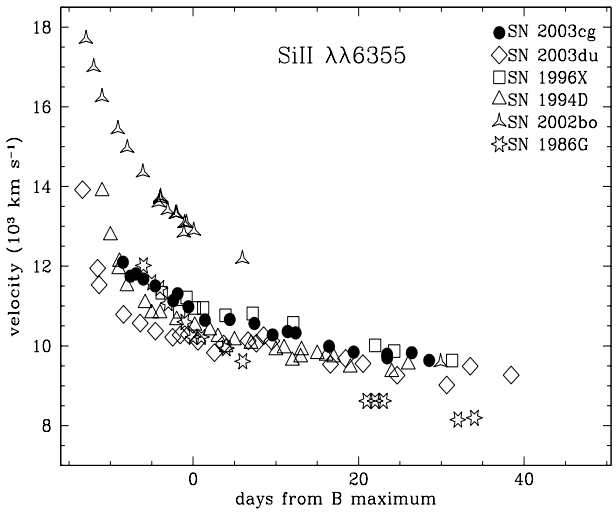

FIGURE 3.20— Evolution of the expansion velocity derived from the minima of Si II 6355 Å for SN 2003cg, compared with other LVG (Benetti et al. 2005a) SNe: SN 2003du (Stanishev et al., in preparation), SN 1996X (Salvo et al. 2001) and SN 1994D (Patat et al. 1996). Also shown are the evolution of the HVG SN 2002bo (Benetti et al. 2004a) and the FAINT SN 1986G (Cristiani et al. 1992).

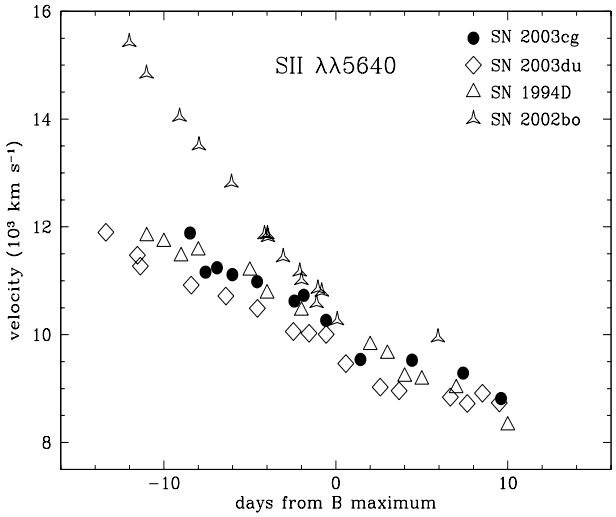

FIGURE 3.21— Evolution of the expansion velocity derived from the minima of S II 5640 Å for SN 2003cg, and two other LVG SNe: SN 2003du, SN 1994D. Also shown is the evolution of the HVG SN 2002bo.

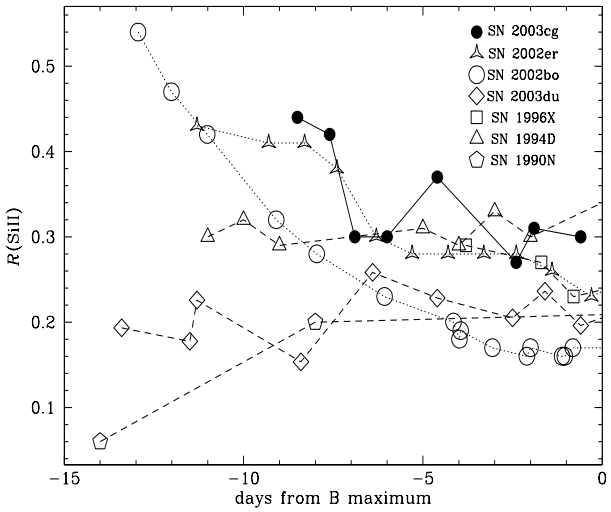

FIGURE 3.22— Pre-maximum evolution of $\mathcal{R}$(Si II) for SN 2003cg, compared with those SNe 2002er, 2002bo (HVG) 2003du, 1996X, 1994D and 1990N (LVG) (Benetti et al. 2005a).

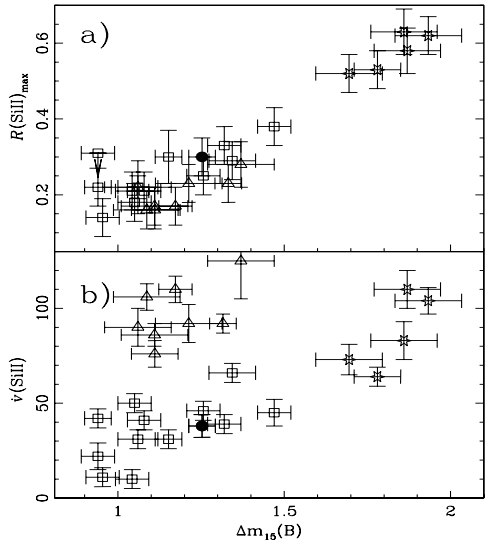

FIGURE 3.23— a) $\mathcal{R}(\mathrm{Si\,II})_{max}$ vs. Δm_{15}(B). b) $\dot{v}$ vs. Δm_{15}(B) for Si IIλ 6355. Filled symbols refer to SN 2003cg, and squares, triangles and stars represent LVG, HVG and FAINT SNe, respectively (Benetti et al. 2005a).

3.4.4 Spectral modelling

We have compared the observed spectra of SN 2003cg with synthetic spectra derived using the Lucy-Mazzali Monte Carlo code, which has been used successfully to model spectra of SNe Ia in the photospheric phase (e.g. Mazzali & Lucy 1993). The code (Mazzali & Lucy 1993; Lucy 1999; Mazzali 2000) assumes that the SN ejecta can be separated by a sharp photosphere into an optically thick region below which all the light is emitted and an optically thin region where line formation occurs. The code's input parameters are the SN luminosity, a photospheric velocity (which is equivalent to radius since $v = r/t$, a density structure and a set of abundances. The density structure used here is that of the W7 model (Nomoto, Thielemann & Tokoi 1984). The flux at the photosphere is assumed to be emitted with a black-body spectrum. The code follows the propagation of photons in the ejecta and their interaction with lines (including the process of branching) and electron scattering. Excitation and ionisation are computed using a nebular approximation, which gives a good description of the conditions in a SN Ia near maximum (Pauldrach et al. 1996). The emerging spectrum is computed using a formal integral.

Days –7.6/–6.5

Here we model the day −7.6 spectrum optical spectrum and day −6.5 NIR spectrum, which were among the earliest obtained. In the model, the SN ejecta above the photosphere is divided into three spherically symmetric shells above 11200, 11600, and 15500 $\mathrm{km\,s^{-1}}$, respectively. All shells are dominated by O (48% to 64% by mass). The outermost shell contains 5% C to account for the C II line (see below). A rather high amount of Si (18% to 25% in the inner shell) is necessary to reproduce the deep Si II features in the spectrum. Also of interest is the high Fe group abundance at this early stage. We find 5% Ni in all shells. The stable Fe abundance, i.e. Fe that is not produced in the Ni decay chain, is between 1.5% near the photosphere, and 0.5% in the outermost shell (for reference the solar mass fraction of Fe is $\approx 0.27\%$ - Gratton et al. 2003). Finally, Ti and Cr of $\approx 0.25\%$ are needed in order to shift the flux from the UV to optical wavelengths (the solar mass fraction is $\approx 6.22 \times 10^{-4}\%$ for Ti and $\approx 3.80 \times 10^{-3}\%$ for Cr - Gratton et al. 2003). The best fit was achieved using $\log_{10} L = 42.88\,(\mathrm{erg\,s^{-1}})$, a photospheric velocity $v_{ph} = 10,300\,\mathrm{km\,s^{-1}}$, and epoch after explosion $t_{exp} = 12.3\,\mathrm{d}$ (i.e. a rise time of 19.9 days, cf. Section 3.3.1). The observed spectrum, dereddened according to the prescription derived above (Section 3.2), and the synthetic spectrum are compared in Figure 3.24 (top), where the main features are also identified.

The model reproduces the overall shape and the individual line profiles reason-

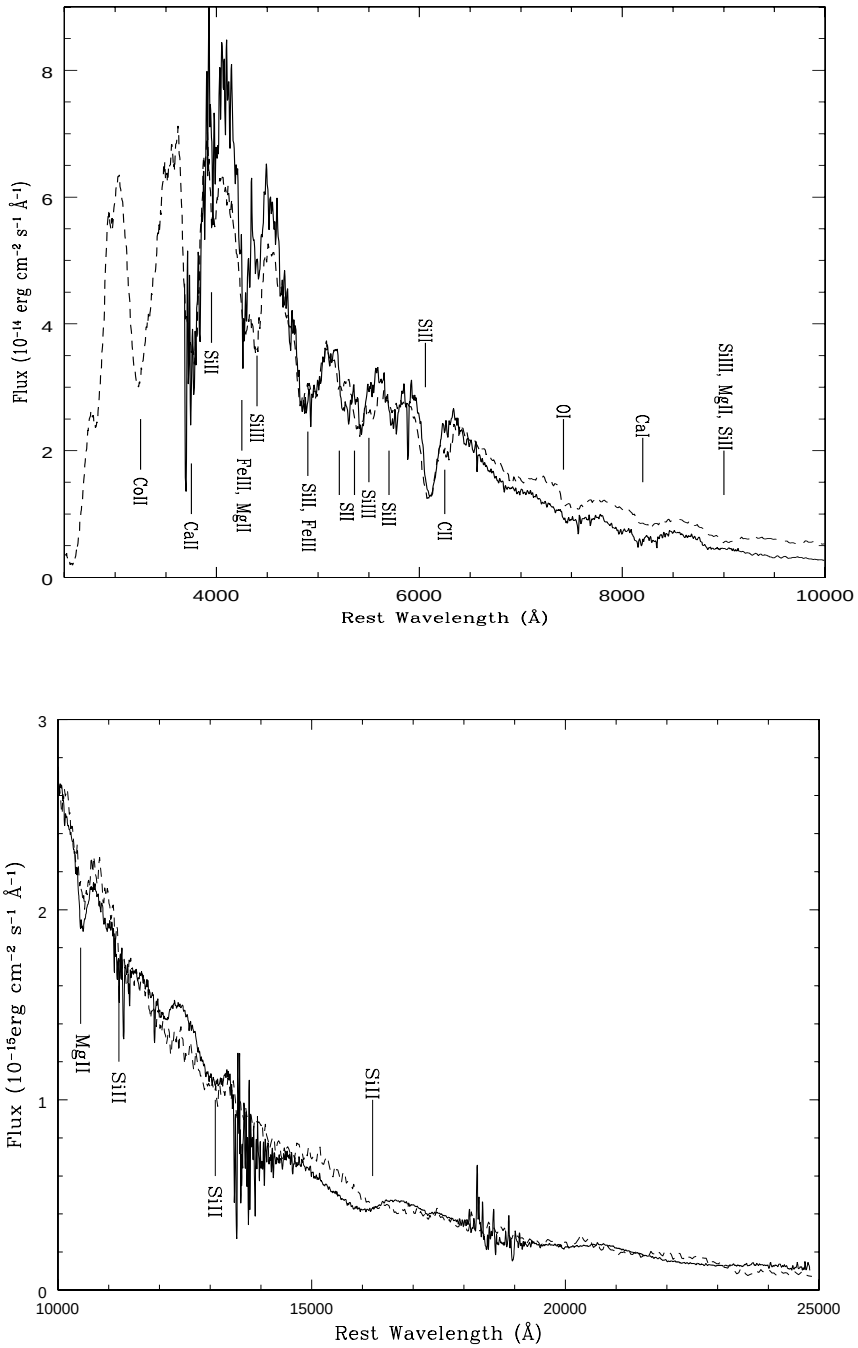

FIGURE 3.24— Observed, dereddened optical (top) and NIR (bottom) spectra of SN 2003cg at day $-7.6/-6.5$ and corresponding spectral models. The model parameters include $\log_{10} L = 42.88\,(\mathrm{erg\,s^{-1}})$, $v_{ph} = 10,300\,\mathrm{km\,s^{-1}}$, $\mu = 31.28$ and $t_{exp} = 12.3\,\mathrm{d}$.

ably well, but it has difficulties matching the very blue $B - V$ colour obtained after dereddening. Achieving a bluer spectrum may require increasing the metal abundance near the photosphere to increase line blocking and therefore transfer more near-UV photons to the B region. Given the lack of information on the U band flux, we cannot constrain this aspect very tightly. In particular, in order to obtain a blue continuum we have to adopt a rather low value for the photospheric velocity. This leads to near-photospheric temperatures that are too high, and results in the presence of lines in the synthetic spectrum that are not present in the observed one. In particular this affects Si III lines.

Starting at the blue end of the spectrum, the strong Ca II H&K near 3800 Å can be seen. The narrow feature at $\approx$ 4000 Å is identified as Si II 4130 Å. The peak near 4000 Å is suppressed in the model due to S III absorptions. This indicates that the temperature near the photosphere is too high. The excessive strength of two other Si III lines, 4565 Å, which is seen in the model near 4400 Å, and 5740 Å, seen near 5500 Å, substantiates this assumption. The absorption at 4250 Å is a combination of Mg II 4481 Å, Fe III 4420 Å, and Si III 4339 Å. The feature slightly blueward of 5000 Å is caused by Si II 5056 Å and Fe III 5128, 5156 Å. In this case the presence of strong Fe III lines is supported by the accuracy with which the observed profile is matched. Near 5300 Å, we recognize the typical S II W-feature, followed by the two Si II lines at 5960 Å and 6350 Å. The weakness of the synthetic Si II 5960 Å line again suggests that the model temperature near the photosphere is too high. The emission component of the Si II 6350 Å line is suppressed in the observed spectrum. This effect is reproduced in the model by C II 6580 Å absorption. This has also been detected in other SNe Ia (e.g. Mazzali 2001). Further to the red only two more lines are clearly identified: O I 7774 Å, and the Ca II IR triplet. Both lines are somewhat deeper in the model. An absorption in the synthetic spectrum near 9000 Å is attributed to a blend of Mg II 9218 Å, Si III 9324 Å, and Si II 9413 Å.

In Figure 3.24 (bottom) we compare the day -6.5 NIR spectrum with the model spectrum described above, extended to the NIR. Owing to the black body lower boundary adopted in the model, the predicted IR continuum exceeds that observed. We attribute this to a drop in opacity which appears redward of $\sim$7000 Å and is not reproduced in the model (see Figure 3.24 - top). Therefore, to match the observed spectrum, the model continuum was multiplied by a factor 0.5. However, apart from the discrepancy in the overall flux level, the shape of the IR continuum and other features are well reproduced by the model at this epoch. Only a few, relatively weak lines are present in the NIR spectrum, primarily due to Si II and Mg II. The feature at 1.05μ is well reproduced by Mg II 10914, 10951 Å. As Hatano et al. (1999) discuss in their work (see also Section 3.4.2), the identification of Mg II at this wavelength implies the presence of other

Mg II features in other parts of the optical/NIR spectrum, some of which have been identified above. In spite of this and due the lower strength of these lines in the observed spectra, we can not exclude the presence of He 10830 Å.

Day –0.6

We have also modelled the SN 2003cg optical spectrum near maximum light. The dereddened day −0.6 spectrum was compared to a synthetic spectrum computed using the following parameters: $t_{exp} = 19.3\,\mathrm{d}$, $\log_{10}L = 43.11\,(\mathrm{erg\,s^{-1}})$ and $v_{ph} = 6000\,\mathrm{km\,s^{-1}}$. The observed spectrum, dereddened as above, and the synthetic spectrum are compared in Figure 3.25, where the main features are also identified.

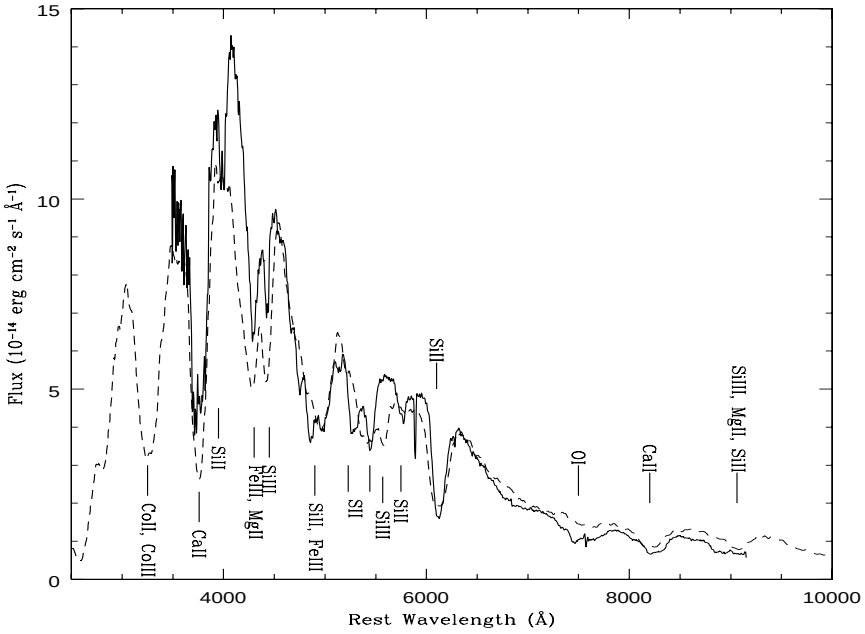

FIGURE 3.25— Observed, dereddened optical spectrum of SN 2003cg at day −0.6 and corresponding spectral model. The model parameters include $\log_{10}L = 43.11\,(\mathrm{erg\,s^{-1}})$, $v_{ph} = 6,000\,\mathrm{km\,s^{-1}}$, $\mu = 31.28$ and $t_{exp} = 19.3\,\mathrm{d}$.

As for the pre-maximum spectrum, we are forced to use a very low velocity for this epoch because the dereddened spectrum is unusually blue. Our synthetic spectrum has $B - V \sim 0.0$, but the dereddened spectrum has $B - V \sim$

−0.2. Therefore, on the one hand our model colour is too red, and on the other our model line features are somewhat too hot compared to the observed ones.

The features present in the spectrum are generally similar to those deduced in the –7.6 day spectrum. In the blue region Ca II H&K is strong. Si II 4130 Å is present in the data but not reproduced in the model. The line near 4300 Å is now dominated by Fe III 4419, 4431 Å and Mg II 4481 Å. Moving redwards, we again identify Si III 4560 Å. This line is strong both in the observed spectrum and in the synthetic one. However, other lines of Si III, notably 5740 Å, which is strong in the model near 5500 Å, but are absent in the data, indicate that the model temperature is too high. The feature near 5000 Å is dominated by Fe III 5127, 5156 Å, with contributions from Si II 5056 Å and Fe II 5169 Å. The observed profile of this feature however suggests that Fe II lines also make an important contribution. The S II W-feature is affected by the presence of Si III 5740 Å. The prominent Si II 6350 Å line is well reproduced with an increased Si abundance (reaching $\sim 40\%$ near the photosphere. The Si II 5960 Å is however not reproduced at all, again indicating that the adopted velocity and luminosity lead to a temperature that is too high. By this epoch, the C II line on top of the Si II 6350 Å emission has vanished. This is because the density in the outermost layers, where carbon is found, is now too low for the line to form. Further to the red we identify strong O I 7774 Å, and the Ca II IR triplet. Finally, we identify another strong absorption at 9000 Å due mostly to Si III 9324 Å.

3.5 Summary

SN 2003cg is a heavily reddened but otherwise normal Type Ia supernova. We have presented the results of an intensive optical/NIR monitoring programme by the ESC using a wide range of telescopes and instruments. Photometry and spectroscopy were acquired spanning day -8 to +414 after B maximum light (plus upper limits on day +624). We have corrected all our photometric measurements for the deviation of each instrumental photometric setup from the Bessell (optical) and Persson (IR) standard systems. This was done using the S-correction method, and was applied up to the latest observed phases.

Besides the atypically red observed colours, evidence for high extinction towards SN 2003cg include (a) its coincidence with a dust lane of NGC 3169, (b) the very strong Na ID interstellar doublet and (c) the presence of a *diffuse interstellar band* (DIB). However, dereddening using a standard extinction law to match a typical SN Ia $B - V$ colour yields a peak absolute magnitude at maximum which is abnormally bright. We therefore allowed R_V to become a free parameter within the CCM extinction law and adjusted R_V and A_V to provide simultaneous matches to a range of colour curves of normal SNe Ia.

From this, we obtained $A_V = 2.39 \pm 0.13$ and $R_V = 1.80 \pm 0.20$ (which give us as excess colour E(B−V) $= 1.33 \pm 0.11$). While the value obtained for R_V is small, such values have been invoked in the past. It implies that the grain size is small compared with the average value for the local ISM. As an alternative explanation, the light echo (LE) hypothesis (Wang 2005), has severe difficulties. It seems unlikely that dust as close as $R_0 \leq 10^{16}$cm could survive the supernova peak luminosity. If a significant proportion did survive it would produce a strong NIR excess, but this is not seen. Other LE effects expected but not seen in SN 2003cg, include (a) a reduced $(B-V)$ color range, (b) temporal variation in the reddening, (c) an anomalously small Δm_{15}, (d) a significantly brighter late phase tail and (e) broader spectral lines (more details in Patat 2005).

The shape of the UBVRIJHK light curves of SN 2003cg are generally typical of a normal Type Ia SN. The U and V light curves show a broader peak and a pronounced shoulder in the post-maximum decay, respectively. Again we believe that this is due to the high reddening, causing the effective λ of these bandpasses to shift to redder wavelengths. We obtain a reddening-corrected $\Delta m_{15}(B)_{obs} = 1.25 \pm 0.05$ for SN 2003cg, which is typical for normal SNe Ia. The intrinsic peak bolometric luminosity is $\log_{10} L = 43.01 \pm 0.05$ (erg s^{-1}).

The spectral evolution of SN 2003cg is also similar to that of other normal Type Ia SN. This includes the spectral features, their ratios and their evolution. The earliest spectra exhibit a weak, but clearly visible, high velocity component of Ca II IR. The late phase spectra show emission features of [Fe II], [Fe III] and [Co II] plus an unusual blend of lines between 7100 and 7350 Å. From the velocity evolution of Si II at 6355 Å and S II at 5640 Å, we classify SN 2003cg as an LVG SN. The same conclusion is indicated by the $\mathcal{R}$(SiII) evolution.

SN 2003cg, the fourth target followed by the ESC, has provided an important addition to the database of well-monitored nearby Type Ia. In addition, further study of the heavy reddening towards SN 2003cg will help us to establish the diversity in the characteristics of dust responsible for astrophysical extinction.

4

SN 2002cv: a heavily obscured Type Ia event

¡Chiquilla!
Tururun tun-tun-tutururun
turun turun turun ...
Jesús Varela López

This kind of stuff!
Avet Harutyunyan

... e tu sei piccolina
che cosa ci puoi far!!
Filomena Bufano & Jairo Mendéz Abreu

We present in this Chapter the study of another interesting, very extinguished SNe Ia, SN 2002cv. This SN exploded in the same host galaxy a few months after the well studied Type Ia SN 2002bo. SN 2002cv is also one of the earliest SNe discovered in the NIR bands (Section 4.1) and one of the most obscured SNe ever observed, it was not visible in the bluer bands (Section 4.2). Our analysis shows that also in the direction of this object there is an atypical extinction law with a small R_V (Section 4.3). In order to compare SN 2002cv with other Type Ia SNe, we developed new methods and relations between optical parameters to simplify its analysis (Section 4.4).

SN 2002cv was discovered in the spiral galaxy NGC 3190 (z=0.0042) in 2002 May 13.7 by Lavionov & Arkharov (2002) while observing SN 2002bo, a

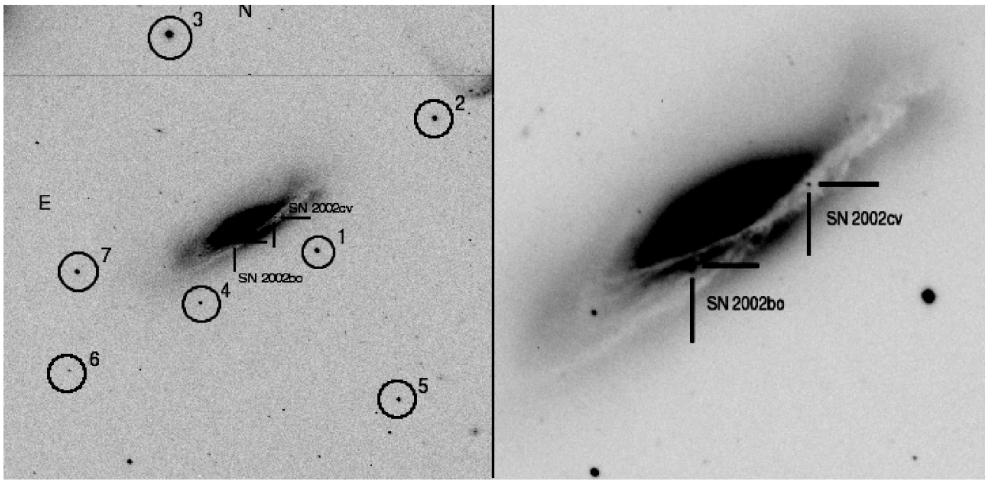

FIGURE 4.1— R band image of SN 2002cv in NGC 3190 taken with the 2.5m Isaac Newton Telescope + WFC on 2002 June 27 (FoV $\sim 8' \times 8'$). SN 2002bo and the local sequence stars are also indicated (cf. Table 4.1).

Type Ia SN extensively studied by Benetti et al. (2004a), Krisciunas et al. (2004b). The new source appeared 18″W and 10″N from the galactic nucleus ($\alpha = 10^h18^m03\overset{s}{.}68$, $\delta = +21^o50'06\overset{''}{.}20$, J2000.0) projected on the dust lane of NGC 3190 (Figure 4.1). An early optical spectrum (Turatto et al. 2002) showed a very red continuum with almost no signal bluewards of 6000 Å which was attributed to very high extinction. Infrared spectra taken at the UKIRT telescope on May 22.3 and 23.3 and reported by Meikle & Mattila (2002) indicated, that SN 2002cv could be a Type Ia SN similar to SN 1991T. This classification was confirmed by Filippenko et al. (2002b).

4.1 Photometry

4.1.1 Data acquisition and reduction

The fact that another Type Ia SN, SN 2002bo, exploded in the same galaxy of SN 2002cv few months before, helped in collecting pre-discovery optical and NIR data and in having templates for photometry reduction. SN 2002cv was observed for almost seven months, from day -10.4 to +206.7 relative to I band maximum light. Here we present the data collected by four different teams, Berkeley University (USA), Imperial College (UK), Padova and Teramo Observatories (Italy) with 9 different instruments.

As described in Chapter 2, the photometric observations of SN 2002cv were

first trimmed and corrected from overscan, bias and flat-field (for the IR bands, we also performed sky subtraction, and image coaddition to improve the signal-to-noise) and later measured the optical and NIR magnitudes using the template subtraction technique (described on Section 2.3.2) due to the strong luminosity gradient at the SN position. Reference images (templates) of NGC 3190 were taken about two months before SN 2002cv discovery during the SN 2002bo follow-up with the Asiago 1.82m Copernico telescope + AFOSC on March 21, 2002, and the AZT-24 telescope + SWIRCAM on March 28, 2002, for the optical and NIR bands respectively. After the subtraction of the template from the SN image, the instrumental magnitude of the SN was measured with the point-spread function (PSF) fitting technique using the SNOoPY (Section 2.3.2) package on the subtracted image. Reference stars in the SN field (Figure 4.1) were also measured using the IRAF PSF fitting routine on the original image.

In order to calibrate the instrumental magnitudes into a standard photometric system, we used the colour term equations for the various instrumental setups. These were derived from the observations during photometric nights of several standard fields (Landolt 1992). In turn, the photometric zeropoints for non-photometric nights were determined using the magnitudes of the local sequence stars in the SN field (Table 4.1). Because of the small number of IR standard fields observed each night, we used the average colour terms provided by the telescope teams. Since in the same host galaxy the well studied SN 2002bo also exploded, we use the average of the optical magnitudes of the local sequence given by Benetti et al. (2004a) and Krisciunas et al. (2004b) to calibrate our data. The order of the local sequence is that given by Benetti et al. (2004a) (see their Figure 1 and Table 1) with the addition of star number 7 which corresponds to the star number 3 of Krisciunas et al. (2004b) (see their Figure 1*e* and Table 1). For the IR magnitudes we calibrate two stars of the local sequence during photometric nights. The IR magnitudes of the single star in common with Krisciunas et al. (2004b) agree to better than 0.02 mag.

We also included the data from Di Paola et al. (2002) (see Section 4.1.2) obtained using the AZT-24 Telescope of the Campo Imperatore Observatory, equipped with the near-infrared camera SWIRCAM. These data were checked and calibrated with our local sequence. In a few cases, we obtained new determinations with respect to their estimates. Some of them were measured again to match the new calibration.

Whereas after colour correction, the SN magnitudes are formally in the standard system, it is well-known that these colour corrections do not work well for the SNe themselves because of the non-stellar SED (Spectral Energy Distribution) of the SNe and significant systematic differences between band-

TABLE 4.1— Magnitudes for the local sequence stars identified in the field of SN 2002cv coded as in Figure 4.1.

star	V	R	I	J	H	K
1	14.41(0.05)	13.98(0.07)	13.59(0.03)	13.05(0.01)	12.71(0.01)	12.67(0.01)
2	14.32(0.08)	13.91(0.08)	13.57(0.04)	-	-	-
3	12.39(0.09)	12.02(0.09)	11.67(0.09)	-	-	-
4	17.20(0.05)	16.35(0.06)	15.65(0.06)	14.83(0.01)	14.20(0.01)	14.12(0.01)
5	15.65(0.08)	15.26(0.09)	14.92(0.02)	-	-	-
6	17.90(0.04)	17.51(0.08)	17.16(0.04)	-	-	-
7	14.93(0.01)	14.49(0.02)	14.08(0.02)	-	-	-

passes of different instruments. During the follow-up of SN 2002cv, we used seven different instruments for the optical and two for the NIR observations. In order to convert the photometry of the target to the standard system we applied S-corrections to our data following the method of Pignata et al. (2004a) described in Section 2.3.2.

We calculated the S-corrections for the VRI bands[1] by using the flux-calibrated spectra of SN 2002cv (Section 4.2). Since our spectra did not cover all photometric epochs, we completed the spectral database by adding spectra of unreddened normal SNe Ia such as SN 1992A (Suntzeff 1996), SN 1994D (Patat et al. 1996) and SN 1996X (Salvo et al. 2001), properly reddened to match those of SN 2002cv (see Section 4.3 for more details).

The corrections for SN 2002cv are in general, relatively small (≤ 0.09), as seen in Figure 4.2 except for the I band of the INT and JKT where the corrections were up to 0.40 because these telescopes use Sloan Gunn i and Harris I passbands respectively, which differ significantly from the Bessell ones. The SN magnitudes calibrated using this technique, agree reasonably well with the other ones (Figure 4.3). The data from TNT and Lick - Nickel 1m Telescopes were not corrected because some of the required instrumental information was not available. In any case, the measurements from these instruments appear in good agreement with those corrected from other instruments as can be seen in Figure 4.3.

Observed and corrected optical photometry is reported in Table 4.2 and NIR measurements are listed in Table 4.3. Magnitudes are presented together with their uncertainties, which were computed as the sum in quadrature of the

[1] We did not compute the S-correction for late time observations and for NIR bands because of the lack of suitable spectra.

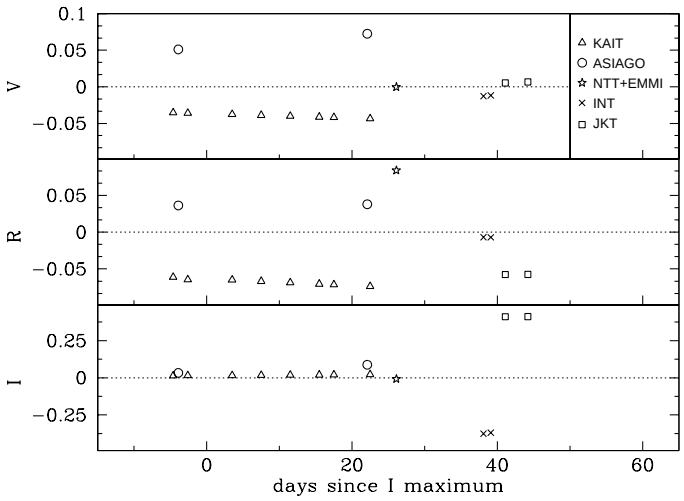

FIGURE 4.2— Summary of the S-corrections derived for the VRI bands of the different instruments (see legend) at early times. These corrections have been added to the first-order corrected SN 2002cv magnitudes to convert them to the standard system values. The dotted line shows the zero correction.

following contributions: PSF fitting error on the subtracted image calibration errors (r.m.s. of the observed magnitudes of the local sequence stars) and errors associated with the S-correction (r.m.s. deviation with respect to the low order polynomial fit over phases) for every set up.

4.1.2 Light curves

The early phases light curves are shown in Figure 4.4. Since SN 2002cv is not visible in the B band, the phases are relative to the epoch of the first I maximum, which occurred on May 19.9 2002 UT (JD = 2452414.42).

The light curves have a good sampling from -10 to +64 days after I maximum, except in V because the early frames were too shallow. SN 2002cv was discovered in the JK bands about 10.4 days before the I maximum, making these measurements among the earliest NIR observations available for SNe Ia.

The secondary maximum typical of the Type Ia SNe is present in all bands confirming the early classification of SN 2002cv as a Type Ia SN. We remind the reader that no certain classification was assigned to SN 2002cv because of the lack of clear spectral features blueward than 6000 Å. Another typical SN Ia signature is the first I maximum occurring before the R and NIR ones (e.g.

TABLE 4.2— S-corrected optical photometry of SN 2002cv.

date	JD (+2400000.00)	Phase* (days)	V	R	I	Instr.
14/05/02	52408.75	-5.6	20.97(0.27)	19.81(0.18)	-	N1mT
14/05/02	52409.37	-4.9	20.48(0.16)	-	17.23(0.14)	TNT
15/05/02	52409.74	-4.6	$\geq$ 20.69	19.62(0.06)	17.45(0.02)	N1mT
15/05/02	52409.75	-4.6	-	19.73(0.12)	17.49(0.05)	KAIT
15/05/02	52410.39	-3.9	-	-	17.18(0.12)	TNT
15/05/02	52410.40	-3.9	-	-	17.32(0.04)	EKAR
16/05/02	52410.74	-3.6	$\geq$ 20.50	19.54(0.06)	16.89(0.03)	N1mT
16/05/02	52411.41	-2.9	-	19.42(0.10)	16.69(0.02)	TNT
17/05/02	52411.75	-2.6	-	19.28(0.09)	-	KAIT
17/05/02	52412.38	-1.9	-	-	16.65(0.05)	TNT
20/05/02	52415.39	1.1	-	-	16.67(0.06)	TNT
23/05/02	52417.75	3.5	-	19.24(0.08)	16.86(0.06)	KAIT
27/05/02	52421.75	7.5	-	19.28(0.12)	17.06(0.08)	KAIT
28/05/02	52423.37	9.1	-	-	17.25(0.04)	TNT
29/05/02	52424.33	10.0	-	-	17.23(0.04)	TNT
30/05/02	52425.36	11.1	-	-	17.24(0.02)	TNT
31/05/02	52425.75	11.5	-	19.58(0.04)	17.35(0.04)	KAIT
01/06/02	52427.28	13.0	-	-	17.19(0.02)	TNT
04/06/02	52429.75	15.5	-	20.05(0.16)	17.33(0.28)	KAIT
06/06/02	52431.75	17.5	-	19.65(0.12)	17.26(0.23)	KAIT
08/06/02	52433.70	19.4	$\geq$ 20.46	20.27(0.12)	17.15(0.03)	N1mT
10/06/02	52436.37	22.1	$\geq$ 20.72	-	17.29(0.03)	EKAR
11/06/02	52436.71	22.4	$\geq$ 20.65	19.65(0.07)	17.08(0.03)	N1mT
11/06/02	52436.75	22.5	-	19.54(0.20)	17.27(0.12)	KAIT
14/06/02	52440.39	26.1	$\geq$ 20.58	19.26(0.08)	17.21(0.02)	EMMI
26/06/02	52452.40	38.1	-	20.09(0.08)	17.78(0.07)	INT
27/06/02	52453.42	39.1	21.37(0.12)	20.07(0.03)	17.96(0.06)	INT
29/06/02	52455.43	41.1	-	-	18.26(0.04)	JKT
02/07/02	52458.45	44.2	-	20.01(0.23)	18.24(0.08)	JKT
05/12/02	52613.93	199.6	$\geq$ 23.27	$\geq$ 23.30	-	N1mT
12/12/02	52620.98	206.7	$\geq$ 23.85	$\geq$ 23.41	$\geq$ 23.28	N1mT

* Relative to I_{max} (JD=2452414.42)
N1mT = Lick - Nickel 1m Telescope + Direct imaging 0.28″/px; TNT = Teramo-Normale Telescope + CCD 0.46″/px; KAIT = Lick - Katzman Automatic Imaging Telescope + CCD 0.80″/px; EKAR = Asiago 1.82m Copernico telescope + AFOSC 0.47″/px; EMMI = ESO NTT + EMMI 0.1665″/px; INT = 2.5m Isaac Newton Telescope * WFC 0.33″/px; JKT = Jacob Keptein 1.0m Telescope + JAG 0.33″/px

TABLE 4.3— Original near-IR photometry of SN 2002cv.

Date	JD (+2400000.00)	Phase* (days)	J	H	K	Instr.
09/05/02◁	52403.86	-10.4	17.05(0.11)	-	16.64(0.11)	AZT
13/05/02◁	52407.85	-6.5	15.46(0.01)	14.92(0.02)	14.73(0.05)	AZT
14/05/02◁	52408.85	-5.5	15.26(0.01)	14.61(0.02)	14.36(0.03)	AZTDP
15/05/02◁	52409.82	-4.5	15.07(0.02)	14.56(0.03)	14.25(0.04)	AZTDP
16/05/02◁	52410.86	-3.4	14.90(0.01)	14.44(0.02)	14.21(0.03)	AZT
17/05/02◁	52411.88	-2.4	14.89(0.01)	14.34(0.01)	-	AZTDP
20/05/02◁	52414.83	0.5	14.75(0.03)	-	13.95(0.03)	AZT
26/05/02◁	52420.93	6.6	-	-	14.06(0.04)	AZT
27/05/02◁	52421.86	7.6	-	-	14.06(0.05)	AZTDP
28/05/02◁	52422.91	8.6	15.37(0.04)	-	-	AZT
29/05/02◁	52423.88	9.6	-	14.74(0.02)	-	AZT
30/05/02	52424.86	10.6	-	-	14.16(0.03)	AZTDP
30/05/02	52425.42	11.1	15.69(0.07)	-	-	AZT
31/05/02◁	52425.91	11.6	15.80(0.02)	-	-	AZTDP
01/06/02◁	52426.83	12.5	15.85(0.04)	14.71(0.03)	14.41(0.04)	AZTDP
05/06/02	52431.36	17.1	16.87(0.08)	14.49(0.04)	14.94(0.07)	AZT
12/06/02	52438.35	24.1	16.33(0.03)	14.41(0.03)	14.26(0.04)	AZT
15/06/02	52441.53	27.2	16.04(0.01)	-	14.17(0.01)	SofI
20/06/02	52446.36	32.1	15.77(0.05)	-	13.95(0.10)	AZT
04/07/02	52460.33	46.0	-	-	14.40(0.06)	AZT
09/07/02	52465.33	51.0	15.87(0.09)	-	-	AZT
10/07/02	52466.33	52.0	-	15.39(0.10)	-	AZT
11/07/02	52467.32	53.0	-	-	14.89(0.07)	AZT
12/07/02	52468.33	54.0	16.50(0.10)	-	-	AZT
22/07/02	52478.30	64.0	-	-	14.25(0.80)	AZT

* Relative to I_{max} (JD=2452414.42)
◁ Photometric night
AZT = AZT-24 Telescope (Campo Imperatore Observatory) + SWIRCAM 1.04″/px; AZTDP = data from Di Paola et al. (2002) using the same configuration of AZT; SofI = ESO NTT + SofI 0.29″/px

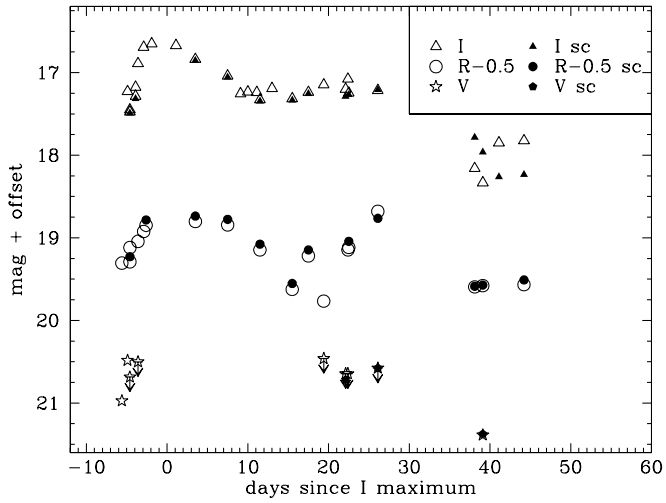

FIGURE 4.3— Comparison between the original VRI band light curves (empty symbols) of SN 2002cv and the corrected one (filled symbols).

Contardo, Leibundgut & Vacca 2000).

The R band light curve presents a pronounced secondary maxima not usual for SNIa. This is probably due to the high reddening suffered by SN 2002cv which shifted the effective wavelength of the R bandpass to the red mimicking the I light curve of an unreddened SN Ia.

We note also that the post-maximum decline of the J light curve is much steeper than in the I band, showing a pronounced J minimum around day +16. On the contrary, a shallow H minimum, occurs few days earlier than those in J, and the K. All these features, except the broad K peak, are typical for Type Ia SN (Meikle 2000).

For comparison, in Figure 4.5 we plot the I light curves of three nearby Type Ia SNe having different Δm_{15}(B): SN 1991T (Δm_{15}(B) = 0.94), SN 1991bg (Δm_{15}(B) = 1.94) and SN 1992A (Δm_{15}(B) = 1.47). The light curves have been shifted to match the I first maximum. As can be seen the light curve of SN 2002cv is best matched by that of SN 1992A even if the first maximum is somewhat narrower in SN 2002cv. Assuming that the two SNe were also similar in the B band we can assign to SN 2002cv a Δm_{15}(B) $\sim$ 1.5.

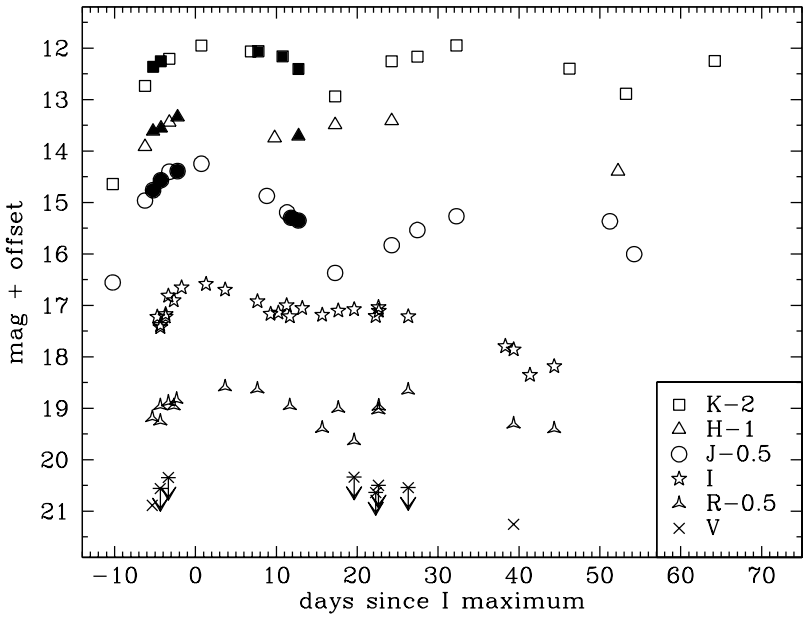

FIGURE 4.4— S-corrected VRIJHK light curves of SN 2002cv during the first weeks past-explosion. The original data measurements by Di Paola et al. (2002) (AZTDP in Table 4.3) are marked as filled symbols. The light curves have been shifted by the amount shown in the legend.

4.1.3 Colour and pseudo bolometric Curves

In Figure 4.6 the evolution of the intrinsic (I-NIR) colours for SN 2002cv (corrected for the reddening as discussed in Section 4.3) is compared with those of a sample of SNe Ia. The colour curves are in general very similar to those of normal SNe Ia such as SN 2001cz (Krisciunas et al. 2004b) or SN 2001el (Krisciunas et al. 2003) but for some differences in the $(I-K)_0$.

The good match of the SN 2002cv colour curve with those of other normal SNe Ia is another confirmation of the classification as SN Ia. This is strengthened by the colour curves present in Figure 4.7, in which the $(I-J)_0$ curve of SN 2002cv is compared with those of other SNe types: SN 2001el (Type Ia, Krisciunas et al. 2003), SN 2004aw (Type Ic, Taubenberger et al. 2006) and SN 2005cs (Type IIP, Pastorello et al. 2007d). During the pre-maximum period all curves have similar colours, but immediately afterwards the three SN types

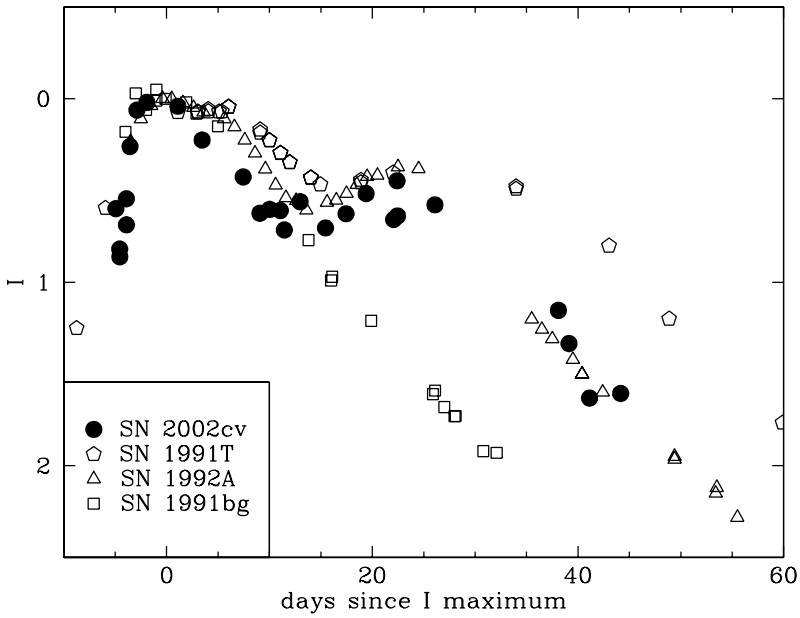

FIGURE 4.5— Comparison between the I band light curve of SN 2002cv and three other Type Ia SNe with different Δm_{15}(B): SN 1991T (Δm_{15}(B) = 0.94), SN 1991bg (Δm_{15}(B) = 1.94) and SN 1992A (Δm_{15}(B) = 1.47) normalized to the I maximum. See Table 4.8 for more information about the SNe.

follow different patterns and SN 2002cv definitely resembles those of SN Ia.

Figure 4.8 shows the "pseudo-bolometric" luminosity evolution of SN 2002cv derived by integrating the flux of the RIJHK bands (with the distance modulus and reddening discussed in Section 4.3). We have also plotted the same pseudo-bolometric light curves of SN 1992A, SN 2002bo and SN 2004eo. In the case of SN 1992A, we added a correction for the unknown NIR contribution following Suntzeff (1996). The reddening-corrected bolometric luminosity at maximum is $\log_{10}L$ (RIJHK) = 42.70 ± 0.20 (erg s^{-1}). The first maximum of SN 2002cv is brighter and earlier than those of the other SNe. SN 2002cv presents a bright and broad secondary maximum similar to that of SN 2004eo. The uncertainties were computed taking into account photometric, reddening and distance errors.

It is well know that for SNIa around maximum most of the flux of SNe Ia is emitted in the UBV bands. From the photometry of SN 2004eo (Pastorello et

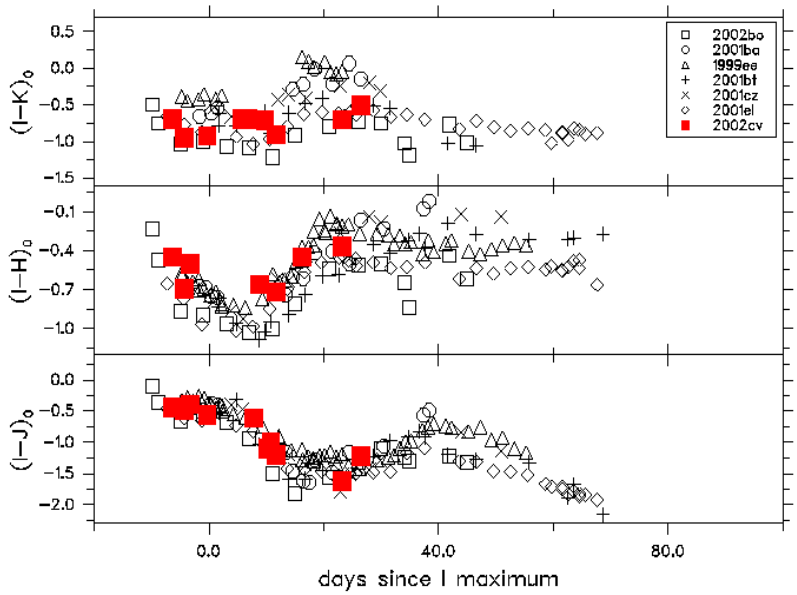

FIGURE 4.6— Colour evolution of SN 2002cv compared with those of SNe 2002bo (Benetti et al. 2004a; Krisciunas et al. 2004b), 2001bt, 2001cz (Krisciunas et al. 2004b), 1999ee, 2001ba (Krisciunas et al. 2004a) and 2001el (Krisciunas et al. 2003). The curves have been dereddened according the values reported in Section 4.3 ($A_V = 8.99 \pm 0.30$ and $R_V = 2.04 \pm 0.30$).

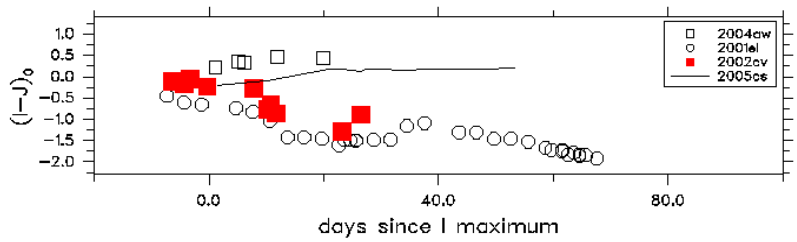

FIGURE 4.7— Colour evolution of SN 2002cv compared with those of SN 2001el (Type Ia SN, Krisciunas et al. 2003), SN 2004aw (Type Ic SN, Taubenberger et al. 2006) and SN 2005cs (Type IIP SN, Pastorello et al. 2007d). The curves have been dereddened according to the values reported in the mentioned papers.

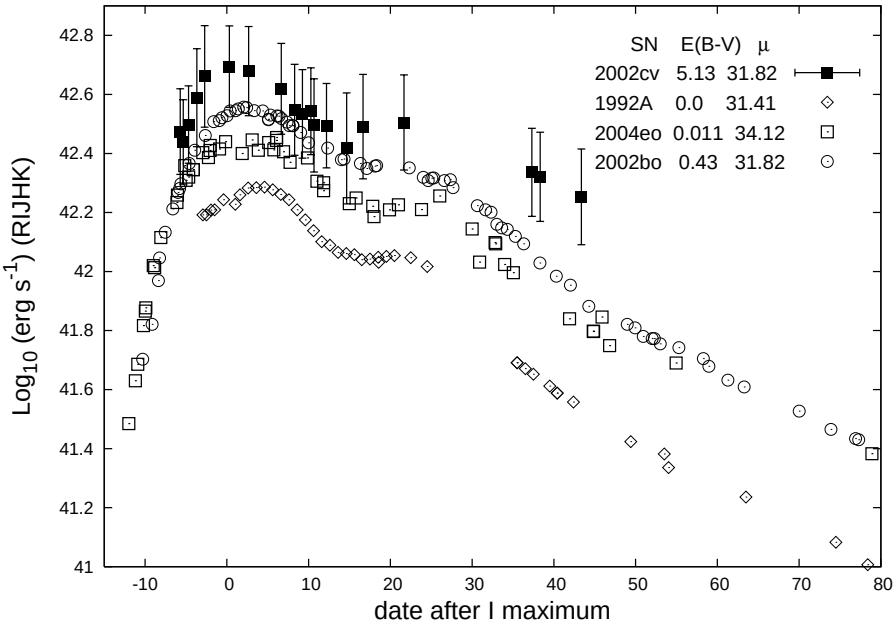

FIGURE 4.8— Pseudo-bolometric (RIJHK) light curve for SN 2002cv (filled squares). Open diamonds, squares and circles give the pseudo-bolometric (RIJHK) light curves for SN 1992A, SN 2004eo and SN 2002bo, respectively. Error bars include photometric, reddening and distance uncertainties.

al. 2007b) we can estimate that the integrated flux carried out by the RIJHK bands is only 39% of the complete flux emitted from U to K band, consistent also with Figure 6 of Contardo, Leibundgut & Vacca (2000). We estimate therefore that the total *uvoir* luminosity at maximum of SN 2002cv was $\log_{10} L_{uvoir} = 43.11$ $(\mathrm{erg\,s^{-1}})$.

Considering that in general the B maximum occurs approximately three days after the I maximum, we can derive the epoch of the I secondary maximum relative to B maximum and read the ^{56}Ni mass from Figure 11 of Kasen (2006). In that work prominence and timing of the I and J secondary maxima were measured and plotted vs. M_{Ni} for I and J band models. Kasen (2006) also computed the ^{56}Ni mass considering the absolute maximum and the deep minimum in J band of their models (Figure 10 of Kasen 2006) and reproduced synthetic model light curves by varying the mass of ^{56}Ni. These models suggest that SN 2002cv should have $M(^{56}\mathrm{Ni}) \leq 0.45\ M_{\odot}$.

TABLE 4.4— Main data of SN 2002cv and its host galaxy.

Host Galaxy Data	NGC 3190	Ref.
α (2000)	$10^h18^m05\overset{s}{.}60$	1
δ (2000)	$+21°49'55''$	1
Galaxy type	SA(s)a pec	1
B magnitude	12.12	1
E(B−V)$_{Gal}$	0.025	2
$v_{r,helio}$ (km s^{-1})*	1271	1
μ	31.82 ± 0.10	3
SN Data	**SN 2002cv**	**Ref.**
α (2000)	$10^h18^m03\overset{s}{.}68$	4
δ (2000)	$+21^o50'06\overset{''}{.}20$	4
Offset SN-Gal. nucleus	$18''W, 10''N$	4
Discovery date (UT)	2002 May 13.7	4
Discovery date (JD)	2452408.20	4
E(B−V)$_{host}$	5.12 ± 1.09	3
$R_{V\,host}$	1.73 ± 0.54	3
$A_{V\,tot}$	8.94 ± 0.95	3
Date of I max (JD)	2452415.09 ± 0.22	3
Magnitude and epoch	V ∼ 19.70; ∼+5.8 (days)	3
at max wrt I max	R = 19.08 ± 0.20; +3.2 (days)	3
	I = 16.57 ± 0.10; 0.0 (days)	3
	J = 14.75 ± 0.01; -0.4 (days)	3
	H = 14.34 ± 0.01; -2.0 (days)	3
	K = 13.91 ± 0.02; +1.6 (days)	3
Magnitude and epoch	I = 17.11 ± 0.10; +23.1 (days)	3
of second IJHK max	J = 15.24 ± 0.19; +41.5 (days)	3
wrt I max	H = 14.40 ± 0.11; +25.9 (days)	3
	K = 13.88 ± 0.29; +35.2 (days)	3
Estimated $\Delta m_{15}(B)_{intrinsic}$	1.46 ± 0.17	3
Absolute magnitude	M_V^{max} ∼ -21.05	3
	M_R^{max} = -18.62 ± 0.67	3
	M_I^{max} = -18.12 ± 0.34	3
	M_J^{max} = -18.76 ± 0.21	3
	M_H^{max} = -18.61 ± 0.16	3
	M_K^{max} = -18.59 ± 0.13	3
$\log_{10}L$ (RIJHK)	42.70 ± 0.20 (erg s^{-1})	3
$\log_{10}L_{uvoir}$	43.11 ± 0.61 (erg s^{-1})	3

* Heliocentric Radial Velocity.
(1) NED; (2) Schlegel, Finkbeiner & Davis (1998); (3) This work; (4) Lavionov & Arkharov (2002).

4.2 Spectroscopy

4.2.1 Data reduction

The spectra were reduced using IRAF or FIGARO (for some IR data) routines as it is described in Section 2.3.3. In the reduction special care was devoted to the background subtraction. The zero points of the wavelength calibration was adjusted against the bright night-sky emission lines. The absolute flux calibration of the spectra checked against the photometry is less than 10%.

The spectroscopic observations are summarised in Table 4.5.

TABLE 4.5— Optical and IR spectroscopic observation of SN 2002cv.

Date	JD (+2400000.00)	Phase* (days)	Grism/Grating	Range (Å)	Instr.
15/05/02	52410.42	-4.0	gm2	5250 - 10300	EKAR
19/05/02	52413.77	-0.7	‡	3300 - 10400	SHANE
08/06/02	52433.75	+19.3	‡	3300 - 10400	SHANE
15/06/02	52440.52	+26.1	gm2	3900 - 9700	EMMI
Date	JD (+2400000.00)	Phase* (days)	Grism/Grating	Range (Å)	Instr.
22/05/02	52417.25	+2.8	gmij	8250 - 13500	UKIRT
23/05/02	52418.25	+3.8	gmk	19800 - 25100	UKIRT
15/06/02	52441.49	+27.1	gmB	9450 - 16512	SofI

* Relative to I_{max} (JD=2452414.42)
‡ grt300/7500+gm600/4310
EKAR = Asiago 1.82m Copernico Telescope + AFOSC; SHANE = Lick - Shane 3m Reflector + Kast Dual Spectrograph; EMMI = ESO NTT + EMMI; UKIRT = United Kingdom Infrared Telescope + CGS4; SofI = ESO NTT + SofI

4.2.2 Optical and NIR spectra

Given the faintness of SN 2002cv, only four spectra in the optical and three in the NIR were secured (Table 4.5).

The sequence of optical spectra of SN 2002cv is shown in Figure 4.9. Our four optical spectra are distributed from -4 days, to +26.1 days relative to I maximum. Spectra are truncated bluewards of 5000 Å because at shorter

wavelengths no signal from the SN was detected. The only feature clearly visible in the optical spectra is the Ca II IR triplet ($\sim$ 8500 Å). In the last spectra there is evidence of Si II-Fe II emission about 6350 Å.

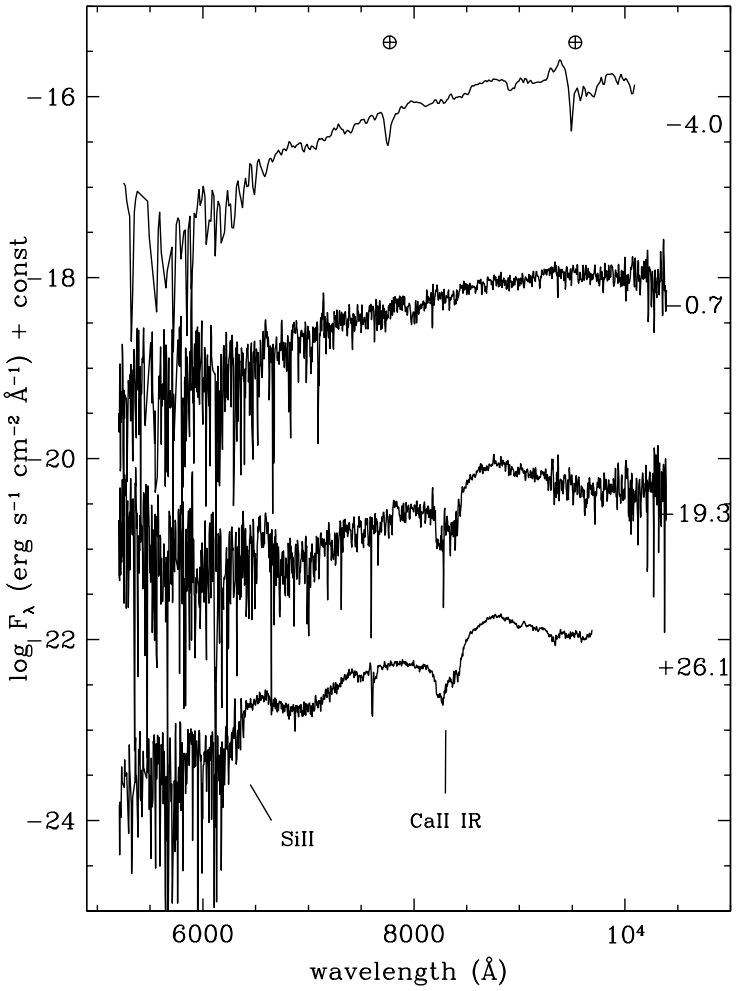

FIGURE 4.9— Optical spectral evolution of SN 2002cv. The ordinate refers to the first spectrum and the others have been shifted downwards by arbitrary amounts (these amounts are -1, -2, -4 and -6.5 from the lowest spectrum to the highest one). Epochs (days) relative to I max are given at the right hand side.

The NIR evolution of SN 2002cv is shown in Figure 4.10. The spectral evolution is typical of SNe Ia. In the earliest spectra the continuum is dominant.

The spectrum at phase $+2.8^d$ shows a weak feature with P-Cygni profile at about 10900 Å (rest wavelength), attributed possibly to Mg II (Meikle et al. 1996; Mazzali & Lucy 1998). A weak emission visible at 20500 Å on day +3.8, may be due to Co II lines (Marion et al. 2003). In the spectrum at +27.1 days, several discrete, doppler-broadened features seem dominate the spectrum. In particular Fe II absorption at ∼12300 Å (Marion et al. 2003) is prominent. Around 15000 Å SN 2002cv shows an abrupt change of the flux observed also in many Type Ia SNe. According to Wheeler et al. (1998) and Marion et al. (2003) the change in slope is because the region between 11000 and 15000 Å has fewer blends of iron-group lines compared to adjacent wavelengths.

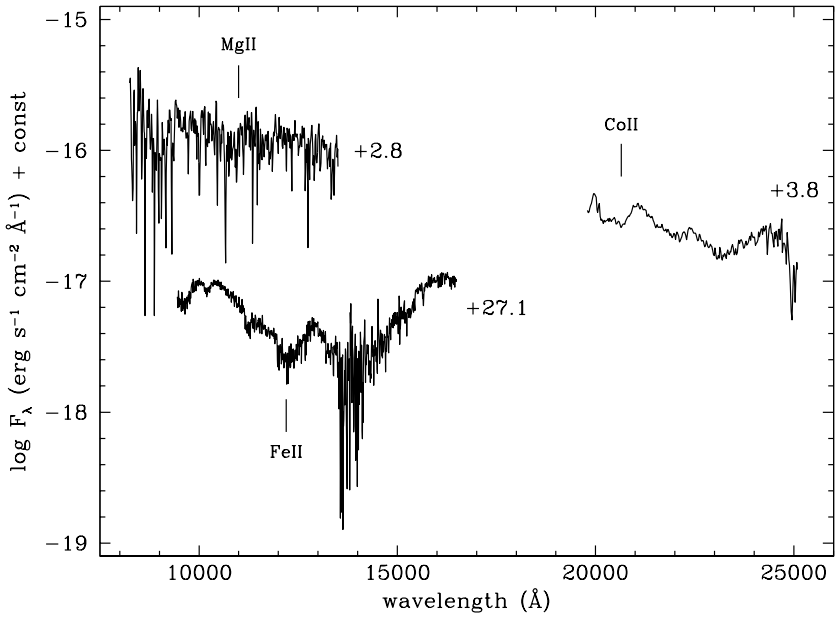

FIGURE 4.10— NIR spectral evolution of SN 2002cv. The ordinate refers to the first spectrum and the others have been shifted downwards by arbitrary amounts (these amounts are -2.5, -1 and 0 from the lowest spectrum to the highest one). Epochs are given at the right hand side.

Figure 4.11 shows the combined nearly-coeval optical and NIR spectra of SN 2002cv (NTT+EMMI at $+26.1^d$ and NTT+SofI at phase $+27.2^d$) compared with similarly aged spectra of SN 2004eo (Type Ia SN, Pastorello et al. 2007b),

SN 2004aw (Type Ic SN, Taubenberger et al. 2006) and SN 1999em[2] (Type II SN, Hamuy et al. 2001; Leonard et al. 2002; Elmhamdi et al. 2003). On this comparison it is clear that SN 2002cv is a Type Ia SN because it presents the same main features seen in SN 2004eo. On the contrary, the pronounced Hα PCygni and Pβ of the Type II SNe (SN 1999em, λ6562.8 and 12818 Å) or the He I and C I around 10830 Å (SN 2004aw) are not present on SN 2002cv.

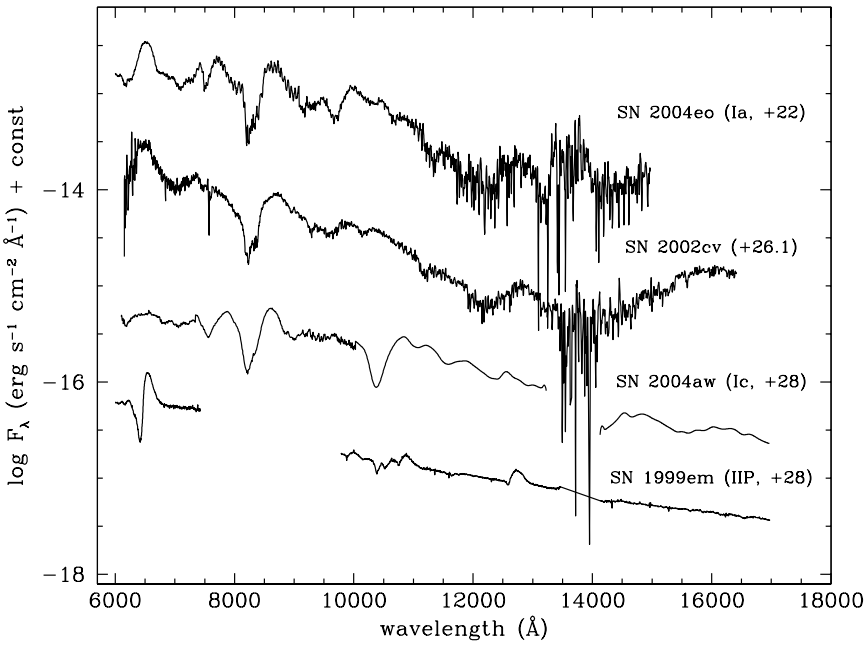

FIGURE 4.11— Comparison between the combined optical and IR spectra of SN 2002cv at +26.1 and +27.1 days after I maximum respectively with those of SN 2004eo (Type Ia SN, Pastorello et al. 2007b), SN 2004aw (Type Ic SN, Taubenberger et al. 2006) and SN 1999em (Type II SN, Hamuy et al. 2001; Leonard et al. 2002). All the spectra have been corrected for redshift and reddening.

4.3 The reddening estimate

As we will discuss in Chapter 6, extinction can be the dominant source of error in the spectrophotometric calibration of SNe Ia.

[2]SN 1999em spectra were downloaded from SUSPECT (The Online Supernova Spectrum Archive): http://bruford.nhn.ou.edu/ suspect/index1.html

Di Paola et al. (2002) derived the extinction of SN 2002cv from the SN absolute magnitudes at maximum via

$$M_\lambda = m_\lambda - \mu - A_\lambda \tag{4.1}$$

for J, H and K bands and with a standard extinction curve estimating $A_V = 7.9 \pm 0.9$.

We have followed the same process using the magnitudes at maximum and the optical absolute magnitudes derived by us (see Section 4.4.3), the mean NIR absolute magnitudes of Type Ia SNe from Krisciunas et al. (2004b) and the distance modulus for NGC 3190 as in Benetti et al. (2004a) for SN 2002bo, $\mu = 31.77$ (this will be discussed below). Then, using the $A_{\lambda,host}$ derived, i.e. for the R band:

$$A_{R,host} = m_R - M_R - \mu - A_{R,Gal} = 19.08 + 19.04^3 - 31.77 - 0.06 = 6.29, \tag{4.2}$$

and the Cardelli, Clayton & Mathis (1989) (hereafter CCM) standard absorption law: $\frac{A_R}{A_V} = 0.751$, $\frac{A_I}{A_V} = 0.479$, $\frac{A_J}{A_V} = 0.282$, $\frac{A_H}{A_V} = 0.190$ and $\frac{A_K}{A_V} = 0.114$, we are able to estimate the A_V, e.g. using the R band only:

$$A_V = \frac{A_{R,host}}{0.751} = 8.37. \tag{4.3}$$

But assuming the canonical value of R_V we could introduce systematic errors if this value is far from the true value. Assuming the canonical $R_V = 3.1$ (Seaton 1979, Savage & Mathis 1979), we obtained an average value for $A_{V,host}$ of 6.15 ± 0.57, which is not close to that obtained by Di Paola et al. (2002).

Because R_V may well be lower than the 3.1, we decided to derive the extinction in the direction to SN 2002cv applying other different methods, which make use of the comparison of the SED and the luminosity of the SN 2002cv with those of other standard SNe Ia.

1. We matched simultaneously the I-J, I-H and I-K colour curves of SN 2002cv with those of other normal SNe Ia (Figure 4.6). Following Elias-Rosa et al. (2006a), it turns out that a unique value of A_V can be obtained only if we adopt a value of R_V smaller than the canonical one. The best match is for $A_V = 9.0 \pm 0.3$ and $R_V = 2.0 \pm 0.3$.

2. We derived the observed extinction curves by comparing the observed optical (> 6000 Å) and NIR SED of SN 2002cv with those of unreddened

[3]This value has been obtained by Prieto, Rest & Suntzeff (2006), see Section 4.4.3

SNe Ia, at similar epochs. The spectra used for this comparison were previously corrected for redshift and Galactic reddening, and scaled to the distance of SN 2002cv (cf. Figure 4.12). This method was applied by Elias-Rosa et al. (2006a) to derive the extinction law to SN 2003cg.

As references we have used the spectra of SN 1992A, SN 1994D, SN 1996X and SN 2004eo (see Table 4.8 for more details about the SNe). With this methods we obtain, as average values: $A_{V,host} = 8.2 \pm 0.6$ and $R_V = 1.5 \pm 0.1$.

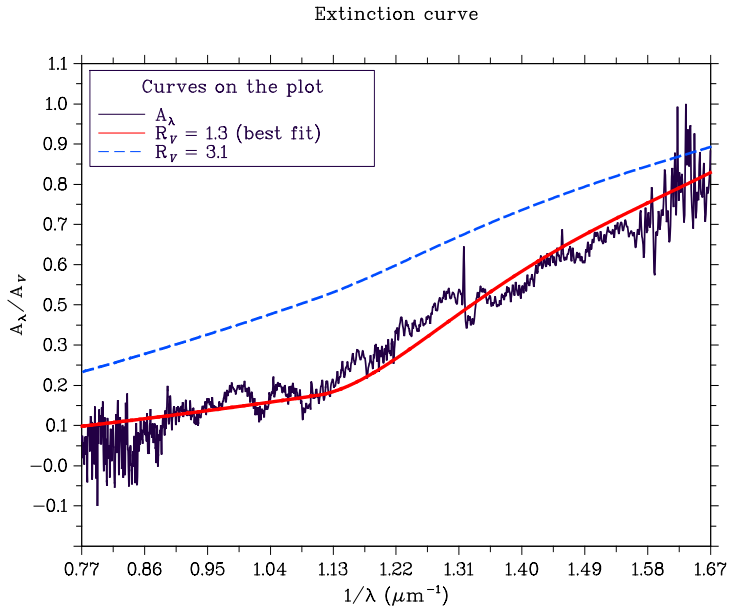

FIGURE 4.12— One of the best fit of the observed extinction law (A_λ/A_V) with the theoretical CCM laws (solid line). The extinction curve of SN 2002cv was obtained with SN 2004eo from 6000 to 12500 Å on day +26. It is also plotted the CCM extinction curve for $R_V = 3.1$ (dashed line) for comparison. From the average of 12 comparisons, we obtained $R_V = 1.5 \pm 0.1$.

3. Another approach to determine A_V and R_V consists of a multi-dimensional maximum likelihood estimation[4] to find the value of A_V, R_V and μ that

[4]The maximum likelihood method is the procedure of finding the value of one or more

TABLE 4.6— Basic input data to find the values of A_V, R_V and μ by multi-dimensional maximum likelihood estimation.

Filter	$m_{\lambda,max}$ [1]	$A_{\lambda,Gal}$	$M_{\lambda,max}$ [2]
R	19.08±0.20	0.064	-19.04±0.13
I	16.57±0.10	0.047	-18.79±0.12
J	14.75±0.03	0.022	-18.61±0.13
H	14.34±0.01	0.014	-18.28±0.15
K	13.91±0.04	0.009	-18.44±0.14

[1] Observed magnitudes at maximum for each band (see Section 4.4.3);
[2] Adopted absolute magnitudes of SN 2002cv. For R and I see 4.4.3, for J, H and K we used the mean absolute magnitudes given by Krisciunas et al. (2004b)

give the best match to the values in column 4 of Table 4.6 from the equation

$$M_\lambda = m_\lambda - \mu - A_{\lambda,Gal} - [A_V(a_\lambda + \frac{b_\lambda}{R_V})]_{host} \tag{4.4}$$

where a_λ and b_λ are wavelength-dependent coefficients given by CCM[5].

Figure 4.13 reproduces the probability contour plot around the derived extinction solution corresponding to a 3, 2 and 1 (the inner one) σ for the 2 parameters A_V and R_V. The uncertainty on R_V and A_V can be read from the 2-σ contour. The biggest value of the maximum likelihood estimation was obtained for $A_V = 9.40 \pm 0.70$, $R_V = 1.70^{+0.52}_{-0.33}$ and distance modulus $\mu = 31.82 \pm 0.10$.

The A_V, and R_V, values found with the three methods are listed in Table 4.7. The averages of these values are $A_V = 8.85 \pm 0.95$ and $R_V = 1.73 \pm 0.54$. Including the galactic extinction component $E(B-V)_{Gal} = 0.025$ (Schlegel, Finkbeiner & Davis 1998), the total extinction suffered by SN 2002cv is $A_{V\,tot} = 8.94 \pm 0.95$, making SN 2002cv one of the most reddened SNe ever observed.

The value of μ found by method (iii) is in excellent agreement with the distance modulus derived using the relative distance from Virgo for NGC 3190 from the (Kraan-Korteweg 1986) catalogue (1.48), $\mu = 31.77$. Moreover, since

parameters for a given statistic which makes the known likelihood distribution a maximum (Myung 2003).

[5] Other values of these coefficients better suited to SNe Ia are also given by Krisciunas et al. (2006) but they are valid only around maximum light.

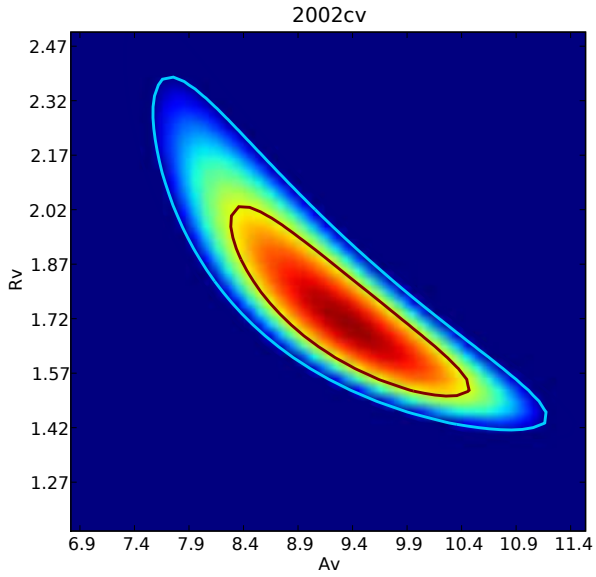

FIGURE 4.13— Multi-dimensional maximum likelihood estimation to derived A_V and R_V. Each contour correspond to 3, 2 and 1 (the inner one) σ. The values found were $A_V = 9.40 \pm 0.70$ and $R_V = 1.70^{+0.52}_{-0.33}$.

TABLE 4.7— Values of the total host extinction in the V band and the ratio of total-to-selective extinction derived from different methods.

Method	$A_{V,host}$	R_V
Colour Evolution	8.99±0.30	2.04±0.30
Comp-CCM	8.17±0.57	1.52±0.11
Multi-dimensional	9.40±0.70	$1.70^{+0.52}_{-0.33}$

NGC 3190 is a member of the Leo III group (García 1993), we can consider the SBF (Surface Brightness Fluctuation - Tonry et al. 2001a) distance of another possible member of the group, NGC 3226 ($\mu = 31.86 \pm 0.24$) as discussed in Krisciunas et al. (2004b) (see Section 2.8 of his paper). All these values are similar to each other. We decided to adopt in the following for NGC 3190 $\mu = 31.82 \pm 0.10$, value obtained in the method (iii).

Finally, as we have seen, the three methods agree on a value of R_V much lower than the canonical $R_V = 3.1$. This is really interesting, because in the

same parent galaxy SN 2002bo exploded, for which an extinction $A_V = 1.18$ was derived using $R_V = 3.1$. Applying the same methods given by Elias-Rosa et al. (2006a) and used before, we matched the B-V, V-R, R-I, V-J, V-H and V-K colour curves of SN 2002bo with those of other normal SNe Ia (Figure 4.14) and we find an A_V in the host galaxy of 1.5 ± 0.3 and a R_V of 3.0 ± 0.3, which confirms the results given by Benetti et al. (2004a) even if SN 2002bo is estimated as brighter by 0.3 mag.

The extinction found for these two objects shows that in NGC 3190 we can find dust with different grain size distributions since R_V is related to the grain size (cfr. Chapter 6). This is not surprising since in the Galaxy we also observe regions with different R_V. We note that, in agreement with Goudfrooij et al. (1994) and Patil et al. (2007), the smaller value of R_V in NGC 3190 is found in the dust lane. This suggests that the observed dust grain size is determined by the time elapsed since the dust lane was accreted from outside (Goudfrooij et al. 1994). These result show us that SNe can be also useful tools in the studies of the dust in other galaxies.

4.4 Photometric parameters

The parameters characterizing the photometric behaviour of the Type Ia SN are usually derived from B and V light curves. For SN 2002cv, B and V bands are heavily extinguished and no detection has been obtained. Hence, to compare this SN to other events we will seek correlations between blue to red light curve parameters.

4.4.1 VRI decline rates vs. Δm_{15}(B)

Hamuy et al. (1996d), using a sample of seven type Ia SNe, showed strong correlations between Δm_{15}(B) and others light curve decline rate parameters, namely Δm_{60}(B), Δm_{20}(V), Δm_{60}(V) and Δm_{60}(I). They also found that for the I band the time between the minimum and secondary maximum is greater for the slow-declining SNe.

Here, we extend the statistics of Hamuy et al. (1996d) to a sample of 20 SNe (Table 4.8) spanning a range between 0.90 and 1.94 in Δm_{15}(B). For each SN we obtained the epoch and magnitude of the maximum light in V, R and I bands, and measured the decay in the first 15, 20, 40 and 60 days after maximum in each band. See Figure 4.15 for a graphical description of these parameters.

Figure 4.16 shows the decline rates of the V light curves versus Δm_{15}(B). The correlations between the different decline rates with Δm_{15}(B) are similar to those found by Hamuy et al. (1996d). We note that the decline rates present in this work are not corrected for the host extinction. Phillips et al. (1999)

showed that Δm_{15}(B) has a weak dependence on reddening. We also checked if a similar correction was required for the other bands using the spectra of three SNe: SN 1994D, SN 1996X and SN 2004eo. We computed Δm_{15}(B), the decline rates for other bands and $\Delta t_{max}(I)$ for (a) the unreddened spectra and (b) the spectra reddened for the Galactic and host galaxy reddening with the law found for SN 2002cv (see Section 4.3). We confirmed the correction for Δm_{15}(B) as given by Phillips et al. (1999) whereas the corrections for the I band parameters turned out to be negligible.

On the contrary, the behaviour of the R band declines rates (Figure 4.17) is different according to the different intervals considered. While there are no correlations between Δm_{15}(B) and Δm_{15}(R) or Δm_{20}(R) except for fast-declining SNe (SN 1991bg), we find a stronger correlation with Δm_{60}(R). This is probably due to the change of opacity and concentration of iron-peak elements in the central regions during these first days (Kasen 2006), which produce the secondary maximum. According to this model, a SN Ia having homogenized abundance stratification shows red light curves where the first and second maxima are indistinguishable. This could be the case for SN 1991bg, which has no secondary maximum and shows high values of the declines also in the redder bands.

In Figure 4.18 we also compared parameters measured from the I light curve with Δm_{15}(B). While it appears that Δm_{15}(I) remains constant, there is a clear correlation between Δm_{40}(I) and Δm_{15}(B) and, though less clear, between Δm_{60}(I) and Δm_{15}(B).

In the I band, the secondary maxima are very pronounced, as seen in the J, H and K light curves. The strength and phase of the secondary maximum was found to correlate with the Δm_{15}(B), being more prominent and later in bright SNe Ia (Hamuy et al. 1996d; Nobili et al. 2005). We measured the magnitude difference ΔI_{max} and time interval $\Delta t_{max}(I)$ between the primary and secondary peaks in the I light curve for the SNe of our sample (see Figure 4.15), and compared them with Δm_{15}(B).

While ΔI_{max} shows no clear correlation with Δm_{15}(B) (Figure 4.19), the correlation between $\Delta t_{max}(I)$ and Δm_{15}(B) is tighter (Figure 4.20) with the phase delay of the secondary maximum longer for slow-declining SNe. Note that SNe with $\Delta m_{15}(\mathrm{B}) \geq 1.8$, similar to SN 1991bg, are not included in the graph because their I light curves do not show a secondary maximum.

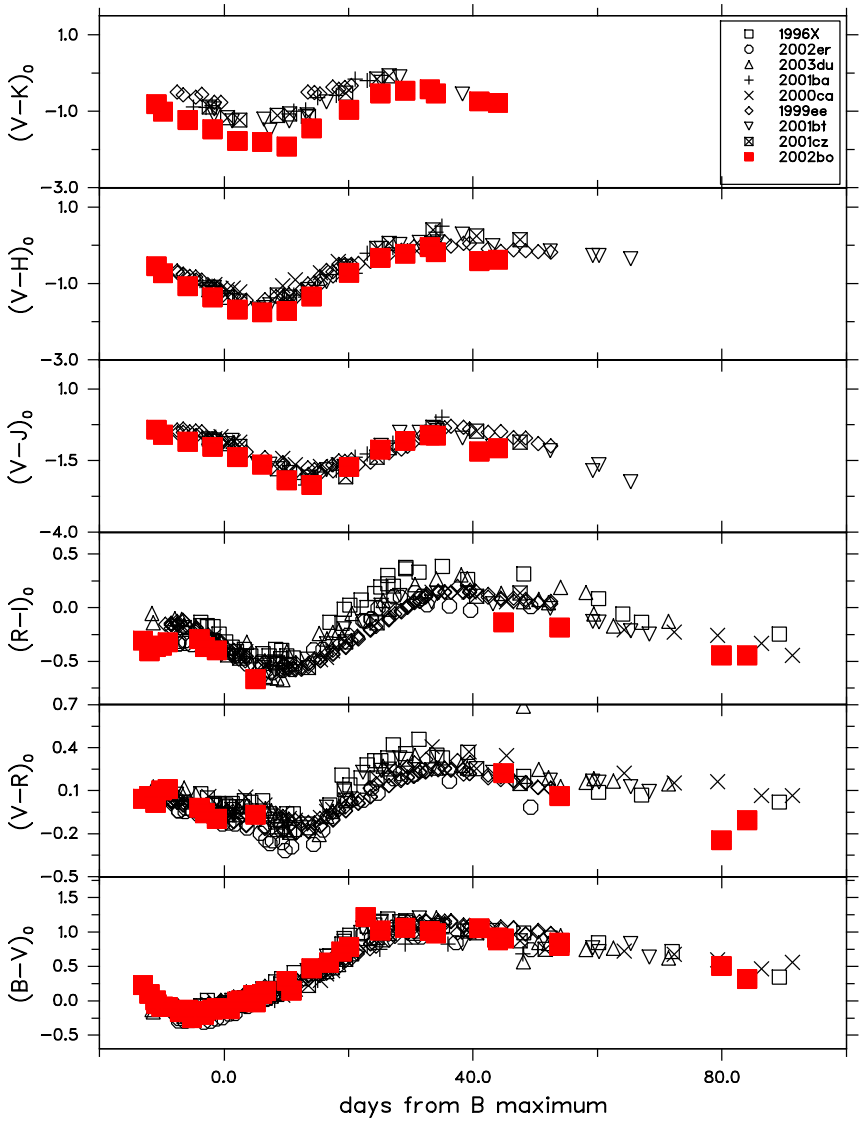

FIGURE 4.14— As in 4.6 for SN 2002bo. The curves have been dereddened according to $A_V = 1.5 \pm 0.3$ and $R_V = 3.0 \pm 0.3$.

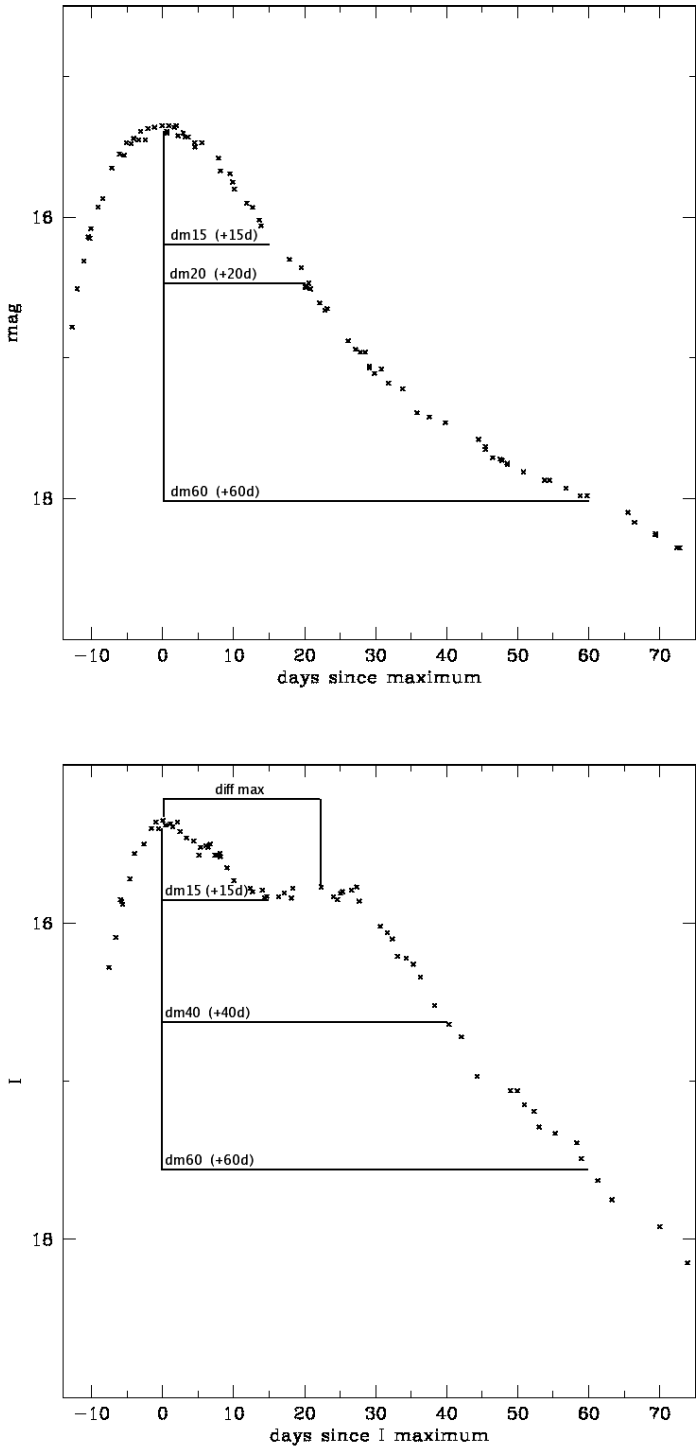

FIGURE 4.15— Graphical representation of the parameters defined in this Section for a general band (top panel) and in particular for I band (bottom panel).

TABLE 4.8— Main parameters for the SNe Ia sample.

SN	$\Delta m_{15}(B)_{obs}$	JD(I_{max}) (+2400000.00)	I_{max}	$\Delta m_{40}(I)_{obs}$	$\Delta max(I)$	μ	$A^*_{I,tot}$	sources
SN 1992bc	0.90(0.05)	48910.84(0.50)	15.56(0.05)	0.98(0.06)	33.13(1.13)	34.56	0.04	0,1,2,3
SN 1991T	0.94(0.05)	48371.60(0.50)	11.62(0.04)	0.69(0.01)	27.75(0.51)	30.74	0.33	0,1,2,4,5,6,7
SN 2003du	1.02(0.05)	52764.92(0.50)	13.83(0.02)	0.97(0.03)	29.78(0.71)	32.42	0.01	0,1,8
SN 1990N	1.05(0.05)	48080.70(0.50)	12.95(0.02)	–	28.86(1.05)	31.07	0.10	0,1,2,6
SN 1992al	1.09(0.05)	48836.86(0.50)	14.93(0.04)	1.02(0.02)	27.50(0.71)	33.82	0.05	0,1,2,3
SN 2005cf	1.11(0.03)	53532.00(0.50)	13.70(0.03)	0.96(0.03)	29.60(0.55)	32.19	0.14	0,1,9
SN 2003cg	1.12(0.05)	52728.22(0.50)	13.82(0.04)	1.13(0.04)	28.08(0.71)	31.28	1.14	0,1,10
SN 2001el	1.13(0.05)	52181.43(1.00)	12.81(0.04)	0.97(0.04)	27.26(1.01)	31.29	0.27†	0,1,2,11
SN 2002bo	1.17(0.05)	52355.50(1.00)	13.49(0.10)	0.98(0.10)	27.94(1.00)	31.77	0.56	0,1,12,13
SN 1995E	1.19(0.05)	49771.00(0.50)	15.33(0.05)	1.01(0.05)	–	33.43	1.01	0,1,2,14
SN 1998dh	1.23(0.17)	51029.32(0.50)	14.10(0.05)	1.21(0.05)	27.50(0.69)	32.92	0.31	0,1,2,15
SN 1994D	1.31(0.05)	49428.50(1.00)	12.11(0.05)	1.31(0.06)	25.02(1.01)	31.14	0.04	0,1,16,17,18,19
SN 1996X	1.32(0.05)	50188.00(1.00)	13.39(0.01)	1.10(0.02)	27.71(1.05)	32.17	0.10	0,1,14,20
SN 2002er	1.33(0.04)	52523.56(0.50)	14.49(0.05)	1.40(0.09)	26.14(0.71)	32.90	0.53	0,1,21
SN 1997E	1.39(0.06)	50466.19(0.50)	15.46(0.05)	1.44(0.07)	22.78(1.41)	33.72	0.28	0,1,2,15
SN 2004eo	1.45(0.04)	53276.30(1.00)	15.36(0.04)	1.26(0.04)	24.13(1.03)	34.12	0.21	0,1,22
SN 1992A	1.47(0.05)	48638.00(0.50)	12.80(0.04)	1.46(0.05)	22.08(0.56)	31.41‡	0.09	0,1,2,7,23
SN 2000cn	1.58(0.12)	51706.93(0.50)	16.63(0.05)	–	–	34.93	0.16	0,1,2,15
SN 1992bo	1.69(0.05)	48984.94(0.50)	15.95(0.05)	1.68(0.05)	20.00(0.71)	34.28	0.08	0,1,2,3
SN 1991bg	1.94(0.05)	48608.60(1.00)	13.51(0.05)	2.42(0.05)	–	31.32	0.06	0,1,2,24,25,26,27

0 = This work; 1 = LED; 2 = Reindl et al. (2005); 3 = Hamuy et al. (1996c); 4 = Schmidt et al. (1994); 5 = Cappellaro et al. (1997); 6 = Lira et al. (1998); 7 = Altavilla et al. (2004); 8 = Stanishev et al. (2006); 9 = Pastorello et al. (2007a); 10 = Elias-Rosa et al. (2006a); 11 = Krisciunas et al. (2003); 12 = Benetti et al. (2004a); 13 = Krisciunas et al. (2004a); 14 = Riess et al. (1999a); 15 = Jha et al. (2006); 16 = Richmond et al. (2005); 17 = Tsvetkov & Pavlyuk (1995); 18 = Patat et al. (1996); 19 = Meikle et al. (1996); 20 = Salvo et al. (2001); 21 = Pignata et al. (2004a); 22 = Pastorello et al. (2007b); 23 = Suntzeff (1996); 24 = Filippenko et al. (1992b); 25 = Leibundgut et al. (1993); 26 = Turatto et al. (1996); 27 = Tonry et al. (2001b); * $A_{I,Gal}$+$A_{I,host}$; † $E(B-V)_{host} = 0.18$, with $R_V = 2.88$; ‡ average μ from different sources.

4.4.2 I magnitudes and Δm_{15}(B)

It is well known that the shape of the B light curve is a characteristic parameter of SN Ia, which correlates with the luminosity class of the events. If the B band is missing, as for SN 2002cv, we are forced to find alternative methods to establish the photometric class of the SN. In Figure 4.5 we have already shown that the I light curve shapes of SNe 2002cv and 1992A were similar and so have similar $\Delta m_{15}(\mathrm{B}) \sim 1.5$. In order to obtain an accurate estimate of Δm_{15}(B), we exploit the previously derived correlations, involving Δm_{40}(I) (SN 2002cv was observed until +44.2 days after I maximum) and the $\Delta t_{max}(I)$. Using the code developed by Akritas & Bershady (1996) for linear regression analysis, we performed a linear fit to the points in Figures 4.18 and 4.20 obtaining respectively:

$$\Delta t_{max}(I) = -17.68(\pm 1.52) \times \Delta m_{15}(B) + 48.80(\pm 1.89), \tag{4.5}$$

and,

$$\Delta m_{40}(I) = 1.55(\pm 0.17) \times \Delta m_{15}(B) - 0.77(\pm 0.23). \tag{4.6}$$

For the equation 4.5 we used 16 SNe and the Pearson correlation coefficient is -0.94. Whereas for equation 4.6 we used 18 SNe and the Pearson correlation coefficient is 0.93[6].

Since Δm_{15}(B) is related to the B luminosities of the Type Ia SNe, we could expect a similar relation between Δm_{40}(I) and M_I^{max} the absolute magnitude of the first I maximum, and even between the $\Delta t_{max}(I)$ and M_I^{max}. Figures 4.21 and 4.22 confirm this expectation though in both cases the dispersion is high but consistent with the uncertainties of the distance modulus used for computing M_I^{max}.

Linear fits to the two relations give:

$$M_I^{max} = -0.05(\pm 0.02) \times \Delta t_{max}(I) - 17.45(\pm 0.68), \tag{4.7}$$

and,

$$M_I^{max} = 1.06(\pm 0.24) \times \Delta m_{40}(I) - 20.14(\pm 0.31). \tag{4.8}$$

For the two relations 15 and 18 SNe were used, obtaining correlation coefficients 0.57 and 0.73 respectively.

[6] In the fit of $\Delta t_{max}(I)$ vs. Δm_{15}(B) we excluded SN 1991T which appears to deviate (as in Hamuy et al. 1996d). Indeed SN 1991T was an abnormal object with a variety of pre-maximum spectroscopic peculiarities (Filippenko et al. 1992a; Phillips et al. 1992)

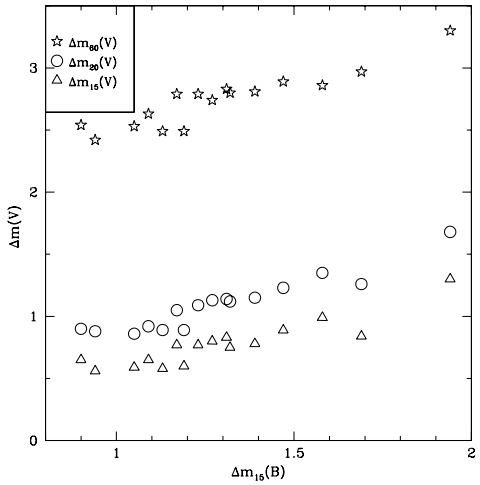

FIGURE 4.16— V light curve decline rates Δm_{15}(V) (triangles), Δm_{20}(V) (circles) and Δm_{60}(V) (stars) vs. $\Delta m_{15}(B)_{obs}$.

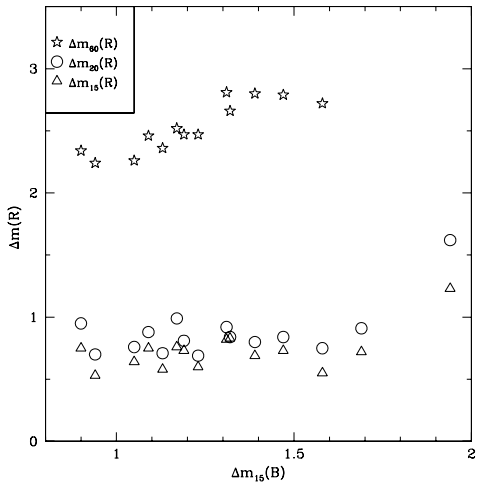

FIGURE 4.17— R light curve decline rates Δm_{15}(R) (triangles), Δm_{20}(R) (circles) and Δm_{60}(R) (stars) vs. $\Delta m_{15}(B)_{obs}$.

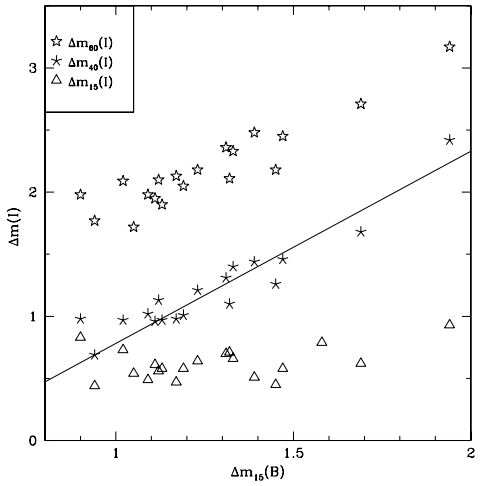

FIGURE 4.18— I light curve decline rates Δm_{15}(I) (triangles), Δm_{40}(I) (asterisks) and Δm_{60}(I) (stars) vs. $\Delta m_{15}(B)_{obs}$.

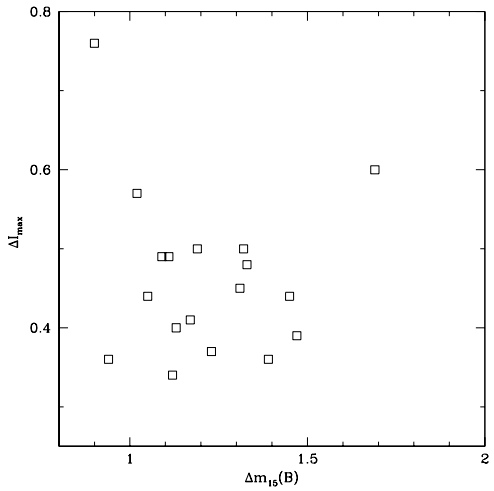

FIGURE 4.19— Difference of magnitude between the primary and secondary maxima of I light curve, ΔI_{max}, vs. $\Delta m_{15}(B)_{obs}$.

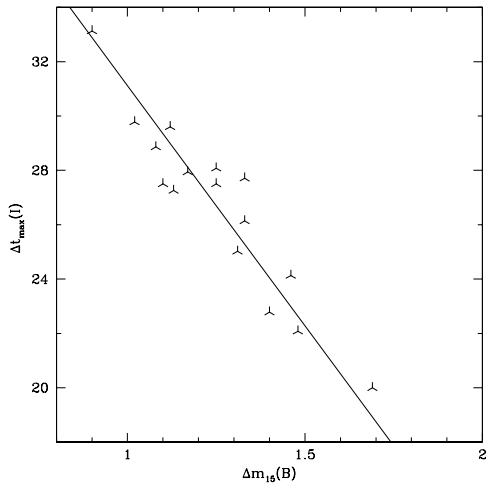

FIGURE 4.20— Difference in phase between primary and secondary maxima of I light curve ($\Delta t_{max}(I)$) vs. $\Delta m_{15}(B)_{obs}$. The straight line is the best fit.

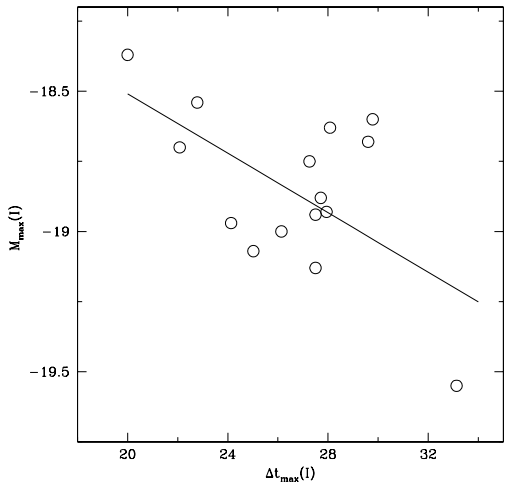

FIGURE 4.21— M_I^{max} vs. $\Delta t_{max}(I)$, for the SNe of Table 4.8. The straight line represent the relation 4.7.

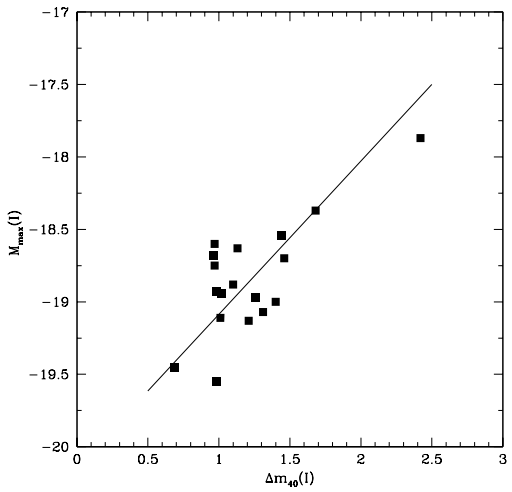

FIGURE 4.22— M_I^{max} vs. Δm_{40}(I), with the best fitting drawn.

4.4.3 Parameters of SN 2002cv

The maximum light epochs and magnitudes for the different bands, reported in Table 4.4, were derived by fitting low order polynomials (lower than 5) to the light curves. The first I maximum is found on JD(I_{max}) = 2452415.09 ± 0.22 (May 20.6 2002 UT) with I_{max} = 16.57 ± 0.10. The I band secondary maximum occurred 23.06 ± 0.59 days after with magnitude 17.11 ± 0.10. In addition we measured Δm_{40}(I) = 1.50 ± 0.32.

Using equations 4.5 and 4.6, we derived a Δm_{15}(B) average value of 1.46 ± 0.17, very close to that of SN 1992A.

Afterwards, from the measured $\Delta t_{max}(I)$ and Δm_{40}(I), we used equations 4.7 and 4.8 to derive an estimate of the intrinsic I absolute magnitude at maximum for SN 2002cv. The values obtained are M_I^{max} = -18.60 ± 0.84 and M_I^{max} = -18.55 ± 0.76 respectively with a weighted average value of $< M_I^{max} >$ = -18.57 ± 0.57. This magnitude is close to the average value for SN Ia found by Saha et al. (1999): $< M_I^{max} >$ = -18.74 ± 0.03 (scaled to H_0 = 72 $\mathrm{km\,s^{-1}} Mpc^{-1}$).

For the I band we can derive the absolute magnitude also through the relation with Δm_{15}(B). Using the known relation between the peak luminosity and the Δm_{15}(B) of Hamuy et al. (1996a) ("peak subsample" case), Phillips

TABLE 4.9— Absolute I magnitude of SN 2002cv derived from different methods and scaled to $H_0 = 72\ \mathrm{km\,s^{-1}}Mpc^{-1}$.

M_I^{max}	Method	Reference
-18.57 ± 0.57	eq. 4.7 and 4.8	this work
-18.52 ± 0.20	M_I^{max} vs. Δm_{15}(B)	Hamuy et al. (1996a)[1]
-18.52 ± 0.28	M_I^{max} vs. Δm_{15}(B)	Phillips et al. (1999)[2]
-18.79 ± 0.12	M_I^{max} vs. Δm_{15}(B)	Prieto, Rest & Suntzeff (2006)[3]

(1) according to the relation given in Table 3 of Hamuy et al. (1996a) (peak luminosity);
(2) according to the relation given in Table 3 of Phillips et al. (1999);
(3) according to the relation given in Table 3 of Prieto, Rest & Suntzeff (2006) (for the complete sample - ALL).

et al. (1999) (see their Table 3) and Prieto, Rest & Suntzeff (2006) (complete sample reported in Table 3), scaled to $H_0 = 72\ \mathrm{km\,s^{-1}}Mpc^{-1}$, we derived M_I^{max} quite close to that estimate with our equations (see Table 4.9). We note that the equation 4.4 and the necessary parameter seen previously, provide M_I^{max} = -18.12 ± 0.34 in agreement for marginally fainter with the above estimation within the calculated errors.

Considering again the Prieto, Rest & Suntzeff (2006) relation, we obtain an analogous measurement for the R band M_R^{max} = -19.04 ± 0.13. Hamuy et al. (1996a) and Phillips et al. (1999) do not provide an average relation in R band. As before, by applying the equation 4.4 we obtain again a marginally fainter value for M_R^{max}, that is -18.62 ± 0.67.

The NIR absolute magnitudes were estimated from the observed peak magnitude and μ. Their values: M_J^{max} = -18.76 ± 0.21, M_H^{max} = -18.61 ± 0.16 and M_K^{max} = -18.59 ± 0.13, are consistent with the average values found by Krisciunas et al. (2004b) within the errors (M_J^{max} = -18.61 ± 0.13, M_H^{max} = -18.28 ± 0.15 and M_K^{max} = -18.44 ± 0.14).

V maximum light was difficult to estimate because due to the high extinction SN 2002cv was hardly visible in this band and only few measurements are available (see Table 4.2 and Figure 4.4). We are able to give an estimate of the expected V_{max} considering M_V^{max} = -19.03 ± 0.13 (using the Prieto, Rest & Suntzeff (2006) relation for V band), μ = 31.82 ± 0.10, $A_{V,Gal}$ = 0.078 and $A_{V,host}$ = 8.85 ± 0.95, and it is V_{max} = 21.72 ± 0.96.

4.5 Summary

We have presented optical and near-infrared data of SN 2002cv and completed the study of this SN (Di Paola et al. 2002). SN 2002cv exploded in the same galaxy as SN 2002bo, a few months later, and it presents an extremely high extinction.

In disagreement with Meikle & Mattila (2002), the shape of the light curves of SN 2002cv are similar to those of SN 1992A, and not to those of SN 1991T.

Moreover, the presence of clear secondary maxima, typical of the Type Ia SNe, in all redder light curves, its colour curves and the features of its spectra, confirms its early classification as a Type Ia SN. SN 2002cv is also one of the earliest SNe discovered in the NIR bands: it was discovered in the JK at phase -10.4 days, during the rise time to maximum.

We have used different methods to estimate the extinction adopting in all cases a standard extinction law (CCM) with R_V as free parameter, and we obtained E(B−V) = 5.12 ± 1.09 and R_V = 1.73 ± 0.54 for the host galaxy, which give a total A_V of 8.94 ± 0.95. It turns out that SN 2002cv is one of the most reddened supernovae ever observed and a new entry in the growing list of SNe with a low value of R_V (e.g. SN 1999cl - Krisciunas et al. 2006, SN 2001el - Krisciunas et al. 2003, SN 2002hh - Pozzo et al. 2006, SN 2003cg - Elias-Rosa et al. 2006a).

We have constructed empirical relations between Δm_{15}(B) and M_I^{max}, the delay of the secondary I maximum ($\Delta t_{max}(I)$) and the decline rate at 40 days in the I band (Δm_{40}(I)). These allow the calibration of the SNe Ia in an independent way, i.e. without the use of the B band. With these average relations we derive for SN 2002cv $\Delta m_{15}(B)_{intrinsic}$ = 1.46 ± 0.17 and a M_I^{max} = -18.57 ± 0.57, which is marginally brighter than that estimated from the observed peak magnitude and μ: -18.12 ± 0.34, probably because of the low intrinsic magnitude of the object.

By considering the results obtained in the study of SN 2002cv, it is clear that this object represents a peculiar SNe Ia, increasing in this way the number of high extinguished SNe. Moreover, the peculiarity of having two observable line of sight in the same host galaxy makes this object fundamental for the study of the extinction in NGC 3190.

5

Peculiar dust around SN 2006X

Es lo que hay.
Roi Alonso Sobrino

¡Pa' habernos matado!.
Nahida Darwich Sobrino

In this Chapter we present early optical photometry and spectroscopy of the reddened Type Ia SN 2006X. The high extinction of this SN was already detected in the classification spectrum, which shows a continuum too red for an unextinguished SN Ia at early phases. The study of the extinction law, carried out in analogy to the other objects of this thesis, shows an atypical law in the direction of this object. The peculiarity of this SN are the Na ID interstellar lines, which were found to evolve with time. This could be explained by the presence of circumstellar material in the vicinity of the explosion location, most likely physically related to the supernova progenitor system. This unique finding adds a new intriguing element to the study of SNe Ia as distance indicators. The results are shown in Sections 5.2, 5.3 and 5.4.

SN 2006X is a bright Type Ia supernova, still visible at the time of writing, in the Virgo cluster galaxy M 100 (NGC 4321), at $\alpha = 12^h22^m53\overset{s}{.}99, \delta = +15^o48'33\overset{''}{.}10$ (2000.0), $12''$W and $48''$S of the nucleus of host galaxy (Figure 5.1). It was discovered by Suzuki & Migliardi (2006) on 4 February 2006 and classified a few days later by Quimby et al. (2006a) as an early Type Ia SN most likely affected by a substantial extinction.

From spectropolarimetric data (range 330-850 nm) of SN 2006X obtained using the Very Large Telescope at the European Southern Observatory, Wang et al. (2006a) found a high continuum polarization, reaching ~ 8 % in the blue and decreasing approximately linearly to about 3.5 % in the red. They reported that the spectropolarization was significantly different from that typically ob-

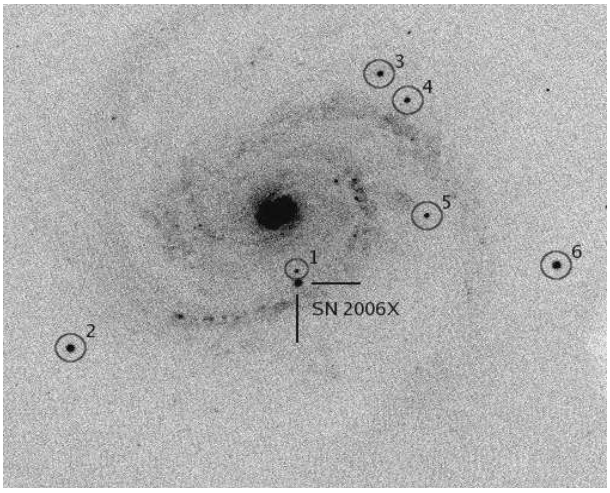

FIGURE 5.1— V band image of SN 2006X in M100 taken with the NOT+ALFOSC on 2006 Feb. 17 (FoV$\sim 6'.5 \times 6'.0$). Local sequence stars are indicated. N is up and E is to the left.

served for extinguished Galactic stars, which may suggest either that the dust properties in NGC 4321 are very different from those of the Galaxy, or that dust and polarization are of circumstellar origin.

Following this argumentation and taking into account the red continuum and the evident Na ID interstellar absorption lines at the velocity of the host galaxy, we consider this object as a ideal target for our study of the absorption toward Type Ia SNe.

5.1 Data acquisition and reduction

SN 2006X was observed in the optical using all the telescopes available to the ESC (Appendix A). 6 different instrumental configurations were used, and the follow-up spanned a period of about 4 months (from February to May 2006). At the time of writing, the SN is still visible at m $\sim$ 22, and nebular data are being taken.

The SN 2006X photometric observations were processed as described in Chapter 2. First, the data were trimmed, corrected for overscan and bias, and flat-fielded. Then, the instrumental magnitudes of the SN and the local standards (see Figure 5.1) were measured using the IRAF point-spread-function (PSF) fitting routine. The SN magnitudes reported in Table 5.1 were calibrated on the basis of two photometric nights. Since we can collect more data of SN 2006X, no S-correction has been applied (see Section 2.3.2 for more de-

tails). The magnitudes were calibrated through linear colour equations, with the colour terms of all instrumental setups determined through observations of Landolt (1992) standard fields or communicated to us by the staff of the observatories.

The spectra were reduced and optimally extracted using standard IRAF routines (see Section 2.3.3). For most spectra the error in the wavelength calibration is $< \pm 2$ Å, and the flux calibration is typically accurate within $\pm 10\%$. The spectroscopic observations are summarised in Table 5.2.

5.2 Photometry

5.2.1 Light curves

The early-time optical light curves of SN 2006X are shown in Figure 5.2. Phases are measured relative to the epoch of the B maximum, which occurred on February 20.8, 2006 UT (JD = 2453787.34). The first point of these light curves is at -3.7 days from B maximum, and the last one is at +59.0 days.

The shapes of the light curves are typical of a normal Type Ia SN, showing secondary maxima longward of the V band, and the first I maximum occurring before the V and R maxima (see Contardo, Leibundgut & Vacca 2000). The epochs and magnitudes of maximum light for the different bands were estimated by fitting low order polynomials to the light curves around their respective maxima. The results are summarized in Table 5.3.

In order to estimate Δm_{15}(B) (the B magnitude decline between the maximum and 15 days later, Phillips 1993) of SN 2006X from our sparsely sampled light curves, we compare the B light curve of SN 2006X with those of other three nearby Type Ia SNe having different Δm_{15}(B) (Figure 5.3): SN 1991T (Δm_{15}(B) = 0.94), SN 1991bg (Δm_{15}(B) = 1.94) and SN 2002bo (Δm_{15}(B) = 1.17)[1]. The light curves have been shifted to match the B maximum. As can be seen from Figure 5.3 the light curve of SN 2006X is best matched by that of SN 2002bo. Considering this comparison, we find a value for SN 2006X of Δm_{15}(B) $\sim$ 1.17.

Estimating the stretch factor in the B band (also described in Chapter 3) to match the template light curves, we find s = 0.96 $\pm$ 0.03 (see Figure 5.4), which corresponds to Δm_{15}(B) = 1.21 $\pm$ 0.07 according to the relation given by Altavilla et al. (2004).

[1]The references of these SNe can be found in Table 4.8

TABLE 5.1— Optical photometry of SN 2006X.

date	JD (+2400000.00)	Phase* (days)	U	B	V	R	I	z'	Instr.
17/02/06	53783.61	-3.7	16.89(0.05)	15.55(0.01)	14.27(0.01)	13.54(0.01)	13.40(0.01)	12.85(0.01)	LT
18/02/06◁	53784.59	-2.8	16.91(0.03)	15.50(0.01)	14.20(0.01)	13.52(0.01)	13.43(0.01)	12.87(0.01)	LT
21/02/06◁	53787.55	0.2	17.15(0.03)	15.37(0.01)	14.11(0.01)	13.34(0.01)	13.49(0.01)	12.80(0.01)	LT
23/02/06	53790.50	3.2	17.24(0.07)	15.55(0.01)	14.03(0.06)	13.42(0.04)	13.56(0.05)	12.86(0.01)	LT
26/02/06	53793.48	6.1	17.44(0.12)	15.68(0.01)	14.12(0.01)	13.59(0.02)	13.79(0.02)	13.01(0.01)	LT
06/03/06	53800.95	13.6	-	16.58(0.06)	14.74(0.05)	14.01(0.01)	13.84(0.02)	-	ASI
13/03/06	53807.54	20.2	18.49(0.03)	17.29(0.01)	14.94(0.01)	14.11(0.01)	13.72(0.01)	-	NSC
16/03/06	53810.54	23.2	18.69(0.01)	17.57(0.01)	15.05(0.01)	14.16(0.01)	13.69(0.01)	-	NSC
21/03/06	53815.54	28.2	19.06(0.01)	18.01(0.01)	15.38(0.01)	14.40(0.01)	13.78(0.01)	-	NSC
26/03/06	53820.57	33.2	-	18.09(0.10)	15.73(0.04)	14.72(0.02)	14.24(0.01)	13.29(0.01)	LT
31/03/06	53825.64	38.3	-	18.28(0.04)	15.94(0.02)	14.95(0.03)	14.58(0.01)	13.62(0.03)	LT
20/04/06	53846.38	59.0	-	18.37(0.06)	16.55(0.02)	15.82(0.05)	15.29(0.06)	-	ASI

* Relative to B_{max} (JD=2453787.34)

◁ Photometric night

LT = Liverpool Telescope + RATCAM 0.14″/px; ASI = Asiago-Ekar 1.82m Copernico telescope + AFOSC 0.47″/px; NSC = Nordic Optical Telescope + StanCam 0.176″/px

TABLE 5.2— Optical spectroscopy of SN 2006X.

Date	JD (+2400000.00)	Phase* (days)	Range (Å)	Instr.
08/02/06	53774.60	-12.7	4550-6950	AS12
10/02/06	53776.57	-10.8	4000-8050	AS12
16/02/06	53782.65	-4.7	3650-9350	TNG
02/03/06	53797.53	10.5	3650-9350	CAF
06/03/06	53801.45	14.1	3650-9350	AS18
16/03/06	53810.53	23.2	3650-9350	TNG
21/04/06	53847.49	60.2	4000-7800	AS18
18/05/06	53873.95	86.6	3600-9350	NAL

* Relative to B_{max} (JD=2453787.34)
AS12 = Asiago-Pennar 1.22m Galilei Telescope + B&C; TNG = Telescopio Nazionale Galileo + DOLORES; CAF = Calar Alto 2.2m + CAFOS; AS18 = Asiago-Ekar 1.82m Copernico Telescope + AFOSC; NAL = NAL = Nordic Optical Telescope + ALFOSC

From the average of these two values of Δm_{15}(B), we estimate that we assume SN 2006X has Δm_{15}(B) of $\sim$ 1.19, which is not far from the value found by K. Krisciunas (1.28, private communication).

5.2.2 Colour curves

In Figure 5.5 (top panel) we present the intrinsic (B-V) colour of SN 2006X compared with that of SN 2002bo. The curves are in general very similar, and the good match between them is another confirmation that SN 2006X is an intrinsically normal type Ia SN. This match was obtained adopting E(B−V) = 1.30 ± 0.04 and the canonical value of R_V (= 3.1). However, significant problems appear when we try to match other colour curves using the same values. For example, we find a global offset between the (V-R) colour curves of SN 2006X and SN 2002bo of about 0.8 magnitudes (see Figure 5.5 - bottom). This is an evident indication that the value of R_V is different from the canonical one, and is probably lower. This issue will be discussed more extensively in Section 5.4.1.

TABLE 5.3— Main data of SN 2006X and its host galaxy.

Host Galaxy Data	NGC 4321 (M100)	Ref.
α (2000)	$12^h22^m54\overset{s}{.}90$	1
δ (2000)	$+15^o49'21''$	1
Galaxy type	SAB(s)bc	1
B magnitude	10.05	1
E(B−V)$_{Gal}$	0.026	2
$v_{r,helio}$ (km s^{-1})*	1571	1
μ (for $H_0 = 72$ km s^{-1} Mpc^{-1})	31.03 ± 0.17	3
SN Data	**SN 2006X**	**Ref.**
α (2000)	$12^h22^m53\overset{s}{.}99$	4
δ (2000)	$+15^o48'33''.10$	4
Offset SN-Gal. nucleus	$12''W, 48''S$	4
Discovery date (UT)	2006 February 7.10	4
Discovery date (JD)	2453773.6	4
E(B−V)$_{host}$	1.27 ± 0.37	5
$R_{V\,host}$	1.56 ± 0.30	5
A$_{V\,tot}$	2.06 ± 0.69	5
Date of B max (JD)	2453787.3 ± 0.1	6
Magnitude at max and	U = 16.64 ± 0.03; -1.6 (days)	6
epoch at max wrt B max	B = 15.41 ± 0.04; 0.0 (days)	6
	V = 14.06 ± 0.04; 2.7 (days)	6
	R = 13.36 ± 0.05; 1.4 (days)	6
	I = 13.41 ± 0.04; -2.6 (days)	6
	Z = 13.55 ± 0.05; -2.6 (days)	6
Magnitude second I max	I = 13.70 ± 0.04; +25.0 (days)	6
and epoch wrt B max		
Estimated $\Delta m_{15}(B)_{obs}$	1.19 ± 0.07	6
Stretch factor in B	0.96 ± 0.03	6
Absolute magnitude	M_U^{max} = -18.83 ± 0.71	6
	M_B^{max} = -19.04 ± 0.71	6
	M_V^{max} = -19.03 ± 0.71	6
	M_R^{max} = -18.99 ± 0.71	6
	M_I^{max} = -18.21 ± 0.71	6

* Heliocentric Radial Velocity.

(1) NED; (2) Schlegel, Finkbeiner & Davis (1998); (3) Ferrarese et al. (1996); (4) Ponticello et al. 2006; (5) K. Krisciunas (private communication); (6) This work.

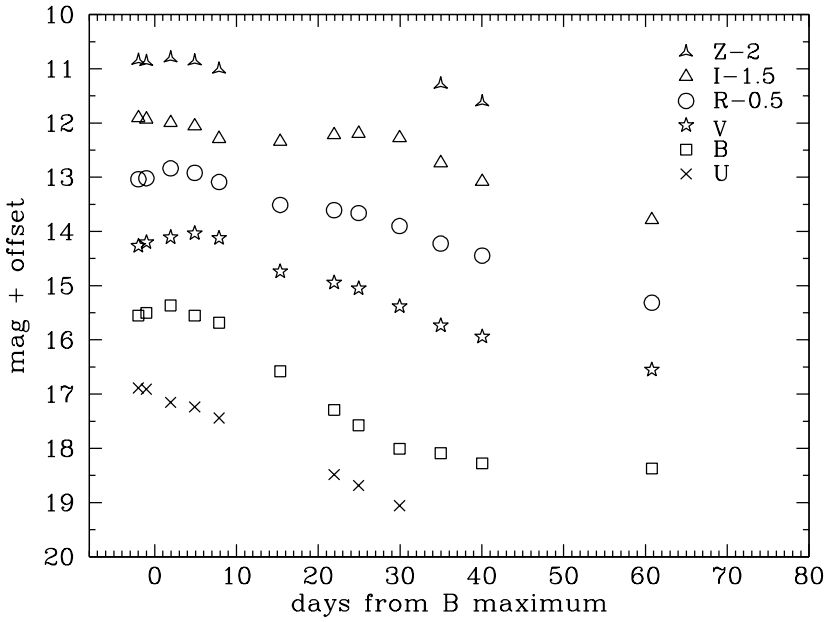

FIGURE 5.2— Optical light curves of SN 2006X during the first months after explosion. The light curves have been shifted along the y axis by the amount shown in the legend.

5.3 Spectroscopy

5.3.1 Spectral evolution

The eight optical spectra of SN 2006X are shown in Figure 5.6. Their phases range from -12.7 to +86.6 days relative to B maximum. They look similar to those of other normal Type Ia SNe but, as already detected in the first spectrum obtained (Quimby et al. 2006a), have a red continuum which gives evidence of high extinction. This idea is supported by the clearly visible Na I D interstellar absorption observed at $\sim$ 5915 Å in the spectra (it will be discussed in detail in the next section). Around maximum light, the P Cygni profile of Si II at $\sim$ 4130 Å is weak. Instead, the spectra show two prominent absorption troughs at $\sim$ 4300 Å and $\sim$ 4900 Å. While the former can be attributed to a combination of Mg II, Fe III and Si III lines, the latter is predominantly formed by transition of Fe III, Si II and S II. The W shaped feature at $\sim$ 5300 Å is almost caused solely by S II. Between 5700 and 6400 Å the spectra are dominated by Si II lines, typical of Type Ia SNe. At $\sim$ 8500 Å we can identify the Ca II IR triplet.

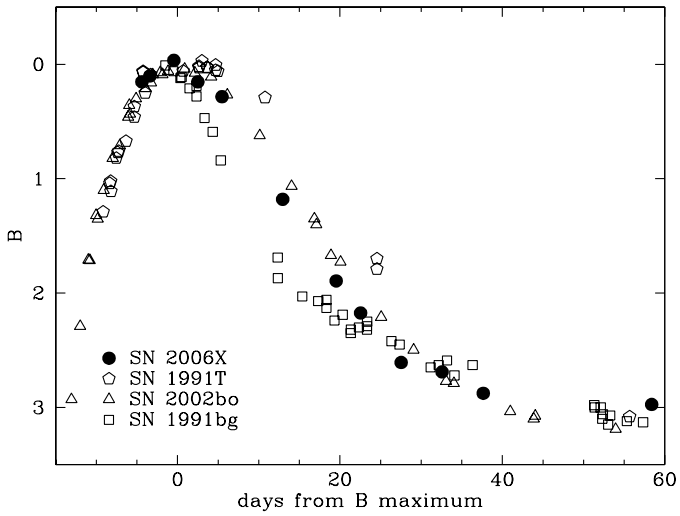

FIGURE 5.3— Comparison between the B band light curve of SN 2006X and three other Type Ia SNe with different Δm_{15}(B): SN 1991T (Δm_{15}(B) = 0.94), SN 1991bg (Δm_{15}(B) = 1.94) and SN 2002bo (Δm_{15}(B) = 1.17) normalized to the B maximum.

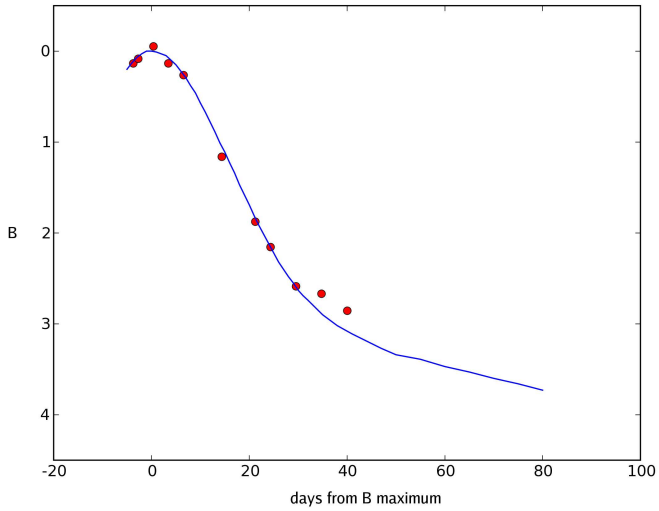

FIGURE 5.4— Best B template match to obtain the stretch factor for SN 2006X (s = 0.96 ± 0.03).

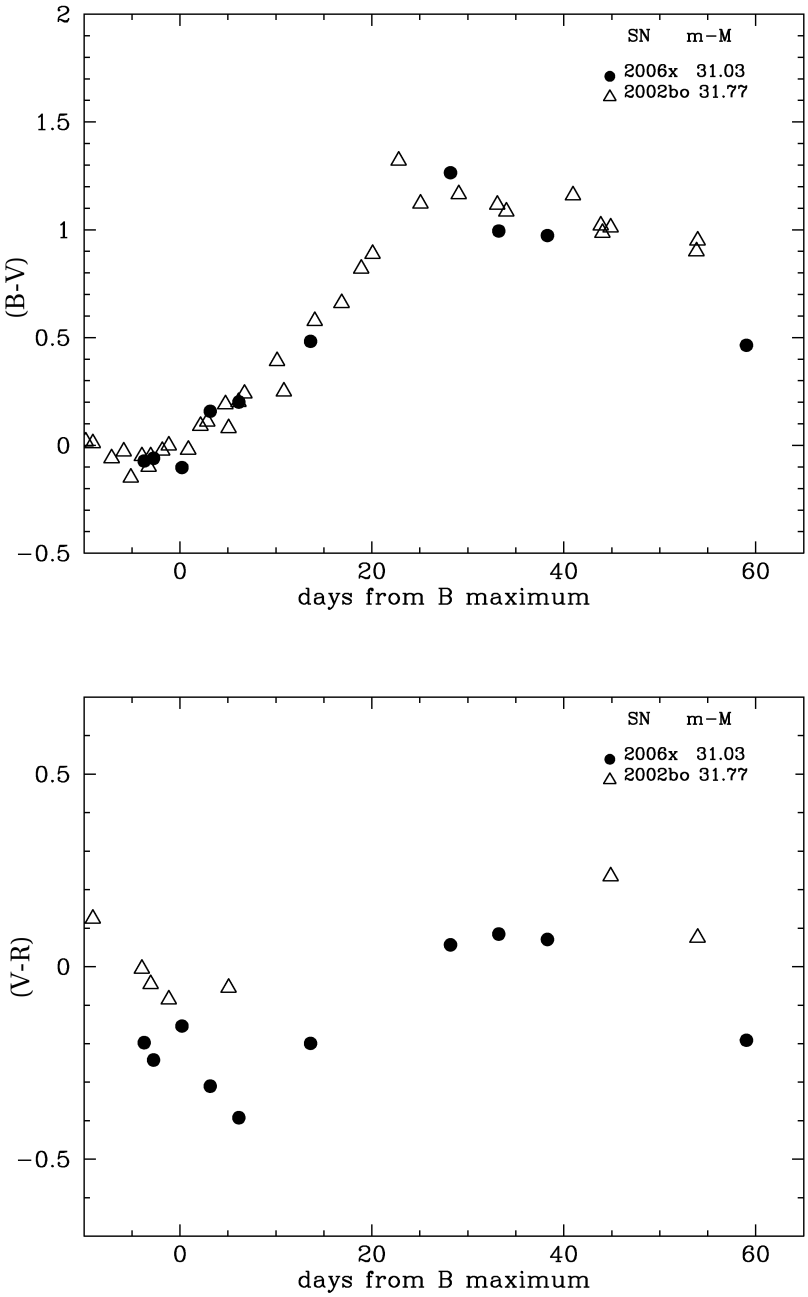

FIGURE 5.5— (B-V) and (V-R) colour curves of SN 2006X (filled circles) compared with those of SN 2002bo (empty triangles) (Benetti et al. 2004a; Krisciunas et al. 2004b). The SN 2006X curves have been dereddened according to E(B−V) = 1.30 ± 0.04 and $R_V = 3.1$.

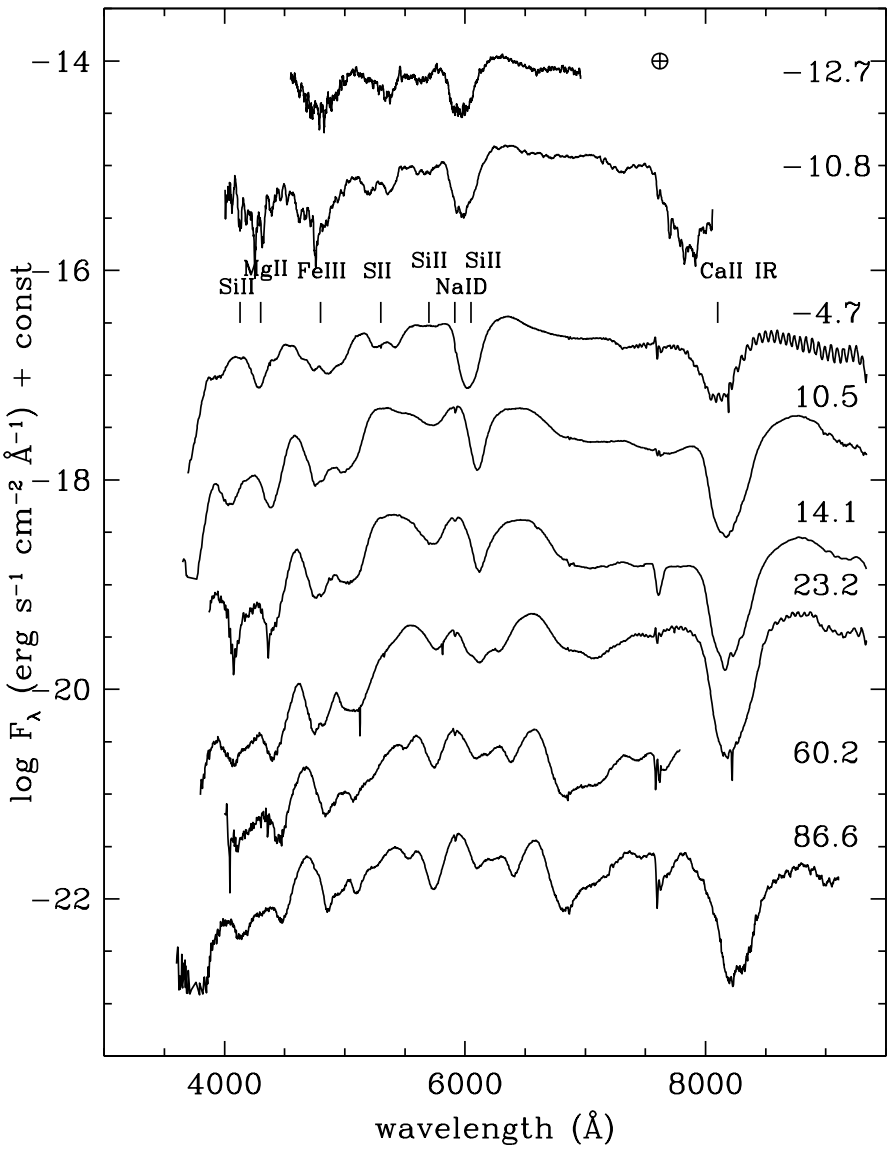

FIGURE 5.6— Optical spectral evolution of SN 2006X. The ordinate refers to the first spectrum and the others have been shifted downwards by arbitrary amounts. Epochs (days) relative to B maximum are given at the right hand side.

In Figure 5.7 we compare the optical spectra of SN 2006X at three epochs, around maximum light, 4 weeks after and three months after, with those coeval of SN 2002bo (Benetti et al. 2004a). The similarity of SN 2006X to SN 2002bo is evident, both SNe showing well-developed and structured features due to intermediate mass elements but with clear differences in the shape of the Si II λ6355 line. In SN 2006X this feature has a fairly symmetrical profile, which is not the case in SN 2002bo. Evident is also the high expansion velocity of this line in SN 2006X (this will be discussed in detail in the next section).

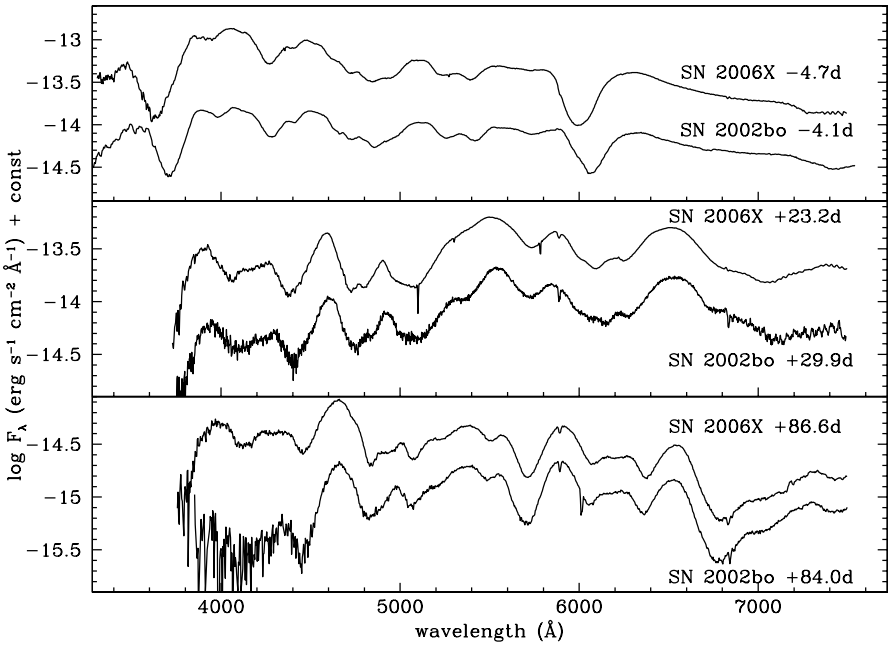

FIGURE 5.7— Comparison between optical spectra of SN 2006X and those of SN 2002bo (Benetti et al. 2004a) at three different phases. All the spectra have been corrected for redshift and reddening (see text).

5.3.2 Velocity gradient

In the previous section we have seen the deep Si II line at 6355 Å rest wavelength present in the SN 2006X spectra. This line is visible from the earliest spectra to more than two weeks after maximum, shifting rapidly redwards with time.

In Section 3.4.3 we have extensively referred to the study of Benetti et al. (2005a) on the diversity of the type Ia SNe. Following that work, we compare

the SN 2006X Si II velocity evolution with that of a sample of SNe Ia (Figure 5.8). Undoubtedly, SN 2006X is one of the SNe with the highest velocity gradients ever seen. It is a member of the HVG group (normal SNe Ia with high velocity gradients, but brighter absolute magnitudes and higher absolute expansion velocities than the FAINT SNe, see Benetti et al. 2005a), with velocity gradient[2]: $\dot{v}_{SN2006X} \sim 165 \pm 6$ km s^{-1} d^{-1} much higher than average $\langle \dot{v} \rangle = 97$ ($\sigma = 16$) km s^{-1} d^{-1}. Notwithstanding, the estimated Δm_{15}(B) and expansion velocity at 10 days past maximum are in agreement with the average values for the SNe of the HVG group: $\Delta m_{15}(\mathrm{B})_{SN2006X} = 1.19 \pm 0.07$ vs. $\langle \Delta m_{15}(\mathrm{B}) \rangle = 1.20$ ($\sigma = 0.1$) and $v_{10}(\mathrm{Si\,II})_{SN2006X} = 13140 \pm 0.10$ km s^{-1} vs. $\langle v_{10}(\mathrm{Si\,II}) \rangle = 12200$ ($\sigma = 1.1$). The absolute magnitudes of SN 2006X (see next section) are slightly fainter that the average $\langle \mathrm{M}_B \rangle$ = -19.3 ($\sigma = 0.3$) but they are within of the range of values established for all the sample of the HVG group. A physical interpretation of such high velocities could be related to the SN progenitor system evolution and explosion dynamics, but it is still under investigation. Benetti et al. (2005a) suggest that the HVG SNe may be delayed detonations with the internal dispersion arising from a range of transition densities, while the LVG SNe might originate from pure deflagrations.

5.4 Extinction

In the previous Chapters we have seen two examples of highly reddened Type Ia SNe, and we have found the necessity for lower R_V values in the extinction law in order to make their various colour curves be consistent with normal Type Ia SNe. Here we present another case of a strongly extinguished object, SN 2006X, this time with evidence of specific behaviour of the Na ID interstellar lines.

5.4.1 Reddening estimate

In Section 5.2.2 we have seen that the (B-V) colour curve of SN 2006X can be matched to that of SN 2002bo by correcting the former with E(B−V) = 1.30 ± 0.04 but we found difficulties when attempting to simultaneously match other colours, e.g. the (V-R) colour curve, using the same values of $R_V = 3.1$. Note that this value is in good agreement with the value obtained by K. Krisciunas (private communication) on a larger set of data with respect to the analysis here reported.

As argued before, this indicates that the value of R_V is different from that usually found for dust in our Galaxy. Including also NIR data which are less

[2] $\dot{v}$ = -$\Delta v/\Delta t$ is derived from least-squares fits of the measurements taken between maximum and either the time the Si II feature disappears.

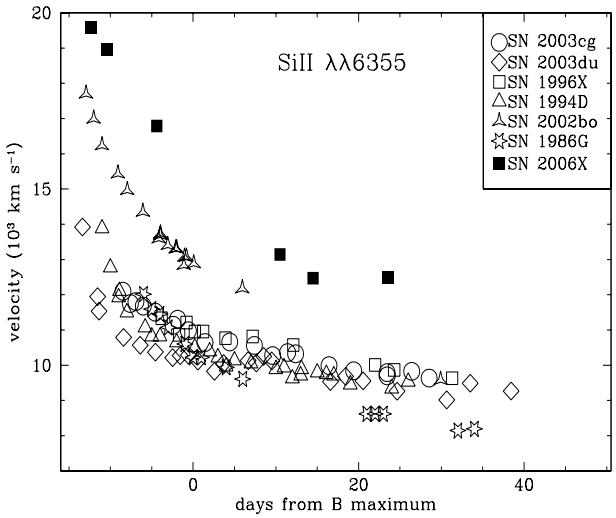

FIGURE 5.8— Evolution of the expansion velocity derived from the minima of Si II 6355 Å for SN 2006X, compared with another HVG, SN 2002bo (Benetti et al. 2004a). Also shown are the evolution of the FAINT SN 1986G (Cristiani et al. 1992) and of a sample of SNe of LVG (Benetti et al. 2005a) SNe: SN 2003cg (Elias-Rosa et al. 2006a), SN 2003du (Stanishev et al., in preparation), SN 1996X (Salvo et al. 2001) and SN 1994D (Patat et al. 1996).

affected by extinction, K. Krisciunas infers a significantly smaller R_V of 1.56 ± 0.30.

Another approach to determine A_V and R_V was introduced by Elias-Rosa et al. (2006a) and in Section 3.2.2. It consists of the comparison of the observed optical spectra with those of unreddened SNe Ia (template) at similar epochs, previously corrected for redshift and Galactic reddening and scaled to the distance of SN 2006X. In this case we used SN 2004eo (Pastorello et al. 2007b) as template because it is an unreddened SN Ia with similar features to SN 2006X. Figure 5.9 shows the best fit obtained, which gives $A_V = 2.08 \pm 0.57$ and $R_V = 1.74 \pm 0.11$. We note that the E(B-V) resulting is in good agreement with that derived by colour curve analysis.

K. Krisciunas (private communication) estimated the extinction of SN 2006X using a data set larger than ours. He also obtained an independent determination of R_V which is in agreement with our finding. Because of the higher precision of his estimation, in the following we will adopt his determination $A_V = 1.98 \pm 0.69$ and $R_V = 1.56 \pm 0.30$ which corresponds to E(B-V) = 1.27 ±

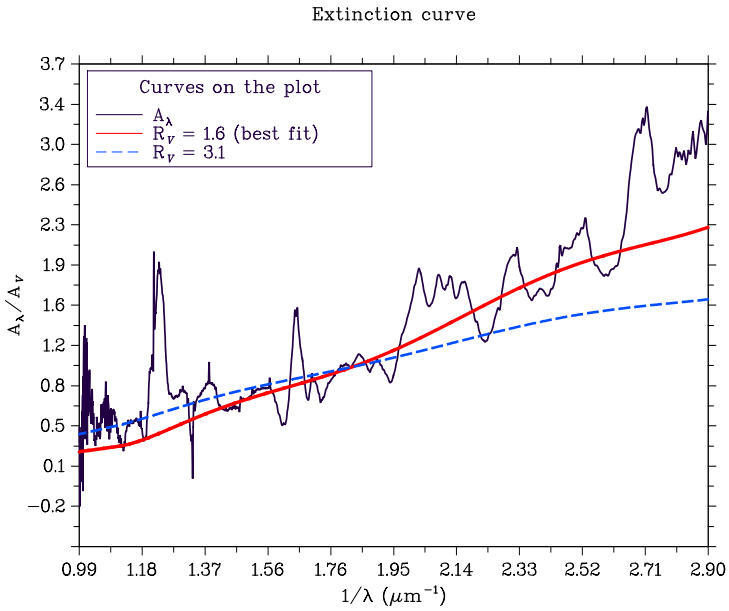

FIGURE 5.9— Best fit of the observed extinction law (A_λ/A_V) with the theoretical Cardelli, Clayton & Mathis (1989) (CCM) laws (solid line). The observed extinction curve of SN 2006X was obtained with SN 2004eo on day +14. The CCM extinction curve for $R_V = 3.1$ (dashed line) is also plotted for comparison. The best match is obtained with $A_V = 2.08 \pm 0.57$ and $R_V = 1.74 \pm 0.11$.

0.37.

With the 16.1 Mpc Cepheid distance of M100 ($\mu = 31.03 \pm 0.17$, Ferrarese et al. 1996), with the observed V magnitude (V = 14.06 mag) and using a A_{Vtot} = 2.06 ± 0.69 (total absorption estimated by K. Krisciunas), we obtained an absolute V magnitude M_V^{max} = -19.03 ± 0.71. On the other hand, if we assume that this is a normal Type Ia SN, with say M_V^{max} = -19.34 ± 0.05 (Gibson et al. 2000 for $H_0 = 72$ km s^{-1} Mpc^{-1}), the apparent V luminosity would imply A_{Vtot} = 2.29, meaning that the extinction could be higher than that estimated by K. Krisciunas. Absolute magnitudes for the other bands estimated with our data are listed in Table 5.3.

5.4.2 Sodium lines

A few days after the discovery of SN 2006X, on 2006 February 13 and 23, high resolution spectra were obtained by Lauroesch et al. (2006). These spectra showed very intense interstellar absorption features, identified as CN, Na I, Ca II and K I, confirming the presence of significant extinction along the line of sight. With the aim of detecting possible evolution in the narrow absorption lines, Patat et al. (2007) observed SN 2006X with the high resolution UVES spectrometer[3]. The very good quality of the data allowed to detect a number of features, both belonging to our own Galaxy and to M100.

In Figure 5.1 we can see as the apparent position of SN 2006X is very close to a spiral arm of M100, which is inclined by 28 degrees with respect to the line of sight (Canzian & Allen 1997). Given the relatively high extinction (see previous section), the SN most probably exploded inside or behind the disk of the host galaxy. Moreover, the SN is projected onto the receding side of the galaxy, since the component of the rotation velocity along the line of sight at the apparent SN location is about 75 $\mathrm{km\,s^{-1}}$ (Rand 1995, Canzian & Allen 1997), which coincides with the strongly saturated Na ID component. This suggests very clear that the very deep absorption (which is very well visible also in the Ca II H&K lines and in the CN vibrational band (0-0), see Patat et al. 2007) arises inside the disk of M100, in a cloud (or system of clouds) which is responsible for the bulk of reddening suffered by SN 2006X.

In Figure 5.10 the spectral region of the Na ID lines is shown. The equivalent widths of the Na ID lines measured in this spectrum are 670.5 and 625.4 mÅ for the D2 and D1 components respectively. The implied total Na I column density, estimated fitting Voigt line profiles with VPFIT[4], is as large as $\log N \sim 14.3$. For a Milky Way-like dust mixture this would turn into a color excess E(B−V) $\sim$ 1.1 (Hobbs 1974). Moreover, the CN lines are clearly visible in this high resolution spectrum. These lines are unusual for extragalactic objects. The equivalent widths measured for the three lines are: EW $[R(0)] = 91 \pm 2$, EW $[R(1)] = 60 \pm 3$ and EW $[P(1)] = 42 \pm 3$ mÅ which, after correcting for saturation effects, correspond to column densities of $\log [NR(0)] = 14.0 \pm 0.1$, $\log[NR(1)] = 13.6 \pm 0.1$ and $\log[NR(1)] = 13.6 \pm 0.1$ respectively. Stars having comparable column densities in our own Galaxy are known to have color

[3]The UVES spectrometer is mounted at the 8.2m ESO Very Large Telescope. The adopted instrumental setup covers simultaneously three wavelength ranges (3290-4500 Å 4780-5740 Å and 5830-6800 Å) with a resolution 7 $\mathrm{km\,s^{-1}}$ (FWHM) at 5900 Å. Patat et al. (2007) observed SN 2006X at several different epochs, here we show the Na ID region of the spectra taken on February 18 2006 (UT), which correspond to -2 days with respect to B band maximum light.

[4]VPFIT has been developed by R. F. Carswell and can be freely downloaded at http://www.ast.cam.ac.uk/rfc/vpt.html

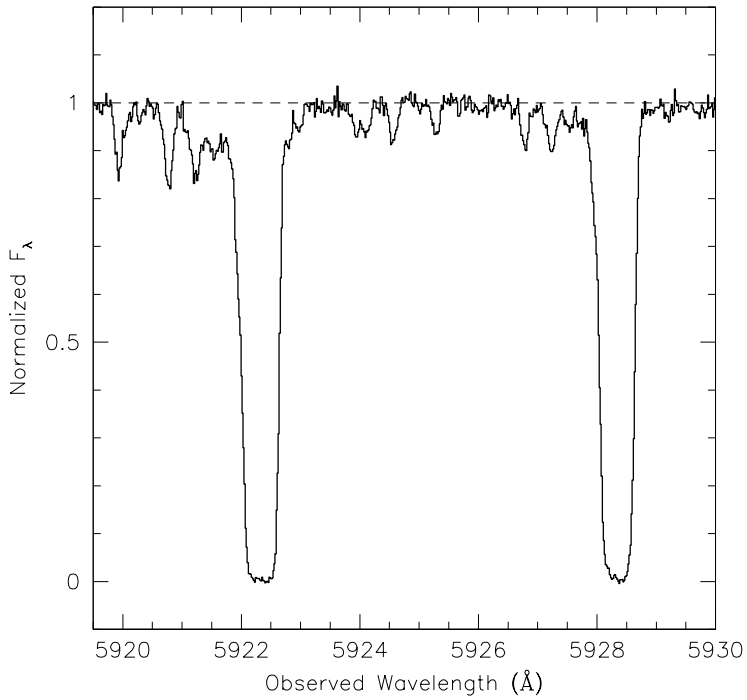

FIGURE 5.10— Detail of the interstellar Na ID region of SN 2006X obtained on 2006 February 18 with the high resolution UVES spectrometer.

excesses larger than E(B−V) = 1 (see for example Crutcher 1985). Applying the method outlined by Meyer & Jura (1985), a temperature of 3.0 ± 0.2 K is derived for this cloud, leading to the conclusion that this material has certainly nothing to do with the SN and is not influenced by its radiation field.

This information in itself is very interesting and, certainly deserve further investigation. However, the most striking result derived from high resolution observations of SN 2006X is that Na ID shows a significant time evolution of the various components (see Figure 5.10 and Patat et al. 2007). We obtained several spectra spaced by several weeks and others are planned.

We believe that the evolution of the profile of the Na ID lines will give us the first direct evidence of circumstellar material for a Type Ia SN, which can be a feature common to all objects of this kind. The study of the interstellar line evolution in SN 2006X and a new program to detect such features in other SNe Ia will provide new information on the nature of the type Ia progenitors

(for more details see Patat et al. 2007).

5.5 Summary

At first glance, SN 2006X seemed to be a typical heavily extinguished Type Ia SN. A more detailed investigation has revealed striking peculiarities, in particular different grain properties of this dust and the variability of the Na ID interstellar lines. Hence, this SN provides clues toward a better characterization of the dust of its host galaxy, M100, which is extensively studied at all wavelengths.

While the E(B−V) of SN 2006X is very similar to that of SN 2003cg, the EW of the Na ID lines is only about one half of that measured in SN 2003cg.

Evidently, SN 2006X is a highly interesting case. The clear evolution of the Na ID absorption features could be caused by the presence of circumstellar material in the vicinity of the explosion location. A yet unresolved question is whether what we have seen in SN 2006X represents the rule or is rather an exceptional case. Following Patat et al. (2007), we think that there are sufficient reasons to suspect that variability of the Na ID lines caused by circumstellar dust may be a common feature in SNe Ia. It may have escaped detection firstly because it requires long integration times on large telescopes and, secondly, because there was no good reason to expect changes along the line of sight on timescales of SN activity.

Here we have presented the main results obtained for SN 2006X. They were extracted from a set of data selected for this thesis in order to sample the most important epochs during the object evolution. We reckon they will not change significantly after the analysis of the whole set of data will be carried out in a forthcoming work.

6

Dust

Calima: existencia de partículas muy pequeñas de polvo o arena en suspensión en la atmósfera.
Wikipedia

Dust is a ubiquitous feature of the cosmos, impinging directly or indirectly on most fields of modern astronomy. Its study is a highly active area of current research. This Chapter aims to give an overview of this phenomenon and of how it can affect our interpretation of the SNe observations.

The study of extinction by interstellar dust probably began with Wilhelm Struve and his analysis of star counts (Struve 1847). Struve demonstrated that the apparent number of stars per unit volume of space declines in all directions with the distance from the Sun. This led him to hypothesize that starlight suffers an absorption proportional to the distance covered. Also William Herschel, in the 18th century, noted the presence of "holes" in the distribution of stars on the sky. Unfortunately these suggestions did not gain acceptance until the beginning of the 20th century, when Kapteyn (1909) recognized the potential significance of extinction:

"Undoubtedly one of the greatest difficulties, if not the greatest of all, in the way of obtaining an understanding of the real distribution of the stars in space, lies in our uncertainty about the amount of loss suffered by the light on its way to the observer"

The confirmation of the interstellar extinction hypothesis came some years later as the result of Trumpler's (1930a, b, c) research, who measured the distance of clusters of stars using two different methods: measuring the apparent luminosities of the stars in a cluster and the apparent diameter of the cluster as a whole. Doing this for many clusters, he found that cluster distances as determined using the luminosities of the stars were systematically larger than those determined using their dimensions and that this discrepancy increases with the distance. He concluded that the space between the stars is not empty, and that there is a component of the interstellar medium (hereafter ISM) that absorbs starlight; hence, a distance-dependent correction must be applied to the apparent brightness and intrinsic luminosity.

Later, in the 1940's, it was shown that obscuration varies with wavelength. In the visible the obscuration scales with wavelength approximately as λ^{-1} indicating that the obscuring material is composed of small, solid particles having dimensions comparable to an optical wavelength.

Today dust particles play a fundamental role in the explanation of many phenomena, are implicated in star formation, in the formation of molecules in interstellar space, drive the mass loss in the stars at the end of their lives and are vital in the formation of planets.

6.1 Interstellar medium

The interstellar medium (or ISM) is the material which fills the space between the stars. It consists of an extremely dilute plasma, gas and dust, consisting of a mixture of ions, atoms, molecules, larger dust grains, electromagnetic radiation, cosmic rays, and magnetic fields. The matter consists of about 99% gas (90% of atomic and molecular hydrogen, 9% of helium) and 1% dust (formed by heavier elements such as carbon, oxygen and nitrogen) by mass. Gas and dust are well mixed. In typical spiral galaxy, dust is located mainly in the galactic disc, producing dark lanes in edge-on spirals. In contrast, there is relatively little dust in elliptical galaxies. Within the disc, most of the material is confined to the spiral arms. The distribution of interstellar matter is largely inhomogeneous, and in our galaxy it is usual to find high density clumps with typical sizes in the range 1-50 pc which are traditionally termed 'clouds'. In general, extinction is proportional to the number of clouds that lie along a given line of sight. The mean rate of extinction for lines of sight close to the plane of the Milky Way and for distances up to a few kpc from the Sun is:

$$\langle \frac{A_V}{L} \rangle \approx 1.8 \; mag \; kpc^{-1}, \tag{6.1}$$

where A_V is the absorption at visual wavelengths and L is the distance along the observed column. The correlation between dust and gas in the galactic disc was studied using ultraviolet absorption-line spectroscopy to measure hydrogen column density of reddened stars (E(B−V) $\geq$ 0.5 mag) within $\sim$ 1 kpc of the Sun (Bohlin, Savage & Drake 1978). They found the following mean ratio of hydrogen column density to reddening as:

$$\langle \frac{N_H}{E(B-V)} \rangle \approx 5.8 \times 10^{21} \; cm^{-2} \; mag^{-1}, \tag{6.2}$$

We noted before that the ISM is inhomogeneous, presenting a typical distribution in clouds. Early models (e.g. McKee & Ostriker 1977) classified the ISM into three phases: the Cold Neutral Medium (CNM), often called clouds; the Warm Ionized Medium or Warm Neutral Medium (WIM or WNM), which is sometimes considered the boundary layers of the CNM; and the Hot Ionized Medium (HIM), which is sometimes referred as the intercloud medium or the coronal gas. The CNM itself seems to contain clouds of several types. The densest clouds, where all the H I is converted to H_2 by grain surface catalysis (see Section 8.1 in Whittet 1992) and are most protected from the UV radiation from stars, are termed dense, dark or *molecular clouds*. The most tenuous clouds, fully exposed to starlight and with H I as the dominant phase, are usually called *diffuse clouds*. Clouds that fall in between these two extremes are often referred as *translucent clouds*. Considering these categories, we adopt here the systematic classification for cloud types given by Snow & McCall (2006) (see Table 6.1); it is also important to remark that the most common situation is to find a mixture of different types of clouds in the lines of sight. Also, in some cases, a line of sight may consist of an "onion-like" structure, with dense cloud material in the centre, surrounded by translucent gas, which is in turn surrounded by more diffuse gas.

6.1.1 Dust grain properties

As said above, dust grains account for only 1% of the total interstellar mass, but their effects are important. Despite their small size, ranging from about 3.5×10^{-4} μm to about 10 μm, dust grains are able to reduce the radiation coming from stars mainly in the visual and ultraviolet bands (Figure 6.1). The dust grains can both absorb and scatter the incoming radiation. While the scattered part is only deviated towards a different line of sight, the absorbed radiation warm the grains making them re-emit the energy as diffuse thermal

TABLE 6.1— Classification of Interstellar Cloud Types.

	Diff. Atomic	Diff. Molec.	Translucent	Dense Molec.
Defining	$f^n_{H_2}$ <0.1	$f^n_{H_2}$ >0.1	$f^n_{C^+}$ <0.5	f^n_{CO} >0.9
characteristic		$f^n_{C^+}$ >0.5	f^n_{CO} <0.9	
A_V(min.)	0	$\sim$ 0.2	$\sim$ 1 - 2	$\sim$ 5 - 10
Typ. n_H (cm^{-3})	10 - 100	100 - 500	500 - 5000?	$>10^4$
Typ. T (K)	30 - 100	30 - 100	15 - 50?	10 - 50
Observational	UV/vis	UV/Vis IR abs.	Vis (UV?) IR abs.	IR abs.
techniques	H I 21-cm	mm abs.	mm abs./em.	mm em.

Diff. = Diffuse; Molec. = Molecular
f^n_X - fraction of a element X, in term of number of densities and in local conditions,
e.g. $f^n_{H_2} = 2n(H_2)/n_H$
$n_H = n(H) + 2n(H_2)$

energy. This process is more efficient towards UV wavelengths. As a result, we experience a lack of UV radiation and an excess of IR radiation along a line of sight dominated by the interstellar dust. For this reason, the extinction process is normally referred to as *reddening*.

Observations give us a lot of information about interstellar grains. The depletion and spectroscopy study allow us to investigate the composition of dust, and the data on extinction, scattering, polarization and emission give information about the distribution of grain sizes. In this work we will concentrate mainly on the extinction phenomena (more detailed information about

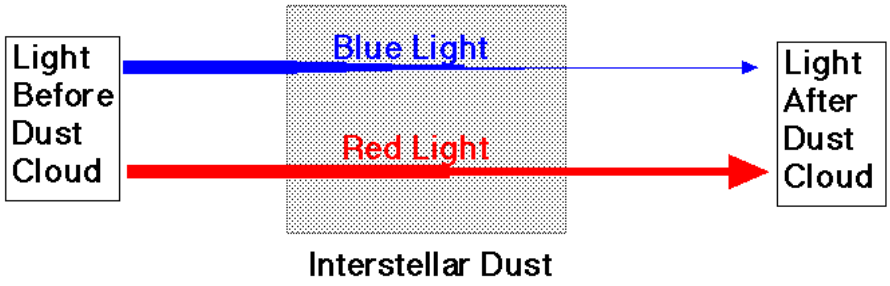

FIGURE 6.1— Blue light is absorbed more than red light when light passes through a dusty medium.

the other processes can be found in Whittet 1992).

Extinction

Let us consider spherical particles, having an extinction cross section C_{ext} (which is the sum of absorption and scattering cross sections[1]: $C_{ext} = C_{abs} + C_{sca}$), distributed along the line of sight with density n_d. The presence of dust along the line of sight reduces the intensity of starlight, I, at a given wavelength resulting from the extinction produced in a element of column with length dL as:

$$\frac{dI}{I} = -n_d C_{ext} dL. \tag{6.3}$$

By integrating equation 6.3 we obtain

$$I = I_0 e^{-\tau}, \tag{6.4}$$

where I_0 is the intensity emitted by the source and

$$\tau = \int n_d dL C_{ext} = N_d C_{ext}, \tag{6.5}$$

is the optical depth of the dust. N_d is the column density of the dust. We can convert this expression in magnitudes by considering the total extinction at some wavelength λ and the equations 6.4 and 6.5:

$$A_\lambda = -2.5 log_{10}(\frac{I}{I_0}) = 1.086 N_d C_{ext} = 1.086 N_d \pi a^2 Q_{ext}, \tag{6.6}$$

where $Q_{ext} = C_{ext}/\pi a^2$ is the extinction efficiency factor and a is the radius of the grain. The extinction efficiency can be split as the sum of corresponding efficiency factors for absorption and scattering ($Q_{ext} = Q_{abs} + Q_{sca}$).

If we consider a distribution of grain sizes such that $n(a)$ da is the number of grains per unit volume in the line of sight with radii in the range a to $a+$ da instead of grains of constant radius a, the equation 6.6 becomes

$$A_\lambda = 1.086 \pi L \int a^2 Q_{ext}(a) n(a) da. \tag{6.7}$$

The extinction efficiency factors were first calculated by Mie (1908) considering the grains as spheres. The efficiency factors are functions of a dimensionless

[1]The cross section is used to express the likelihood of interaction between particles. It can therefore characterize the probability of a particle being absorbed by a nucleus, or the statistical nature of scattering events. The cross section is expressed in units of area, usually in barn.

size parameter X = 2πa/λ and of the complex refractive index of the grain material: m = n - ik where n and k, the "optical constants", are functions of the wavelength.

When the particles are small compared with the wavelength (X << 1), for dielectric material (such as ices and silicates) $Q_{sca} \propto \lambda^{-4}$ and $Q_{abs} \sim 0$ and for absorbing material (such as metals) $Q_{sca} \propto \lambda^{-4}$ and $Q_{abs} \propto \lambda^{-1}$. When X becomes large (X < 20), Q_{ext} becomes constant indicating that the extinction is neutral (wavelength independent).

The extinction is most reliably determined using the *pair method*: comparing spectrophotometry of two stars of the same spectral type and luminosity class but unequal reddening (see Figure 6.2). The apparent magnitude of each star as a function of wavelength may be written:

$$\begin{aligned} m_1(\lambda) &= M_1(\lambda) + 5logd_1 + A_1(\lambda) \\ m_2(\lambda) &= M_2(\lambda) + 5logd_2 + A_2(\lambda), \end{aligned} \tag{6.8}$$

where M, d and A are the absolute magnitude, distance and total extinction respectively; indexes 1 and 2 correspond to the "reddened" and "comparison" stars. Assuming $M_1(\lambda) = M_2(\lambda)$ and $A(\lambda) = A_1(\lambda) \gg A_2(\lambda)$, the magnitude difference $\Delta m(\lambda) = m_1(\lambda)$ - $m_2(\lambda)$ is reduced to

$$\Delta m(\lambda) = 5log(\frac{d_1}{d_2}) + A_\lambda. \tag{6.9}$$

Normalization with respect to two standard wavelengths λ_1 and λ_2 allows us to eliminate the distance:

$$E_{norm} = \frac{\Delta m(\lambda) - \Delta m(\lambda_2)}{\Delta m(\lambda_1) - \Delta m(\lambda_2)} = \frac{A_\lambda - A_{\lambda_2}}{A_{\lambda_1} - A_{\lambda_2}} = \frac{E(\lambda - \lambda_2)}{E(\lambda_1 - \lambda_2)}, \tag{6.10}$$

where $E(\lambda_1 - \lambda_2)$, the difference in extinction between the specified wavelengths, is the colour excess, for instance E(B−V) = (B -V) - (B -V)$_0$.

The pair method has been used to measure extinction curves for many lines of sight, finding, in general, a similar form. Savage & Mathis (1979) and Seaton (1979) presented the average extinction curve of our Galaxy at various wavelengths. Figure 6.3 shows values of mean normalized extinction at various wavelengths taken from the previous works as a function of the inverse of the wavelength. This plot shows several distinctive features. It is almost linear in the visible from 1 to 2 μm^{-1}, with changes in slope in the blue near 2.2 μm^{-1} (the "knee") and in the infrared near 0.8 μm^{-1} (the "toe"). The most

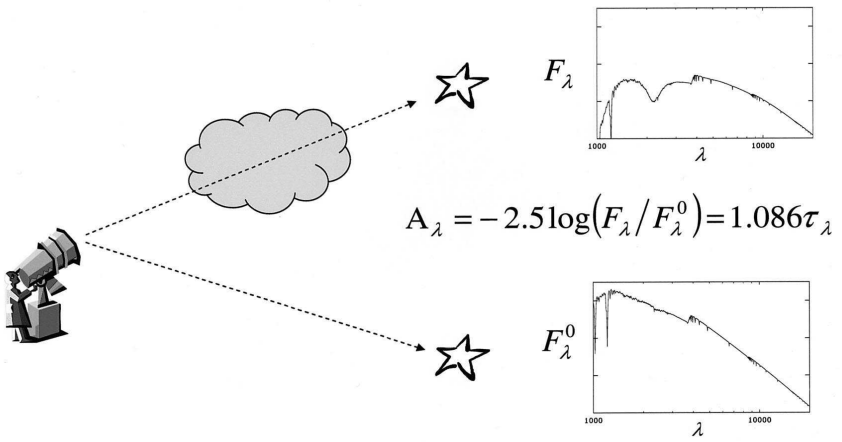

FIGURE 6.2— Schematic illustration of the Pair Method: comparing spectrophotometry of two stars of the same spectral class (from Fitzpatrick 2004).

prominent characteristic of the observed extinction curve is a broad, symmetric peak in the mid-ultraviolet centred at $\sim 4.6\ \mu m^{-1}$: this is the 2175 Å "bump". Beyond the bump, a decrease occurs near $\sim 6\ \mu m^{-1}$, followed by a steep rise into the far-ultraviolet (FUV, $\lambda^{-1} > 6 \mu m^{-1}$).

A common measure of the slope of the extinction curve in the optical region is the dimensionless quantity $R_V = A_V\ /\ (A_B\ -\ A_V) = A_V\ /\ \mathrm{E(B-V)}$. Very large grains would produce gray extinction with $R_V \to \infty$. Rayleigh scattering ($A_V \propto \lambda^{-4}$) would produce very steep extinction with $R_V \approx 1.2$ (Draine 2003). Pair method determinations of the reddening law for many lines of sight indicate that $R_V \approx 3.1$ for the average extinction law for diffuse clouds in the local Milky Way (Savage & Mathis 1979, Cardelli, Clayton & Mathis 1989).

Cardelli, Clayton & Mathis (1989, hereafter CCM) were the first to demonstrate a link between UV and the optical/IR region extinction by showing that R_V correlates with the level of UV extinction. It means that lines of sight with large R_V values tend to have low UV extinction, and viceversa. CCM derived a mean extinction law (for $0.12\ \mu m^{-1} < \lambda < 3.5\ \mu m^{-1}$) that depends only on the parameter R_V. They found that the extinction curves of their sample constitute a one-parameter family, the parameter being R_V:

$$\frac{A_\lambda}{A_V} = a_x + \frac{b_x}{R_V}, \tag{6.11}$$

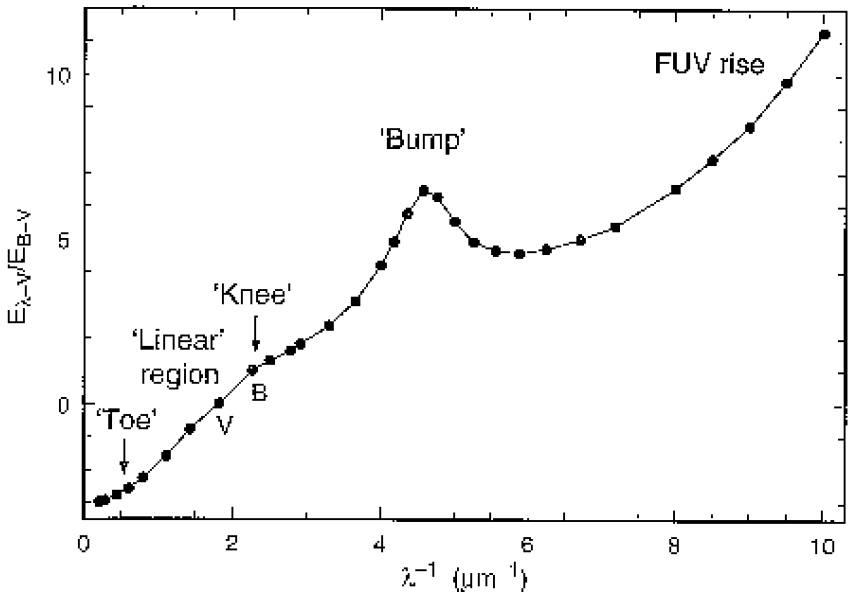

FIGURE 6.3— Average interstellar extinction curve as a function of λ^{-1}. Points correspond to values of mean normalized extinction at various wavelengths taken from Savage & Mathis (1979), Seaton (1979) and Whittet (1988). The positions of the B and V passbands selected for normalization are also indicated (from Whittet 1992).

where x = 1 / λ, and a_x and b_x are wavelength-dependent coefficients. In Figure 6.4 extinction curves obtained using the CCM law for different values of R_V are shown.

As we have said, in the Milky Way the dust varies from one direction to another. Our knowledge of the extinction law for dust in other galaxies is derived basically from the Large and Small Magellanic Clouds (LMC and SMC), where it has been possible to study the extinction for individual stars. Several lines of sight in the LMC appear to suffer extinction laws similar to that for the Milky Way diffuse clouds, obtaining also a $R_V = 3.1$ in most cases (Fitzpatrick 1986, Misselt, Clayton & Gordon 1999). In the SMC, stars in the "bar" region have extinction curves which appear to lack the 2175 Å feature. In M31, Bianchi et al. (1996) found an extinction law similar to the average Milky Way extinction curve but with the 2175 Å feature somewhat weaker than in our Galaxy. The variation in the extinction properties seen in the Magellanic Clouds and M31 may be due to several factors, for example different environments (e.g. star formation regions where large amounts of UV radiation and shocks are present)

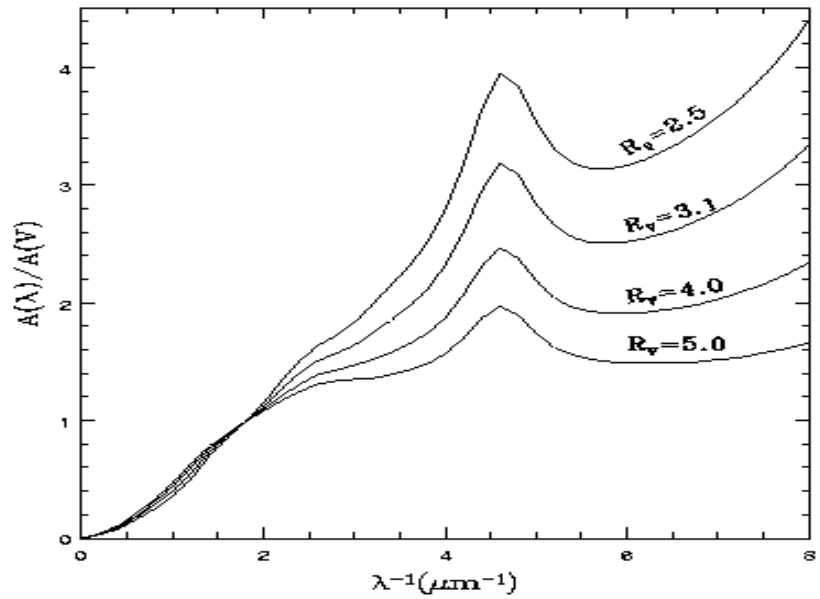

FIGURE 6.4— Example of extinction curves obtained using the Cardelli, Clayton & Mathis (1989) law for different values of R_V (from Geminale 2006).

(Clayton 2004).

For other galaxies where individual stars cannot be resolved, there are different approaches to determine the extinction curve for dust. The dust extinction law can be determined when a foreground galaxy overlaps a background galaxy, or using observations of the overall emission spectrum in starburst galaxies or from analysis of QSO spectra (Draine 2003).

Evolution of the grain population

The size distribution of interstellar grains is a consequence of the balance of constructive and destructive processes (see Figure 6.5).

There are two mechanisms for the growth of dust particles: (i) coagulation, as a consequence of grain-grain collisions, and (ii) mantle growth when gas-phase atoms accumulate on grains surface. The former process redistributes the grain mass, the latter creates a new grain material and increases the dust-to-gas ratio. The collisions that lead to coagulation take place when the speed of dust is $v_d < 1$ km s^{-1} (Jones, Tielens & Hollenbach 1996). In a dense cloud, R_V is often enhanced as a consequence of coagulation. In fact, this mechanism reduces the number of small grains, increases the number of large

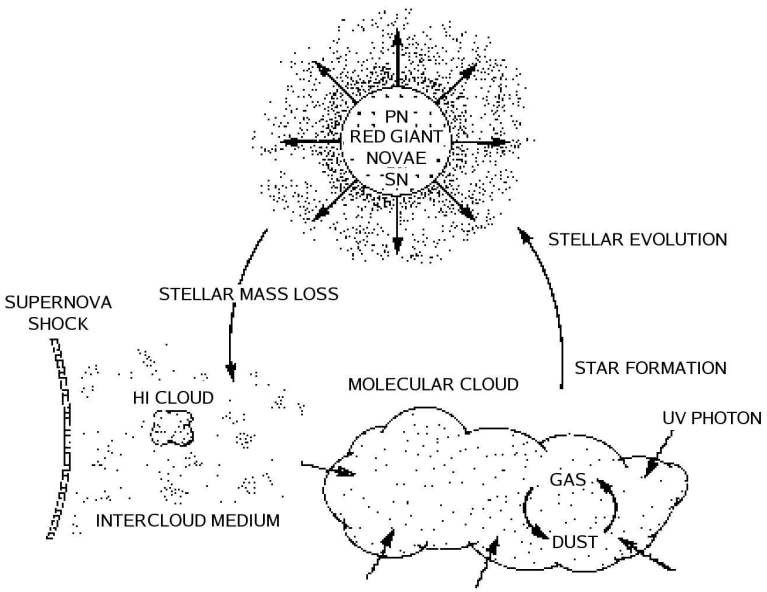

FIGURE 6.5— Schematic representation of the evolution of cosmic dust. Grains of "stardust" in the atmospheres and outflows of evolved stars are ejected into low-density phases of the interstellar medium, where they are exposed to UV irradiation and to destruction by shocks. Grains grow within molecular clouds, and later are dissipated by subsequent star formation (from Tielens & Allamandola 1987).

grains and it has a systematic effect on the shape of the extinction curve (Mathis & Whiffen 1989; Kim & Martin 1996a; Mathis 1996; O'Donnell & Mathis 1997; Weingartner & Draine 2001).

In the densest regions of molecular clouds atoms of C, N and O that reach the grain surface form molecules of OH, CH, and NH and, in a second phase, may form ice of H2O, NH3 and CH4 (d'Hendecourt, Allamandola & Greenberg 1985; Tielens & Hagen 1982). When there are no more available atoms of H a secondary mantle of CO, O2 and N2 it is formed. These mantles on grains may undergo sublimation or crystallization when luminous stars form within the dense clouds.

There are two main mechanisms that destroy the grains: (i) sputtering and (ii) grain-grain collisions (Barlow 1978a; Barlow 1978b; Draine & Salpeter 1979; Seab 1988; Draine 1989a; McKee 1989; Tielens et al. 1994). The former can be chemical or physical. Chemical sputtering arises when gas atoms reach the grain surface at low velocity and react with the atoms on the grain forming molecules that are desorbed. If the particle impinging on the grain has high

kinetic energy the sputtering is physical and it involves the removal of surface atoms by energetic impact.

Both sputtering and grain-grain collisions destroy the grains in the diffuse ISM as a consequence of a supernova shock wave (Draine & McKee 1993; Jones et al. 1994; Barlow 1978b; Tielens et al. 1994; Borkowski & Dwek 1995). Destruction by shocks is more efficient in the diffuse ISM than in dense clouds because the shock is decelerated when it encounters a cloud with density higher than that of the diffuse ISM. In high velocity shocks large enhancements of the gas-phase silicon abundance are observed in both diffuse and dense clouds (van Dishoeck, Jansen & Phillips 1993). Moreover, in high velocity shocks grain destruction is dominated by sputtering which creates a deficiency of small dust particles compared to the preshock gas. Instead, in low velocity shocks ($v <$ 200 km s^{-1}) grain fragmentation and vaporization by grain-grain collision create an excess of small dust particles compared to the unshocked gas. Borkowski & Dwek (1995) described two type of collisions: cratering and catastrophic collisions. At low energies only a limited region around the grain will be affected by the shock. Most of the mass of the grain remains intact. This is a cratering collision. At higher impact energies the grain is broken up into fragments characterized by a wide range of sizes. These are catastrophic collisions. Cratering collisions produce a strong excess of fragments, ranging from small to large sizes, because smaller grains are expected to be produced in more frequent and less energetic events rather than in catastrophic collisions. The velocity at which sputtering occurs decreases with increasing mass of the incident particle because of the greater kinetic energy at a given velocity. Then, in low velocity shocks ($10 < v <$ 50 km s^{-1}) sputtering by heavy particles dominates and in high velocity shocks ($v >$ 50 km s^{-1}) sputtering is dominated by H and He impact (Draine & Salpeter 1979; Tielens et al. 1994).

Moreover, the compression of the magnetic field B parallel to the shock front accelerates the charged grains producing gas-grain velocity comparable to the shock velocity. This acceleration is the mechanism of grain destruction for shock velocities in the range 50 - 200 km s^{-1} (Spitzer 1976; Cowie 1978).

Grain distribution

The size distribution is governed by the balance of destruction and re-growth. In the last 60 years, several works concerning the size distribution of dust particles appeared, from the work of Oort & van de Hulst (1946)[2] to that of Weingartner

[2]Their size distribution was characterized by a steep drop at large sizes, beginning at a radius smaller than the wavelength of light (0.5 μm). They used only extinction data at visible wavelength and their grains were mainly ice.

and Draine (2001, hereafter WD01), where each one presents an improvement on a previous one.

This last is the most recent work on distribution of grain sizes and we adopt this model to reproduce the extinction curves. The WD01 model is an extension of the Mathis, Rumpl & Nordsieck (1977) (hereafter MRN) model. They showed that the extinction curve from the near infrared to the far ultraviolet requires a power law for the dust grain size of two separate populations of bare spherical silicate and graphite grains. The power law is the result of formation and destruction processes that modify grain sizes. The power law distribution is given by $n(a) \propto a^{-3.5}$. All the successive models, based on new observational data, can be considered an extension of the MRN model that was constructed considering only extinction through diffuse clouds. Indeed the extinction curve shows variations depending on the considered interstellar environment.

The WD01 model consists of spherical grains of two types: amorphous silicates and carbonaceous grains. These last grains are composed of graphite grains and PAH[3] molecules with very small sizes. The WD01 model is able to reproduce both emission and extinction properties in different regions in our Galaxy and in regions of the Small and Large Magellanic Clouds. At present, the abundance of very small grains required to reproduce the observed IR emission is not well determined.

Figure 6.6 shows how the model reproduces the extinction curve for $R_V = 3.1$ and ${b_C}^4 = 6 \times 10^{-5}$. WD01 adopt the normalization for the "observed" extinction curve: $A(\lambda)$ / $(2.6 \times 10^{-22}$ cm$^2)$, which was suggested by Cardelli, Clayton & Mathis (1989)[5].

6.2 Circumstellar medium

Circumstellar dust consists of dust grains that are closely associated with an individual star rather than being uniformly distributed through space. In general, we can assume that the properties of circumstellar dust are similar to those of interstellar dust at about 1pc from the central star. The nature of circumstellar dust grains is different from that of interstellar grains. Their size and chemical composition depend on the nature of the star with which they are associated,

[3]Polycyclic aromatic hydrocarbons. They are big molecules containing 5% of the total C available. They are made of benzene rings and have dimension of about 10 Å.

[4]b_C is the number of carbon atoms per total H atoms in the log-normal population (see Weingartner & Draine 2001). $b_C = 6 \times 10^{-5}$ is the best value found by Li & Draine (2001b) to reproduce the IR emission from dust and the extinction curve for R_V 3.1.

[5]Cardelli, Clayton & Mathis (1989) found that $A(\lambda)/A(I)$ appears to be independent of R_V for $\lambda > 0.9$ μm (= I band), suggesting that the diffuse cloud value of $A(I)/N_H = 2.6 \times 10^{-22}$ cm^2 may also hold for dense clouds (see, e.g. Draine 1989b).

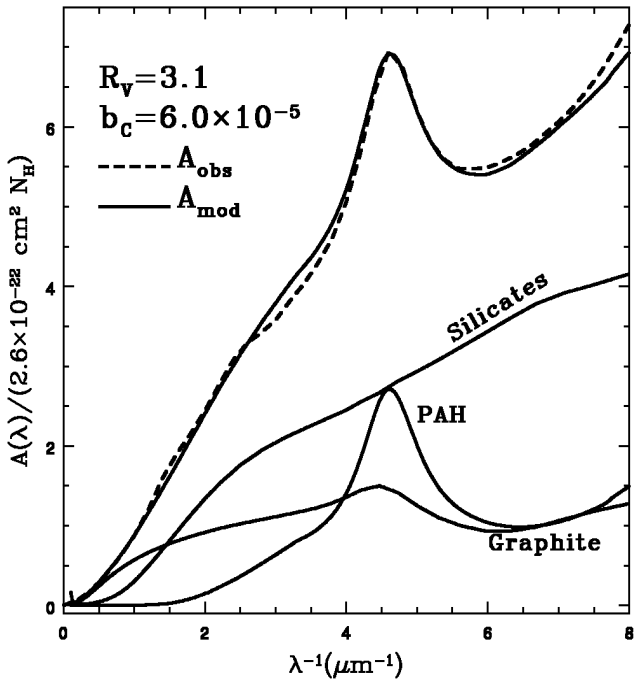

FIGURE 6.6— Extinction curve model for the average Galactic extinction with $R_V = 3.1$. The contribution of every dust component is included in the figure. b_C is the number of carbon atoms per total H atoms in the log-normal population (see Weingartner & Draine 2001), and $A(\lambda)/(2.6 \times 10^{-22}\ \mathrm{cm}^2)$ is taken from Cardelli, Clayton & Mathis (1989).

whereas the interstellar grain population is a mixture of all the grains ejected into the surrounding medium.

Dust in the stellar ejecta

The elements that will form dust can reach the interstellar medium from the inner regions of the stars only under particular conditions, for example if there is a mixing of the shell regions and envelope material or if the star becomes a supernova. This star can produce iron in the core, but when the temperature rises as a consequence of the contraction, the Fe nucleus is destroyed to form neutrons. This event is important for the enrichment of the ISM by heavy elements.

Stars of $1 < M < 8\ M_\odot$ do not follow all the sequence of thermonuclear processes and stop the nucleosynthesis with a C-rich and/or O-rich core. These

elements can reach the surface by a process called dredge-up which is a consequence of an instability.

Interstellar dust can form around post-main-sequence stars with photospheric temperatures between 2000 and 3500 K such as red giants, supergiants and AGB stars. The formation of dust of a given composition takes place at a distance from the star where the gas temperature is below the condensation temperature corresponding to that composition; the maximum distance from the star where dust forms is where the temperature and density become comparable with those of interstellar medium.

The composition of dust depends on the abundance ratio N(C)/N(O). C and O atoms form CO molecules, but the less abundant of these will remain locked in the gas phase within the CO molecules and so it will not be available to form solids. Silicate grains form where N(C) < N(O). This happens in outflows from oxygen-rich stars where the 10 μm silicate feature is observed. Fe, Mg, SiO and H_2O produce grains at T $\sim$ 1200 - 800 K: enstatite ($MgSiO_3$), fosterite (Mg_2SiO_4), olivine ((Mg,Fe)SiO_4). H_2O-ice mantles can condense onto grains when T < 200 K. The 10 μm feature is not seen in outflows from stars with N(C) > N(O), where a feature at 11.3 μm may be found instead . This has been attributed to mixture of amorphous carbon and SiC submicron grains (Treffers & Cohen 1974; Blanco et al. 1998). Also amorphous carbon or PAHs are formed when N(C) > N(O). The ring segment C=CH reacts with C_2H_2 molecules to form a stable ring (Tielens 1990) that attaches other C_2H_2 units. So, PAH molecules containing several rings (Frenklach & Feigelson 1989) or amorphous carbon when ring clusters are randomly grouped may be formed.

Planetary nebulae, nova outbursts and supernovae produce dust. During its evolution in the AGB phase, the star loses a high quantity of mass. This mass forms an envelope around the star that becomes a planetary nebula when the outer layers expand, the mass loss rate declines and the envelope expands becoming a luminous nebula heated by the star. Grains formed during AGB phase may be destroyed (Pottasch et al. 1984, Lenzuni et al. 1989), swept up and reprocessed.

As SNe manufacture many condensable elements, it is natural to presume that they are important sources of dust. Of the various classes, Type II SNe are the most important. In the expanding envelope there is nucleation and growth of material produced during the star's life (Gehrz & Ney 1987).

In the IR spectrum of evolved O-rich stars the features at 9.7 μm and 18.5 μm due to Si-O stretching and bending modes of silicates can be seen; in C-rich objects instead of a silicate profile there is the 11.2 μm emission feature produced by silicon carbide (SiC). Ice spectral features at 3.1 μm are formed in the outer layers of O-rich stellar atmosphere that are shielded from photospheric

radiation (Gillett & Soifer 1976; Soifer et al. 1981; Roche & Aitken 1984; Geballe et al. 1988; Smith, Sellgren & Tokunaga 1988; Omont et al. 1990; Meyer et al. 1998).

Stars later than M1-M2 spectral type have high mass loss rates (up to 10^{-4} $M_\odot$ yr^{-1}) and photospheric temperatures T < 3600 K. These stars have dusty envelopes detected by their infrared emission and it seems that dust conveys momentum to the gas, driving it away from the star (Wannier et al. 1990; Knapp 1986; Dominik et al. 1990). For a star of mass M, luminosity L and radius R, the mass loss rate is given by $dM/dt \propto GM/R^2$ where G is the gravitational acceleration at the stellar surface. The force due to gravity acting on grains is $F_{gr} = GMm_d/r^2$ where m_d is the dust mass and r is the radial distance from the center of the star. The force due to radiation pressure (in a direction opposed to gravity) is given by $F_{pr} = \pi a^2 < Q_{pr} > L/(4\pi r^2 c)$ where Q_{pr} is the radiation pressure coefficient factor. If $F_{pr}/F_g > 1$ the grains are accelerated by radiation pressure and encountering the gas they transfer momentum to it. In this way a star with a dusty envelope may lose its mass (Elitzur & Ivezic 2001).

In an expanding envelope the grains undergo multiple collisions and the consequence is a power law size distribution $n(a) \propto a^{-3.5}$ (Biermann & Harwit 1980). When dust reaches the ISM it is produced and destroyed but again the size distribution is a power law. The quantity of stardust ejected in the ISM can be estimated considering all dust sources. For stars of intermediate mass (1 - 8 $M_\odot$) the mass-loss occurs during AGB phase and during the ejection of a planetary nebula. The grand total mass loss rate is about 1.3 $M_\odot$ yr^{-1} for the Milky Way (Jura & Kleinmann 1989; Maciel 1981) over the entire post-main-sequence lifetime of intermediate-mass stars. The contribution of SNe may be estimated from the product of frequency and ejecta mass, obtained a rate of $\sim$ 0.2 $M_\odot$ yr^{-1} for Galaxy.

6.3 Dust and Supernovae

As we have seen in previous sections, the SNe play an important role in generation and evolution of the interstellar medium. In particular, for what concerns dust, they contribute the 8% of dust content of the interstellar medium (Gehrz 1989). On the other side the dust of the Galaxy and of the host galaxy along of the line of sight alters the Spectral Energy Distribution (SED) and the flux received by the SN. Indeed, the extinction is a crucial factor in SNe study and has to be taken carefully into account in their calibration process. Typically, dust extinction is larger in the case of core collapse SNe (CCSNe) because they are preferentially located in dust-rich environments, and smaller for Type Ia

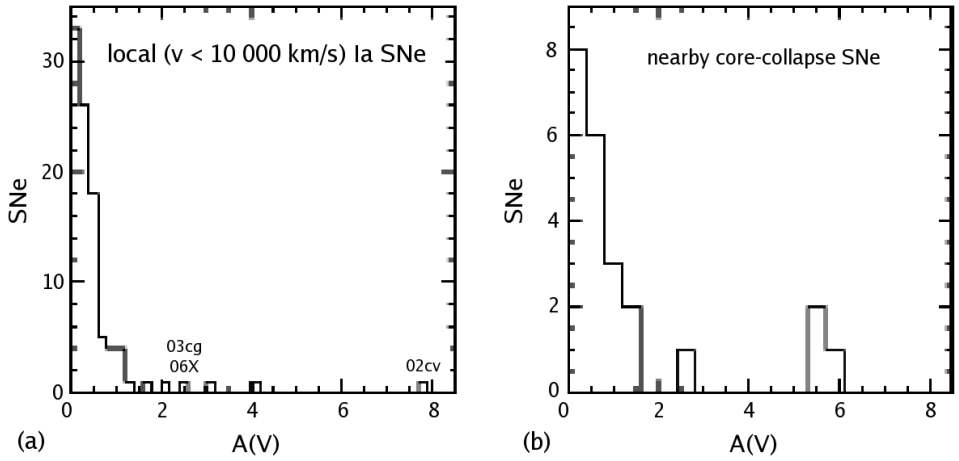

FIGURE 6.7— Histogram of the host galaxy extinction of nearby Type Ia SNe (a) and CCSNe (b). The SNe discussed in this work are marked in the figure (from Mattila, Meikle & Greimel 2004).

SNe, particulary for those exploding in elliptical galaxies, which are, in general, almost dust-free (see e.g. Riess et al. 1996b). Nonetheless, there are several examples of Type Ia SNe showing moderate to high extinction (see Figure 6.7), such as the examples presented in the previous Sections: SN 2002cv, SN 2003cg and SN 2006X.

Thanks to their overall homogeneity, SNe Ia are well suitable to make the inverse process, i.e. to derive the reddening suffered by their light and thus, the dust properties of the interstellar medium. By measuring the colour excess of a large sample of Type Ia SNe, it is possible to see that the majority of SNe Ia suffer a reddening lower than 0.40 mag (see Figure 6.7). In this case the changes of the SED are small and comparable to the photometric calibration. The few cases left with very high extinction studied in the previous Chapters have a fundamental role and can help to shed light on different extinction laws followed by the interstellar medium inside the parent galaxies.

As we have seen, all methods we have used to estimate the extinction suffered by SNe rely on the deformed SED: either using the SN colours and photometry or using spectra with good S/N. In both cases, we have obtained more robust results if we combine optical and IR bands. For each of the SNe presented in this thesis (Chapters 3, 4 and 5), we have discussed in depth different methods used to compute their extinction.

In the discussions of previous Chapters we have often mentioned other effects that dust has on the observable of SNe Ia. It is well known that the E(B−V) depends by the colour of the source, that is the effective wavelength change with the SED (Kim, Goobar & Perlmutter 1996b). In the case of SN, because the SED changes with time, the E(B−V) also changes with time and so does the extinction which changes the light curve. For the decline rate, Phillips et al. (1999) found a relationship between true and observed Δm_{15}(B) (we recall that is the difference in magnitude between maximum light and 15 days later) as a function of E(B-V)$_{intrinsic}$

$$\Delta m_{15}(B)_{intrinsic} = \Delta m_{15}(B)_{obs} + 0.1E(B-V)_{intrinsic}, \tag{6.12}$$

so that the light curves of SNe Ia get broader from the peak to +15 days, as the SNe become more extinguished by dust. We have demonstrated for SN 2003cg or SN 2002cv (Sections 3.3.1 and 4.4.1) that this relations is also valid for highly extinguished SNe.

Nugent, Kim & Perlmutter (2002) measured the shift to the red of the effective wavelength λ_{eff} (Figure 6.8) inside a given photometric band for a heavy reddened SN which can produce changes in the characteristic shape of the light curve. We have attributed to this effect the relatively broad maximum of the U light curve and the unusual hint of secondary maximum visible in the V light curve of SN 2003cg (Section 3.3.1).

Both Nugent, Kim & Perlmutter (2002) and Jha (2002) have measured the variation with time of $R_X = A_X$ / E(B-V), where X is a selected band, using spectral templates (see Section 5 of Nugent, Kim & Perlmutter 2002) and a sample of 91 spectra (described in Section 4.2.2 of Jha 2002). Variations of R_X caused by the rapid evolution of the SED of SNe Ia around maximum light are more evident over the first 60 days after the explosion. Figure 6.9 shows an example of this evolution given by Wang (2005), which used the dust model of Weingartner & Draine (2001) and the SN Ia spectral template as described in Knop et al. (2003).

As we have already specified in Section 1, the study of the SNe Ia provided the first indication that the expansion of the Universe is accelerating (Perlmutter et al. 1999; Riess et al. 1998). Supernova magnitudes at peak brightness and redshifts are the ingredients that allow their use as cosmological probes. But, as we also know, dust in the host galaxy dim the light coming from the SN

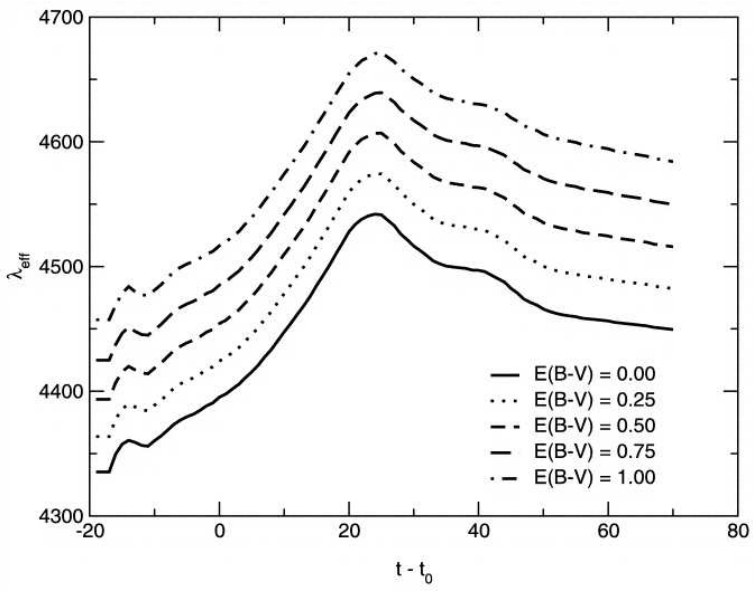

FIGURE 6.8— Variation of λ_{eff} in time for various levels of extinction in the B bands (from Nugent, Kim & Perlmutter 2002).

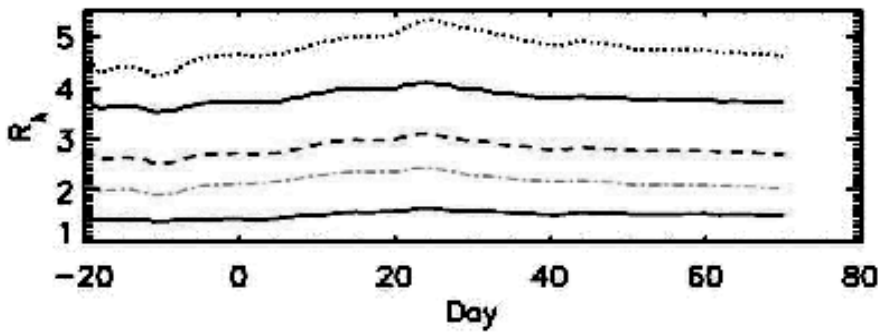

FIGURE 6.9— Variation with time of the selective to total extinction ratio in U (dotted line), B (solid line), V (dashed line), R (dot-dashed line) and I (bottom solid line) bands for Type Ia SNe (from Wang 2005).

and might hamper the results obtained with SNe. Sullivan et al. (2003) found that at high-redshift the dust extinction in the host galaxies is the main cause of the scatter in the Hubble diagram. It means that the morphology of the host galaxies of the SNe Ia is correlated closely with the scatter observed in this diagram[6]. This scatter is smaller for SNe Ia occuring in early-type host galaxies and larger for those occurring in late-type galaxies[7]. However, considering both early-type galaxies and late-type galaxies, the cosmological parameter Ω_Λ suffers a modest shift continuing to be > 0 at nearly the 98% confidence level (Knop et al. 2003; Filippenko 2005).

Sometime it happens that the light reflected off dust particles travels for a longer distance, arriving at the observer with a time delay with respect to unaffected light. This is the so called light echo phenomenon studied by Chevalier (1986), and more recently by Sugerman (2003), Patat (2005) and Patat et al. (2006). Light echo is a phenomenon which can give us important insights into the progenitor's nature, a matter which is still under debate. Due to the typical number density of dust particles which are responsible for the light scattering, light echoes are expected to have an integrated brightness about ten magnitudes fainter than the SN at maximum. This has the simple consequence that it is much easier to observe such a phenomenon in a SN Ia than in any other SN type, due to its high intrinsic luminosity. Five cases of SNe are known showing light echo: SN 1991T (Schmidt et al. 1994; Sparks et al. 1999), SN 1998bu (Cappellaro 2001) and the Type II SNe 1987A (Crotts, Kunkel & McCarthy 1989; Crotts & Kunkel 1991; Crotts, Kunkel & Heathcote 1995; Xu, Crotts & Kunkel 1994; Xu, Crotts & Kunkel 1995), 1993J (Sugerman & Crotts 2002) and 2003gd (Van Dyk, Li & Filippenko 2006). The study of light echoes induced by dust is beyond the aim of the present work.

After this quick view of the effects of dust on SNe, it is clear how important is the knowledge of the extinction law suffered by light coming from SNe.

6.4 Diffuse interstellar bands in supernovae

In the Section 3.2 we introduced the *diffuse interstellar bands* or DIBs, which are weak absorption features observed in the spectra of celestial objects obscured and reddened by interstellar dust (Herbig 1995).

The first DIBs were detected more than 80 years ago (Heger 1922) and

[6]It is assumed that early-type host galaxies have very low internal extinction.

[7]On average, the SNe Ia in late-type host galaxies are slightly fainter ($\sim 0.14 \pm 0.09$ mag) and at the peak brightness their colours are marginally redder.

their interstellar nature was established 12 years later (Merrill 1934). During the last decades of DIB studies almost 130 DIBs have been detected, mainly within the Milky Way. Only in a handful of cases, have DIBs been observed in extragalactic sources (e.g. Vladilo et al. 1987; Heckman & Lehnert 2000; Ehrenfreund et al. 2002).

These absorptions are seen between 4000 and 13000 Å and their intensity is associated with the reddening. Since there are variations of the R_V (next section) and this is related to the grain size, we might think that DIB intensity reflects such a change in grain properties. Unfortunately, the DIB intensity does not follow this variation (Herbig 1993). Besides, the DIB intensity is correlated with the amount of Na I in the line of sight (Herbig 1993).

The carriers of the DIBs still remain unknown. It seems that at least in some cases, the DIBs are due to large molecules/ultrasmall grains, possibly of PAH composition, or to optical and near-infrared transitions for fullerenes[8] and buckyonions (multishell fullerenes) (Iglesias-Groth 2004).

There are many advantages in searching for DIBs in supernova spectra. When they are present, we can study DIBs in the parent galaxies since galactic and extragalactic component do not overlap because of redshift. But, the supernova spectrum is made up of broad lines, so, very broad DIBs are not easy to disentangle.

DIBs have been found towards SN 1987A in LMC (Vladilo et al. 1987), SN 1986G in the nearby galaxy NGC 5128 (Rich 1987; D'Odorico et al. 1989), SN 1989M in NGC 4579 (Steidel, Rich & McCarthy 1990), and SN 2001el and SN 2003hn in NGC 1448 (Sollerman et al. 2005). As the DIBs are associated with reddening, we have checked for the presence of DIBs in the spectra of the three highly reddened SNe which are the subject of this thesis. Most of our spectra are of low resolution and the detection of narrow weak absorption features is problematic. We did not detect DIBs in SNe 2002cv and 2006X, even though for SN 2006X we have high resolution UVES spectra. However, SN 2003cg presents several DIBs which are reported in Table 6.2 and marked in Figure 6.10. We searched for DIBs at wavelengths where they were found in SN 2001el and among those listed in the Herbig (1995) tables.

The 5780.37 Å and 6283.85 Å DIBs are the most intense and are visible practically in all spectra of SN 2003cg, even at low resolution. On the other hand, the other DIBs listed in Table 6.2 are seen only in the WHT spectrum having resolution $\sim$ 1.5 Å. There are other DIBs from the list of Herbig (1995)

[8]The fullerenes are molecules composed entirely of carbon, in the form of a hollow sphere, ellipsoid, or tube. They are similar in structure to graphite, which is composed of a sheet of linked hexagonal rings, but they contain pentagonal (or sometimes heptagonal) rings that prevent the sheet from being planar.

TABLE 6.2— Diffuse Interstellar Bands of SN 2003cg.

λ^a_{DIB} (Å)	λ^b_{observ} (Å)	EW (Å)	FWHM (Å)	v_{DIB} kms^{-1}
4726.40	4727.93	0.30	4.59	97.05
	5730.88	0.23	2.27	
5780.37	5779.61	0.78	4.38	39.42
5796.97	5795.69	0.15	2.65	66.20
6203.08	6201.09	0.48	6.78	96.27
6283.85	6282.12	1.55	6.82	82.54
6307.00	6305.45	0.22	6.70	73.91
6318.00	6316.52	0.27	6.97	70.08
6613.56	6611.24	0.34	6.20	105.17
6660.64	6658.95	0.05	2.33	76.07

[a] λ of the DIB from the table of Herbig (1995) and in the spectra of SN 2001el (Sollerman et al. 2005).
[b] λ of the DIB identified in SN 2003cg spectra (corrected by redshift and reddening).

that seem to appear in the SN 2003cg WHT spectrum, but they are too weak to be measured. In Figure 6.10 is also possible to see a relatively strong narrow absorption around 5730 Å which does not correspond to any DIBs of the lists, nor is attributable to bad pixels or cosmic rays.

Herbig (1995) suggested that DIBs are weaker in dense clouds, and that the strong DIBs usually appears in the atomic hydrogen gas. In this hypothesis the reddening of SN 2003cg is due to diffuse clouds while in SN 2006X, which also got very high reddening, the density of interstellar clouds was higher. We can say little on SN 2002cv since we have not got any spectra of high resolution for SN 2002cv.

6.5 Estimation of the relative grain sizes for the parent galaxies

In previous Chapters, we have obtained the extinction curves along the line of sight to three highly reddened SNe. We can estimate the characteristic grain size, relative to that of the Milky Way, which produced the observed extinction following the same procedure outlined by Goudfrooij et al. (1994) and Patil et al. (2007), i.e. using the R_λ $[\equiv \frac{A_\lambda}{E(B-V)}]$ derived from our extinction curves.

In Figure 6.11 we have plotted the R_λ values obtained from the extinction curves of our SNe along with those for the Milky Way (they are listed in Table

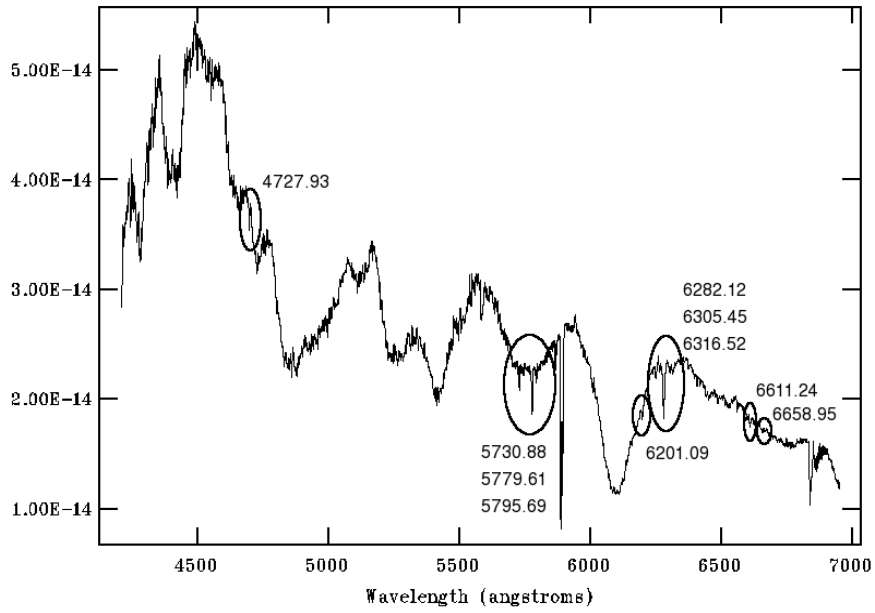

FIGURE 6.10— Diffuse Interstellar Bands in a medium-resolution spectrum of SN 2003cg obtained on March 22, 2003 with the WHT + ISIS (Elias-Rosa et al. 2006a).

6.3 with those for the Milky Way taken from Rieke & Lebofsky 1985). This figure demonstrates that, on average, extinction curves for our galaxies are practically parallel to that of our Galaxy, and this should imply that the dust extinction properties in the extragalactic environment are similar to those of the Milky Way. However, R_V is found to be different from the canonical value 3.1 of the Milky Way.

As we have said before, assuming that the chemical composition of dust grains in the extragalactic environment is similar (on average) to that of our Galaxy, smaller R_V values imply that the dust grains responsible for interstellar reddening are smaller.

An attempt to estimate the relative grain sizes can be provided by the extinction efficiencies (Q_{ext}). As mentioned in Section 6.1.1, the size of a grain can be expressed in terms of the (dimensionless) parameter X defined by

$$X = \frac{2\pi a}{\lambda}, \tag{6.13}$$

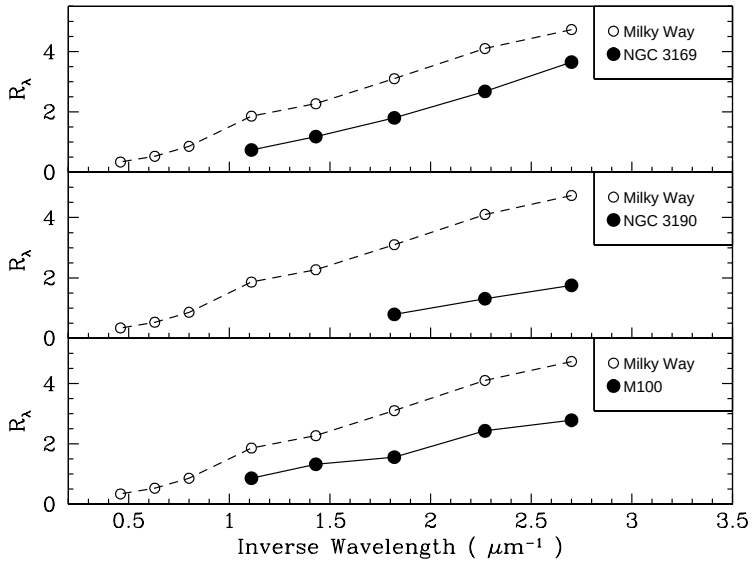

FIGURE 6.11— Extinction curves for the parent galaxies in the direction to the three highly extinguished SNe Ia of this thesis (filled circles, solid lines) compared with the canonical curve for the Milky Way (open circles, dashed lines).

where a is the grain radius. For small grains, $Q_{ext} \propto \lambda^{-1}$ i.e. for $X \leq 1$. Since the extinction curve in the optical part of the spectrum varies proportional to λ^{-1}, Q_{ext} is proportional to X. For a given Q_{ext}, the mis-match between the extinction curve for the Milky Way and those for our parent galaxies is attributed to the difference in grain size between the parent galaxies and the Milky Way.

Considering the Equation 6.13 and the condition for small grains, we can write

$$a \leq \frac{1}{2\pi\lambda^{-1}}, \tag{6.14}$$

and from this equation

$$\frac{\langle a \rangle}{a_G} \leq \frac{\lambda_G^{-1}}{\lambda_G^{-1} + \Delta(\lambda^{-1})}, \tag{6.15}$$

calling $\frac{\langle a \rangle}{a_G}$ the grain size (mean) of our parent galaxies relative to the Milky

TABLE 6.3— R_λ values and relative grain sizes.

Object	R_U	R_B	R_V	R_R	R_I	$\langle a \rangle / a_G$
NGC 3169	3.65(0.20)	2.68(0.20)	1.80(0.20)	1.18(0.20)	0.74(0.20)	0.75(0.07)
NGC 3190	—	—	1.75(0.55)	1.31(0.55)	0.79(0.55)	0.52(0.06)
M 100	2.78(0.30)	2.43(0.30)	1.56(0.30)	1.32(0.30)	0.86(0.30)	0.71(0.07)
Milky Way	4.73	4.10	3.10	2.27	1.86	1.00

NOTE: NGC 3169, NGC 3190 and M100 are the host galaxies of SN 2003cg, SN 2002cv and SN 2006X, respectively.

Way dust grains size, λ_G^{-1} is the inverse wavelength for the Milky Way, and $\Delta(\lambda^{-1})$ is the difference of the inverse wavelength between both extinction curves (parent galaxy and Milky Way), i.e. the required quantity need to overlap the two extinction curves.

Therefore, one can estimate the relative grain size by shifting the observed extinction curve along the λ^{-1} axis until it best matches the Galactic extinction curve, in the sense that the extinction curve lying below the Galactic curve will correspond to smaller grain size relative to that of Galactic dust grains. The relative grain sizes derived for the line of sights inside the parent galaxies are listed in Table 6.3.

It must to be stressed that the values reported in Table 6.3 are not average values for those galaxies as those reported by Goudfrooij et al. (1994) and Patil et al. (2007), but specific to the line of sight of the studied SNe. Indeed, for NGC 3190 we have studied another line of sight in the direction to SN 2002bo which has provided a standard extinction curve, hence standard grain size. This on one side highlights how variable is the extinction curve inside the same galaxy, and on the other confirm the finding by Goudfrooij et al. (1994) and Patil et al. (2007) which noted that the grain properties inside the dust lane are different from the rest of the galaxy.

6.6 Equivalent width of Na ID line and reddening in SNe

In the interstellar medium, together with dust particles is intermixed also gas. The gas properties have been determined by observing the absorption effects at ultraviolet, optical and infrared wavelengths, and the emission at radio and millimetric wavelengths. The first direct evidence which pointed to the existence of interstellar gas was obtained by Hartmann (1904) when he detected Na and Ca^+ optical absorption lines in a spectroscopic binary. Spitzer (1948) or Münch (1968), among others, reviewed on the formation of interstellar lines

and the theory of the curve of growth; others like Münch (1957), Hobbs (1969a, 1969b, 1974, 1978a, 1978b), Welsh et al. (1991), Bertin et al. (1993) or Sembach, Danks & Savage (1993) have provided experimental data.

By measuring interstellar absorption lines it is possible in principle to obtain the total column density of the absorbing gas along the line of sight. This can be in turn related to the amount of interstellar dust because, as we know, the interstellar medium is a mix of gas and dust, although with a dust-to-gas ratio which may vary. So, measuring the equivalent width (hereafter EW) of the narrow interstellar lines, in particular the Na ID doublet (5890.0, 5895.9 Å), we can obtain directly an estimate of the reddening which is a crucial ingredient in the calibration of SNe. A first study on SNe was performed by Barbon et al. (1990) on low resolution spectra. They found the linear relation E(B−V) = 0.25 × EW (Å) over the whole range $0.0 \leq$ E(B−V) ≤ 1.0. Munari & Zwitter (1997) made a similar study on high resolution spectra of 32 O and early B stars. They confirmed a relation for Na ID and extended the work at high reddening using K I line. Finally, Turatto, Benetti & Cappellaro (2003b) reviewed the Barbon et al. (1990) work increasing the sample with the SNe Ia provided by Phillips et al. (1999) and other objects with similar prescription. They found that SNe Ia occupy a large area of the EW(Na ID) vs. E(B-V) plane and seem to favour two regions derived by the linear relations:

$$E(B-V) = 0.16 \times EW(NaID) \tag{6.16}$$

$$E(B-V) = 0.51 \times EW(NaID) \tag{6.17}$$

The limit of that work was due to the use of low resolution spectra which, on one side reduces the accuracy of the measurements at low EW, on the other blends components of different intensity and does not account for line saturation.

Here we rediscuss the EW(Na ID) vs. E(B−V) relation on a larger sample of SNe of all types. This work is based only on the measurements of the Na ID lines. We do not consider the K I (7699.0 Å) line which saturates later that the Na ID lines, because it is too weak in our low resolution spectra. We collected the equivalent width of the Na ID and the reddening both in the Milky Way and in the host galaxies for a sample of 90 SNe of all types. The values of the EW(Na ID) come from direct measurements on the low resolution spectra of the Asiago Supernova Archive (Barbon et al. 1999) or from literature. The E(B−V) can be determined in different manners. For SNe Ia we have favored

the determinations based on the colour curves at epochs between 30 and 90 days past maximum (cfr. Section 1.4.1). For Core-Collapse SNe the estimates are in general less reliable and homogeneous. They come from comparison of colour curves of objects of similar classes, from the study of the SED with theoretical models and study of the high resolution component of interstellar lines. In Table 6.4 are listed the SNe and their values. In Figure 6.12 is shown the entire distribution of SNe on the EW(Na ID) vs. E(B−V) plane while Figure 6.13 shows a zoom for EW(Na ID) < 2 Å and E(B−V) < 0.5.

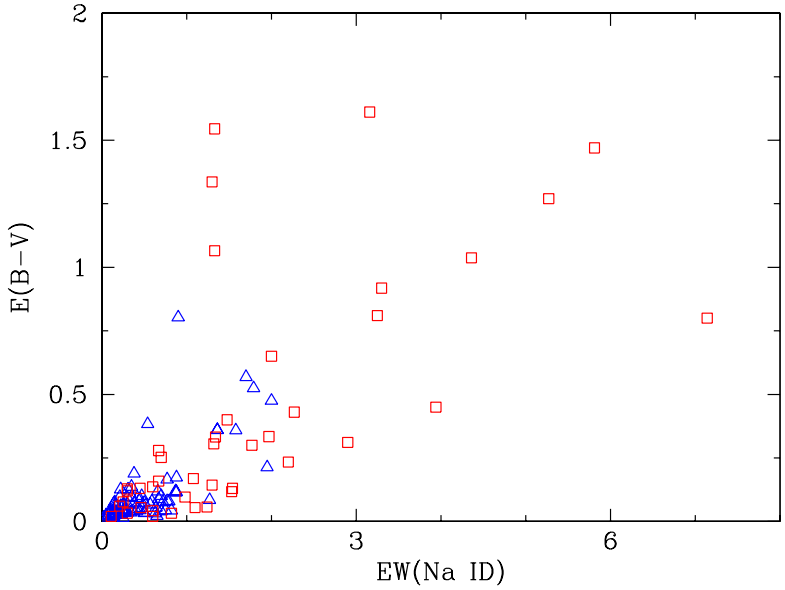

FIGURE 6.12— Relation between equivalent width of Na ID and reddening for the 90 SNe of our sample. Triangles and squares correspond to measurements for the Milky Way and the SN host galaxies, respectively.

To investigate the possible causes of the observed distribution we first introduce some theoretical considerations which could help in the subsequent analysis (see e.g. Bowers & Deeming 1984).

Suppose that an absorption line is formed in a the plane, parallel layer of uniform physical properties (temperature, density, pressure). Its equivalent width is generally expressed as:

$$EW_\lambda = \int [\frac{I_\lambda(0) - I_\lambda}{I_\lambda(0)}] d\lambda = \int (1 - e^{-\tau_\lambda}) d\lambda, \tag{6.18}$$

TABLE 6.4— Sample of SNe treated in this section.

SN	Type	$A_{B,G}$	EW(Na ID)$^{\dagger}_{G}$ (Å)	E(B-V)$_H$	EW(Na ID)$^{\ddagger}_{H}$ (Å)	Ref.$^{\diamond}$
SN 1976B	Ib	0.13	—	1.22±0.10	2.00±0.50	0,1,2,1
SN 1979C	IIB-L	0.11	0.08±0.07	—	—	0,1,–,–
SN 1980K	IIB-L	1.47	1.58±0.51	—	—	0,1,–,–
SN 1981B	Ia	0.08	0.14±0.11	0.04±0.03	—	0,1,3,–
SN 1986G	Iapec	0.50	—	1.04±0.05	4.36±0.29	0,–,4,1
SN 1987A	IIF	0.32	0.79±0.12	—	—	0,1,–,–
SN 1989B	Ia	0.14	—	0.31±0.02	2.90±0.41	0,–,3,1
SN 1989M	Ia	0.18	0.82±0.09	0.13±0.05	1.54±0.12	0,1,5,1
SN 1990B	Ic	0.14	0.30±0.20	0.80±0.20	7.14±1.15	0,1,6,1
SN 1990K	II	0.06	0.02±0.13	—	0.50±0.12	0,1,–,1
SN 1990M	Ia	0.15	0.25±0.70	—	—	0,1,–,–
SN 1990U	Ic	0.48	0.66±0.37	—	—	0,1,–,–
SN 1990W	Ib/c	0.71	0.88±0.40	—	—	0,1,–,–
SN 1991M	Ia	0.16	0.41±0.10	—	—	0,1,–,–
SN 1991S	Ia	0.11	—	0.06±0.04	0.21±0.06	0,–,4,1
SN 1991T	Iapec	0.10	0.11±0.19	0.14±0.06	1.30±0.18	0,1,2,1
SN 1991al	II	0.22	0.47±0.22	—	—	0,1,–,–
SN 1991bd	Ia	1.95	2.00±0.82	—	2.06±0.33	0,1,–,1
SN 1991bg	Iapec	0.18	0.25±0.15	0.03±0.05	—	0,1,4,–
SN 1992G	Ia	0.08	0.14±0.11	—	0.83±0.55	0,1,–,1
SN 1992ao	II	0.77	0.38±0.31	—	0.31±0.09	0,1,–,1
SN 1992ba	II	0.25	0.22±0.07	—	—	0,1,–,–
SN 1993J	IIb	0.35	1.27±0.38	0.40±0.00	1.48±0.04	0,1,7,1
SN 1993K	II	0.27	0.25±0.04	—	0.41±0.45	0,1,–,1
SN 1994I	Ic	0.15	—	0.45±0.5	3.94±0.34	0,–,8,1
SN 1994L	II	0.26	0.15±0.08	—	—	0,1,–,–
SN 1994U	Ia	0.25	0.17±0.26	—	1.29±0.02	0,1,–,1
SN 1994ae	Ia	0.13	—	0.03±0.03	0.30±0.30	0,–,3,1
SN 1994ai	Ic	0.11	0.22±0.06	—	1.89±0.11	0,1,–,1
SN 1995H	II	0.14	0.09±0.11	—	0.17±0.12	0,1,–,1
SN 1995V	II	0.15	0.27±0.16	—	2.25±0.59	0,1,–,1
SN 1995ac	Iapec	0.18	0.45±0.34	0.02±0.00	0.60±0.26	0,1,3,1
SN 1995ad	II	0.15	0.34±0.11	—	0.07±0.03	0,1,–,1
SN 1995ak	Ia	0.17	—	0.06±0.08	0.46±0.47	0,–,3,1
SN 1995bd	Iapec	2.15	1.79±0.83	0.31±0.10	1.32±0.92	0,1,3,1
SN 1996D	Ic	0.66	—	1.47±0.50	5.81±0.34	0,–,5,1

SN 1996L	IIL	0.41	0.70±0.20	—	0.12±0.09	0,1,–,3
SN 1996W	II	0.18	0.19±0.20	—	1.13±0.13	0,1,–,3
SN 1996Z	Ia	0.27	0.57±0.11	0.33±0.02	1.34±0.13	0,1,3,1
SN 1996ai	Ia	0.06	0.25±0.10	1.61±0.11	3.16±0.30	0,1,3,1
SN 1996aq	Ic	0.17	0.10±0.15	—	0.13±0.11	0,1,–,3
SN 1996bl	Ia	0.40	0.35±0.10	0.04±0.01	0.60±0.15	0,1,3,1
SN 1996bw	II	0.12	0.23±0.10	—	0.41±0.21	0,1,–,3
SN 1997X	Ic	0.12	0.16±0.25	—	0.53±0.33	0,1,–,3
SN 1997Z	II	0.56	0.35±0.20	—	0.36±0.18	0,1,–,3
SN 1997bp	Iapec	0.19	0.27±0.09	0.17±0.10	1.08±0.55	0,1,3,1
SN 1997bq	Ia	0.10	0.05±0.05	0.16±0.10	0.70±0.20	0,1,3,1
SN 1997br	Iapec	0.49	0.87±0.22	0.25±0.03	0.67±0.20	0,1,3,9
SN 1997cw	Iapec	0.31	0.72±0.10	0.33±0.08	1.97±0.34	0,1,3,1
SN 1997de	Ia	0.26	—	0.28±0.06	1.77±0.42	0,–,5,1
SN 1998A	II	0.52	0.22±0.10	—	—	0,1,–,–
SN 1998bp	Ia	0.33	0.77±0.02	—	—	0,1,–,–
SN 1998bu	Ia	0.11	0.19±0.10	0.28±0.06	0.67±0.17	0,1,3,1
SN 1998bw	Ic	0.25	0.25±0.16	—	0.04±0.01	0,1,–,3
SN 1998co	Ia	0.18	0.29±0.20	—	0.82±0.70	0,1,–,3
SN 1998dh	Ia	0.29	0.38±0.05	0.12±0.06	0.30±0.05	0,1,3,1
SN 1998dk	Ia	0.19	0.14±0.03	0.13±0.03	0.45±0.21	0,1,3,1
SN 1998es	Iapec	0.14	0.50±0.20	0.06±0.04	1.10±0.25	0,1,3,1
SN 1999E	IIn	0.38	0.42±0.18	—	1.97±0.92	0,1,–,3
SN 1999ac	Iapec	0.20	0.42±0.12	0.08±0.04	0.25±0.20	0,1,3,1
SN 1999as	Ia	0.14	0.50±0.20	—	0.04±0.89	0,1,–,1
SN 1999cl	Ia	0.16	0.70±0.20	0.92±0.28	3.30±0.50	0,10,3,10
SN 1999cz	Ic	0.28	0.30±0.15	1.68±0.50	5.62±1.05	0,1,5,1
SN 1999dn	Ib	0.23	0.64±0.16	—	0.37±0.14	0,1,–,1
SN 1999dq	Iapec	0.47	0.88±0.18	0.01±0.03	0.98±0.05	0,1,3,1
SN 1999ee	Ia	0.09	0.05±0.07	0.23±0.08	2.20±0.20	0,1,3,1
SN 1999em	IIP	0.17	—	0.06±0.03	1.24±0.13	0,–,11,1
SN 1999ga	II	0.87	1.95±0.60	—	—	0,1,–,–
SN 2000C	Ic	0.18	0.75±0.25	—	0.57±0.63	0,1,–,1
SN 2000E	Ia	1.57	0.54±0.33	0.14±0.03	0.60±0.20	0,1,3,1
SN 2000cu	Ia	0.39	0.30±0.15	—	—	0,1,–,–
SN 2000cx	Iapec	0.35	0.45±0.19	—	—	0,1,–,–
SN 2000dj	II	0.32	0.59±0.06	—	—	0,1,–,–
SN 2000eo	IIn	0.36	0.67±0.37	—	—	0,1,–,–
SN 2001el	Ia	0.06	—	0.13±0.05	0.30±0.01	0,–,3,12
SN 2001V	Ia	0.09	—	0.03±0.03	0.82±0.37	0,1,3,1

SN 2001bg	Ia	0.17	0.37±0.20	—	0.89±0.41	0,1,–,1
SN 2001cz	Ia	0.40	0.21±0.15	—	1.17±0.13	0,1,–,1
SN 2001fh*	Iapec	3.29	0.9 ±0.30	—	1.60±0.50	0,13,–,13
SN 2002ap	Icpec	0.30	0.50±0.01	0.02±0.00	0.11±0.01	0,1,14,1
SN 2002bo	Ia	0.11	0.12±0.07	0.43±0.10	2.27±0.20	0,1,15,1
SN 2002cm	II	0.29	0.14±0.56	0.81±0.10	3.25±0.11	0,1,5,1
SN 2002cs	Ia	0.47	0.87±0.10	—	—	0,1,–,–
SN 2002dj	Ia	0.41	0.47±0.28	—	—	0,1,–,–
SN 2002er	Ia	0.68	0.77±0.22	0.20±0.05	1.53±0.36	0,1,16,1
SN 2002hh1°	II	1.48	1.36±0.07	1.07±0.30	1.33±0.07	0,17,18,17
SN 2002hh2°	II	1.48	1.36±0.07	1.55±0.20	1.33±0.07	0,17,18,17
SN 2003cg	Ia	0.13	0.63±0.07	1.27±0.20	5.27±0.50	0,19,19,19
SN 2004aw	Ic	0.09	0.65±0.03	0.35±0.02	2.17±0.11	0,1,20,1
SN 2005aj	Ic	2.33	1.70±0.20	—	1.10±0.20	0,21,–,21
SN 2006X	Ia	0.11	0.13±0.01	1.34±0.03	1.30±0.01	0,1,22,5

† Values for the Milky Way.
‡ Values for the host galaxy.
◇ Reference for column 3, 4, 5 and 6 respectively.
* Host galaxy has a galactic latitude < 5 deg and it can create some problem with the extinction estimates (NED, Schlegel, Finkbeiner & Davis 1998).
° A 2-component extinction model was proposed for SN 2002hh (Pozzo et al. 2006). SN 2002hh1 is relative to Component 1, and SN 2002hh2 to Component 2.
References: 0 = NED, $A_{B,G}$ from Schlegel, Finkbeiner & Davis (1998); 1 = Asiago Supernova Archive (Barbon et al. 1999); 2 = de Vaucouleurs, de Vaucouleurs & Odewahn (1981); 3 = Reindl et al. (2005); 4 = Phillips et al. (1999); 5 = This work; 6 = Clocchiatti et al. (2001); 7 = Benetti et al. (1994); 8 = Richmond et al. (1996); 9 = Qiao et al. (1997); 10 = Garnavich et al. (1999); 11 = Utrobin (2006); 12 = Sollerman, Leibundgut & Lundquist (2001); 13 = Matheson et al. (2001); 14 = Takada-Hidai, Aoki & Zhao (2002); 15 = Benetti et al. (2004a); 16 = Pignata et al. (2004a); 17 = Peter Meikle, private communication; 18 = Pozzo et al. (2006); 19 = Elias-Rosa et al. (2006a); 20 = Taubenberger et al. (2006); 21 = Filippenko & Foley (2005); 22 = Kevin Krisciunas, private communication.

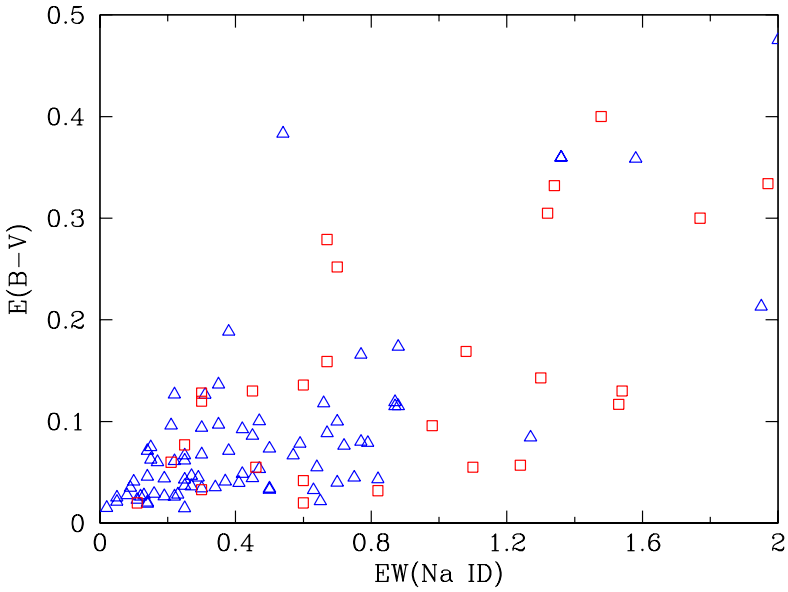

FIGURE 6.13— Relation between Na I D equivalent width and extinction for the SNe of our sample in the range EW(Na I D) < 2 Å and E(B−V) < 0.5. Empty triangles and squares correspond to measurements for the Milky Way and the host galaxies respectively.

where we have taken into account the radiation intensity emerging from the layer

$$I_\lambda(h) = I_\lambda(0)e^{-k_\lambda h} = I_\lambda(0)e^{-\tau_\lambda}. \tag{6.19}$$

The optical thickness of this layer, whose physical thickness is h, is

$$\tau_\lambda = \int n a_\lambda dh = \int k_\lambda dh = k_\lambda h, \tag{6.20}$$

where k_λ is the absorption coefficient per unit volume, n is the number density of atoms and a_λ is the absorption coefficient per unit mass. Assuming the line profile is pure Doppler broadening, we can write

$$a_\lambda = \frac{\sqrt{\pi}e^2\lambda_0^2}{mc^2\Delta\lambda_D} f e^{-(\frac{\lambda-\lambda_0}{\Delta\lambda_D})^2} (= a_0 e^{x^2}), \tag{6.21}$$

where f is the oscillator strength and $\Delta\lambda_D$ is the Doppler width of the line in λ units or $\Delta\lambda_D = \lambda_0 v_D/c$ ($v_D = \sqrt{2KT/m}$ - v_T^2, where v_T^2 is the microturbulent

velocity but that we neglect here).

If we consider optically thin gas ($\tau_0 \ll 1$), the equivalent width of an absorption line is

$$EW_\lambda = \int [1 - e^{-a_0 nh e^{x^2}}] dx. \tag{6.22}$$

A series expression for this can be obtained by writing

$$e^{-x} = 1 + \Sigma_{n=1}^{\infty} \frac{(-x)^n}{n!}, \tag{6.23}$$

and this give

$$EW_\lambda = \sqrt{\pi} \Delta\lambda_D \tau_0 \; (1 - \frac{\tau_0}{2!\sqrt{2}} + \frac{\tau_0^2}{3!\sqrt{3}} - \frac{\tau_0^4}{4!\sqrt{4}} + ...), \tag{6.24}$$

where $\tau_0 = a_0 nh = \frac{\sqrt{\pi} e^2 \lambda_0^2}{mc^2} \Delta\lambda_D f$.
Then, for $\tau_0 \ll 1 \Rightarrow$

$$EW_\lambda \propto \tau_0 \propto N. \tag{6.25}$$

where N ($= nh$) is the column density of the ion producing the line.

The EW cannot continue to increase indefinitely and linearly as the column density increases. When n becomes sufficiently large, most of the photons have been absorbed, and even for a large increase in their number the central intensity of the line will no change at all, hardly giving any change in the EW. This is called *saturation*. At this point, it is possible to prove that the asymptotic form for τ_0 (Bowers & Deeming 1984) give:

$$EW_\lambda \simeq 2\Delta\lambda_D \sqrt{\ln \tau_0} \; (1 + \frac{0.2886}{\ln \tau_0} - \frac{0.1355}{(\ln \tau_0)^2} + ...). \tag{6.26}$$

So, for $\tau_0 \gg 1 \Rightarrow$

$$EW_\lambda \propto \sqrt{\ln \tau_0} \propto \sqrt{\ln N}. \tag{6.27}$$

When further atoms are added, although the central depth cannot become deeper, the wings of the profile start to add to the EW, and the EW increases again, although rather more slowly than during the optically thin stage. In this case, we assume pure damping broadening and consider $\alpha = \gamma / 4\pi\Delta\nu_D$ to determine the wings of the line (Chapter 6 of Bowers & Deeming 1984) where γ is the classical damping constant ($= 2.47 \times 10^{-22} \nu_0^2 sec^{-1}$) and $\Delta\nu_D$ the Doppler width of the line in frequency units ($= (\nu_0/c) v_D = (\nu_0/c)\sqrt{2kT/m}$). It is important to underline that the core of the line is produced by the Doppler

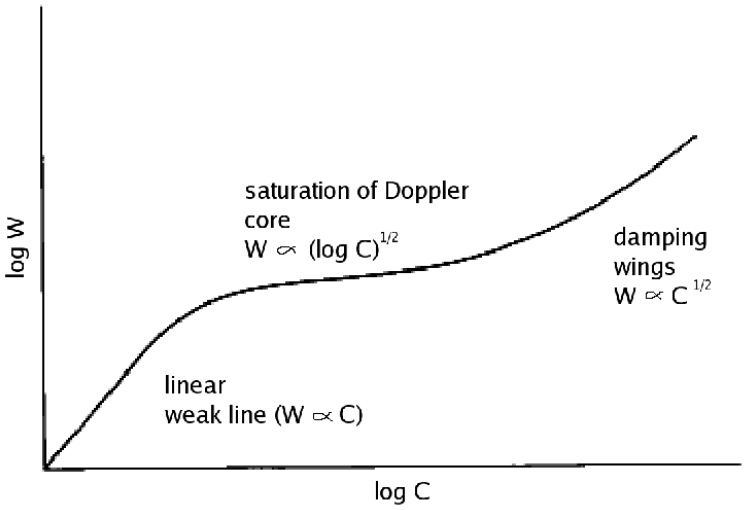

FIGURE 6.14— Equivalent line width (curve of growth) versus optical depth at the line center. Note that in our nomenclature $W \equiv$ EW and $C \equiv \tau_0$ (Bowers & Deeming 1984).

effect and the wings are produced by damping. In the wings of the line, $v \gg \alpha$, and the Voigt function ($H(\alpha, v)$) is given quite accurately by $H(\alpha, v) \simeq \frac{\alpha}{\sqrt{\pi}} \frac{1}{v^2}$, so we can approximate a_λ by:

$$a_\lambda = a_0 H(\alpha, v) \sim a_0 \frac{\alpha}{\sqrt{\pi}} \frac{1}{v^2}, \tag{6.28}$$

which allows us to write

$$EW_\nu \approx \sqrt{\alpha \pi^{1/2}} \sqrt{\tau_0} \Delta\nu_D \tag{6.29}$$

Thus, for $\tau_0 > 10^3 \Rightarrow$

$$EW_\lambda \propto \sqrt{\tau_0} \propto \sqrt{N}. \tag{6.30}$$

The total effect of these three stages is summarized in Figure 6.14 which is know as a *curve of growth*.

We try to understand which are the sources of the observed scatter in the Figures 6.12 and 6.13.

Position and type of the host galaxies

Since we are working with SNe in different host galaxies, we first consider the study of the position and type of the parent galaxies of the SNe with larger

values of EW(Na ID) or E(B-V) (see Figure 6.12) in order to find a reason for the distribution of the EW(Na ID) vs. E(B−V) plane. But unfortunately our research did not have success.

According to Spitzer (1948) and Spitzer & Oke (1952), we studied the distribution of interstellar sodium for the galaxies of our sample without find any variations of the EW(Na ID) with the distance.

Type and inclination[9] of the host galaxies were also collected but again we do not find any segregation.

Therefore, by considering this approach, we cannot obtain any explanation to the distribution of our plane EW(Na ID) vs. E(B−V).

Not constant dust-to-gas ratio

As we have seen in previous relations, EW(Na ID) is related to the column density of gas (see equations 6.25, 6.27 and 6.30) and E(B−V) is related through A_V to the column density of dust grain (see equations 6.5 and 6.6). They are connected by the dust-to-gas ratio (ρ_d/ρ_g).

It is known that ρ_d/ρ_g depends on the chemical composition ISM, on the physical conditions of the clouds and on the depletion of their most abundant elements. This implies different values of ρ_d/ρ_g even within the same galaxy (e.g. for the Milky Way see Barbaro et al. 2004). Average values for the Milky Way are $\frac{\rho_d}{\rho_g} = 10\times10^{-3}$ and for the Magellanic Clouds 2.88×10^{-3} and 1.84×10^{-3} for the Large and Small Magellanic Cloud, respectively, but our knowledge of the average dust-to-gas ratio in other galaxies is still scarce. Studies of column density of atomic hydrogen, molecular gas and grain populations are needed.

Each SN of our sample represents not only a different host galaxy but also a different line of sight inside of it. The large dispersion of the points in the plane EW(Na ID) vs. E(B−V) proves the variation of ρ_d/ρ_g, but we should also find more dispersion for large values, and this is not found.

Not-unique value of R_V

To relate E(B−V) with the τ of the dust, the parameter R_V has to be taken into account. As we have seen before, there are SNe for which R_V is lower than the standard $R_V = 3.1$. Then, the wide range of possible values of R_V is another source of dispersion in Figure 6.12. Considering that R_V can range from 0.70 to 5.5 (see Section 6.7), we should experience a larger distribution dispersion in the plane EW(Na ID) vs. E(B−V).

[9] Line of sight from a inclined galaxy could present more extinction than that from a galaxy seen face on.

Indeed, in order to remove the dependence on R_V, we consider also the possibility of representing the SNe in the EW(Na ID) vs. A_V plane instead of EW(Na ID) vs. E(B−V) (Figure 6.15).

Nevertheless, A_V is not directly derived from the observations and needs the knowledge of R_V. Moreover, the points in the EW(Na ID) and A_V are more concentrated with respect to the ones in the EW(Na ID) - E(B−V) diagram, making the later more favourable to find single deviations from the average behaviour.

Therefore, also this new representation does not solve the degeneracy due to R_V and we prefer to remain in the EW(Na ID) vs. E(B−V) plane which is closer to the direct observations.

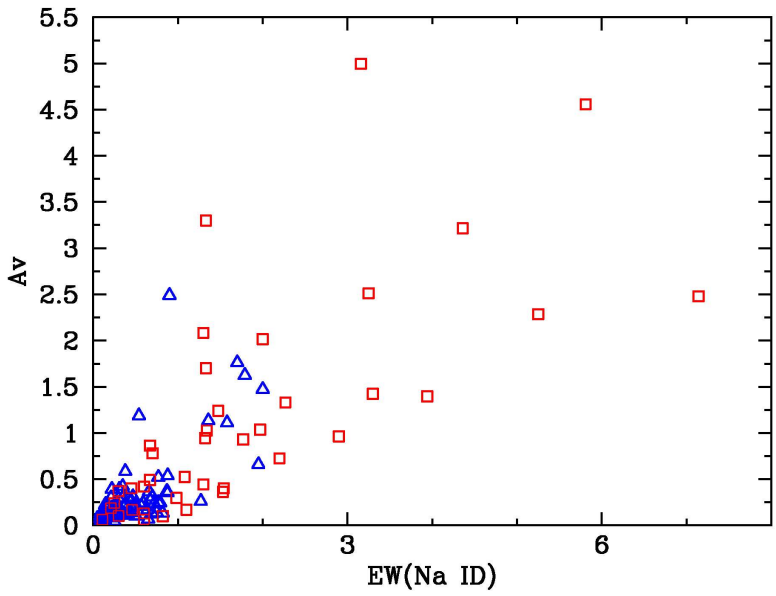

FIGURE 6.15— EW(Na ID) vs. A_V of the sample listed in Table 6.4. It was considered R_V =3.1 for all SNe except for SN 1999cl (R_V = 1.55), SN 2001el (R_V = 2.88), SN 2002hh (R_V = 1.1/3.1), SN 2003cg (R_V = 1.80) and SN 2006X (R_V = 1.56). Empty triangles and squares correspond to measurements for the Milky Way and the host galaxy components, respectively.

Number of clouds and saturated lines

The ideal way to derive column densities from the Na ID absorption lines is to record spectra at a sufficiently high resolution (hereafter HR) and good signal-to-noise ratio.

In view of the early total saturation of the sodium, and in order to better understand the behaviour of the line saturation in spectra of low resolution (hereafter LR), we generated synthetic spectra with IRAF task MK1DSPEC at different EW where both lines of sodium are perfectly distinguished and have gaussian profiles. Then, we convolved them to obtain low resolution spectra and measured again the EW. In the process, we took into account that EW the two lines of Na I are not independent. In fact, the ratio of the oscillator strengths for the two sodium lines is

$$\frac{3^2S_{1/2} - 3^2P^0_{3/2}(5890\mathring{A})}{3^2S_{1/2} - 3^2P^0_{1/2}(5896\mathring{A})} = \frac{0.631}{0.318} \sim 2.0 \tag{6.31}$$

We did several tests changing the number of the clouds and their velocity (supposing that the dispersion of velocity of a cloud is smaller than the slit used to obtain the spectrum), and proved that it is possible to consider

$$EW(D_1)_{hr} + EW(D_2)_{hr} = EW(D)_{lr} \tag{6.32}$$

where hr and lr means high and low resolution respectively, and also that for n clouds in the line of sight, the EW is equal to n times the EW of a single cloud. So, the total EW of saturated and unsaturated lines has the same value for low and high resolution.

After this, we check by how much the different types of clouds (Table 6.1) can affect the EW. By considering the different range of column density and temperature for each type of cloud and by applying these values to the three stages of the curve of growth of the sodium shown in Figure 6.14 (corresponding to equations 6.24, 6.26 and 6.29), we found that the EW is only slightly affected by the temperature (assuming a fixed mean value of the column density for each cloud) for three stages. On the contrary, the EW changes with the column density (assuming now a fixed mean value of the temperature for each cloud).

We superimpose on Figure 6.12 curves of growth for one to seven clouds, obtaining Figure 6.16. These curves were created by adding to the relation found by Munari & Zwitter (1997) between E(B−V) and EW(Na ID1) (i.e.

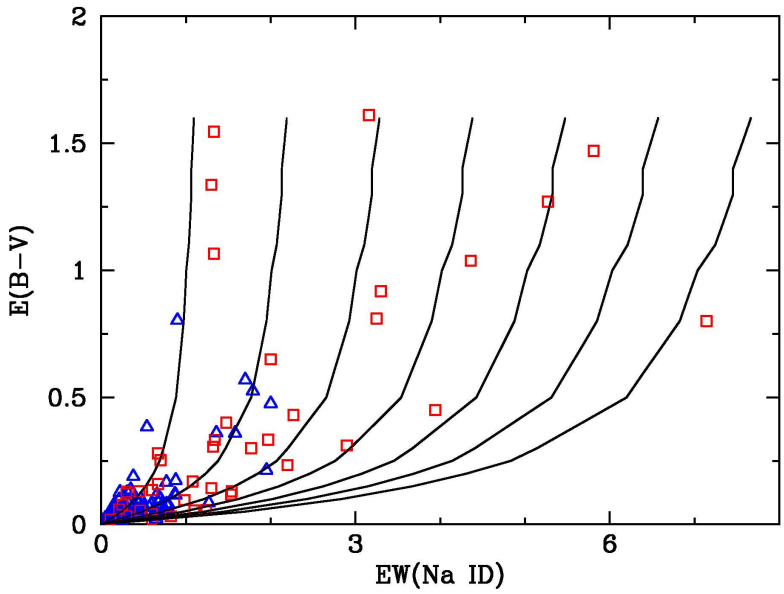

FIGURE 6.16— Superimposition of curves of growth on plane EW(Na ID) vs. E(B−V) from one to seven clouds.

for a single component) the contribution of a second component, taking into account equation 6.31.

So, a possible explanation of the behaviour of EW(Na ID) vs. E(B−V) that we find is that each line of sight from us to the SN (it means at each point of the diagram) passes through a different number of clouds of different column density. These curves are clearly an approximation because we have assumed constant values of a dust-to-gas ratio and R_V (Munari & Zwitter 1997). Nevertheless they can explain in qualitative way the observations.

We retrieved HR spectra of some of the most extinguished SNe in the figure from our archive or from literature, and measured separately the EW of both lines of the doublet. It is known that if the doublet ratio is close to 1.1, it means that the lines are saturated and probably by the presence of cold clouds; if it is around 2.0, it means that the lines are unsaturated indicating probably the presence of warmer clouds (e.g. Spitzer 1948). The doublet ratio of SNe on the lower shaded area of our plane EW(Na ID) vs. E(B−V) of Figure 6.17 is close to the unsaturated value (see Table 6.5) and the other ones have a ratio

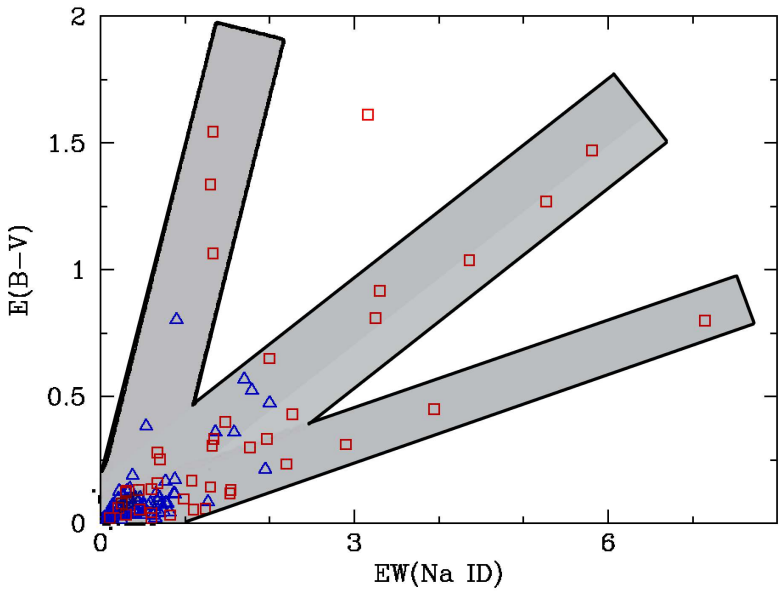

FIGURE 6.17— Same as Figure 6.12 where we have highlighted the region of linear growth (bottom) and those of saturation.

around 1.1. This could mean that light from SNe like SN 1990B, SN 1994I and SN 1989B (lower area of Figure 6.17) probably passes through diffuse clouds (warmer cloud and low column density) without saturating the sodium lines which are kept close to linear stage of the curve of growth. For the other SNe, considering always those with large values, the sodium lines are close to saturation (doublet ratio close to 1.1) probably because the radiation travels through clouds with more atoms and in other stages of the curve of growth.

Therefore, this scenario seems to explain better the distribution in the plane EW(Na ID) - E(B−V) shown in Figures 6.12 to 6.17, but we cannot rule out that the other possibilities described have some effect. Probably the reason for the presence of only three well-distinguished lines in the plot lies in the small sample of high extinguished SNe.

The study of an enlarger sample of SNe has shown that the distribution of SNe in the EW(Na ID) vs. E(B−V) plane is sparse. No clear empirical relation between these two quantities can be derived even if it provides lower limits to

TABLE 6.5— Ratio of equivalent widths of the components of the NaI D doublet.

Lower line†		Medium line‡		Upper line*	
SN◇	Ratio	SN	Ratio	SN	Ratio
SN 1990B	—	SN 1996D	—	SN 2002hh2	1.33±0.07
SN 1994I	2.15±0.02	SN 2003cg	1.24±0.10	SN 2006X	1.10±0.02
SN 1989B	2.70±0.10	SN 1986G	1.19±0.05	SN 2002hh1	1.33±0.07
SN 1999ee	—	SN 2002cm	—	SN 2001fh	—
		SN 1999cl	—	SN 2000E	—
		SN 1976B	—		

† Lower area of the Figure 6.17.
‡ Medium area of the Figure 6.17.
* Upper area of the Figure 6.17.
◇ Each SN of the list corresponds to a point of the line in decreasing order of EW from top to bottom.

the reddening as a function of EW of the form

$$E(B-V) = 0.11 \times EW(Na\,ID) - 0.01. \tag{6.33}$$

Several can be the causes of this dispersion, different dust-to-gas ratios, different extinction law, and the effect of superposition of several saturated and not saturated lines. Probably all this effect are mixed together and difficult to disentangle.

The study of reddened SNe at high resolution will help in the comprehension of this phenomenon.

6.7 Low total-to-selective extinction ratios in SNe

As we have seen before, the total-to-selective extinction ratio, R_V, has been well studied in the Milky Way obtaining a mean value of $R_V = 3.1$. However, for a few directions, values ranging from $R_V = \sim 2$ to ~ 5.5 have been found (Fitzpatrick 2004; Geminale & Popowski 2005). In other galaxies, we have relatively poor information about the extinction parameters. The studies of R_V from SNe have provided values ranging from 0.70 (Capaccioli et al. 1990) to 3.1 (Pozzo et al. 2006) (in Section 3.2.1 there is a more complete list of values of R_V found in the literature).

In previous Chapters we have shown three examples of highly reddened Type Ia SNe, and in all these three cases we have found values for R_V definitely lower

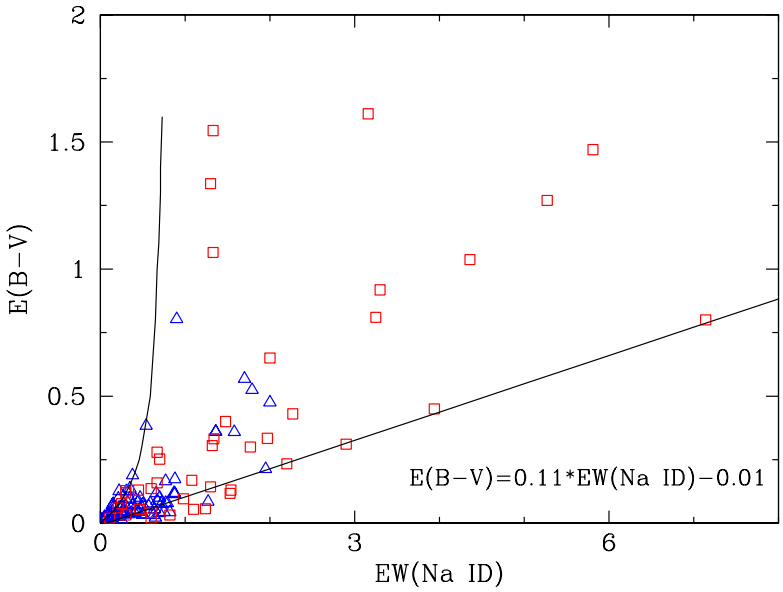

FIGURE 6.18— Limits on the plane EW(Na ID) vs. E(B−V). The upper limit is the curve of growth of a single cloud (see text) and the lower limit is reproduced by the relation E(B-V) = 0.11 × EW(Na ID) - 0.01.

than the canonical value. As was already mentioned, R_V is probably related to the averaged characteristics of dust grains that contribute to extinction along the line of sight. It is possible deduce that small values of R_V correspond to small size of the dust grains. From the recent works of Goudfrooij et al. (1994) and Patil et al. (2007), small values of R_V are measured in galaxies with well-defined dust lanes, and actually, our SNe are projected on dust lanes of the host galaxies (see respectively Chapters 3 and 4).

In general, taking into account of a grain size distribution model like that seen in 6.1.1 ($n(a) \propto a^{-3.5}$), an acceptable fit to the mean extinction curve (e.g. Figure 6.3) can be obtained with values of grain sizes ranging from $a_{min} \approx 0.005\mu m$ to $a_{max} \approx 0.25\mu m$ (Whittet 1992). According to Witt (2000), it is possible to divide the size distribution of interstellar grains (Kim, Martin & Hendry 1994; Zubko, Smith & Witt 1999) into three separate domains: typical, small and very small (see Table 6.6 for more information). By considering the value of R_V, for our three SNe we find that the dust grains along the line of sight to these SNe must be very small. This kind of grains should be related to

TABLE 6.6— Size Domains of Interstellar Grains (from Witt 2000).

Domain	Radius[a] (μm)	Mass (g)	Relative Abundance
typical	0.1 - 1	$10^{-14} - 10^{-11}$	1
small (SG)	0.005 - 0.1	$10^{-19} - 10^{-14}$	$\sim 10^3$
very small (VSG)	0.0003 - 0.005	$10^{-21} - 10^{-19}$	$\sim 10^6$

[a] Assuming spherical grains.

diffuse clouds because studies in dense clouds confirm that these grains grow by coagulation, which implies a large R_V (Whittet 1992).

Focusing on the SN Ia, Branch & Tammann (1992) summarized the possibilities why the total-to-selective extinction ratios in SN Ia are so small without to arrive to some resolution: (1) because of the different dust in the host galaxy with respect to the Galactic dust, (2) the observed spread of (B-V) at maximum might be inflated by observational errors, (3) the assumption of a unique intrinsic $(B-V)_0^{max}$ for all Type Ia SNe could be invalid, (4) due to circumstellar dust with very particular optical properties. Some years later, Riess et al. (1996b) demonstrated from the study of 20 distant SNe Ia that on average, the optical properties of dust in distant galaxies are not drastically different from those of the Milky Way and that the variation of the R_V is not caused by circumstellar dust but by interstellar dust, because, if not, we would expect the measured A_V to be independent of galaxy morphology, which it is not, as shown in Figure 6 of Riess et al. (1996b).

An alternative explanation was introduced by Wang (2005) who considers that dust in the immediate neighborhood of SNe Ia can explain the anomalous reddening seen in SNe Ia. This idea implies light echo scenarios where the light is scattered out of and into our line of sight. In this work it is found that light echo from a dust cloud, having an inner radius 10^{16} cm would produce a significant reduction in R_V. In Figure 6.9 we have seen the evolution with time of R_V in UBVRI bands for Type Ia SNe, while in Figure 6.19 we present again the evolution of R_V but considering dust around the SNe with a inner radius of 10^{16} cm (Wang 2005)[10]. By comparing both figures, it is clear that R_λ is reduced around the optical maximum if dust scattering effects are included.

[10](Wang 2005) defined $R_\lambda^0 = A_\lambda / E^0(B-V)$, where $E^0(B-V) \equiv (A_B^{max} - A_V^{max})$, $A_B^{max} = B_d^{max} - B^{max}$ and $A_V^{max} = V_d^{max} - V^{max}$, and B^{max} and V^{max} are the B and V band maximum magnitudes with no dust extinction, respectively, and B_d^{max} and V_d^{max} the B and

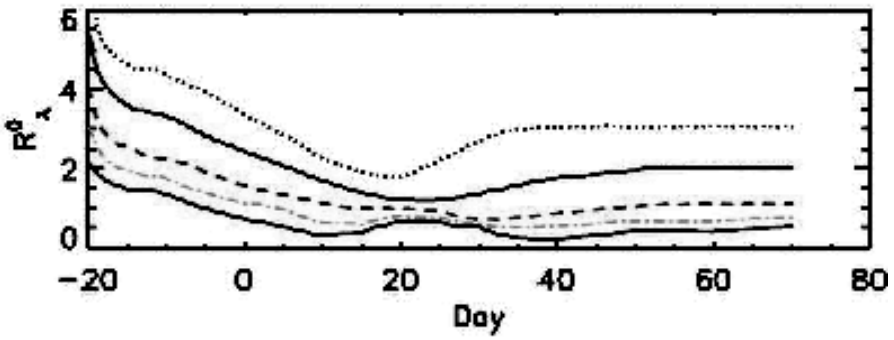

FIGURE 6.19— Variation in the time of extinction properties in U (dotted line), B (solid line), V (dashed line), R (dot-dashed line) and I (bottom solid line) bands for Type Ia SNe considering dust scattering. It was assumed a spherically symmetric distribution of dust with an inner radius of 10^{16} cm and an optical depth of 1.45 in B band (from Wang 2005).

However, as seen in Section 3.2.3, there are some difficulties for this interpretation. Firstly, the possibility of grain survival at such a small distances are low, then, we expect to observe other effects at later times such as a strong near-IR excess, a temporal variation in the reddening, an anomalously small Δm_{15}, a significantly brighter late phase tail or a broader spectral lines (Patat 2005), which are not seen.

We conclude, therefore, that low values of R_V we observed are caused mainly by effects in the interstellar medium due to grains of small size along the line of sight. In general, most of the host galaxies have different properties from the Milky Way, and also, as we have seen (Chapter 4), there are cases where for a single galaxy we find SNe whose R_V is different. Our hypothesis could be supported by the possibility that the radiation due to SNe explosion might have partially eroded the dust grains, increasing the number of small grains. Moreover, it supports the hypothesis that "circumSN" dust is the cause of these variations, but it is not the only possibility, there are still some open question in this explanations.

V band maximum magnitudes with dust extinction.

7

Conclusions

Lui si che è bravo!
Massimo Turatto

Ancora qua!
Stefano Benetti

The determination of the extinction by dust is one of the most crucial ingredients in the calibration of SNe for their use as distance indicators. Indeed the correction for such effect has been studied in the past but no convincing solutions have been found. Often the analysis of the reddening in nearby SNe has given hints of anomalous reddening. A practical solution to the problem is to remove reddened objects from the samples when statistical studies are done. This removes the problem but does not solve it.

In this thesis I have studied in great detail three nearby SNe Ia which showed clear signatures of significant reddening. I have determined the extinction law and verified "a posteriori" that they were intrinsically normal objects thus confirming the hypothesis on which the extinction law was determined.

The three examples of highly reddened Type Ia SNe: SN 2002cv, SN 2003cg and SN 2006X, were collected, reduced, and analyzed in the framework of the *European Supernova Collaboration*. The available densely sampled observations of these SNe allowed me to carry out a detailed comparison between them and other well observed unreddened SNe Ia and to analyze their reddening laws.

For all the objects I have estimated a very low value of R_V, the total-to-selective extinction ratio, by mean of the comparison of the SED (Spectral

Energy Distributions) with photometric and spectroscopic methods. The SNe of this work are new entries in the growing list of SNe with a low value of R_V: SN 1999cl was reddened by dust with $R_V = 1.55 \pm 0.08$ (Krisciunas et al. 2006); SN 2001el with $R_V = 2.88 \pm 0.15$ (Krisciunas et al. 2003); SN 2002hh with two extinction components, $A_V = 3.3$, $R_V = 1.1$ and $A_V = 1.7$, $R_V = 3.1$ respectively (Pozzo et al. 2006).

- SN 2003cg was a heavily reddened, but otherwise normal, Type Ia supernova as shown by the shape of its UBVRIJHK light curves or its spectral evolution. This object presented several indications that reddening was an important issue: (a) SN 2003cg appeared projected into a dust lane of NGC 3169; (b) the U and V light curves showed broader peaks and a pronounced shoulder in the post-maximum decay, respectively; (c) its optical spectrum showed a very strong Na I D interstellar doublet and (d) *diffuse interstellar bands* (DIBs). However, dereddening the B light curve with a standard extinction law and the E(B-V) derived matching the average SN Ia (B-V) colour curve, would yield an abnormally bright peak in the absolute magnitude. I therefore allowed R_V to become a free parameter within the Cardelli, Clayton & Mathis (1989) extinction law and adjusted R_V and A_V to provide simultaneous matches to a range of colour curves of normal SNe Ia or to a derived extinction curve from spectral comparison. As result I obtained for line of sight inside the host galaxy of SN 2003cg: $A_V = 2.39 \pm 0.13$ and R_V 1.80 ± 0.20 (which give me as excess colour E(B-V) = 1.33 ± 0.11).

- SN 2002cv was a rare event for two main reasons: it exploded a few months after and in the same host galaxy of the well studied Type Ia SN 2002bo, and its extinction was extremely high (it was not detectable bluewards of 6000 Å). Due to this lack of clear spectral features, no certain classification was attributed to SN 2002cv. Our analysis shows the presence of clear secondary maxima, typical of the Type Ia SNe, in all red and IR light curves and IR spectral features compatible with SNe Ia, thus classifying this object beyond any doubt. The study of the SED shows that in the direction of this object there is an atypical extinction law with a small $R_V = 1.75 \pm 0.55$ and $A_V = 8.54 \pm 0.89$ (E(B-V) = 4.88 ± 1.61).

- In the case of SN 2006X a high extinction was already detected in the classification spectrum, because of a continuum too red for an unextinguished SN Ia at early phases. The study of the extinction law has been carried out in analogy with the other objects of this thesis on the material

already collected, and showed a $A_V = 1.98 \pm 0.21$ and $R_V = 1.56 \pm 0.30$ (which give an E(B-V) = 1.27 ± 0.37) in the direction to this object. The peculiarities of this SN are the high velocity of its spectral lines and the Na ID interstellar lines, which were found to evolve with time. This could be explained by the presence of circumstellar material in the vicinity of the explosion location, most likely physically related to the supernova progenitor system.

A yet unresolved question is whether the variation I observed in the Na ID interstellar lines in SN 2006X is the rule or an exceptional case. Following Patat et al.'s (2007) conclusions, I believe that there are sufficient reasons to suspect that the variability of the Na ID lines caused by circumstellar may be a common feature in SNe Ia. Until now, it may have escaped detection mainly because it requires high resolution spectroscopy, i.e. long integration times on large telescopes.

These SNe are an important addition to the database of well-monitored nearby Type Ia, which is of crucial interest in calibrating nearby SNe Ia for cosmological studies.

The study I am carrying out of the heavy reddening towards these SNe is helping to establish the diversity in the physical characteristics of dust responsible for extinction which is also relevant in other astrophysics studies. I have found lower values of R_V in the line of sight to our three SNe, which is probably caused by different types of grains, those of small size being predominant. Grain sizes relative to our galaxy: $\langle a \rangle / a_G$, was derived for the line of sight inside the parent galaxies: 0.75 ± 0.07 for NGC 3169 (SN 2003cg), 0.52 ± 0.06 for NGC 3190 (SN 2002cv) and 0.71 ± 0.07 for M100 (SN 2006X). I note that the line of sight inside NGC 3190, toward SN 2002bo, show normal values for the total-to-selective extinction ratio R_V. A plausible hypothesis about these small sizes could be attributable to the radiation due to SN explosions which could have partially eroded the dust grains, increasing the number of small grains. In this case, the dust responsible for the low value of R_V found in the SNe Ia should be of circumstellar origin. I note however that similar values for R_V have been found along the line of sight in dust lanes of early type galaxies (Patil et al. 2007). Therefore other possibilities cannot be excluded.

In this work I have re-analysed an independent method for estimating the reddening via the equivalent width (EW) of the narrow interstellar Na I D doublet, by studying an enlarged sample of SNe. The points representing the SNe are more dispersed on the EW(Na I D) vs. E(B-V) plane than in previous

studies, thus I am able to provide only lower and upper limits to the reddening once E(B-V) is known. A full explanation is not provided because several effects probably play a role. I believe that the lower limit is formed by SNe whose light passes through diffuse clouds (warmer cloud and low column density) without saturating the sodium lines which are kept on the first part (linear stage) of the curve of growth. For the other SNe, with large values of E(B-V), the sodium lines are close to the saturation (doublet ratio close to 1.1) probably because the radiation travels through clouds with larger column density and in other stages of the curve of growth. The problem is complicated by the possible presence of several clouds and/or by other effects, e.g. different or variable R_V. But this explanation is not unique and does not exclude other possibilities described above.

The general conclusion of this work is that it appears that the most reddened SNe Ia studied so far seem to obey a non canonical extinction law with low values of R_V. Whether this is the case only for high extinction objects is not yet clear. Certainly there are other objects that seem to follow the normal law, such as SN 2002bo in the same galaxy as SN 2002cv. What is the relative frequency of different values of R_V and what are the causes is not clear. The possible sources of different extinction laws might be either local to the SN environment or the statistical effect of the projection of different clouds along the line of sight. Understanding this is extremely important both for understanding the nature of the exploding stars and for the calibration of SNe Ia for cosmological use.

To solve this issues more extended studies based on larger samples of SNe, possibly also with the use of high resolution spectroscopy, are needed. The extension of similar work also on Core-Collapse SNe will help in disentangling the local effects due to the parent population from those due to projection along the line of sight. In turn, the information on individual SNe will provide new independent data to understand the overall behaviour and distribution of dust in galaxies.

7.1 Future work

Several studies are already in progress with this aim:

1. Extension of the preliminary work on several SNe (among which SN 2006X, discussed here) to other wavelengths, in particular extension to the UV domain by using data collected with the Swift satellite. The inclusion of the short wavelengths is very important to improve the study of the extinction effect.

2. Reduction and analysis of other ESC targets not yet studied in order to study the physics of their explosion.

3. Study of high resolution spectra of SNe Ia (and other SN types) at different epochs to check if the variability of the interstellar absorption is a common feature.

A

European Supernova Collaboration

The theoretical and observational investigation of local SNe Ia was the main motivation of the European Supernova Collaboration (ESC)[1]. It was an European RTN (Research Training Network) funded by the European Community for 4 years (2002-2006) and formed by 10 European Institutions (Max Plank für Astrophysik and European Southern Observatory in Germany, Imperial College, University of Oxford and Cambridge Institute of Astronomy in UK, Isaac Newton Group of Telescopes and Astronomy Department of the Barcelona University in Spain, Padova Observatory in Italy, Supernova Group University of Paris VI & VII in France and Physics Department in & Observatory of the Stockholm University in Sweden) + the Research School of Astronomy & Astrophysics and the Mt. Stromlo & Siding Springs Observatories in Australia.

A.1 Research objectives

Currently, our poor understanding of the Type Ia supernova physics is the major systematic uncertainty in measurements of the accelerated expansion of the universe and in determinations of its "dark energy" content. In addition, SNe Ia are still the best tool that can be used to constrain the physical nature of the dark energy and its time evolution (if there is any).

Only after their light curves have been calibrated can Type Ia supernovae become very good cosmic distance indicators. However, the distant supernovae exploded at a time when the solar system was just forming. There is no guarantee that they are the same as the nearby ones on which the empirical calibrations

[1] http://www.mpa-garching.mpg.de/∼rtn/

are based. Only after we understand the physics of the explosions can we assess with confidence whether SNe Ia can be used as reliable distance indicators, and whether it is necessary to search for new physics beyond the standard models of particle physics and cosmology. This goal can only be achieved by studying very nearby supernovae in great detail.

This collaboration was born with the conviction that the only way to make a decisive jump in understanding the physics of SNe Ia is to compare realistic models of thermonuclear explosions (and the emerging radiation) with a complete and detailed set of homogeneously-acquired observations by a combined action of all major groups working in this field in Europe. For the first time homogeneous sets of light curves and spectra for a rather large sample of Type Ia supernovae were obtained through systematic and targeted observations, while at the same time the quality and predictive power of theoretical models was increased.

Consequently, an "alert group" was established which was in charge of quick responses to newly discovered supernovae and of coordinating the monitoring campaigns.

In addition, there is a global objective which cover all those ones, the training of young researchers (PhD students, Post-Doc), in which I took part.

A.2 Major successes

The RTN obtained very good to excellent data for 15 Type Ia SNe (SNe 2002bo - Benetti et al. 2004a, 2002cv - Elias-Rosa et al. in prep., 2002dj - Pignata et al. in prep., 2002er - Pignata et al. 2004a, Kotak et al. 2005, 2003cg - Elias-Rosa et al. 2006a, 2003du - Stanishev et al. submitted, 2003gs, 2003kf, 2004dt - Altavilla et al. submitted, 2004eo - Pastorello et al. 2007b, 2005W, 2005bl, 2005cf - Pastorello et al. 2007a, Garavini et al. 2007, 2005hk and 2006X) and one Type Ic SN (SN 2004aw - Taubenberger et al. 2006). In some cases the reason for losing targets was bad weather at most of the telescope sites the RTN had access to, but also technical difficulties in coordinating up to 12 different telescopes for our observing campaigns, something which had never been attempted before by any other group. With these SNe was carried out the kind of investigation that was the main scientific goal of the RTN. However, due to these technical difficulties we have been unable to reduce and analyze all data yet, although the work is being continued by several partners (MPA, ESO, Padua) by means of core funding.

In total we have more than tripled the number of Type Ia SNe observed starting well before maximum light and followed with very good time and wavelength coverage, both spectroscopically and photometrically all the way into the

nebular phase. We also have more than doubled the number of Type Ia SNe with good infrared data. All these data are needed if attempts are to be made to obtain a complete physical picture of the explosions.

In this thesis we have present three of these Type Ia SNe of the ESC.

Another major success was that the companion star of a Type Ia supernova could be identified for the first time, supporting the single-degenerate scenario of the progenitors.

On the theoretical side, "abundance tomography" was carried out for two of the RTN SNe: SN 2002bo and SN 2003du, and it was demonstrated that accurate data make it indeed possible to analyze the physical reasons behind the observed diversity of SNe Ia, which was the main scientific objective of the RTN. Moreover, synthetic light curves and abundances in velocity space were computed from first principles for the first time and were shown to agree well with observations and, in particular, with the results we had obtained from the abundance tomography of individual explosions.

The conclusion from all these efforts is that indeed most (if not all) Type Ia SNe are the result of the explosion of a Chandrasekhar-mass white dwarf, presumably in a binary system with an ordinary star as the companion. In addition we could show beyond doubt that the empirical single-parameter calibration of their peak luminosity is insufficient and needs to be refined. Besides the mass of radioactive nickel, the additional parameter that most probably needs to be considered is the kinetic energy of the explosion, as measured by the spectra. We expect that the scatter in the Hubble diagrams of Type Ia SNe will decrease, and thus their precision as distance indicators will increase, if this effect is included.

A.3 Research results

As we have discussed before, the scientific objective of the RTN was to investigate the nature of thermonuclear supernova explosions by means of a combined effort of groups working on the observations and on modelling these events. The RTN started its operation in mid July of 2002, and by the end of the funding period (July 2006) reached its main goals.

An extensive study, varying physical parameters such as the composition and the ignition conditions, was carried out and published by the MPA group (Röpke et al. 2006a), and metallicity effects on the peak luminosity of SNe Ia were investigated in order to search for systematics in the empirically derived luminosity - light curve shape relations which is critical for cosmological applications (Travaglio, Hillebrandt & Reinecke 2005). Along the same line, the effect of different C/O ratios on the luminosity was investigated but in contra-

diction to expectations no significant effect was found (Röpke & Hillebrandt 2005, Röpke et al. 2006a). Also rather different ignition conditions were modelled (Röpke et al. 2006b). These ignition conditions were chosen in accord with numerical studies (Iapichino et al. 2006). Results from the various models were used to compute synthetic light curves and spectra, and to compare them with observations (Blinnikov et al. 2006, Stehle et al. 2005,Kozma et al. 2005, Sauer, Hoffmann & Pauldrach 2006).

ESO continued its collaboration in various projects within the RTN. For example groups at ESO made a detailed comparison of the spectra of distant Type Ia SNe with those of nearby objects, while others investigated the global parameters of the thermonuclear explosions. This last work, in connection with explosion models and radiative transport calculations, allowed us to check the complete chain of assumptions with observations. The validity and limits of Arnett's rule describing the relation between a supernova luminosity and mass of synthesised ^{56}Ni has been demonstrated (Stritzinger et al. 2006).

The activity of the Padova node during the course of the RTN collaboration was focused on the following aspects: collection of new data on SNIa discovered before or at maximum light, data analysis, study of SNIa at intermediate redshifts, and development of archiving tools for the collaboration. This node was in charge of the coordination of the observations performed with the telescopes/instruments available at ESO La Silla and Paranal (Chile), at the Telescopio Nazionale Galileo at La Palma (Spain) and Asiago (Italy). The activity ranged from the preparation of the observing proposals, to the preparations of the Phase 2 (when required), the management of the daily observations in ToO (Target of Opportunity, see B), the observations at the telescopes in visitor mode, and the coordination with the telescopes managed by other teams.

A detailed study of four of the SNe of the ESC was developed by this node. One of them was SN 2002bo, the first target of the collaboration (Benetti et al. 2004a). The other three objects have been shown and analyzed in the Chapters 3, 4 and 5.

A detailed analysis of the photometric and spectroscopic properties of 26 well-observed Type Ia Supernovae (SNe Ia) has been performed with the aim of exploring the SN Ia diversity as a collaborative effort of several groups of the RTN (and the Padua and Garching nodes in particular). The sample included normal SNe, as well as extreme events such as SN 1991T and SN 1991bg, while the highly peculiar SNe Ia, SN 2000cx and SN 2002cx, were not included. The statistical treatment revealed the existence of three different groups as we have seen in previous chapters. The first group (FAINT) consists of faint SNe Ia similar to SN 1991bg, with low expansion velocities and rapid evolution of Si II velocity. A second group consists of normal SNe Ia, also with high temporal

velocity gradient (HVG), but with brighter mean absolute magnitude $\langle M_B \rangle$ = -19.3 and higher expansion velocities than the FAINT SNe. The third group includes both normal and SN 1991T-like SNe Ia: these SNe populate a narrow strip in the Si II velocity evolution plot, with a low-velocity gradient (LVG), but have absolute magnitudes similar to HVGs. While the FAINT and HVG SNe Ia together seem to define a relation between $\mathcal{R}$(Si II) and Δm_{15}(B), the LVG SNe either do not conform to that relation or define a new, looser one. The $\mathcal{R}$(Si II) pre-maximum evolution of HVGs is strikingly different from that of LVGs. This new evidence has a deep impact on the understanding of SN Ia diversity, in terms of explosion mechanisms, degree of ejecta mixing, and ejecta-circumstellar material interaction (Benetti et al. 2005a, Mazzali et al. 2005).

SN 2002er was spectroscopically classified by the Cambridge and ICL RTN nodes. Photometrically and spectroscopically, we found that SN 2002er fell into the regime of normal Type Ia SNe, e.g. it had a striking resemblance to the typical type Ia supernova SN 1996X. The early-time spectra were compared with model spectra generated by a Monte Carlo code based on the W7 explosion model. With a homogeneous abundance distribution in the atmosphere a fair match to the observations was obtained, but only by pushing the adopted distance and rise time close to the observational limits. We also compared the late-time spectrum with a single-zone spectral synthesis model constructed at ICL. From this we inferred a ^{56}Ni mass of 0.69 $M_\odot$, consistent with that derived from the light curve (Pignata et al. 2004a, Kotak et al. 2005).

Optical and near-IR light curve monitoring of Type Ia supernovae using the Liverpool Robotic Telescope (LT) on La Palma commenced in mid-2005. This provided optical light curves for a number of RTN targets e.g. SNe 2004dt, 2004eo, 2005bl, 2005cf.

The SuperNova Integral Field Spectrometer (SNIFS) instrument, built in France during the period 2002-2004 and in operation since July 2004 was used to observe about 50 nearby Supernovae during the July 05 to July 06 period. During this period, detailed spectro-photometry of about 20 of these SNe was obtained at multiple epochs. A first paper was published reporting observations of SN 2006gj, a unusual Type 1a Supernova in a massive circumstellar envelope. The rest of the data set is being analyzed with the aim of providing precisely calibrated spectro-photometry of SN Ia. The project will continue gathering data for two more years beyond the initially planned end in 2006. It is expected to have accumulated a set of about 200 Type Ia supernovae with spectroscopic observations for at least 10 epochs. This unprecedented data set will be used to improve distance measurements with Type Ia supernovae as well as improve our understanding of the Type Ia supernovae mechanism (Garavini et al. 2005,

Nobili et al. 2005, Conley et al. 2006).

A campaign to search for circumstellar matter in SNe Ia using various telescopes was conducted by the group at Stockholm Observatory. The telescopes used are the ESO Very Large Telescope (VLT), Subaru and the radio array ATCA in Australia. Special emphasis was put on the nearby SNe 2000cx and 2001el, and upper limits on the mass loss rate of circumstellar matter from the progenitors of these events have been derived (e.g. Mattila et al. 2005). SN 2002ic is one of two SNe Ia which has shown clear evidence of circumstellar matter, and we have obtained X-ray data of it using Chandra.

The group at Stockholm Observatory had also, together with other nodes in the network, made observations and spectral models of the late emission of SNe Ia (e.g., Sollerman et al. 2004, Kozma et al. 2005). One of the aims was to test explosion models of SNe Ia. Also the group at the Physics Department had a leading role in the use of Type Ia SNe in cosmology through their participation in the Supernova Cosmology Project, the Supernova Legacy Survey (SNLS) program and SNAP (Supernova Acceleration Probe) which is focused on the systematic effects involved in the determination of cosmological parameters, e.g. Jönsson et al. (2006). The SNLS data were used to test extra dimension models. Also, through a combined analysis of SN data, as well as Cosmic Microwave Background (CMB) and Large Scale Structure (LSS), an important upper limit was derived on the sum of the neutrino masses by Goobar et al. (2006).

The Barcelona node was leading an effort to identify the companion star to Tycho Brahe's supernova (SN 1572). The companion was found to be a rather normal main-sequence star, giving strong support to the "single-degenerate" scenario for the progenitors of Type Ia supernovae (Ruiz-Lapuente et al. 2005).

Most of the data have been published by now and some will be published in the near future. In order to make full use of the unprecedented data set collaborations between several of the groups involved will continue beyond the formal end of this RTN.

Finally, besides the many papers published by the collaboration in refereed journals and conference proceedings more than 100 IAU-Circulars were published in the past years, mostly giving fast identifications and classifications of nearby supernovae.

B

Spectroscopic Classification of Supernovae

SNe are discovered by comparison between new and reference images. Discovery images do not give information on types, although the location and the type of the parent galaxy can already provide useful information. It is therefore crucial, for any program devoted to SNe studies, to get the SNe classification as soon as possible.

This has been also important in this thesis devoted to the study of reddened SNe. Only through the information provided by the first spectra has been possible to understand whether the SNe were heavily reddened and, consequently, to start an intensive study. The photometric indications like absolute magnitudes, colour evolution, etc. can be used to study the amount of reddening when the data have already been collected, but already with a single optical spectrum (e.g. that used for the classification of the SN) we can have indication from the SED (Spectral Energy Distribution) and presence of interstellar features.

Therefore, during the period of my PhD, I took care also of the organization of this activity for the Padova SNe Group.

In last several years, the Padova SNe Group has classified a fair fraction of the new, nearby supernovae (brighter than 18 magnitudes) with the Asiago, ESO and TNG telescopes.

Contrary of what I was expecting, I searched my emails, not the sky, to find new SNe. A number of observers, both amateur and professional, are engaged

in the search for SNe. The notification and confirmation of these candidates is communicated to the International Astronomical Union (IAU)'s Central Bureau for Astronomical Telegrams (CBAT)[1] and reported in the IAU Circulars or Central Bureau Electronic Telegrams (CBETs). Generally, spectroscopic classification of the new objects is obtained by others, and reported separately in the IAU Circulars.

The candidate SN for classification are selected according to their position in the sky, the duration of their observability, brightness and distance, as well as possible peculiarities.

In the following, we present a brief report and spectroscopic comparison (for the cases with spectra of sufficient signal-to-noise) of a set of new SNe classified in last four years, the period during which I have been directly involved. This comparison have been performed with PASSparTOO (Padova Asiago Supernovae Spectra ComPARison TOOl) (Harutyunyan et al. 2005). This program, written in Python, compares a given SN spectrum with a set of SN spectra of known type and age (template spectra) of the Padova-Asiago Supernovae Archive to find the best fit. It takes a wavelength calibrated spectrum from input and, after redshift correction, normalises it dividing by the continuum. To the template spectra is applied the same processing. Then the input spectrum is compared to each of the template spectra and the best match is selected by minimization of the differences. A list of the SNe classified are also presented in Table B.1

B.1 Supernova 2003hg in NGC 7771

SN 2003hg was discovered in NGC 7771 (Moore, Li & Boles 2003), a SBa galaxy with a NED[2] heliocentric recession velocity of 4298 $\mathrm{km\,s^{-1}}$, at $\alpha = 23^h51^m24\overset{s}{.}13, \delta = +20^o06'38\overset{''}{.}30$ (J2000.0). Elias-Rosa et al. (2003) reported, from the inspection of a spectrum (range 355-780 nm; resolution 2.4 nm) obtained on Aug. 22.48 UT with the Asiago 1.8-m telescope (+ AFOSC), that SN 2003hg was a type-II supernova caught shortly after explosion. In Figure B.1 there is the spectroscopic comparison using PASSPARTOO, which confirms this classification and a phase around maximum light. The spectrum is dominated by Hβ and Hγ with P-Cyg profiles, while Hα still had a pure emission profile. The expansion velocity deduced from the Hβ and Hγ absorptions and from the Hα FWHM is about 11300 $\mathrm{km\,s^{-1}}$. A broad He I 587.6 nm emission is also present. A detection of a deep (EW about 0.2 nm) interstellar Na ID

[1] http://cfa-www.harvard.edu/iau/cbat.html
[2] http://nedwww.ipac.caltech.edu/

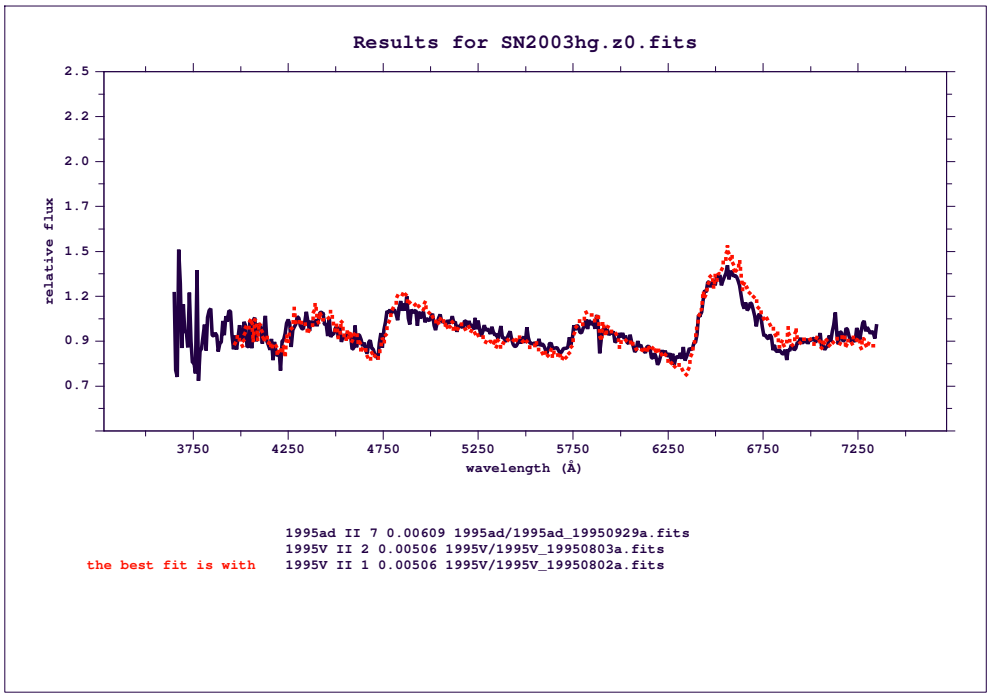

FIGURE B.1— Spectral comparison of SN 2003hg with the SNe of the Padova-Asiago Supernovae Archive producing the best fit, the type II SN 1995V (Evans et al. 1995). The spectra in the graph are converted to the host galaxy rest frame and normalized to the continuum flux so that the intensity and shape of the continuum are removed. At the bottom are reported the three SNe giving the best match along with the type, epoch, redshift and name of the file in the archive.

feature suggests high reddening for SN 2003hg.

B.2 Supernova 2003ie in NGC 4051

The inspection of a spectrum (range 370-750 nm; resolution 2.4 nm), obtained on Sept. 22.78 UT with the Asiago 1.8-m telescope (+ AFOSC), shows that SN 2003ie (Arbour & Boles 2003) is a type-II supernova (Benetti et al. 2003). It was located at $\alpha = 12^h03^m18\overset{s}{.}15, \delta = +44^o31'34\overset{''}{.}60$ (J2000.0), which is $91''$east and $18\overset{''}{.}6$ south of the centre of NGC 4051 (SBbc galaxy with a NED heliocentric recession velocity of 697 km s^{-1}). Its spectrum is dominated by a red continuum and unusually strong P-Cyg lines of Fe II at 492.4, 501.8, and 516.9 nm; Sc II at 552.7, 565.8, and 624.5 nm; Na ID; and Ba II at 614.2 nm. The mean expansion velocity deduced from these lines is 5450 +/- 200 km s^{-1}. Hβ and Hα are also present with P-Cyg profiles and expansion velocities of 5700

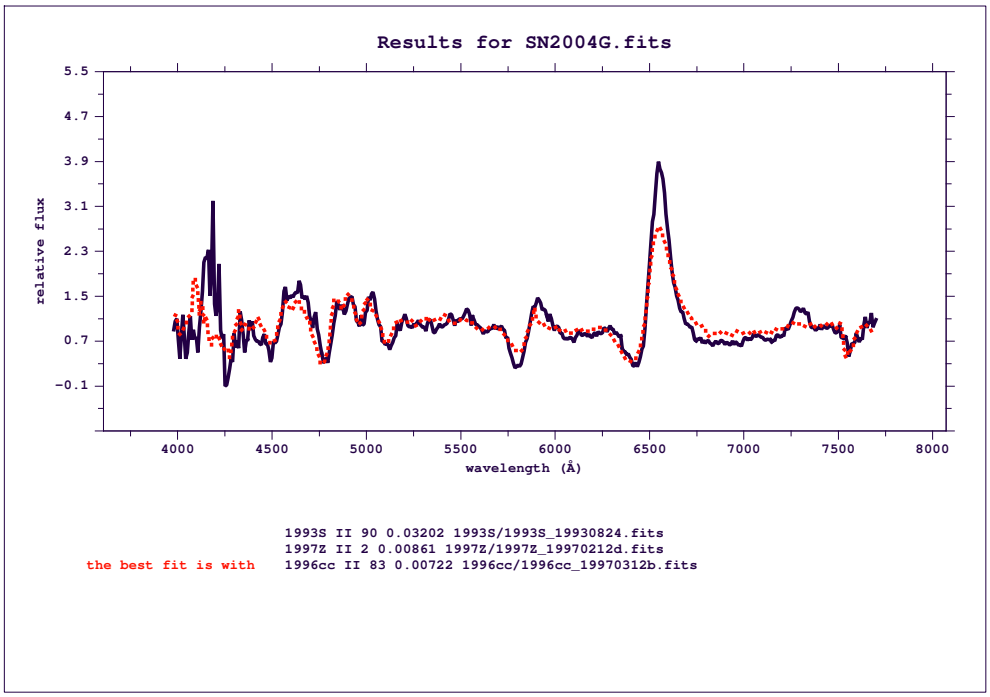

FIGURE B.2— As Figure B.1 for SN 2004G. The best fit is obtained with Type II SNe about 3 months after explosion.

and 5500 km s^{-1}, respectively. A broad and asymmetric absorption centred at 629.0 nm does not have a clear identification, but it could be due to a blend of several metal (mostly Ti II and Ba II) lines.

B.3 Supernova 2004G in NGC 5668

SN 2004G was discovered at $\alpha = 14^h33^m21\overset{s}{.}40, \delta = +04^o26'49\overset{''}{.}50$ (J2000.0), which is 43″west and 12″.5 south of the centre of NGC 5668 (nearby spiral galaxy with a NED heliocentric recession velocity of 1582 km s^{-1}) by Nakano et al. (2004). Figure B.2 shows that this SN is similar to Type II SNe about 3 months after explosion. This confirms the classification given by Elias-Rosa et al. (2004a). The spectrum of SN 2004G was obtained on Jan. 21.15 UT with the Calar Alto 2.2-m reflector (+ CAFOS; range 380-880 nm; resolution 1.1 nm). Expansion velocities of about 6600 and 4300 km s^{-1}can be deduced from the Hα and Hβ absorptions, respectively.

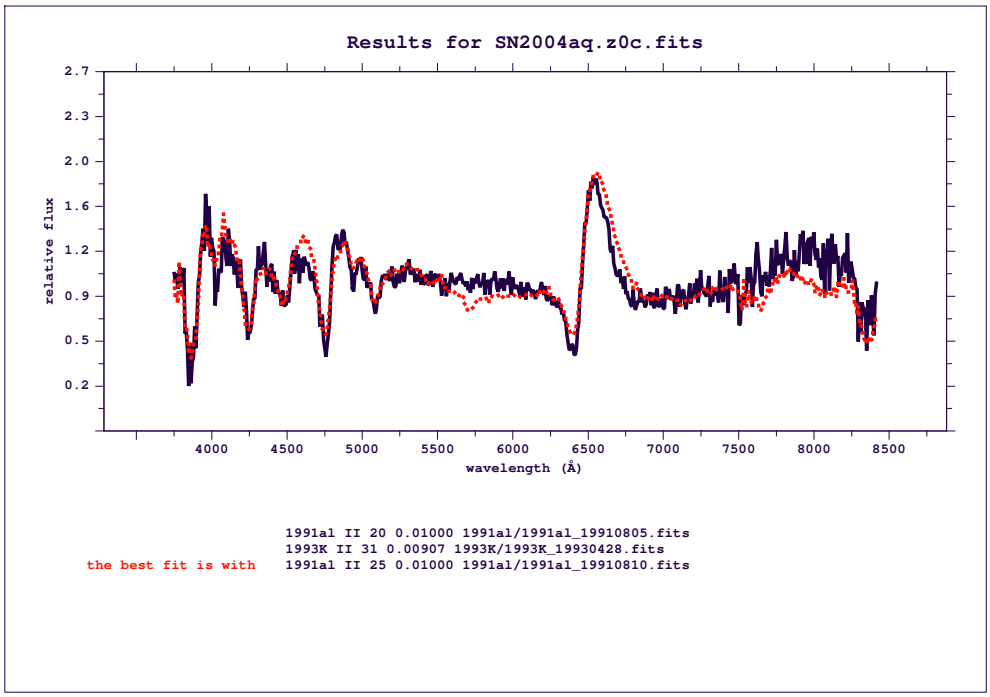

FIGURE B.3— As Figure B.1 for SN 2004aq. The best fit is obtained with a Type II SN around 1 month after explosion.

B.4 Supernova 2004aq in NGC 4012

The discovery of SN 2004aq was reported by M. Armstrong (Armstrong & Buczynski 2004). This SN is located at $\alpha = 11^h58^m27\overset{s}{.}25, \delta = +10^o01'04\overset{''}{.}50$ (J2000.0), which is $4\overset{''}{.}6$ west and $12\overset{''}{.}8$ south of the centre of NGC 4012 (Sb galaxy with a NED heliocentric recession velocity of 4188 $\mathrm{km\,s^{-1}}$). This supernova was classified of type-II, about 1 month after explosion (Elias-Rosa et al. 2004b) by the inspection of a spectrum (range 320-910 nm, resolution 1.7 nm), obtained on Mar. 10.01 UT with the NOT (+ ALFOSC) at La Palma (Figure B.3). The spectrum is dominated by P-Cyg lines of H, Ca II, and Fe II overimposed on a relatively blue continuum. The expansion velocities deduced from the Hα and Hβ absorptions are about 7700 and 6500 $\mathrm{km\,s^{-1}}$, respectively.

B.5 Supernova 2004aw in NGC 3997

SN 2004aw was discovered in NGC 3997 by T. Boles and by K. Itagaki (Boles et al. 2004). Boles measured the position of SN 2004aw as $\alpha = 11^h57^m50\overset{s}{.}24, \delta = +25^o15'55\overset{''}{.}10$ (J2000.0), which is approximately $27\overset{''}{.}7$ east and $19\overset{''}{.}8$ south of

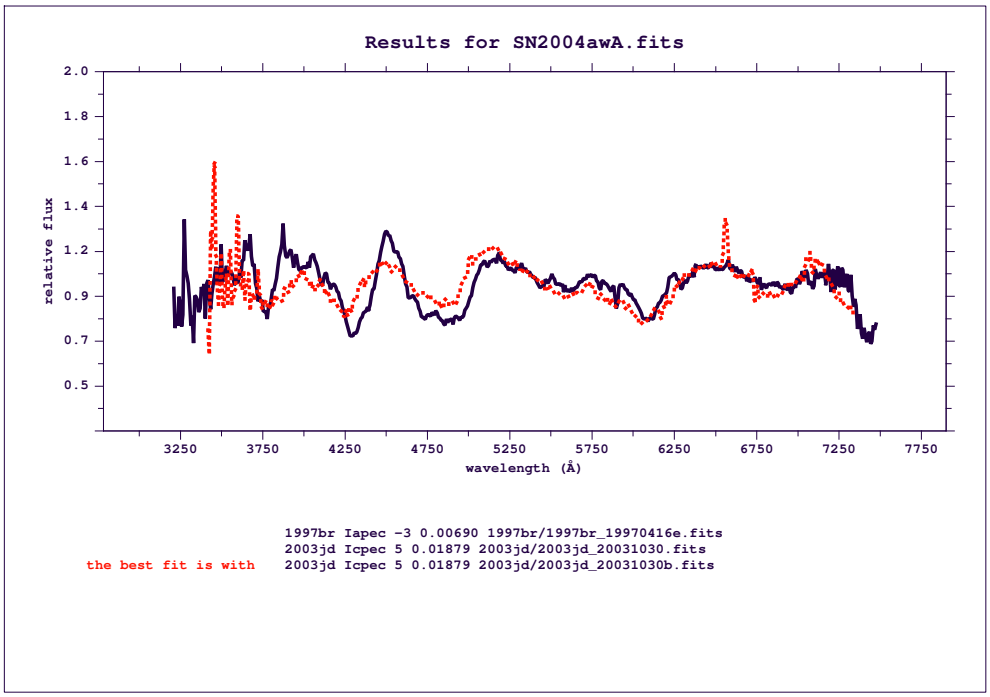

FIGURE B.4— As Figure B.1 for SN 2004aw. The best fit is obtained with a Type Ic SN 5 days after B band maximum.

the centre of NGC 3997 (SBb pec galaxy with a NED heliocentric recession velocity of 4742 km s^{-1}). A first classification of SN 2004aw, provided by Matheson et al. (2004), reported that it was of type I, but the exact classification was unspecified. Benetti et al. (2004b) obtained a spectrum of SN 2004aw with the TNG (+ Dolores; range 335-995 nm; resolution 1.4 nm) on Mar. 24.94 UT and claimed that the supernova resembled the spectrum of SN 1991T, a few days after maximum, and was therefore classified as type Ia. Finally, Filippenko et al. (2004) reclassified SN 2004aw as a SN Ic on a spectrum taken at later epoch. From the spectrum of the classification (phase +1 day after B band maximum from Taubenberger et al. 2006), PASSparTOO provides a best fit with Type Ia SN 1997br. However the comparison of the spectrum at +4.6 days, gives the best fit with the type Ic SN 2003jd as we can see in Figure B.4.

In the first place this is not surprising since it is well known that the spectra of SNe Ic at early epochs resemble those of SNe Ia. On the other hand it warns us how the classification base on a single epoch can be misleading also even using objective classification criteria and analysis tools.

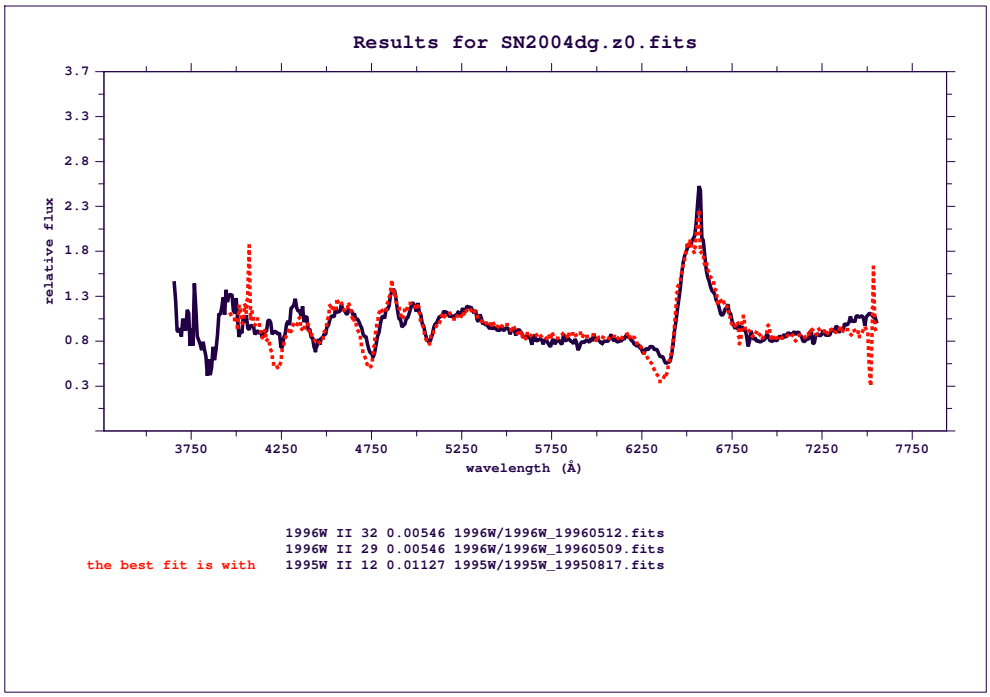

FIGURE B.5— As Figure B.1 for SN 2004dg. The best fit is obtained with a Type II SN around 1 month after explosion.

B.6 Supernova 2004dg in NGC 5806

SN 2004dg was discovered (Vagnozzi et al. 2004) at $\alpha = 14^h59^m58^s.96, \delta = +01^o53'25''.60$ (J2000.0), which was approximately 19″west and 3″south of the centre of NGC 5806 (Sb galaxy with a NED heliocentric recession velocity of 1359 km s^{-1}). The inspection of a spectrogram obtained on July 21.87 UT with the Asiago 1.8-m telescope (+ AFOSC; range 355-780 nm, resolution 2.4 nm), indicated that SN 2004dg was a type-II supernova, about 1 month after explosion Elias et al. (2004). The spectrum was dominated by P-Cyg lines of H I, Ca II H&K, Fe II, and Ti II (Figure B.5). A narrow Hα feature (from a nearby H II region) is visible on the top of the broad emission, from which the observers deduced a recession velocity of about 1720 km s^{-1}, which in turn is substantially higher than the galaxy's heliocentric recession velocity given by NED (1359 km s^{-1}). The expansion velocities deduced from the Hα and Hβ absorptions are about 8270 and 6760 km s^{-1}, respectively.

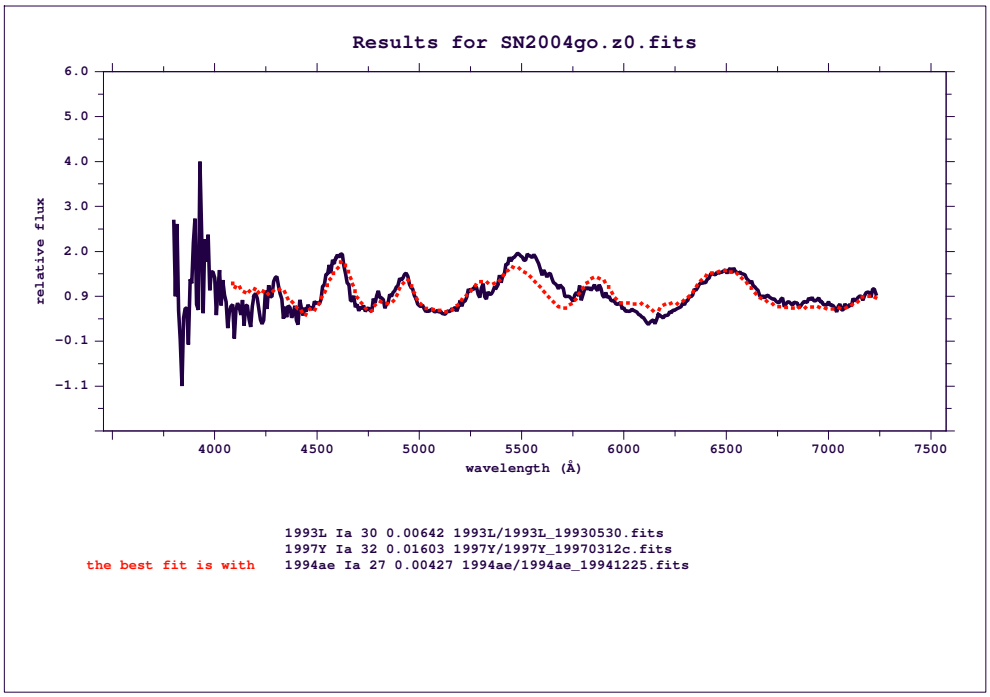

FIGURE B.6— As Figure B.1 for SN 2004go. The best fit is obtained with a Type Ia SN around 1 month after explosion.

B.7 Supernova 2004go in IC 270

SN 2004go was located at $\alpha = 02^h55^m41\overset{s}{.}76, \delta = -14^o14'14\overset{''}{.}50$ (J2000.0), which was $34\overset{''}{.}8$ west and $105\overset{''}{.}7$ south of the nucleus of IC 270 (S0 galaxy with a NED heliocentric recession velocity of 8717 km s^{-1}) (Pugh & Li 2004), and was classified by Morrell et al. (2004) and by Navasardyan et al. (2004) as a type-Ia supernova, 3-4 weeks past maximum light. Figure B.6 shows this SN is comparable with others Type Ia SNe around 1 month after maximum light.

B.8 Supernova 2005G in UGC 8690

J. Graham and W. Li reported the discovery of SN 2005G (Graham et al. 2005), located at $\alpha = 13^h44^m32\overset{s}{.}79, \delta = +04^o46'44\overset{''}{.}30$ (J2000.0), so, at $13\overset{''}{.}4$ west, $12\overset{''}{.}0$ north of the center of UGC 8690 (Scd galaxy with a NED heliocentric recession velocity of 6938 km s^{-1}). It was classified as a Type Ia SNe about 10 days past maximum by Ganeshalingam, Serduke & Filippenko (2005) and Navasardyan et al. (2005). The former mentioned some peculiarity in the spectrum namely unusually narrow Si II 635.5 nm absorption and blend of the

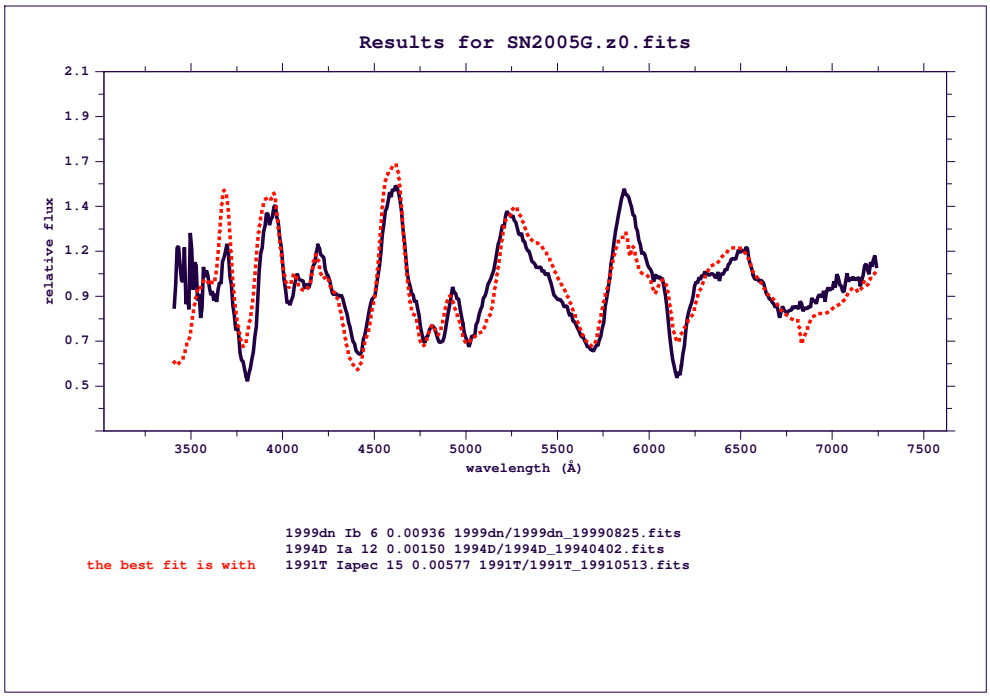

FIGURE B.7— As Figure B.1 for SN 2005G. The best fit is obtained with a Type Ia SN around 15 days after explosion.

two S II absorption lines near 550 nm, and a optical continuum very blue. The latter reported that a spectrum obtained on Jan. 18.16 UT with the Asiago 1.8-m telescope (+ AFOSC; range 355-780 nm, resolution 2.4 nm) closely resembled that of SN 1994D (Patat et al. 1996) and indeed this SN is one of the best fits given by PASSparTOO (Figure B.7). The expansion velocity deduced from the Si II 635.5 nm minimum was 9400 $\mathrm{km\,s^{-1}}$ (adopting the NED recession velocity of 6938 $\mathrm{km\,s^{-1}}$ for the parent galaxy).

B.9 Supernova 2005H in NGC 838

On Jan. 15.57 UT was obtained a noisy spectrum of SN 2005H exploded in NGC 838 (a starburst galaxy with a NED heliocentric recession velocity of 3851 $\mathrm{km\,s^{-1}}$) at $\alpha = 02^h09^m38\overset{s}{.}52, \delta = -10^o08'43\overset{''}{.}60$ (J2000.0) (Graham et al. 2005). The analysis of this spectrum led Pastorello et al. (2005) to classify the SN as a young type-II supernova (Figure B.8). The spectrum was dominated by a blue continuum with a broad Hα emission flanked by a shallow broad absorption. Hβ, Fe II 501.8 and 516.9 nm, and He I 587.6 nm lines are also

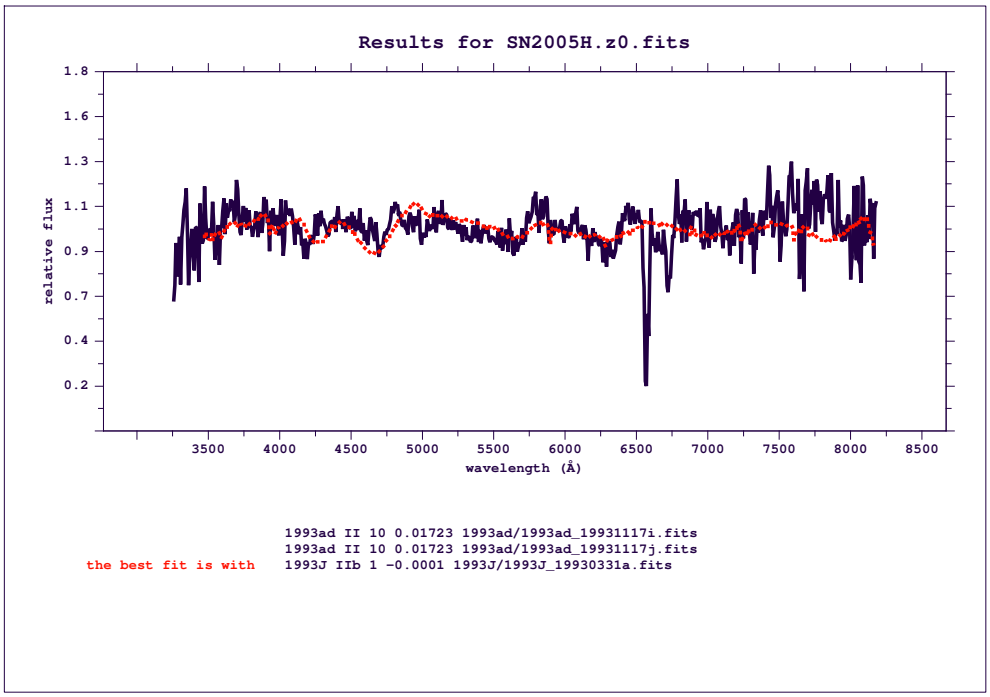

FIGURE B.8— As Figure B.1 for SN 2005H. The best fit is obtained with Type II SNe close to the maximum light. The deep absorption close to 6500 Å is due to a spike in the galaxy background subtraction to the SN spectrum.

present with well-developed P-Cyg profiles. The expansion velocity deduced from the Hα minimum was about 12000 km s^{-1}, while that deduced from Hβ and He I 587.6 nm was about 10400 km s^{-1}.

B.10 Supernova 2005I in IC 983

SN 2005I was located at 21″west and 40″south of the centre of IC 983 (SBcd galaxy with a NED heliocentric recession velocity of 5443 km s^{-1}) at $\alpha = 14^h10^m02\overset{s}{.}86, \delta = +17^o43'22\overset{''}{.}40$ (J2000.0) (Graham et al. 2005). Pastorello et al. (2005) classified this SN as a type-II supernova, about 3 months after the explosion. Figure B.9 shows the best fit at 3 months after explosion (epochs of SN 2003gd reported on the figure correspond to days after discover, which implies 100 days after explosion - Hendry et al. 2005) from the inspection of a spectrogram of SN 2005I, taken on Jan. 18.22 UT with the Calar Alto 2.2-m telescope (+ CAFOS; range 330–880 nm). The spectrum was characterized by a red continuum with relatively strong and narrow P-Cyg lines of H, Ca II, Fe II, Sc II, Ba II, and Ti II. The expansion velocities, deduced by the minima of

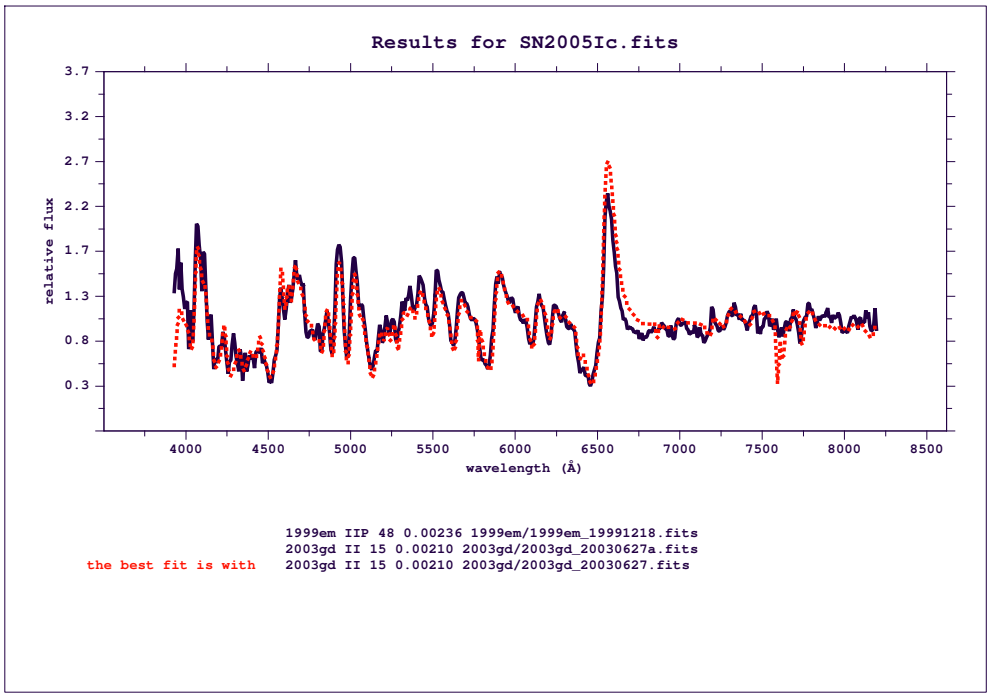

FIGURE B.9— As Figure B.1 for SN 2005I. The best fit is obtained with a Type II SN around 3 months after explosion. Note that the epochs of SN 2003gd reported on the figure correspond to days after discovery, which implies 100 days after explosion (Hendry et al. 2005).

the main features, were 4800 km s^{-1} for Hα, 3300 km s^{-1} for Na ID, and 2500 km s^{-1} for the Fe II lines. The supernova spectrum did not show evidence of interstellar Na lines at the rest wavelength of the host galaxy, suggesting no significant reddening.

B.11 Supernova 2005W in NGC 691

The position of SN 2005W (discovered by Nakano & Li 2005a) was measured at $\alpha = 01^h50^m45\overset{s}{.}75, \delta = +21^o45'35\overset{''}{.}60$ (J2000.0), which was 56″east and 1″south of the center of NGC 691 (Sbc galaxy with a NED heliocentric recession velocity of 2665 km s^{-1}). Before, Elias-Rosa et al. (2005a) reported that a spectrogram of SN 2005W, obtained on Feb. 2.7 UT with the Asiago 1.8-m telescope (+ AFOSC; range 355-780 nm, resolution 2.4 nm), showed it to be a Type Ia supernova close to maximum. The spectrum closely resembles that of SN 2002bo (Benetti et al. 2004a) at comparable phase and the expansion velocity deduced from the Si II 635.5 nm minimum was about 11600 km s^{-1}.

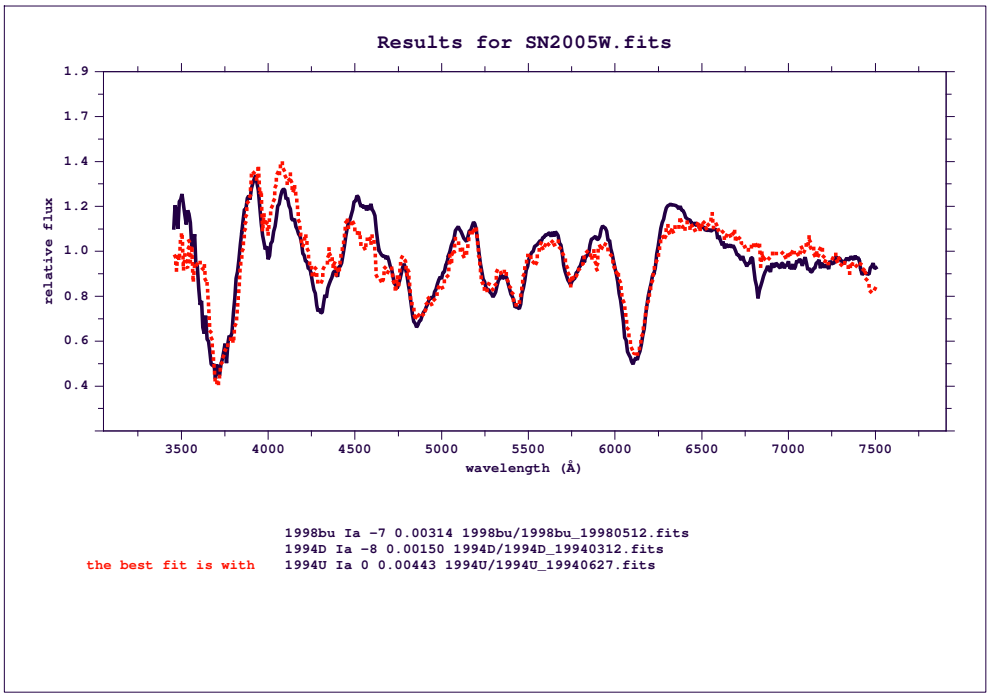

FIGURE B.10— As Figure B.1 for SN 2005W. The best fit is obtained with Type Ia SNe around maximum light.

In Figure B.10 we can see this spectrum and its comparison with SN 1994U around maximum light.

B.12 Supernova 2005ab in NGC 4617

SN 2005ab, discovered by Nakano & Kadota (2005b) on Feb. 5.638 UT at $\alpha = 12^h41^m05\overset{s}{.}18, \delta = +50^o22'56\overset{''}{.}20$ (J2000.0), which is 7″west and 40″south of the centre of the type Sb galaxy ($v_{helio} = 4624$ km s^{-1}) NGC 4617, was classified by Benetti & di Mille (2005c) during a 'RTN Winter School on Supernovae' in Asiago (Italy) as a type-II supernova shortly after explosion A noisy spectrum (range 390-815 nm, resolution 2.3 nm) taken with the Asiago 1.22-m telescope (+ Boller and Chivens spectrograph) is shown in Figure B.11. Note that due to the poor signal-to-noise, the third best fit SN is type Ia.

B.13 Alleged Supernova in NGC 4656

Rich, Yamaoka & Itagaki (2005) reported the discovery of a possible supernova (mag about 18.0) located at $\alpha = 12^h43^m45\overset{s}{.}84, \delta = +32^o06'15\overset{''}{.}00$ (J2000.0),

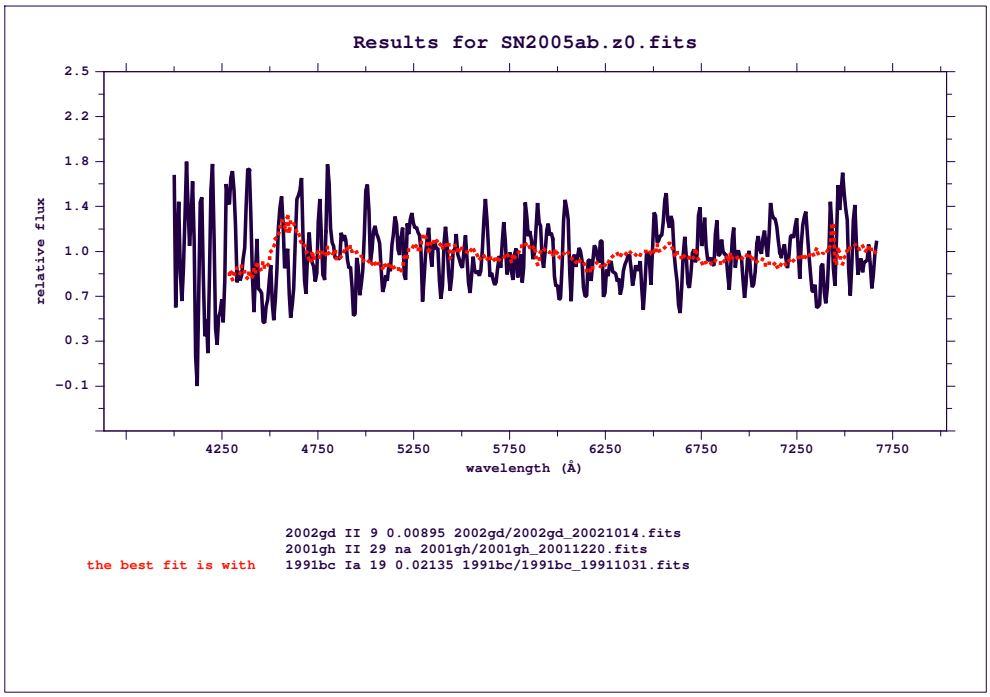

FIGURE B.11— As Figure B.1 for SN 2005ab. Two of the three best fit compare this SN with Type II SNe after explosion.

which was about 151″west and 230″south of the center of NGC 4656 (SB pec galaxy with a NED heliocentric recession velocity of 646 km s^{-1}). Elias-Rosa et al. (2005b) obtained an spectrum at those coordinates on Mar. 23.9 UT with the TNG telescope (+ Dolores; range 350-800 nm, resolution 1.2 nm), which showed a narrow (730 km s^{-1}) Hα emission, while the other Balmer lines were not visible. The broader component of the Hα line often seen in type-IIn supernovae was not apparent. The spectrum also showed narrow (1.5 nm) absorptions due to H and K of Ca II. It was claimed that this object may be a superoutburst of a luminous blue variable rather than a real supernova, similar to SN 1997bs (Treffers et al. 1997; Van Dyk et al. 2000) and 1999bw (Filippenko, Li & Modjaz 1999). In Figure B.12 we can see this spectrum.

B.14 Supernova 2006G in NGC 521

SN 2006G, located by Baek et al. (2006) at $\alpha = 01^h24^m35\overset{s}{.}83, \delta = +01^o43'15\overset{''}{.}80$ (J2000.0), at 32$\overset{''}{.}$4 east and 38$\overset{''}{.}$3 south S of the centre of NGC 521 (SBbc pec galaxy with a NED heliocentric recession velocity of 5018 km s^{-1}), was classi-

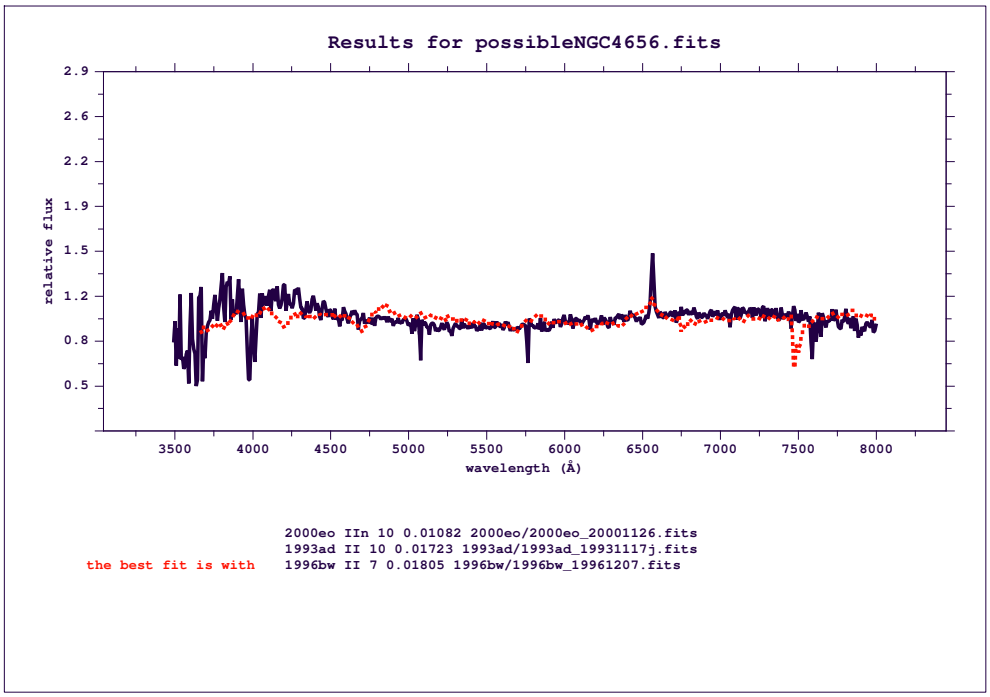

FIGURE B.12— As Figure B.1 for an alleged supernova in NGC 4656. It can be a Type II but there are many uncertainties.

fied as a type-II supernova by Morrell et al. (2006) and Benetti et al. (2006a), who found strong Hα P-Cyg feature and some metallic lines. Also weak Hβ was detected in absorption, indicating an expansion velocity of 10000 km s^{-1}. The presence of Fe II 516.9 nm and the high expansion velocity derived from Hβ suggest that the supernova was 2 or 3 weeks old.

B.15 Supernova 2006W in UGC 9265

SN 2006W was discovered by Ponticello et al. (2006) at $\alpha = 14^h27^m26\overset{s}{.}09, \delta = +25^o31'09\overset{''}{.}80$ (J2000.0), which was at $1\overset{''}{.}2$ east and $17\overset{''}{.}5$ north of the centre of UGC 9265 (Sbc galaxy with a NED heliocentric recession velocity of 4757 km s^{-1}). Navasardyan et al. (2006) reported it to be a type-II supernova, according to a spectrogram (range 370-780 nm), obtained on Feb. 7.167 UT with the Copernicus 1.82-m telescope (+ AFOSC). The spectrum displays broad P-Cyg profiles of the Balmer series, but for Hα shows only a broad (FWHM about 7400 km s^{-1}) asymmetric emission (Figure B.13).

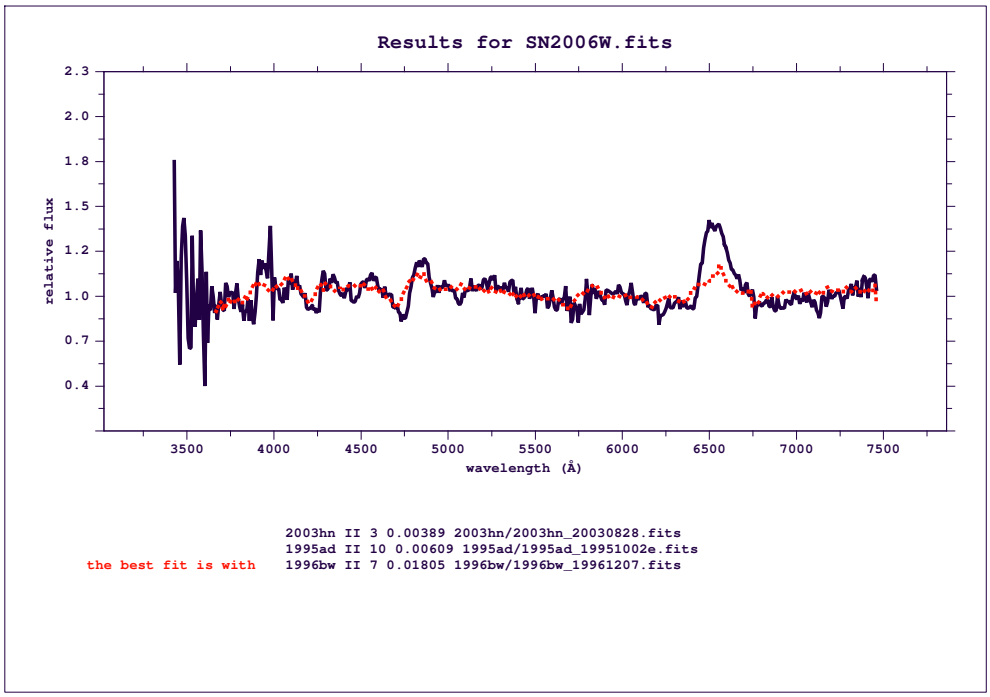

FIGURE B.13— As Figure B.1 for SN 2006W. The best fit is obtained with a Type II SN around 1 week after maximum light.

B.16 Supernova 2006dk in NGC 4161

Dimai & Migliardi (2006) reported the discovery of an apparent supernova called SN 2006dk (mag about 16.3) at $\alpha = 12^h11^m34\overset{s}{.}35, \delta = +57^o44'26\overset{''}{.}30$ (J2000.0), which is 6″east and 11″north of the nucleus of NGC 4161 (Sbc galaxy with a NED heliocentric recession velocity of 4946 km s^{-1}). Dennefeld et al. (2006), reported that a noisy spectrogram (range 368-732 nm, resolution 0.5 nm), obtained with the Carelec spectrograph on the 1.93-m telescope at Haute-Provence Observatory, showed that SN 2006dk was a type-II supernova caught close to explosion (Figure B.14). The spectrum was dominated by a relatively blue continuum having overimposed a broad and faint Hα emission (FWHM about 11700 km s^{-1}). A broad and faint He I 587.6 nm feature with a P-Cyg profile could be spotted, and from its absorption an expansion velocity of about 11500 km s^{-1} was deduced.

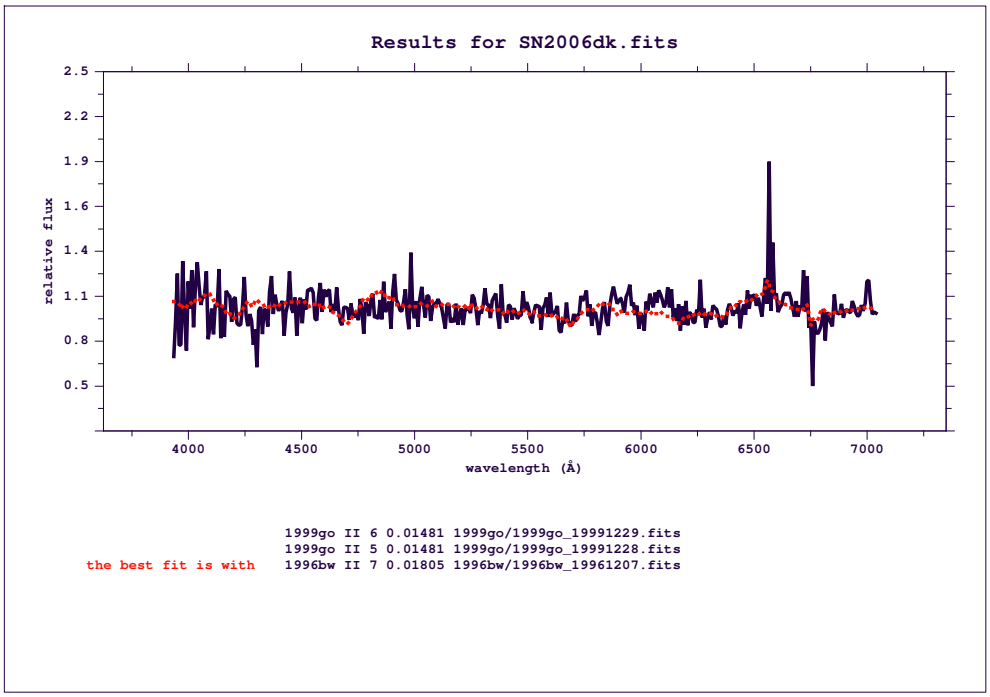

FIGURE B.14— As Figure B.1 for SN 2006dk. The best fit is obtained with a Type II SN around 1 week after maximum light.

B.17 Supernova 2006en in MCG +05-54-41

SN 2006en was discovered at $10\farcs9$ east and $3\farcs8$ south of the nucleus of MCG +05-54-41 (Sc galaxy with a NED heliocentric recession velocity of 9575 km s^{-1}) at $\alpha = 23^h10^m05\fs06, \delta = +30^o13'24\farcs00$ (J2000.0) (Puckett & Peoples 2006a; Puckett et al. 2006b). From the spectrum of SN 2006en obtained with the Telescopio Nazionale Galileo (+ Dolores; grism LR-B, spectral range 350-800 nm, resolution 1.2 nm), Elias-Rosa et al. (2006b) classified this SN as a normal type-Ia supernova around maximum light (Figure B.15). The expansion velocity deduced from the Si II 635.5 nm minimum is 10200 km s^{-1}. An interstellar Na ID absorption feature was visible in the host galaxy rest frame with EW about 0.2 nm, suggesting a reddening E(B-V) > 0.3 mag (Turatto, Benetti & Cappellaro 2003b). Taking into account the apparent magnitudes reported by Puckett & Peoples (2006a), it appears that SN 2006en was very bright object, but this seems inconsistent with the above spectrophotometry and with the normal expansion velocity.

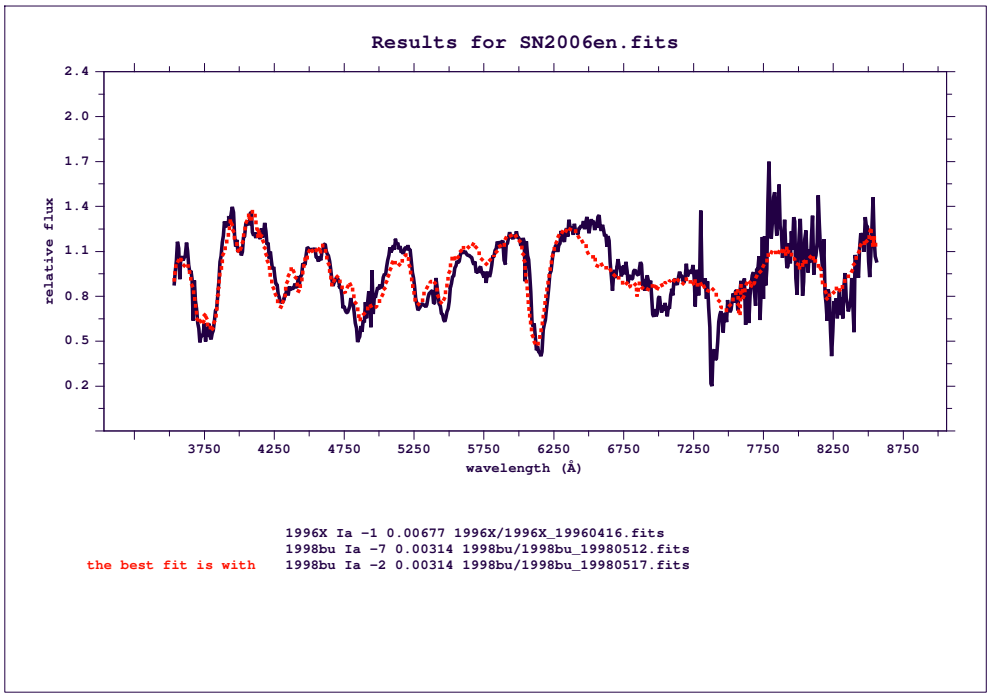

FIGURE B.15— As Figure B.1 for SN 2006en. The best fit is obtained with Type Ia SNe around maximum light.

B.18 Supernova 2006et in NGC 232

SN 2006et was discovered in the spiral galaxy ($v_{helio} = 6647$ km s^{-1}) NGC 232 (Schwehr et al. 2006) at $\alpha = 00^h42^m45\overset{s}{.}82, \delta = -23^o33'30\overset{''}{.}40$ (J2000.0), at $0\overset{''}{.}3$ east and $11\overset{''}{.}0$ north of the nucleus. From the analysis of a spectrum obtained with the Asiago 1.8-m telescope (+ AFOSC; range 345-780 nm, resolution 2.4 nm), Elias-Rosa et al. (2006c) noticed that this SN was similar to the slow-declining, type-Ia supernovae (e.g., SNe 1995ac and 1997br, Padova-Asiago Supernovae Archive) around maximum light. Indeed Figure B.16 shows that the best fit is obtained with Type Ia SNe around maximum light. The expansion velocity deduced from the Si II 635.5 nm minimum is about 9400 km s^{-1}. An interstellar Na ID absorption feature is visible in the host-galaxy rest frame with an equivalent width of about 0.6 nm, suggesting high reddening, E(B-V) $>$ 1 mag (Turatto, Benetti & Cappellaro 2003b).

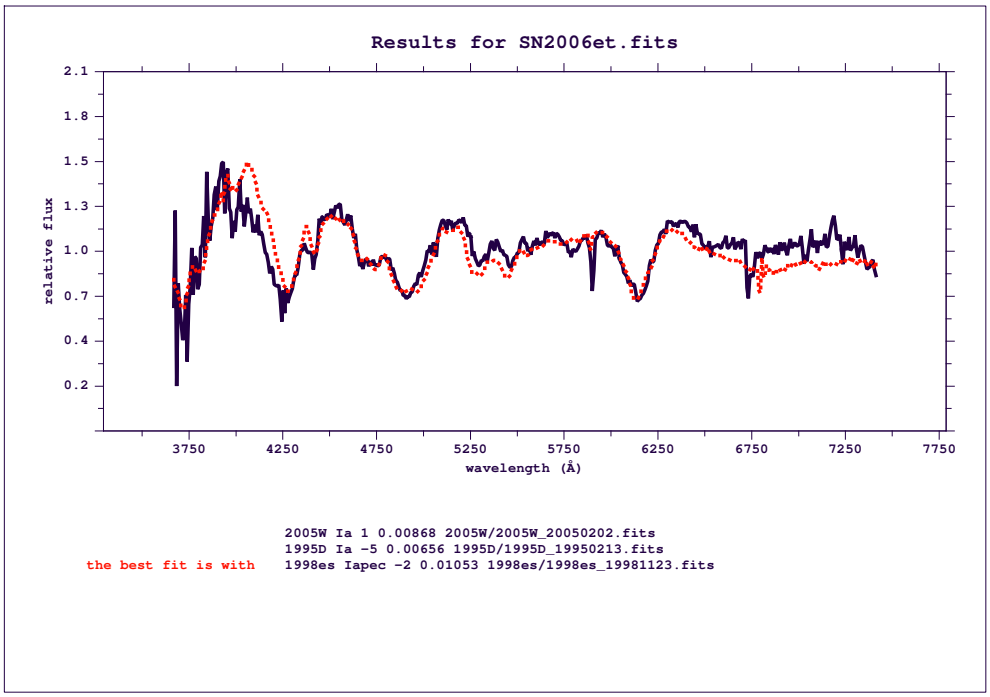

FIGURE B.16— As Figure B.1 for SN 2006et. The best fit is obtained with a Type Ia SN around maximum light.

B.19 Supernova 2006gy in NGC 1260

Quimby (2006b) reported the discovery of SN 2006gy in unfiltered CCD images taken with the 0.45-m ROTSE-IIIb telescope at the McDonald Observatory. SN 2006gy was located at $\alpha = 03^h17^m27\overset{s}{.}06, \delta = +41^o24'19\overset{''}{.}50$ (J2000.0), which is $2\overset{''}{.}0$ west and $0\overset{''}{.}4$ north of the centre of NGC 1260 (spiral galaxy with a NED heliocentric recession velocity of 5753 km s^{-1}). Harutyunyan et al. (2006) classified SN 2006gy as a type-II supernova caught soon after explosion. The spectrum (Figure B.17), obtained with the 3.5-m TNG (+ DOLORES; range 340-920 nm, resolution 1.2 nm) was heavily contaminated by the parent galaxy. It seemed dominated by a relatively red continuum with superimposed Hβ with a P-Cyg profile, and Hα with a complex profile consisting of three emission components: a narrow unresolved one, an intermediate (FWHM about 2500 km s^{-1}) one, and a broad one (FWHM about 9500 km s^{-1}). The He I 587.6 nm emission was also present. An interstellar Na ID absorption feature was visible in the host-galaxy rest frame with an equivalent width of about 0.6 nm. Adopting for the parent galaxy the recession velocity of 5753 km s^{-1},

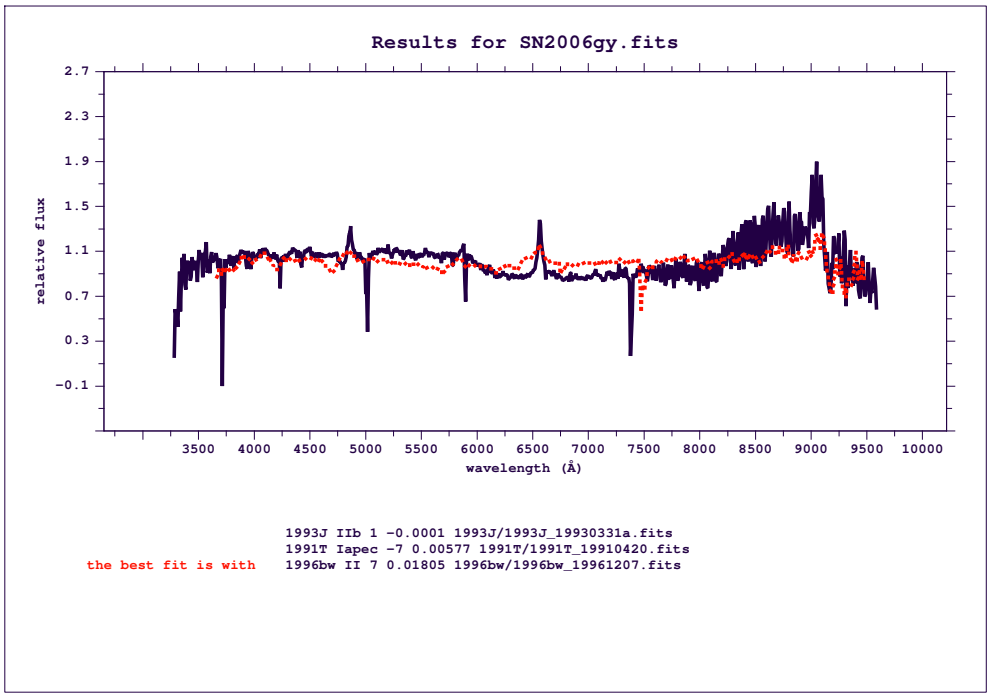

FIGURE B.17— As Figure B.1 for SN 2006gy. The best fit is obtained with a Type II SN around explosion.

as measured from the Na ID absorption, for the parent galaxy, the expansion velocity derived from the Hβ minimum was about 4500 km s^{-1}.

B.20 Supernova 2006jc in UGC 4904

SN 2006jc is a very peculiar supernova. It was found on unfiltered CCD images by Itagaki et al. (2006) at $\alpha = 09^h17^m20\overset{s}{.}78, \delta = +41^o54'32\overset{''}{.}70$ (J2000.0), 11″west and 7″south of the centre of UGC 4904 (spiral galaxy with a NED heliocentric recession velocity of 1189 km s^{-1}). SN 2006jc appears to be a peculiar type-Ib/c supernova although there were discordant classification reports (Crotts et al. 2006; Fesen, Milisavljevic & Rudie 2006a; Benetti et al. 2006b; Fesen, Milisavljevic & Rudie 2006b; Modjaz et al. 2006).

Benetti et al. (2006b) noted that this SN was probably related to type Ib, but of a rare variety. Indeed, the closest comparison that they were able to find was with SN 1999cq (Matheson et al. 2000) and SN 2002ao (Filippenko & Chornock 2002a), which were characterized by strong He I emission lines. There are some distinct differences, however, perhaps indicating a different phase of

TABLE B.1— Summary of the SNe classified.

SN	α	δ	Host galaxy	Type
SN 2003hg	$23^h51^m24^s.13$	$+20^o06'38''.30$	NGC 7771	II
SN 2003ie	$12^h03^m18^s.15$	$+44^o31'34''.60$	NGC 4051	II
SN 2004G	$14^h33^m21^s.40$	$+04^o26'49''.50$	NGC 5668	II
SN 2004aq	$11^h58^m27^s.25$	$+10^o01'04''.50$	NGC 4012	II
SN 2004aw	$11^h57^m50^s.24$	$+25^o15'55''.10$	NGC 3997	Ic
SN 2004dg	$14^h59^m58^s.96$	$+01^o53'25''.60$	NGC 5806	II
SN 2004go	$02^h55^m41^s.76$	$-14^o14'14''.50$	IC 270	Ia
SN 2005G	$13^h44^m32^s.79$	$+04^o46'44''.30$	UGC 8690	Ia
SN 2005H	$02^h09^m38^s.52$	$-10^o08'43''.60$	NGC 838	II
SN 2005I	$14^h10^m02^s.86$	$+17^o43'22''.40$	IC 983	II
SN 2005W	$01^h50^m45^s.75$	$+21^o45'35''.60$	NGC 691	Ia
SN 2005ab	$12^h41^m05^s.18$	$+50^o22'56''.20$	NGC 4617	II
Alleged-SN	$12^h43^m45^s.84$	$+32^o06'15''.00$	NGC 4656	superoutburst
SN 2006G	$01^h24^m35^s.83$	$+01^o43'15''.80$	NGC 521	II
SN 2006W	$14^h27^m26^s.09$	$+25^o31'09''.80$	UGC 9265	II
SN 2006dk	$12^h11^m34^s.35$	$+57^o44'26''.30$	NGC 4161	II
SN 2006en	$23^h10^m05^s.06$	$+30^o13'24''.00$	MCG +05-54-41	Ia
SN 2006et	$00^h42^m45^s.82$	$-23^o33'30''.40$	NGC 232	Ia
SN 2006gy	$03^h17^m27^s.06$	$+41^o24'19''.50$	NGC 1260	II
SN 2006jc	$09^h17^m20^s.78$	$+41^o54'32''.70$	UGC 4904	pec. Ib/c

development or considerable heterogeneity within this peculiar subclass. Actually, Modjaz et al. (2006) added that there are notable differences from SN 1999cq such as a very blue continuum or additional emission lines consistent with He I 388.9, 447.1, and 501.5 nm (rest) that have widths of 1500-6500 km s^{-1} (FWHM), and the absence of the broad peak at around 540 nm. Unfortunately we can not obtain a good comparison with other SNe of the Padova-Asiago Supernova Archive, because of its peculiarity. An extensive work on this object has been just submitted (Pastorello et al. 2007c).

Bibliography

Akritas M. G. & Bershady M. A., 1996, ApJ, 470, 706

Alard C., 2000, A&AS, 144, 363

Altavilla G. et al., 2004, MNRAS, 349, 1344

Arbour R. & Boles T., 2003, IAUC 8205

Armstrong M. & Buczynski D., 2004, IAUC 8301

Astier P. et al., 2006, A&A, 447, 31

Axelrod T.S., 1980, PhD thesis, Univ. California at Santa Cruz

Baade W., 1938, ApJ, 88, 285

Baek, M., Li W., Puckett T., Sostero G., Garzia S., 2006, IAUC 8660

Barbaro G., Geminale A., Mazzei, P. & Congiu E., 2004, MNRAS, 353, 760

Barbon R., Ciatti F. & Rosino L., 1973, A&A, 25, 241

Barbon R. et al., 1990, A&A, 237, 79

Barbon R., Buondí V., Cappellaro E. & Turatto M., 1999, A&AS, 139, 531

Barlow M. J., 1978a, MNRAS, 183, 367

Barlow M. J., 1978a, MNRAS, 183, 397

Benetti S., Patat F., Turatto M., Contarini G., Gratton R., Cappellaro E., 1994, A&A, 285, L13

Benetti S., 2000, MmSAI, 71, 323

Benetti S. et al., 2003, IAUC 8207

Benetti S. et al., 2004a, MNRAS, 348, 261

Benetti S., Elias-Rosa N., Blanc G., Navasardyan H., Turatto M., Zampieri L., Cappellaro E., Pedani M., 2004b, IAUC 8312

Benetti S. et al., 2005a, ApJ, 623, 1011

Benetti S., 2005b, in Turatto M., Benetti S., Zampieri L. & W. Shea, eds., Supernovae as Cosmological Lighthouse. Astron. Soc. Pac., San Francisco, p. 235

Benetti S. & di Mille F., 2005c, IAUC 8480

Benetti S. et al., 2006a, CBET 394

Benetti S. et al., 2006b, CBET 674

Benetti S., Cappellaro E., Turatto M., Taubenberger S., Harutyunyan A., Valenti S., 2006c, ApJ, 653, L129

Benvenuti P., Sanz Fernandez de Cordoba L., Wamsteker W., Machetto F., Palumbo G. C., Panagia N., 1982, An Atlas of UV Spectra of Supernovae (Noordwijk: ESA Scientific and Technical Publications Branch)

Bertin P., Lallement R., Ferlet R. & Vidal-Madjar A., 1993, A&A, 278, 549

Bianchi L., Clayton G. C., Bohlin R. C., Hutchings J. B. & Massey P., 1996, ApJ, 471, 203

Biermann P. & Harwit M., 1980, ApJ, 241, 105

Blanco A., Borghesi A., Fonti S. & Orofino V., 1998, A&A, 330, 505

Blinnikov S. I. & Sorokina E. I., 2000, A&A, 356, L30

Blinnikov S. I., Röpke F. K., Sorokina E. I., Gieseler M., Reinecke M., Travaglio C., Hillebrandt W., Stritzinger M., 2006, A&A, 453, 229

Branch D., 1981, ApJ, 248, 1076

Branch D. & Venkatakrishna K. L., 1986, ApJ, 306, L21

Branch D., 1987, ApJ, 316, L81

Branch D. & Tammann G. A., 1992, ARA&A, 30, 359

Branch D. & Miller D. L., 1993a, ApJ, 405, L5

Branch D. & van den Bergh S., 1993b, AJ, 105, 2231

Branch D. Romanishin W. & Baron E., 1996, ApJ, 465, 73

Branch D. et al., 2006, PASP, 118, 560

Brown P. J. et al., 2005, ApJ, 635, 1192

Boles T., Itagaki K., Nakano S. & Kushida Y., 2004, IAUC 8310

Bohlin R. C. Savage B. D. & Drake J. F., 1978, ApJ, 224, 132

Borkowski K. J. & Dwek E., 1995, ApJ, 454, 254

Bowers R. L. & Deeming T., 1984, Astrophysics, Vol. 1,2. Jones and Bartlett Publ., Boston.

Bufano F., 2003, ...Univ. Padua (Italy)

Calzetti D., 2001, PASP, 113, 1449

Canzian B. & Allen R. J., 1997, ApJ, 479, 723

Capaccioli M. et al., 1990, ApJ, 350, 110

Cappellaro E., Mazzali P. A., Benetti S., Danziger I. J., Turatto M., della Valle M. & Patat F., 1997, A&A, 328, 203

Cappellaro E., 2001, ApJ, 549, L215

Cappellaro E., 2005, in Turatto M., Benetti S., Zampieri L. & W. Shea, eds., Supernovae as Cosmological Lighthouse. Astron. Soc. Pac., San Francisco, p. 71

Cardelli J. A., Clayton G. C. & Mathis J. S., 1989, ApJ, 345, 245

Chevalier R. A., 1996, ApJ, 308, 225

Chini R. & Wargau W. F., 1990, A&A, 227, 213

Conley A. et al., 2006, ApJ, 644, 1

Contardo G., Leibundgut B. & Vacca W. D., 2000, A&A, 359, 876

Cowie L. L., 1978, ApJ, 225, 887

Clayton G. C., 2004, in Witt A. N., Clayton G. C. & Draine B. T., eds., ASP Conf. Ser. Vol. 309, Astrophysics of Dust. Astron. Soc. Pac., San Francisco, p. 57

Clocchiatti A. et al., 2001, ApJ, 553, 886

Cristiani S. et al., 1992, A&A, 259, 63

Crotts A. P. S., Kunkel W. E. & McCarthy P. J., 1989, ApJ, 347, L61

Crotts A. P. S. & Kunkel W. E., 1991, ApJ, 366, L73

Crotts A. P. S., Kunkel W. E. & Heathcote S. R., 1995, ApJ, 438, 724

Crotts A., Eastman J., Depoy D., Prieto J. L., Garnavich P., 2006, CBET 672

Crutcher R. M., 1985, ApJ, 288, 604

Curtis H.D., 1921, Bull. Natl. Res.Counci1 (US), vol.2, part 3, p.171

Della Valle M. & Panagia N., 1992, AJ, 104, 696

Dennefeld M., Bonnet-Bidaud J. M., Benetti S., Cappellaro E., Elias-Rosa N., Harutyunyan A., 2006, CBET 565

de Vaucouleurs G., de Vaucouleurs A. & Odewahn S., 1981, PASP, 93, 181

d'Hendecourt L. B., Allamandola L. J. & Greenberg J. M., 1985, A&A, 152, 130

Dimai A. & Migliardi M., 2006, CBET 561

Di Paola A., Larionov V., Arkharov A., Bernardi F., Caratti o Garatti A., Dolci M., Di Carlo E. & Valentini G., 2002, A&A, 393, L21

Dominik C., Gail H. P., Sedlmayr E. & Winters J. M., 1990, A&A, 240, 365

D'Odorico S. et al., 1989, A&A, 215, 21

Dopita M. A. et al., 1984, ApJ, 287, L69

Draine B. T. & Salpeter E. E., 1979, ApJ, 231, 438

Draine B. T., 1989a, in Bonetti A. et al., eds.. Evolution of Interstellar Dust and Related Topics. North Olland, Amsterdam, p. 103

Draine B. T., 1989b, in Kaldeich B. H., eds.. Infrared Spectroscopy in Astronomy. ESA, Paris, p. 93

Draine B. T. & McKee C. F. , 1993, ARA&A, 31, 373

Draine B. T., 2003, ARA&A, 41, 241

Ehrenfreund P. et al., 2002, ApJ, 576, 117

Elias J. H., Frogel J. A., Hackwell J. A., Persson S. E., 1981, ApJ, 251, L13

Elias J. H., Matthews K., Neugebauer G., Persson S. E., 1985, ApJ, 296, 379

Elias de la Rosa N. et al., 2004, IAUC 8376

Elias-Rosa N. et al., 2003, IAUC 8187

Elias-Rosa N. et al., 2004a, IAUC 8273

Elias-Rosa N., Benetti S., Stanishev V., Goobar A., Jaervinen A., 2004b, IAUC 8301

Elias-Rosa N., Navasardyan H., Harutunyan A., Benetti S., Turatto M., Pastorello A., Patat F., 2005a, IAUC 8479

Elias-Rosa N., Benetti S., Cappellaro E., Dolci M., Pastorello A., Boschin W., Pinilla Alonso N., 2005b, IAUC 8498

Elias-Rosa N. et al., 2006a, MNRAS, 369, 1880

Elias-Rosa N., Benetti S., Cappellaro E., Harutyunyan A., Pastorello A., Mazzali P., Taubenberger S., Andreuzzi G., 2006b, CBET 608

Elias-Rosa N., Navasardyan H., Harutyunyan A., Benetti S., Cappellaro E., Turatto M., 2006c, CBET 619

Elitzur M. & Ivezic Z., 2001, MNRAS, 327, 403

Elmhamdi A. et al., 2003, MNRAS, 338, 939

Evans A., 1994, in John Wiley & Sons, eds., The Dusty Universe. Praxis Publishing Ltd, Chichester, England

Evans R. O., Jarman J., Cragg T., Dopita M., Trung Hua C., Benetti S., 1995, IAUC 6197

Ferrarese L. et al., 1996, ApJ, 464, 568

Fesen R., Milisavljevic D. & Rudie G., 2006a, CBET 672

Fesen R., Milisavljevic D. & Rudie G., 2006b, CBET 674

Filippenko, A. V., 1982, PASP, 94, 715

Filippenko A. V., 1989, PASP, 101, 588

Filippenko A. V. et al., 1992a, ApJ, 384, L15

Filippenko A. V. et al., 1992b, AJ, 104, 1543

Filippenko A. V., Li W. & Modjaz M., 1999, IAUC 7152

Filippenko A. V. & Chornock R., 2002a, IAUC 7825

Filippenko A. V., Chornock R., Foley R.J. & Li W., 2002b, IAUC 7917

Filippenko A. V., Desroches L., Ganeshalingam M., Chornock R., Serduke F. J. D., 2004, IAUC 8331

Filippenko, A. V., 2005, in Sion E. M., Vennes S. and Shipman H. L., eds. AASL, Vol. 332: White dwarfs: cosmological adn galactic probes. Springer, Dordrecht, p. 97

Filippenko, A. V. & Foley R. J., 2005, IAUC 8493

Fitzpatrick E. L., 1986, AJ, 92, 1068

Fitzpatrick E. L., 2004, in Witt A. N., Clayton G. C. & Draine B. T., eds., ASP Conf. Ser. Vol. 309, Astrophysics of Dust. Astron. Soc. Pac., San Francisco, p. 57

Freedman W. L. et al., 2001, ApJ, 553, 47

Frenklach M. & Feigelson E. D., 1989, ApJ, 341, 372

Ganeshalingam M., Serduke F. J. D. & Filippenko A. V., 2005, IAUC 8468

Garavini G. et al., 2005, AJ, 130, 2278

Garavini G. et al., 2007, A&A, in press (astro-ph/0702569)

García A. M., 1993, A&AS, 100, 47

García-Senz D. & Bravo E., 2003, in Leibundgut B., Hillebrandt W., eds, Proc. to the ESO/MPA/MPE Workshop (an ESO Astrophysics Symp.) From Twilight to Highlight the Physics of Supernovae. Springer-Verlag, Berlin, p.158

Garnavich P. M., Jha S., Kirshner R., Challis P. & Calkins M., 1999, IAUC 7190

Garnavich P. M. et al., 2004, ApJ, 613, 1120

Gaskell C. M., 1984, PASP, 96, 789

Gaskell C. M. & Keel W. C., 1986, BAAS, 18, 953

Geballe T. R., Kim Y. H., Knacke R. F. & Noll K. S., 1988, ApJ, 326, L65

Gehrz R. D. & Ney E. P., 1987, Proc. Natl Acad. Sci., 84, 6961

Gehrz R. D., 1989, in Allamandola L. J. and Tielens A. G. G. M., eds. (an IAU Symp. 135) Interstellar Dust. Kluwer Academic Publishers, Dordrecht, p. 445

Gehrels N. et al., 2004, ApJ, 611, 1005

Geminale A. & Podowski P., 2005, preprint (astro-ph/0502540)

Geminale A., 2006, PhD thesis, Univ. Padova (Italy).

Germany L. M., 2000, PhD Thesis, the Australian National University

Gibson B. K. et al., 2000, ApJ, 529, 723

Gillett F. C. & Soifer B. T., 1976, ApJ, 207, 780

Goldhaber G. et al., 2001, ApJ, 558, 359

Goobar A., Hannestad S., Mörtsell E., Huitzu T., 2006, JcAP, 06, 019

Goudfrooij P., de Jong T., Hansen L., Nørgaard-Nielsen H. U., 1994, MNRAS, 271, 833

Graham J., Li W., Schwartz M. & Trondal O., 2005, IAUC 8465

Graham J., Li W., Trondal O. & Schwartz M., 2005, IAUC 8467

Gratton R. G. et al., 2003, A&A, 404, 187

Hachinger S., Mazzali P.A. & Benetti S., 2006, MNRAS, 370, 299

Hamuy M. et al., 1991, AJ, 102, 208

Hamuy M. et al., 1992, PASP, 104, 533

Hamuy M. et al., 1994, PASP, 106, 566

Hamuy M., Phillips M. M., Maza J., Suntzeff N. B., Schommer R. A., Avilks R., 1995, AJ, 109, 1

Hamuy M., Phillips M. M., Suntzeff N. B., Schommer R. A., Maza J. & Aviles R., 1996a, AJ, 112, 2391

Hamuy M., Phillips M. M., Suntzeff N. B., Schommer, R. A., Maza J., Aviles R., 1996b, AJ, 112, 2398

Hamuy M. et al., 1996c, AJ, 112, 2408

Hamuy M., Phillips M. M., Suntzeff N. B., Schommer R. A., Maza J., Smith R. C., Lira P. & Aviles R.et al., 1996d, AJ, 112, 2438

Hamuy M. et al., 2001, ApJ, 558, 615

Hamuy M. et al., 2002, AJ, 124, 417

Hamuy M. et al., 2003, Nature, 424, 651

Hartmann J., 1904, ApJ, 19, 268

Harutyunyan A., Benetti S., Cappellaro E. & Turatto M., 2005, in Turatto M., Benetti S., Zampieri L. & W. Shea, eds., Supernovae as Cosmological Lighthouse. Astron. Soc. Pac., San Francisco, p. 258

Harutyunyan A., Benetti S., Turatto M., Cappellaro E., Elias-Rosa N., Andreuzzi G., 2006, CBET 647

Hatano K. et al., 1999, ApJ, 525, 881

Heckman T. M. & Lehnert M. D., 2000, ApJ, 537, 690

Heger M. L., 1922, Lick Obs. Bull., 10, 146

Hendry M. A. et al., 2005, MNRAS, 359, 906

Henry R. B. C. & Branch D., 1987, PASP, 99, 112

Herbig G. H., 1993, ApJ, 407, 142

Herbig G. H., 1995, ARA&A, 33, 19

Hernandez M. et al., 2000, MNRAS, 319, 223

Hillebrandt W. & Niemeyer J. C., 2000, ARA&A, 38, 191

Hobbs L. M., 1969a, ApJ, 157, 135

Hobbs L. M., 1969b, ApJ, 157, 165

Hobbs L. M., 1974, ApJ, 191, 381

Hobbs L. M., 1978a, ApJ, 222, 491

Hobbs L. M., 1978b, ApJS, 38, 129

Höflich P., 1991, A&A, 246, 481

Höflich P., Gerardy C., Linder E., Marion G. H., 2003, in Stellar Candles for the Extragalactic Distance Scale, Edited by D. Alloin and W. Gieren, Lecture Notes in Physics, vol. 635, p.203-227

Howell D. A. et al., 2006, Nature, 443, 308

Huchra J. P., Vogeley M. S. & Geller M. J. ,1999, ApJS, 121, 287

Iapichino L., Brüggen M., Hillebrandt W., Niemeyer J. C., 2006, A&A, 450, 655

Iglesias-Groth S., 2004, ApJ, 608, L37

Immler S. et al., 2006, ApJ, 648, L119

Itagati K. & Arbour R., 2003, IAUC 8097

Itagaki K. et al., 2006, IAUC 8762

Jansen R. A. et al., 1994, MNRAS, 270, 373

Jha S., 2002, PhD thesis, Harvard University

Jha S. et al., 2006, AJ, 131, 527

Jones A. P., Tielens A. G. G. M., Hollenbach D. J. & McKee C. F., 1994, ApJ, 433, 797

Jones A. P., Tielens A. G. G. M. & Hollenbach D. J., 1996, ApJ, 469, 740

Jönsson J., Dahlen T., Goobar A., Gunnarsson C., Mörtsell E., Lee K., ApJ, 639, 991

Jura M. and Kleinmann S. G., 1989, ApJ, 341, 359

Kapteyn J. C., 1909, ApJ, 29, 46

Kasen D., 2006, ApJ, 649, 939

Keel, 1996, AJ 111, 696

Kim S. H., Martin P. G. & Hendry P. D., 1994, ApJ, 422, 164

Kim S. H. & Martin P. G., 1996a, ApJ, 462, 296

Kim S. H., Goobar A. & , Goobar & Perlmutter S., 1996b, PASP, 108, 190

Knapp G. R., 1986, ApJ, 311, 731

Knop R. A. et al., 2003, ApJ, 598, 102

Kotak R. ,Meikle W. P. S. & Patat F., 2003, IAUC 8099

Kotak R. et al., 2004, MNRAS, 354, L13

Kotak R. et al., 2005, A&A, 436, 1021

Kozma C., Fransson C., Hillebrandt W., Travaglio C., Sollerman J., Reinecke M., Röpke F. K., Spyromilio J., 2005, A&A, 437, 983

Kraan-Korteweg R. C., 1986, A&AS, 66, 255

Kirshner R. P. et al., 1993, ApJ, 415, 589

Krisciunas K. et al., 2000, ApJ, 539, 658

Krisciunas K. et al., 2001, AJ, 122, 1616

Krisciunas K. et al., 2003, AJ, 125, 166

Krisciunas K. et al., 2004a, AJ, 127, 1664

Krisciunas K. et al., 2004b, AJ, 128, 3034

Krisciunas K., Prieto J. L., Garnavich P. M., Riley J.-L. G., Rest A., Stubbs C., McMillan R., 2006, AJ, 131, 1639

Krisciunas K. et al., 2007, AJ, 133, 58

Landolt A.U., 1992, AJ, 104, 340

Lauroesch J. T., Crotts A. P. S., Meiring J., Kulkarni P., Welty D. E., York D.G., 2006, CBET 421

Lavionov V. & Arkharov A., 2002, IAUC 7901

Leibundgut B., 1988, PhD thesis, Univ. Basel

Leibundgut B. et al., 1991, ApJ, 371, L23

Leibundgut B. et al., 1993, AJ, 105, 301

Leibundgut B. & Suntzeff N. B., 2003, in Supernovae and Gamma-Ray Bursters, Weiler K., eds., Lecture Notes in Physics, Supernovae and Gamma-Ray Bursters. Edited by K. Weiler., Lecture Notes in Physics, Springer-Verlag, Berlin, vol. 598, p. 77 (astro-ph/0304112)

Lenzuni P., Natta A., and Panagia N., 1989, ApJ, 345, 306

Leonard D. C. et al., 2002, PASP, 114, 35

Li W., Filippenko A. V., Treffers R. R., Riess A.G., Hu J., Qiu Y., 2001a, ApJ, 546, 734

Li A. & Draine B. T., 2001b, ApJ, 554, 778

Li W. et al., 2001c, PASP, 113, 1178

Lidman C., 2002, ApJ, 339, 1093

Lira P., 1995, M. S. thesis, University of Chile

Lira P. et al., 1998, AJ, 115, 234

Livne E., 1999, ApJ, 527, 97

Lucy L.B., 1999, A&A, 345, 211

Lundmark K., 1920, Sven. Vet. Handlingar, 60, 8

Marion G. H. et al., 2003, ApJ, 591, 316

Maciel W. J., 1981, A&A, 98, 406

Matheson T., Filippenko A. V., Chornock R., Leonard D. C., Li W., 2000, AJ, 119, 2303

Matheson T., Jha S., Challis P., Kirshner R. & Berlind P., 2001, IAUC 7748

Matheson T. et al., 2003, IAUC 8099

Matheson T., Challis P., Kirshner R. & Berlind P., 2004, IAUC 8311

Mathis J. S., Rumpl W. & Nordsieck K. H., 1977, ApJ, 217, 425

Mathis J. S. & Whiffen G., 1989, ApJ, 341, 808

Mathis J. S., 1996, ApJ, 472, 643

Mattila S., Meikle W. P. S. & Greimel R., New Astronomy Reviews, 48, 595

Mattila S., Lundqvist P., Sollerman J., Kozma C., Baron E., Fransson C., Leibundgut B., Nomoto K., 2005, A&A, 443, 649

Mazzali P. A. & Lucy L. B., 1993, A&A, 279, 447

Mazzali P. A. & Lucy L. B., 1998, MNRAS, 295, 428

Mazzali P. A. et al., 1998, ApJ, 499, L49

Mazzali P. A., 2000, A&A, 363, 705

Mazzali P. A., 2001, MNRAS, 321, 341

Mazzali P. A. et al., 2005, ApJ, 623, L37

McKee C. F. & Ostriker J. P., 1977, ApJ, 218, 148

McKee C. F., 1989, in Allamandola L. J. and Tielens A. G. G. M., eds. (an IAU Symp. 135) Interstellar Dust. Kluwer Academic Publishers, Dordrecht, p. 431

Meikle W. P. S. et al., 1996, MNRAS, 281, 263

Meikle W. P. S., 2000, MNRAS, 314, 782

Meikle P. & Mattila S., 2002, IAUC 7911

Merrill P. W., 1934, PASP, 46, 206

Metlova N. V., 1985, IBVS, 2780, 1M

Meyer D. M. & Savage B. D., 1981, ApJ, 248, 545

Meyer D. M. & Jura M., 1985, ApJ, 297, 119

Meyer A. W., Smith R. G., Charnley S. B. & Pendleton Y. J., 1998, AJ, 115, 2509

Mie G., 1908, Ann. Phys., 25, 377

Minkowski R., 1941, PASP, 53, 224

Misselt K. A., Clayton G. C. & Gordon K. D., 1999, ApJ, 515, 128

Modjaz M., Blondin S., Kirshner R., Challis P., Matheson T., Mamajek E., 2006, CBET 677

Moore M., Li W. & Boles T., 2003, IAUC 8184

Morrell N., Hamuy M., Folatelli G. & Phillips M., 2004, IAUC 8450

Morrell N., Folatelli G., Hamuy M. & Phillips M. M., 2006, CBET 368

Münch G., 1957, ApJ, 125, 42

Münch G., 1968, in Middlehurst B. M. andAller L. H. eds., Star and Stellar Systems. VII. Nebulae and Interstellar Matter. Univ. of Chicago Press, p. 365

Munari U. & Zwitter T., 1997, A&A, 318, 269

Myung J., 2003, Journal of Mathematical Psychology, 47, 90

Nakano S., Kushida R., Kushida Y. & Itagaki K., 2004, IAUC 8272

Nakano S. & Li W., 2005a, IAUC 8475

Nakano S. & Kadota K., 2005b, IAUC 8478

Navasardyan H., Turatto M., Harutunyan A., Benetti S., Elias-Rosa N., Pastorello A., Viotti R., Rossi C., 2004, IAUC 8454

Navasardyan H., Benetti S., Elias-Rosa N., Harutunyan A., Pastorello A., 2005, IAUC 8468

Navasardyan H., Benetti S., Harutyunyan A., Bufano F., Elias-Rosa N., Zampieri L., Turatto M., Cappellaro E., 2006, IAUC 8667

Neufeld D. A., Wolfire M. G. & Schilke P., 2005, ApJ, 628, 260

Niemeyer J., Reinecke M., Travaglio C., Hillebrandt W., 2003, in Leibundgut B., Hillebrandt W., eds, Proc. to the ESO/MPA/MPE Workshop (an

ESO Astrophysics Symp.) From Twilight to Highlight the Physics of Supernovae. Springer-Verlag, Berlin, p.151

Nobili S. et al., 2003, A&A, 404, 901

Nobili S. et al., 2005, A&A, 437, 789

Nomoto K., Thielemann F. K. & Tokoi K., 1984, ApJ, 286, 644

Nomoto K. et al., 2003, in Leibundgut B., Hillebrandt W., eds, Proc. to the ESO/MPA/MPE Workshop (an ESO Astrophysics Symp.) From Twilight to Highlight the Physics of Supernovae. Springer-Verlag, Berlin, p.115

Nomoto K., Maeda K., Tominaga N., Ohkubo T., Deng J., Mazzali P., 2005, Ap&SS, 298, 81

Nomoto K., Saio H., Kato M. & Hachisu I., 2007, ApJ, in press (astro-ph/0603351)

Nugent P. et al., 1995, ApJ, 455, L147

Nugent P., Kim A. & Perlmutter S., 2002, PASP, 114, 803

O'Donnell J. E., 1994, ApJ, 422, 158

O'Donnell J. E. & Mathis J. S., 1997, ApJ, 479, 806

Oke J. B., 1990, AJ, 99, 1621

Omont A., Moseley S. H., Forveille T., Glaccum W. J., Harvey P. M., Likkel L., Lowenstein R. F., Lisse C. M., 1990, ApJ, 355, L27

Oort J. H. & van de Hulst H. C., 1946, Bull. Astron. Inst. Netherlands, 10, 187

Panagia N., Van Dyk S. D., Weiler K. W., Sramek R. A., Stockdale C. J., Murata K. P., 2006, ApJ, 646, 369

Pastorello A., Taubenberger S., Patat F., Benetti S., Harutyunyan A., Elias-Rosa N., Alises M., 2005, IAUC 8467

Pastorello A. et al., 2007a, MNRAS, in press (astro-ph/0702566)

Pastorello A. et al., 2007b, MNRAS, in press (astro-ph/0702565)

Pastorello A. et al., 2007c, Nature, submitted

Pastorello A. et al., 2007d, MNRAS, in prep.

Patat F. et al., 1996, MNRAS, 278, 111

Patat F., 2005, MNRAS, 357, 1161

Patat F., Benetti S., Cappellaro E. & Turatto M., 2006, MNRAS, 369, 1949

Patat F. et al., 2007, Science, submitted

Patil M. K., Pandey S. K., Sahu D. K. & Kembhavi A., 2007, A&A, 461, 103

Pauldrach, A.W.A. et al., 1996, A&A 312, 525

Peebles P. J. E. & Ratra B., 2003, Modern Physics, 75, 559

Perlmutter S. et al., 1997, ApJ, 483, 565

Perlmutter S. et al., 1998, Nature, 392, 311

Perlmutter S. and the Supernova Cosmology Project, 1999, ApJ, 517, 565

Persson S. E. et al., 1998, AJ, 116, 2475

Phillips M. M. et al., 1987, PASP, 99, 592

Phillips M. M., Wells L. A., Suntzeff N. B., Hamuy M., Leibundgut B., Kirshner R. P. & Foltz C. B., 1992, AJ, 103, 1632

Phillips M. M., 1993, ApJ, 413, L105

Phillips M. M. et al., 1999, AJ, 118, 1766

Pignata G. et al., 2004a, MNRAS, 355, 178

Pignata G., 2004b, PhD thesis, Univ. Padova (Italy)

Ponticello N. J. et al., 2006, IAUC 8667

Pottasch S. R., Baud B., Beintema D., Emerson J., Habing H. J., Harris S., Houck J., Jennings R. & Marsden P., 1984, A&A, 138, 10

Pozzo M. et al., 2006, MNRAS, 368, 1169

Prieto J. L., Rest A. & Suntzeff N. B., 2006, ApJ, 647, 501

Pskovskii YuP., 1977, Sov. Astron., 21, 675

Pskovskii YuP., 1984, Sov. Astron., 28, 658

Puckett T. & Peoples M., 2006a, CBET 606

Puckett T., Peoples M., Joubert N., Madison D. R., Mostardi R., Khandrika H., Li W., Foley R. J., 2006b, IAUC 8741

Pugh H. & Li W., 2004, IAUC 8448

Qiao Q.-Y., Wu H., Wei J.-Y. & Li W.-D., 1997, IAUC 6623

Quimby R., Brown P., Gerardy C., Odewahn S. C., Rostopchin S., 2006a, CBET 393

Quimby R., 2006b, CBET 644

Rand R. J., 1995, ApJ, 109, 2444

Reindl B. et al., 2005, ApJ, 624, 532

Rich R. M., 1987, AJ, 94, 651

Rich D., Yamaoka H. & Itagaki K., 2005, IAUC 8497

Richmond M. W. et al., 1996, AJ, 111, 327

Richmond M. W. et al., 1995, AJ, 109, 2121

Rieke G. H. & Lebofsky M. J., 1985, ApJ, 288, 618

Riess A. G., Press W. H. & Kirshner R. P., 1995, ApJ, 438, L17

Riess A. G., Press W. H. & Kirshner R. P., 1996a, ApJ, 473, 88

Riess A. G., Press W. H. & Kirshner R. P., 1996b, ApJ, 473, 588

Riess A. G. et al., 1998, AJ, 116, 1009

Riess A. G. et al., 1999a, AJ, 117, 707

Riess A. G. et al., 1999b, AJ, 118, 2688

Riess A. G. et al., 2004, ApJ, 607, 665

Roche P. F. & Aitken D. K., 1984, MNRAS, 209, 33

Röpke F. K. & Hillebrandt W., 2005, A&A, 431, 635

Röpke F. K., Hillebrandt W., Niemeyer J. C., Woosley S. E., 2006a, A&A, 448, 1

Röpke F. K., Gieseler M., Reinecke M., Travaglio C., Hillebrandt W., 2006b, A&A, 453, 203

Röpke F. K., Hillebrandt W. & Blinnikov S. I., 2006c, preprint (astro-ph/0609631)

Röpke F. K., Woosley S. E. & Hillebrandt W., 2006d, preprint (astro-ph/0609088)

Ruiz-Lapuente P., Comeron F., Mendez J., Canal R., Smartt S., Filippenko A. V., Kurucz R. L., Chornock R., Foley R., 2005, Nature, 431, 1069

Saha A., Sandage A., Tammann G. A., Labhardt L., Macchetto F. D. & Panagia N., 1999, ApJ, 522, 802

Salvo M. E. et al., 2001, MNRAS, 321, 254

Salvo M. E., 2006, PhD thesis, The Australian National University

Sauer D. N., Hoffmann T. L. & Pauldrach A. W. A., 2006, A&A, 459, 229

Savage B. D.& Mathis J. S., 1979, Ann. Rev. Astr. Ap., 17, 73

Schaefer B., 1995, ApJ, 450, L5

Schlegel D. J., Finkbeiner D. P. & Davis M., 1998, ApJ, 500, 525

Schmidt B. P., Kirshner R. P., Leibundgut B., Wells L. A., Poter A. C., Riuz-Lapuente P., Challis P., Filippenko A. V., 1994, ApJ, 434, L19

Schwehr J., Lee N., Li W., Itagaki K., Nakano S., 2006, IUAC 8745

Seaton M. J., 1979, MNRAS, 187, 73p

Seab C. G., 1988, in Bailey M. E. & William D. A., eds.. Dust in the Universe. Cambridge University Press, Cambridge, p. 303

Sembach K. R., Danks A. C. & Savage B. D., 1993, A&AS, 100, 107

Smith R. G., Sellgren K. & Tokunaga A. T., 1988, ApJ, 334, 209

Snow T. P. & McCall B. J., 2006, ARA&A, 44, 367

Soifer B. T., Willner S. P., Capps R. W. & Rudy R. J., 1981, ApJ, 250, 631

Sollerman J., Leibundgut B. & Lundquist P., 2001, IAUC 7723

Sollerman J. et al., 2004, A&A, 428, 555

Sollerman J., Cox N., Mattila S., Ehrenfreund P., Kaper L., Leibundgut B. and Lundqvist P., 2005, A&A, 429, 559

Sparks W. B., Macchetto F., Panagia N., Boffi F. R., Branch D., Hazen M. L., Della Valle M., 1999, ApJ, 523, 585

Spitzer L. Jr., 1948, ApJ, 108, 276

Spitzer L. Jr. & Oke J. B., 1952, ApJ, 115, 222

Spitzer L. Jr., 1976, Comments Asrophys., 6, 177

Stanishev V., et al., 2006, MNRAS, in press

Starrfield S., in Leibundgut B., Hillebrandt W., eds, Proc. to the ESO/MPA/MPE Workshop (an ESO Astrophysics Symp.) From Twilight to Highlight the Physics of Supernovae. Springer-Verlag, Berlin, p.128

Steidel C. C., Rich R. M. & McCarthy J. K., 1990, AJ, 99, 1476

Stritzinger M. et al., 2002, AJ, 124, 2100

Stritzinger M., Leibundgut B., Walch S., Contardo G., 2006, A&A, 450, 241

Struve F. G. W., 1847, Etudes d'Astronomie Stellaire

Stehle M. et al., 2005, MNRAS, 360, 1231

Stephenson F. R. & Green D. A., 2005, in Turatto M., Benetti S., Zampieri L. & W. Shea, eds., Supernovae as Cosmological Lighthouse. Astron. Soc. Pac., San Francisco, p. 63

Sugerman B. E. K. & Crotts A. P. S., 2002, ApJ, 581, L97

Sugerman B. E. K., 2003, AJ, 126, 1939

Sullivan M. et al., 2003, MNRAS, 340, 1057

Suntzeff N. B., 1996, in McCray R., Wang Z., eds, Proc. IAU Colloquium 145, Supernovae and Supernova Remanants, Cambridge: University Press, p. 41

Suntzeff N. B., 2000, American Institute of Pysics Conference Series, 522, 65

Suntzeff N. B., 2003, in Leibundgut B., Hillebrandt W., eds, Proc. to the ESO/MPA/MPE Workshop (an ESO Astrophysics Symp.) From Twilight to Highlight the Physics of Supernovae. Springer-Verlag, Berlin, p.183

Suzuki S. & Migliardi M., 2006, IAUC 8667

Takada-Hidai M., Aoki W. & Zhao G., 2002, PASJ, 54, 899

Tanaka M., Mazzali P. A., Benetti S., Nomoto K., Elias-Rosa N., Kotak R., Pignata G., Stanishev V., Hachinger S., 2006, ApJ, submitted

Taubenberger S. et al., 2006, MNRAS, 371, 1459

Thielemann F.-K. et al., 2003, in Leibundgut B., Hillebrandt W., eds, Proc. to the ESO/MPA/MPE Workshop (an ESO Astrophysics Symp.) From Twilight to Highlight the Physics of Supernovae. Springer-Verlag, Berlin, p.331

Tielens A. G. G. M. & Hagen W., 1982, A&A, 114, 245

Tielens A. G. G. M. & Allamandola L. J., 1987, in Morfill G. E. & Scholer M., eds.. Physical Processes in Interstellar Clouds. Reidel, Dordrecht, p. 333

Tielens A. G. G. M., 1990, in J. Tarter et al., eds., Carbon in the Galaxy:Studies from Earth and Space. NASA, Washington DC, p. 59

Tielens A. G. G. M., McKee C. F., Seab C. G. & Hollenbach D. J., 1994, ApJ, 431, 321

Tonry J. L., Blakeslee J. P., Ajhar E. A. & Dressler A., 2001a, ApJ, 475, 399

Tonry J. L., Dressler A., Blakeslee J. P., Ajhar E. A., Fletcher A. B., Luppino G. A., Metzger M. R. & Moore C. B., 2001b, ApJ, 546, 681

Travaglio C., Hillebrandt, W. & Reinecke M., 2005, A&A, 443, 1007

Treffers R. R. & Cohen M., 1974, ApJ, 188, 545

Treffers R. R., Peng C. Y., Filippenko A. V., Richmond M. W., Barth A. J., Gilbert A. M., 1997, IAUC 6627

Trimble V., 1982, Rev. of Modern Physics, 54, 4

Trumpler R. J., 1930a, Lick Obs. Bull., 14, 154

Trumpler R. J., 1930b, Publ. Astron. Soc. Pacific, 42, 214

Trumpler R. J., 1930c, Publ. Astron. Soc. Pacific, 42, 267

Tsvetkov D. Y. & Pavlyuk N. N., 1995, AstL, 21, 606

Turatto M. et al., 1990, AJ, 100, 771

Turatto M., Benetti S., Cappellaro E., Danziger I. J., della Valle M., Gouiffes C., Mazzali P. A. & Patat F., 1996, MNRAS, 283, 1

Turatto M., Desidera S., Benetti S., Altavilla G., Pastorello A., Riello M. & Cappellaro E., 2002, IAUC 7901

Turatto M., 2003a, in Supernovae and Gamma-Ray Bursters, Weiler K., eds., Lecture Notes in Physics, Supernovae and Gamma-Ray Bursters. Edited by K. Weiler., Lecture Notes in Physics, Springer-Verlag, Berlin, vol. 598, p. 21 (astro-ph/0301107)

Turatto M., Benetti S. & Cappellaro E., 2003b, in From Twilight to Highlight the Physics of Supernovae, Leibundgut B., Hillebrandt W., eds., Springer-Verlag, Berlin, p. 200

Utrobin V. P., 2007, A&A, 461, 233

Vagnozzi A. et al., 2004, IAUC 8375

van Dishoeck E. F., Jansen D. J. & Phillips T. G., 1993, A&A, 279, 541

Van Dyk S. D., Peng C. Y., King J. Y., Filippenko A. V., Treffers R. R., Li W., Richmond M. W., 2000, PASP, 112, 1532

Van Dyk S. D., Li W. & Filippenko A. V., 2006, PASP, 118, 351

Vaughan T. E., Branch D., Miller D. L., Perlmutter S., 1995, ApJ, 439, 558

Vladilo G., Crivellari L., Molaro P. & Beckman J. E., 1987, A&A, 182, 59

Wang L., Goldhaber G., Aldering G., Perlmutter S., 2003, ApJ, 277, 355

Wang L., 2005, ApJ, 635, L33

Wang L., Baade D., Patat F., Wheeler J. C., 2006a, CBET, 396

Wang L., Baade D. & Patat F., 2006b, Science, 315, 212

Wang X. et al., 2005, ApJ, 620, L87

Wannier P. G., Sahai R., Anderson B. G. & Johnson H. R., 1990, ApJ, 358, 251

Weiler K. W., Panagia N., Montes M. J., Sramek R. A., 2002, ARA&A 40, 387

Weingartner J. C. & Draine B. T., 2001, ApJ, 548, 296

Welsh B. Y., Vedder P. W., Vallerga J. V. & Craig N., 1991, ApJ, 381, 462

Witt A. N., 2000, Journal of Geophysical Research, 105, 10299 (astro-ph/9910259)

Wheeler J. C. & Harkness R. P., 1990, Reports of Progress in Physics, 53, 1467

Wheeler J. C. et al., 1998, ApJ, 496, 908

Wheeler J. C. & Benetti S., 2000, in Arthur N. Cox eds., 18th Chapter of "Allen's Astrophysical Quantities", IVth edition. AIP Press, p. 451

Whittet D. C. B., 1988, in Bailey M. E. & William D. A., eds., Dust in the Universe. Cambridge University Press, Cambridge, p. 25

Whittet D. C. B., 1992, in Birkinshaw M., Elvis M. & Silk J., eds., Series in Astronomy and Astrophysics, Dust in the Galactic Environment. Institute of Physics Publishing, Bristol and Philadelphia.

Wood-Vasey W. M. et al., 2007, ApJ, in press (astro-ph/0701041)

Xu J., Crotts A. P. S. & Kunkel W. E., 1994, ApJ, 435, 274

Xu J., Crotts A. P. S. & Kunkel W. E., 1995, ApJ, 451, 806

Zubko V. G., Smith T. L. & Witt A. N., 1999, ApJ, 511, L57

Zwicky F., 1938, PASP, 50, 215